CALIFORNIA INSTITUTE OF TECHNOLOGY

SOIL MECHANICS LABORATORY

A STUDY OF HIGH-FREQUENCY STRONG GROUND MOTION FROM THE SAN FERNANDO EARTHQUAKE

by
John Beauchamp Berrill

1975

A STUDY OF
HIGH-FREQUENCY STRONG GROUND MOTION
FROM THE SAN FERNANDO EARTHQUAKE

Thesis by

John Beauchamp Berrill

In Partial Fulfillment of the Requirements

for the Degree of

Doctor of Philosophy

California Institute of Technology

Pasadena, California

1975

(Submitted March 12, 1975)

ACKNOWLEDGEMENTS

The writer wishes to express his thanks to his adviser, Professor R. F. Scott, for first suggesting this topic, and for his encouragement, guidance and help during the investigation, and in many other facets of the writer's stay at the Institute.

Thanks are also due to Dr. T. C. Hanks for his assistance in the seismological aspects of the thesis and for many helpful and lively discussions.

Discussions with Professor P. C. Jennings and Dr. A. G. Brady also contributed significantly to this work, and they are gratefully acknowledged.

The writer is grateful to the Institute for financial assistance, part of which came from National Science Foundation funds.

ABSTRACT

This thesis describes an investigation of the attenuation of strong earthquake ground motion in the 0.4 to 16 Hz frequency band during the M = 6.4, February 9, 1971, San Fernando, California earthquake. It is found that Fourier amplitudes of ground acceleration decay according to a simple expression incorporating a geometric spreading term, and a material attenuation term with constant specific attenuation Q. The scatter in the amplitude data about an expected level given by the simple decay expression is nearly constant with respect to both frequency and focal distance. Fourier amplitudes of acceleration corrected to a reference hypocentral distance agree well with those determined by a two-parameter source model of the San Fernando earthquake. Focusing of energy to the south by the southward propagating rupture is observed at frequencies below 8 Hz. The propagation of rupture was incoherent with respect to higher-frequency components.

The relationship between intensity of ground motion and site geology is examined. It is found that while, in general, sedimentary sites were accelerated more strongly than basement rock sites, no clear difference could be found between sedimentary sites classified as "soft" by Trifunac and Brady (1975) (generally recent alluvium) and those classified as having "medium" soil stiffness, generally consisting of older alluvium and sedimentary rock. The difference between amplitudes recorded on basement rock and sediments is more complex. In general, smoothed amplitude spectra from accelerograms recorded

on basement rock are lower than smoothed amplitudes at corresponding sedimentary sites. However, basement site spectra show marked isolated peaks, as high as those from sedimentary sites at similar distances. This is attributed to the focusing effects of the irregular topography normally accompanying basement rock outcrops. In the frequency band considered, it is concluded that for the purposes of aseismic design of structures no discrimination should be made between the intensity of ground motion expected on basement rock, sedimentary rock, and coarse-grained alluvium typical of Southern California.

The agreement between the recorded strong motion amplitudes and those predicted by a simple two-parameter source model suggests that the model can be used for the assessment of strong ground motion to be used in design procedures. A procedure for estimating design earthquakes using the source model and the amplitude decay expression is presented.

TABLE OF CONTENTS

Table of Contents Continued

Table of Contents Continued

1. INTRODUCTION

This investigation studies the high frequency components of strong ground motions, those in the frequency band of 0.4 to 16 Hz, generated by the M = 6.4, February 9, 1971, San Fernando, California earthquake. This earthquake is unique in that it was the first and, to date, the only earthquake to be recorded by a large number of strong-motion* accelerographs, with 241 accelerograms being recorded in all. This large body of data is particularly well-suited to the study of the propagation of strong ground motion, since the variables arising from the differences between one earthquake rupture mechanism and another are not present. The large number of recordings and particularly their spatial distribution, allows some details of the rupture itself to be studied.

This investigation treats two specific problems in engineering seismology.* They are: (a) the decay of Fourier amplitude of ground acceleration as a function of both distance and frequency, and (b) how well average strong-motion amplitudes can be predicted by simple, recently-developed seismic source models. These problems are addressed in Chapters 2 and 3, respectively. It is found that the average Fourier amplitudes obey a simple decay expression and that, to within a factor of two to three, average amplitudes corrected to a reference hypocentral distance* agree with those predicted independently by a two-parameter source model. The engineering use of this

*A glossary of terms may be found in Appendix 5.

information in predicting earthquake ground motion is illustrated by an example in Chapter 4.

The frequency band of interest in earthquake engineering is governed by the natural frequencies of engineering structures. Long suspension bridges, for example, may have fundamental periods of vibration of as much as 20 seconds. Mechanical equipment and very rigid structures, on the other hand, have natural frequencies of up to, say 20 Hz. Thus the frequency band of engineering interest runs from approximately 0.05 Hz to 20 Hz.

The study was confined to the high frequency components of strong ground motion since there is an essential difference in complexity between high- and low-frequency components in both their generation and in their propagation. The criterion is wavelength. If the wavelength of the components being considered is long compared to the dimensions of the area ruptured, a simple waveform is emitted; the complexity of its subsequent propagation depends principally upon whether or not the wavelength is large compared to the dimensions of the inhomogeneities in its travel path. Hanks (1974b), finds that ground displacement wave forms (characterizing components with frequency, $f \leq 0.3$ Hz, say) from the San Fernando earthquake were propagated coherently* over distances of tens of kilometers. On the other hand, high frequency components are emitted erratically as the rupture progresses along the fault, and they are further modified by inhomogeneities in the propagation path. Crouse (1973) observed that

*See glossary.

acceleration wave forms (characterizing components with $f > 3$ Hz, say) do not propagate coherently for distances of more than a few hundred meters. It is probable that the components contributing to ground accelerations recorded at a particular location and at a particular frequency result from the superposition of several different waves arriving by different propagation paths. It is unlikely that these waves will arrive in phase. More likely, they will interfere, causing relatively high amplitudes of ground acceleration at some frequencies and at some locations, and relatively low amplitudes at other frequencies and locations. In these circumstances, while phase coherence is lost, it is possible that average amplitudes do propagate coherently, and, in fact, this is found to be the case in the data studied. Thus, on the basis of previous observations that acceleration waveforms do not propagate coherently, but in the expectation that their amplitudes might, Fourier amplitudes of accelerations were studied.

The remainder of this chapter reviews some problems of engineering seismology, and describes some currently used methods of predicting future ground shaking for the purpose of designing earthquake resistant structures.

1.1. Some problems in engineering seismology.

This section provides a background to the investigation that follows. For a complete review of engineering seismology, reference may be made to Bolt (1970a, b), Housner (1973a), Hudson (1972a, 1974), and Newmark and Rosenblueth (1971).

An engineer wishing to design a building to withstand earthquakes must first estimate the strength and frequency content of the maximum ground shaking the building is likely to experience during its life. Providing such estimates is the principal problem in engineering, or strong-motion, seismology. Since small earthquakes are more frequent than large, the engineer would like to know the ground motion characteristics expected from a number of different sized events, and the probability of occurrence of each. With this knowledge, the risk of damage can be compared with the cost of providing additional strength and insurance. However, the details of the cause and mechanism of earthquake rupture are not completely understood, and methods are not available for solving the resulting problem of wave propagation from the source through the laterally inhomogeneous earth's crust to a building site. Hence precise estimates of future earthquake ground motion cannot be made, and approximate methods that make use of available knowledge must be resorted to.

There are several ways in which ground motion can be characterized. The simplest is a single-parameter characterization of wave amplitude, often by peak acceleration. However, since the frequency content of seismic waves, as well as their strength, varies from earthquake to earthquake (Aki, 1972b) and is further modified during transmission (Bullen, 1963), this is not likely to be sufficient. Using peak values of acceleration, velocity, and displacement allows a three parameter representation of frequency content, and empirical relationships exist between these parameters and pseudo-velocity

response spectra for a damped, single-degree-of-freedom linear oscillator (Esteva and Rosenblueth, 1963; Brady and Trifunac, 1975). The characterization of ground motion by response spectra is extremely useful since they can be readily used in structural analysis (Hudson, 1956; Newmark and Rosenblueth, 1971).

Power spectral density functions (or Fourier amplitude spectra) afford more complete representations than the three peak ground values, and can be used in structural analysis in various ways. The power spectral density can be used directly with random vibration theory to estimate the response of a single-degree-of-freedom oscillator (Caughey and Stumpf, 1961), the response of multi-degree-of-freedom systems being obtained by modal superposition (Merchant and Hudson, 1962). Alternatively the power spectrum can be used to generate either a single artificial accelerogram, or an ensemble of accelerograms with a statistical distribution corresponding to the uncertainties in estimating the effects of earthquake source and transmission path (Jennings, et al., 1968). Response spectra may in turn be computed from these accelerograms, or the accelerograms may be used directly as input to a numerical structural model from which the distribution of response is determined. The latter use represents the most advanced technique currently in routine use in earthquake engineering (Housner, 1973b).

As a matter of convenience in terminology, any such predicted ground motion will be referred to as a "design earthquake".

Any procedure for estimating design earthquakes should be based as much as possible on what is known of the physics of the

several mechanisms causing the earthquake ground motion, and should resort to empirical methods only when physical understanding or computational capability fails. For research purposes, it is desirable that a procedure be separated into steps corresponding to the various related mechanisms contributing to generation and propagation of earthquakes so that each step may be up-dated as further knowledge becomes available.

The broad physical processes in the generation of an earthquake are as follows:

(1) Large scale tectonic movements; these lead to stress build-up in the earth's crust and rupturing as a mode of stress relief.

(2) The earthquake rupture mechanism. Since the triggering of rupture depends upon details of the mechanism itself, (2) is closely related to (1).

(3) Propagation of seismic waves away from the source.

In the design earthquake estimation problem, there are the following steps:

(1) Prediction of the spatial and temporal distribution of earthquakes with rupture mechanisms described by a particular set of source parameters.*

(2) Obtaining an estimate of the seismic waves radiated from the source region, given a description of the rupture process by the source parameters.

---

*See glossary.

(3) Modification of both amplitude and frequency content of seismic waves during propagation between source and site, including the effects of local site conditions.

The theory of plate tectonics (Jacobs, et al., 1974) provides a general understanding of why earthquakes occur, and explains why they are much more prevalent in certain regions of the world, along plate boundaries, than in others. But to make precise predictions of the occurrence and nature of earthquakes requires a much more complete understanding than exists at present of the cause of crustal plate movements, of the material properties and stress state in the crust, and detailed knowledge of rupture mechanisms. The theory does, however, allow the seismic and geologic history of a region to be used with more confidence in predicting earthquake return periods. However, long historic records, even where they exist do not provide a complete solution to the problem of estimating the likelihood of earthquake occurrence. For example, records have been kept of earthquakes for nearly 3000 years in the Kansu Province of China, yet for one 800 year interval, from 200 A.D. to 1000 A.D., earthquake activity was very low, with intensive activity both before and after that period (Mei, 1960). Ambraseys (1961) has translated an historical record of earthquakes in the Middle East, and it shows a similar irregular history of activity.

Some details of rupture mechanisms are not known, but it is accepted that shallow focus earthquakes, which, as the most damaging, are of prime interest to engineers, are the result of shear dislocations in the earth's crust under the stress field imposed by inter-plate movement (Reid, 1911; Housner, 1955; Steketee, 1958;

Jacobs et al., 1964). While no exact dynamic solutions exist for shear dislocation sources even under idealized material and geometric conditions (Randall, 1973), there is intensive geophysical research in progress into approximate source models, which capture the general features of the mechanism in a small number of source parameters. This work is reviewed by Brune (1971b) and Aki (1972a).

Brune (1970, 1971a) proposed a simple model from which a far-field* shear wave spectrum is obtained, given estimates of two independent parameters of the fault (e.g. seismic moment and source dimension; total dislocation and fault plane area). Results from Brune's model have been found to be in good agreement with independent teleseismic observations over a wide range of the model's parameters (Randall, 1973). It does not follow that the model should also prove satisfactory in regions of strong ground motion where the far-field assumption is not so clearly satisfied. However, it is seen in Chapter 3 that amplitudes predicted by the model from independent estimates of the San Fernando earthquake source parameters are in good agreement with those observed from the strong motion data. While the model is quite simple, in that the amplitude spectrum is approximated by its high and low frequency asymptotes, its use in design earthquake prediction offers an advance over the use of magnitude alone, and brings the procedure closer to the underlying physics.

---

*See glossary.

The third problem, that of propagation of seismic waves through the earth's crust from an earthquake source to an engineering site, also is difficult to solve because of material inhomogeneity and irregular surface topography. At present, no analytical solutions exist for wave propagation through a laterally inhomogeneous crust (Bolt, 1970a). There are numerical techniques available, but due both to cost and computational difficulties at present they are feasible only for low frequency components with periods of a few seconds or longer (Mal, 1974). Furthermore, it is pointed out by Housner (1973a) that even if computation techniques did exist for the realistic strong motion propagation problems, there would be practical difficulties in applying them. Obtaining sufficient knowledge of the material properties and geometric configuration of the geology along the propagation path would be an almost impossible task, and well beyond the resources of a normal engineering project. As an illustration of this difficulty, consider a 5 Hz wave travelling through sediments at a velocity of, say, 1 km/sec. It has a wavelength of 200 meters. Since waves are scattered by inhomogeities with dimensions of the order of one wavelength, the geology should be known to a resolution of better than 200 meters. Housner concludes that a statistical approach to the propagation problem is necessary.

A large number of the strong motion accelerograms from the San Fernando earthquake were obtained within fairly narrow ranges of direction from the epicenter, mainly to the south, but also in smaller groups to the north and south-east. These groups of accelerograms form excellent sets of data from which experimental studies of strong

motion propagation can be made with relative freedom from source details.

1.2. Previous attenuation studies and design earthquake estimation methods.

Previous studies of the amplitude decay of strong ground motion generally involved only correlations between earthquake magnitude and recorded peak ground motion values, and did not consider details of the rupture mechanism and the geology of overall wave path between source and recording site. Many different expressions have resulted from these investigations. Generally, the decay of ground motion amplitudes has been accounted for by a factor of $1/r^n$, where r is hypocentral distance and n is an empirical parameter adjusted to obtain the best fit of the expression to the data set being studied. Scott (1972) was one of the first in earthquake engineering to employ two separate decay terms corresponding to the two physical phenomena contributing to amplitude decay: geometric spreading, and energy absorption or material attenuation by the travel path medium.

Prior to the 1971 San Fernando earthquake only a few strong-motion recordings had been made of a single earthquake, and studies of earthquake ground motion had, of necessity, included measures of the source strength; Richter magnitude was generally employed for this purpose. However, single parameters do not adequately represent either the source or resulting ground motion, since the strength of both is a function of frequency. Further difficulties arise when correlations are attempted between earthquake magnitude and peak ground acceleration since magnitude characterizes lower-frequency components than those developing peak acceleration (Trifunac, 1972). It should be pointed out, however, that early investigators did not have digital

computers to integrate accelerograms and compute Fourier spectra, and that peak acceleration and magnitude were the only parameters readily available. Models offering a more comprehensive source characterization are very recent, and are still at an early stage of development.

An early design earthquake prediction method was given by Esteva and Rosenblueth (1963), who published a procedure for estimating response spectra from peak ground motion values. The high frequency range of the response spectrum was scaled in proportion to peak acceleration, the intermediate in proportion to peak velocity, and the low frequency range of the spectrum according to peak displacement. They obtained expressions by regression analysis for the three peak values as functions of focal distance r, and earthquake magnitude M, from a set of data based mainly upon that of Housner (1961). The expressions are:

$$a = \frac{2000}{r^2} e^{0.8M} \tag{1.1a}$$

$$v = \frac{16}{r^{1.7}} e^{M} \tag{1.1b}$$

and

$$x = \left(\frac{1}{r^{1.4}} + \frac{1}{r^2} \right) e^{1.2M} \tag{1.1c}$$

where

a is peak ground acceleration (cm/sec^2),

v is peak ground velocity (cm/sec), and

x is peak ground displacement (cm).

Noting that high-frequency components of ground motion give rise to acceleration peaks, intermediate frequency components to velocity peaks and low frequency components to displacement peaks, the increasing importance of magnitude with decreasing frequency can be seen in the equations. Larger magnitude earthquakes apparently radiate a greater proportion of low frequency wave components. Also, it can be seen from the exponents of r which include both geometrical and material attenuation effects that the rate of attenuation increases with increasing frequency; peak acceleration being attenuated more rapidly with distance than peak velocity, which in turn is attenuated more rapidly than peak displacement.

The authors plot the peak acceleration and peak velocity data, normalized with respect to magnitude by multiplying the peak values by $e^{-0.8M}$ and e^{-M} respectively, against focal distance. At a given distance, the normalized acceleration values are scattered over two orders of magnitude. The velocity data are less scattered, probably due to better correlation with M, and also to less sensitivity of velocity peaks to variations in the source and the propagation path. If we denote expected values of peak acceleration and velocity computed by equations (1.1a), (1.1b) by $\bar{a}$ and $\bar{v}$, respectively, and the corresponding realized values from the data by a and v, and define the uncertainty factors k_a and k_v by the relationships

$$k_a = \frac{a}{\bar{a}}, \quad k_v = \frac{v}{\bar{v}}, \tag{1.2}$$

then the distributions of k_a and k_v can be computed. From the authors' confidence interval plots, the upper semi-intervals at 90 percent confidence have the values $k_a = 3.8$ and $k_v = 2.0$. That is, there is a 90 percent probability that a recorded acceleration will be less than 3.8 times the value predicted by equation (1.1a). On this basis, peak velocities show only half as much scatter as peak velocity data. Nevertheless, these values both represent large uncertainties in values predicted by equations (1.1a) and (1.1b). This is expected because of the number of different earthquakes involved in the study.

Similarly large scatter is found in other measures of ground shaking; for example, in response spectra (Adu, 1971) and in the Fourier amplitudes of acceleration of this study. Particularly in high frequency components large uncertainties are associated with any estimate of earthquake ground motion that can be made at the present time, and it is imperative that confidence intervals or some other measure of scatter be given with design earthquake estimates so that the structural designer is aware of this.

Seed et al. (1969) proposed a method for generating design earthquakes based on the device of scaling existing accelerograms according to peak acceleration. The first step in this procedure is to estimate peak acceleration at a hypothetical bedrock-soil interface. The authors present an empirical relationship between magnitude, distance and peak acceleration on "bedrock" based on the same data as that of equation (1.1a) but arbitrarily modified to give lower peak acceleration values with the rationale that the original data base included records from both soil and rock sites and that rock sites "ought" to have lower peak accelerations. The attenuation relationship has subsequently been revised by Schnabel and Seed (1973) to conform more to the San Fernando data. An existing accelerogram selected on a basis of magnitude, site, and distance similarity is then scaled to have

the same peak acceleration value in "bedrock". The greater attenuation of higher frequency components is allowed for to some extent by scaling the time base of the accelerogram according to "predominant period", a parameter referred to in Gutenberg and Richter (1956). The scaled accelerogram is then used as input to the vertically-propagating shear wave model of Idriss and Seed (1968), to obtain an accelerogram of motion at ground surface.

This procedure has found widespread use in engineering practice, despite its serious limitations. Chief among these are sole reliance upon peak acceleration to scale the ground motion, and use of the one-dimensional soil model whose assumptions of uniform horizontal soil layers and vertical wave propagation are seldom met in practice. These points are taken up in Sections 1.2.1 and 1.2.2.

Davenport (1972) obtained an empirical relationship between M and a, having the same functional form as that of Esteva and Rosenblueth (1963), but from a larger data set which included data from eleven earthquakes recorded since 1963. With data from a total of 46 North and South American earthquakes, he found the following expression using a least-squares parameter estimation technique:

$$a = \frac{270}{r^{1.64}} e^{0.8M} \qquad (1.3)$$

For Davenport's data and equation (1.3), the distribution of k_a, defined as before by equation (1.2), was approximately log normal, with $\sigma_{\log_e k} = 0.74$. The value of k (the subscript is no longer necessary) at

the upper limit of the 90 percent confidence interval computed from a log normal distribution with $\sigma_{\log_e k} = 0.74$ is 3.3, which is in reasonable agreement with the value of 3.8 given by Esteva and Rosenblueth. Using data from the San Fernando earthquake only, but without further separation into groups according to source-station azimuth or site geology, he found the following relationship:

$$a = \frac{840}{r^{1.48}} e^{0.65M} \tag{1.4}$$

with $\sigma_{\log_e k} = 0.46$.

Equations (1.1a) and (1.3) have the same magnitude dependence. However, their initial constants and exponents of r are quite different, with the larger constant of equation (1.1a) being compensated for to some extent by a larger exponent of r. The difference between the two expressions can be seen by dividing equation (1.1a) by equation (1.3), which yields

$$\frac{a_E}{a_D} = \frac{7.4}{r^{0.36}}, \tag{1.5}$$

where a_E denotes the peak acceleration value at distance r from Esteva and Rosenblueth's relationship, and a_D that from Davenport's expression. The ratio is plotted against distance in Figure 1.1, where it is seen that for $r \leq 100$ km, Esteva and Rosenblueth's expression yields values at least 1.5 times greater than those from Davenport's expression. The differences between these expressions are further demonstrated by Figure 1.2 in which peak acceleration values computed from equations (1.1a), (1.3), and (1.4), normalized with respect to M,

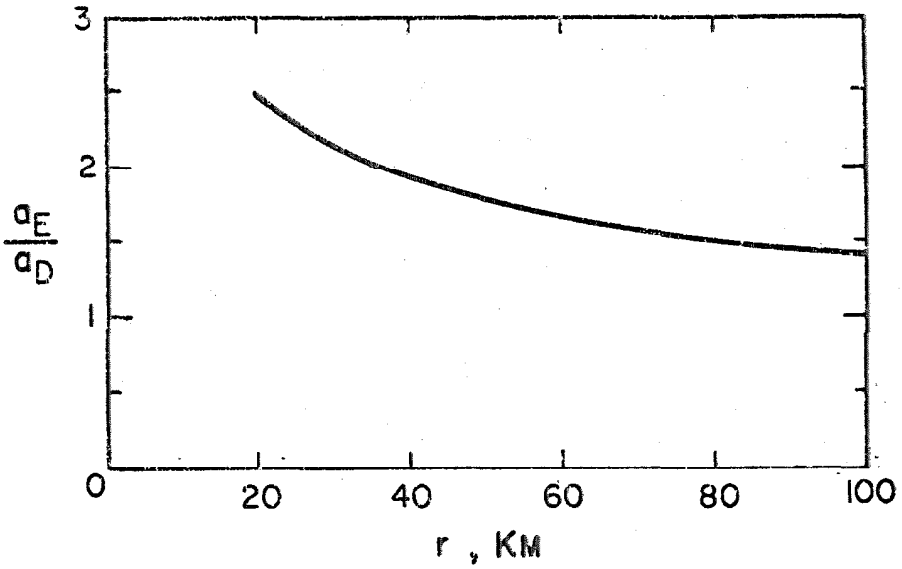

Figure 1.1. Ratio between estimates of peak ground acceleration a_E by Esteva and Rosenblueth's formula and a_D by Davenport's (1972) formula, equation (1.3). Ratio is independent of M.

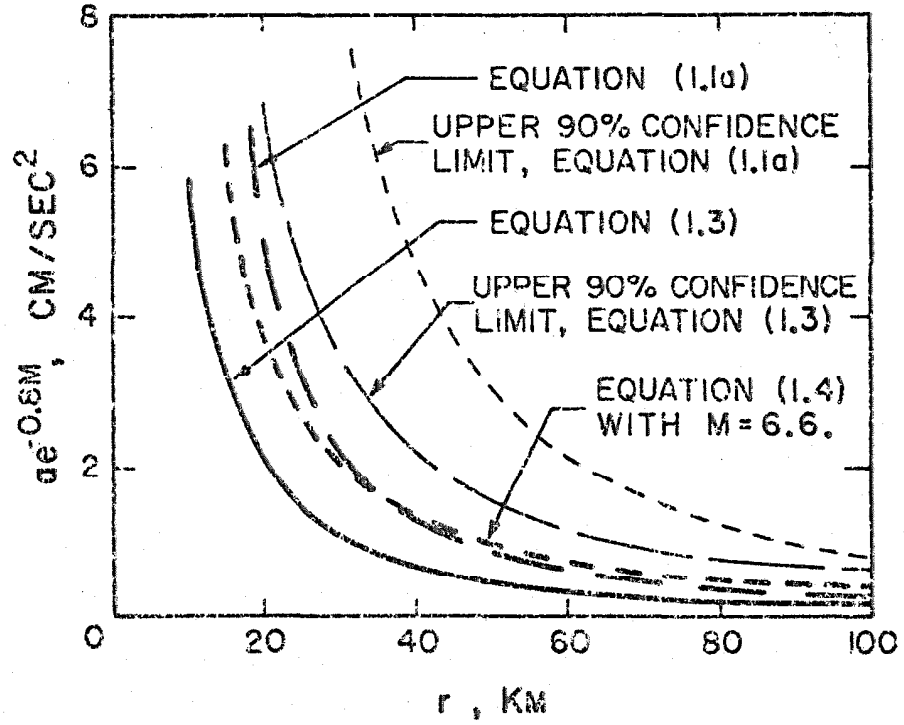

Figure 1.2. Peak accelerations normalized w.r.t. M given by Esteva and Rosenblueth's (1963) equation (1.1a) and Davenport's equation (1.3), and (for San Fernando earthquake alone) equation (1.4).

are plotted against the focal distance. The large differences between the expressions and the height of the confidence limits shows the amount of uncertainty involved.

There is a lower scatter in peak accelerations from the San Fernando earthquake alone, seen in the lower value of $\sigma_{\log_e k}$. This suggests that further factors such as the overall propagation-path geology and details of the rupture mechanism contribute significantly to the recorded ground motion. Further uncertainties may be introduced by differences in instrument response. For example the 1.1 g peak recorded at Pacoima Dam would have registered .60 to 0.7 g on the Japanese SMAC accelerograph (Hudson, 1972).

A similar correlation has been made by Donovan (1973) using a data set that includes some Japanese and South Pacific earthquakes.

There is an implicit assumption in empirical, statistical correlations such as these that the greater the number of earthquakes included in the study the better. This is not necessarily so, because more earthquakes also means more variation in the data from variables (such as hypocentral depth and rupture mechanism) not considered in the simple correlations. The correct procedure is to select the events to be included in the data set in such a way as to reduce the number of variables that should be considered. For this to be done, consideration must be given to the underlying physics of the problem. The validity of this point is illustrated by the differences in standard deviation between Davenport's study of the San Fernando data alone and that of the large group of earthquakes.

Johnson (1973) presents an empirical method for obtaining 5 percent critically damped pseudo-velocity response spectrum ordinates

S_v as functions of magnitude and epicentral distance, s. At each of 14 discrete frequencies in the band 0.4 to 11.0 Hz, he estimates the parameters C and α in the equation

$$S_v = C\,10^{\alpha M_s m} \qquad (1.6)$$

using the method of least squares. His data are taken from 23 Western United States earthquakes (in large part, those used in the correlations described above), with magnitudes between 5.3 and 7.7. Values of the attenuation exponents m, which are different for each frequency, are taken from a study of Lynch (1969) of response spectra of ground shaking due to nuclear explosions. The value of m varies from -1.14 at 0.4 Hz, generally decreasing, to -1.40 at 18 Hz. As seen from the exponents of r in equations (1.1), the variation in m again shows higher frequency components of ground motion being attenuated more rapidly with distance than the lower frequency components.

Only two San Fernando earthquake records are included in Johnson's data, so his method is not greatly biased by that event. Six examples are given in which spectra are estimated for accelerograms not included in the data set. When compared with response spectra computed from the actual accelerograms, three are in good agreement, two are underestimated over a wide frequency band by a factor of about 2 to 3, and the sixth is overestimated by about the same amount. Again, large uncertainties are associated with the predictions.

Johnson's procedure is inconsistent in putting so much detail into the frequency dependence of the resulting spectrum, while at the same time using only a single source parameter M. However, it

does take into account the frequency dependence of attenuation; and a measure of the average frequency dependence of the source emissions of earthquakes in the data set is included in the coefficients C and α. This method compares favorably with the procedure of scaling according to peak acceleration, where each frequency component is scaled equally.

1.2.1. Some shortcomings of magnitude-peak acceleration correlations

Two deficiencies in empirical ground motion investigations employing M and a to represent the source strength and site motions respectively have been noted in the previous sections: (1) Because similarity with respect to frequency components is not preserved from one earthquake to another, a single parameter is insufficient to represent either source strength or ground motion; and (2) M and a, representing different frequency bands, are not strongly correlated.

A particular shortcoming of the use of magnitude, pointed out by Housner (1965), arises from the way in which magnitude is determined. Magnitude is an arbitrary, relative instrumental measure of earthquake strength and is defined as the peak response recorded on a standard Wood-Anderson seismograph at an epicentral distance of 100 km. Since instruments situated much closer than 100 km to epicenters of large earthquakes go off-scale during the earthquake, magnitude determinations are usually made from observations at greater distances, corrected back to 100 km. Housner (1965) notes that at distances of 100 km or more, high frequency components of seismic waves have been attenuated and the peak instrument

response is most probably caused by wave components with frequencies near or below that of the instrument's natural frequency. Thus, while the natural frequency of 1.25 Hz gives the appearance that magnitude measures the center of the frequency band of general interest to engineers, in fact, due to high frequency attenuation, it actually measures lower frequency components.

Furthermore, in some cases magnitude determinations are made from 20-second period surface waves, rather than the components near 1 Hz from which local magnitude is determined. For example M = 7.7 for the 1952 Kern County earthquake, and M = 7.1 for the 1940 Imperial Valley earthquake are both surface wave magnitudes determined at teleseismic distances.

Peak ground accelerations, on the other hand, have been observed to develop generally at frequencies of 3 to 5 Hz or more (Brady and Trifunac, 1975) and, hence, depend on different components of ground motion than do magnitude estimations. Thus, the two measures are not necessarily related.

The lack of correlation between M and a has been demonstrated by Donovan (1972) who fitted an attenuation curve with the same functional form as equations (1.1a), (1.3), and (1.4) to a set of peak acceleration data from American and Japanese earthquakes. The standard deviation of the data scatter measured by $\log_e k$ was $\sigma_{\log_e k} = 0.92$. He then normalized the acceleration data with respect to magnitude by dividing each data point by the magnitude term of the attenuation curve equation, $e^{0.58M}$ The "best fit" curve was

then estimated again, and $\sigma_{\log_e k}$ was found in this case to be 0.84. Thus, normalizing the peak acceleration data to remove the influence of M resulted in a very small reduction in scatter, indicating a poor correlation between M and a.

To sum up the foregoing, magnitude alone is not a good measure of the earthquake source, both because a single parameter does not provide an adequate spectral description and also because magnitude as the parameter in particular measures mainly low-frequency wave components. Similarly, any single parameter does not adequately measure earthquake ground motion; peak acceleration, measuring high frequency components, is an especially bad choice for a ground motion parameter, since, when correlated with M, it tells little of the strength of intermediate and low frequency components which often have the greatest influence on the earthquake response of structures.

1.2.2. One-dimensional modeling of local geology.

Much attention has been given in recent years to modeling the effects of local soil conditions on incoming seismic waves by use of a simple one-dimensional shear wave model. This procedure has been applied in a wide range of situations, even though the assumptions upon which it is based are extremely restrictive. There is a growing body of evidence, reviewed by Salt (1974), that its range of validity is, in fact, much more limited than was first thought, and in almost all circumstances its use is not justified.

Several particular models have been put forward, differing in the way in which material and radiation damping are introduced, and in

whether the model is formulated for transient or for steady state excitation. All are based on the two assumptions:

(1) that the soil occurs in uniform horizontal layers whose lateral dimensions are large compared to their depth, and

(2) that the base of the soil layer system is excited uniformly in a horizontal direction.

The latter assumption requires either vertically propagating shear waves or long wavelength Love waves. (Some models will also treat vertically propagating P-waves.) The reader is referred to Tsai (1969). for examples of advanced one-dimensional models, and for a discussion of their relative merits.

In general, motion at the surface of a soil-layer system satisfying the two assumptions of this model, and in which soil stiffness increases with depth is amplified relative to the motion that would have occurred at the surface of the underlying stiffer medium in the absence of the soil layers. For linear, elastic layers, large amplifications occur near the natural frequencies of the system, with little amplification occurring between them. However, the tendency for motions to be amplified is opposed by damping, which for most soils increases with strain level and also increases with decreasing soil stiffness (Seed and Idriss, 1970). For this reason, sites which, under low levels of shaking, may exhibit the narrow band amplification predicted by the model, do not necessarily show the same behavior under strong shaking.

Practical criteria are needed for determining how closely the geometric assumptions must be met before the model can be applied,

and for what soil types, or range of soil properties, it may be used. At the present time no such rules are available.

Experimental evidence from strong ground motion observations does not resolve this problem, but it does put bounds upon it. On the one hand, there is clear evidence that amplification by a well-defined soft soil layer is the cause of narrow band spectral peaks at about 0.4 Hz in ground motion records made at Mexico City (Zeevaert, 1964). Similarly, amplification by a soft layer of younger bay mud beneath the Southern Pacific Building, San Francisco, accounts for pronounced spectral peaks near 0.9 Hz during the 1957 San Francisco earthquake (Borcherdt, 1970). On the other hand, however, there is a growing number of studies citing situations in which the type of behavior expected from the one-dimensional shear model did not occur. Some of these are noted below.

Tsai (1969) analyzed two separate shocks from the 1968 Borrego Mountain, California, earthquake, recorded at San Onofre, California at a distance of 110 km. Although the shocks were separated by about six seconds, both originated in the same area and thus both traveled essentially the same path to the recording site. Tsai could find no similarities in their spectra and hence concluded that the differences between the recorded motions were due entirely to their respective source mechanisms.

Udwadia (1972) analyzed 15 different strong motion accelerograms recorded at El Centro, California, from earthquakes occurring over a wide range of distances and directions from the recording station. He could find no recurring peaks in their Fourier amplitude

spectra. He concluded that the source mechanism and overall propagation path played the major rôles in determining the nature of ground shaking at El Centro.

Hall et al. (1973) noted that if amplification did occur according to the simple shear model, then both horizontal components of ground motion records should be affected. They searched 20 strong motion recordings (those in Part A, Volume IV of Hudson, ed., 1972) and could find no pronounced spectral peaks that were common to both horizontal components of the same record. They concluded that the one-dimensional model was adequate for predicting site effects only at exceptionally soft sites. Trifunac and Udwadia (1974) reached a similar conclusion from the study of a different group of Southern California strong motion accelerograph records.

Further insights into the complexity of the local geology problem, even with relatively simple geometric configurations, have been provided by Trifunac (1971) and Wong and Trifunac (1974). They consider the problems of semi-cylindrical and semi-elliptical sediment filled valleys in a half-space respectively, subjected to harmonic SH-wave excitation. Both the material filling the valley and the half spaces were assumed to be homogeneous, isotropic and linearly elastic. They found complicated wave interference within the valley, and a highly variable pattern of amplification along the valley surface, strongly dependent on the direction of the incoming waves. Peak amplifications of the order of 10 were found; however it is likely that lower amplifications would be observed under transient excitation (Wong and Jennings, 1975) or when damping is present in the valley

material. It is clear from these models that wave propagation in sediment-filled valleys is very complicated. In real valleys with less regular basement rock-sediment interfaces, and with inhomogeneous valley materials, more complex interference patterns can be expected. Since the direction of approach of future earthquake wave motion is not likely to be known in advance, precise deterministic computations of the effects of local geology on high frequency ground motion components when the soils and their geometric configurations are not uniform, is clearly impossible. The suggestion by Housner (1973a) that a statistical approach be taken, indeed seems to offer the only hope for estimating the effects of propagation path geology on the high frequency components of strong ground motion.

2. ATTENUATION OF STRONG GROUND MOTION FROM THE SAN FERNANDO EARTHQUAKE

In this chapter, propagation of the high frequency components of strong ground-motion from the M = 6.4, February 9, 1971, San Fernando California earthquake is studied by observing the behavior of Fourier amplitudes of acceleration computed from the horizontal components of 95 strong motion accelerograms recorded within 200 km of the epicenter. Correlations are made between the Fourier amplitudes and overall propagation path geology between the source and station, local site geology, and average source-station azimuths of groups of records in approximately the same direction from the epicenter.

Many strong motion accelerograms recorded in the United States, including those from the San Fernando earthquake, have been digitized and published by the California Institute of Technology Earthquake Engineering Research Laboratory (EERL). Each accelerogram has been assigned a reference number by the EERL, for example, C041, from the Pacoima Dam during the San Fernando earthquake. These numbers will be used throughout this text to identify both the record itself, and the recording station or site. The "C" in this example signifies that the record appears in Part C of the appropriate volume. Four volumes of data derived from the digitized accelerograms have been, or are in the process of being, prepared: Volume I, consisting of the uncorrected accelerograms; Volume II, consisting of corrected accelerograms, velocities, and displacements;

Volume III, consisting of response spectra; and Volume IV, Fourier amplitude spectra. For further details of the series as a whole, reference may be made to Hudson (1969).

In this study, use will be made of the corrected accelerograms, found in Volume II of the series, Strong Motion Earthquake Accelerograms (Hudson, et al., 1971), and of Fourier amplitudes of acceleration found in Volume IV of the series (Hudson, ed., 1972). Also some preliminary work is described which made use of peak values of ground displacement, velocity and acceleration from Volume II. Henceforth these volumes of data will be referred to simply as Volume II and Volume IV.

The ground velocities and displacements given in Volume II were obtained from the accelerations by an iterative procedure of integration and baseline adjustment. Details of the digitizing, correction and integration procedures are given in Part A of Volume II. The principal corrections are for long period errors in the digitized records and for recording instrument response characteristics. Errors in the corrected, digitized accelerograph data have been analysed by Trifunac et al. (1973) and Hanks (1973) who have concluded that the corrected records represent the ground motion faithfully in the frequency band 0.125 Hz to 25 Hz, and that for accelerograms recorded on 6 in. and 12 in. paper (about 50 percent of the San Fernando records) the lower limit may be extended to 0.07 Hz. Evidence of digitizing noise was found in the high frequency components of low amplitude records in the course of this study. It will be observed in plots of the 16 Hz Fourier amplitude data, where

digitization noise is seen to dominate the signal at epicentral distances greater than 60 km.

2.1. Preliminary study.

Before starting on the large amount of computing necessary to obtain Fourier transforms of the set of 95 accelerograms, a preliminary study of a smaller group of records was made, using computed data already available. This preliminary study brings out some essential features of strong ground motion propagation and is described below.

When peak accelerations from the San Fernando earthquake are plotted against focal distance, they show considerable amounts of scatter. (See, for example, Hudson, 1972b Figure 3.) In order to find if some of the scatter could be attributed to variations in azimuth, data recorded over a fairly small range of source-station azimuths, south-east of the epicenter,were examined. Site locations are shown in Figure 2.1.

The peak value data taken from Volume II are shown in Figure 2.2, where they are plotted against epicentral distances. By comparison with Figure 3 of Hudson (1972) it can be seen that the range of scatter of the peak accelerations in Figure 2.2 is smaller by a factor of about 0.6 than that of the complete set of San Fernando accelerograms. Thus variations with azimuth in such factors as source radiation and overall propagation path geology do appear to influence the intensity of strong ground motion.

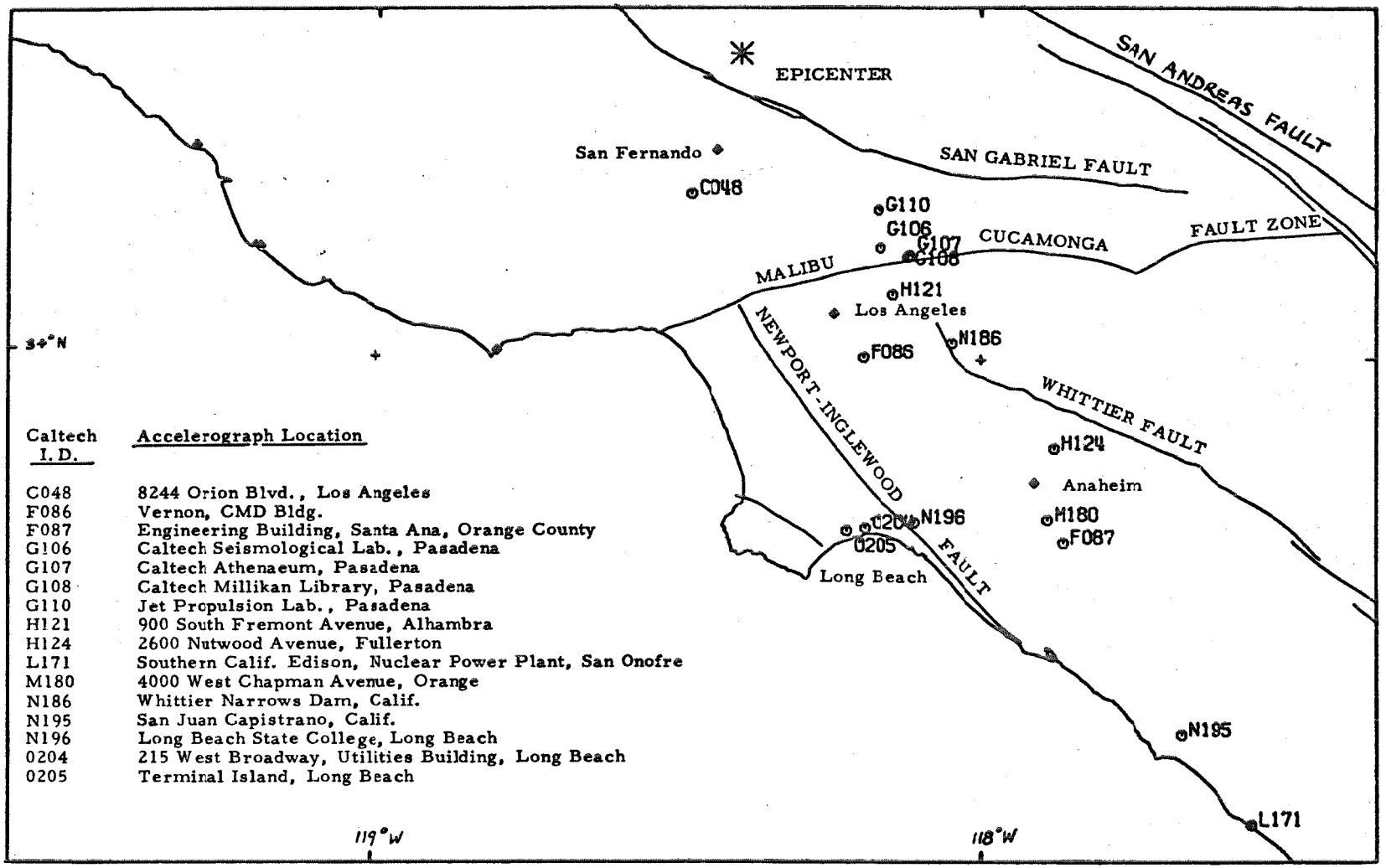

Caltech I.D.	Accelerograph Location
C048	8244 Orion Blvd., Los Angeles
F086	Vernon, CMD Bldg.
F087	Engineering Building, Santa Ana, Orange County
G106	Caltech Seismological Lab., Pasadena
G107	Caltech Athenaeum, Pasadena
G108	Caltech Millikan Library, Pasadena
G110	Jet Propulsion Lab., Pasadena
H121	900 South Fremont Avenue, Alhambra
H124	2600 Nutwood Avenue, Fullerton
L171	Southern Calif. Edison, Nuclear Power Plant, San Onofre
M180	4000 West Chapman Avenue, Orange
N186	Whittier Narrows Dam, Calif.
N195	San Juan Capistrano, Calif.
N196	Long Beach State College, Long Beach
0204	215 West Broadway, Utilities Building, Long Beach
0205	Terminal Island, Long Beach

Figure 2.1. Accelerograph stations in preliminary study.

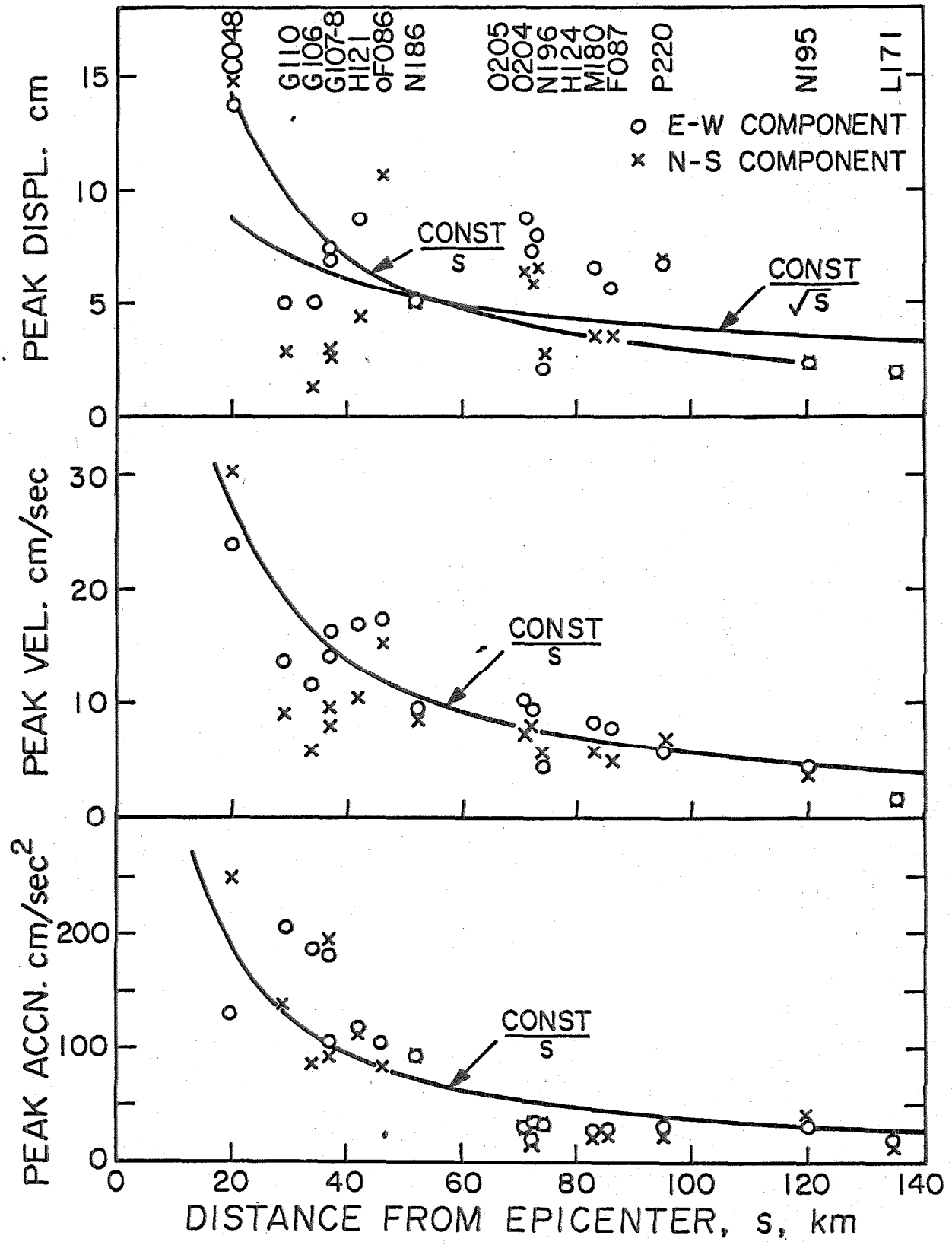

Figure 2.2. Peak ground motion values at sites shown in Figure 2.1.

It is seen from Figure 2.2 that the peak displacement data are more scattered than peak velocities, which, in turn, are more scattered than peak accelerations. This is in contrast to the data of Esteva and Rosenblueth (1963) in which peak accelerations were more scattered than peak velocities. Since their data had been normalized with respect to magnitude, this may be due to a closer relationship between magnitude and peak velocity than between magnitude and peak acceleration. However, that explains only the wider scatter seen in Esteva and Rosenblueth's peak accelerations, which were obtained from many earthquakes. It does not explain why in Figure 2.2 the acceleration peaks are less scattered than the velocity peaks, since they are obtained from the same earthquake. Furthermore they were recorded within a narrow range of azimuths, eliminating source-station direction as a variable. The principal variable remaining is local geology, in this instance referring to the upper 10 to 15 km of the crust. From an examination of the Volume II plots of acceleration, velocity and displacement—in which the peak values are marked—it is seen that acceleration peaks occur early in the accelerograms, peak displacements generally occur several seconds later, with velocity peaks occurring between the two. This suggests that the high frequency components contributing to the development of acceleration peaks (frequencies above 5 Hz; Brady and Trifunac, 1975) travel a larger proportion of their propagation paths in basement rock whereas to some extent, the middle range frequencies at which velocity peaks develop, and particularly the low frequency components developing peak displacements travel

considerable distances as surface waves in the low-velocity surface sediments. The relatively low scatter in acceleration peaks may then be attributed to their more uniform, basement-rock travel paths.

On the other hand, the anomalous appearing growth in peak displacement from sites G110 to F086 has been attributed by Hanks (1974b) to the development of surface waves. At station G110 (The Jet Propulsion Laboratory, Pasadena) which rests on a small depth of alluvium relative to the wavelengths developing displacement peaks, Hanks identified the displacement waveform as predominantly one of body wave arrivals. As the waves move out across the increasing depths of sediment in the San Gabriel Valley and Los Angeles Basin (see Figure 2.7), surface waves are seen to develop in the displacement records with increasing amplitudes until site F086, the Vernon CMD Building, is reached. At this point the Basin sediments are 20,000 feet deep (Yerkes et al., 1965) and should contribute to the formation of Love waves. Beyond Vernon, wave dispersion and geometric attenuation apparently dominate, and the displacement peaks again decay with increasing epicentral distance. The high amplitude at station C048, the Holiday Inn, 8244 Orion Boulevard, Los Angeles, can also be explained by the development of surface waves across the deep, sediment-filled San Fernando Valley (Drake and Mal, 1972).

As with the peak displacements, peak velocities increase, rather than decay, with distance from G110 to F086, but the increase is not as marked as that seen in the peak displacements. Since peak velocities are developed by higher frequency components of motion [approximately 0.3 to 3 Hz (Brady and Trifunac, 1975)] than peak

displacements, it appears that the influence of surface waves is not as strong in this mid-frequency range as it is at the lower frequencies characterizing peak displacements.

In a homogeneous, isotropic, linearly elastic, unbounded solid, except at small distances, body-wave amplitudes decay by geometric spreading in proportion to the inverse of distance from the earthquake source. Surface-wave amplitudes on a similarly idealized half space decay in proportion to the inverse of the square root of distance (see Bullen, 1963, for example). Energy absorption by the propagation medium further attenuates the amplitudes of waves travelling in real materials. This effect is referred to as material damping or material attenuation. The curves plotted in Figure 2.2 enable a comparison to be made between the observed amplitude decay and that expected in an idealized solid.

Because of the amount of scatter in the peak displacement values, it is difficult to tell whether or not they are better fitted by the curve whose ordinates are inversely proportional to epicentral distance or by that with ordinates proportional to the inverse of the square root of epicentral distance. The general trend in velocity peaks is more clearly proportional to the inverse of epicentral distance. Peak acceleration data appear to decay at a greater rate than the inverse of epicentral distance. Since peak accelerations are developed by high frequency components (≥ 5 Hz, Brady and Trifunac, 1975), this suggests the presence of some frequency-dependent material attenuation. Development of surface waves does not appear to be reflected in peak acceleration values. The high values in records

G110 and G106 are consistent with lower material attenuation expected from crystalline rock propagation paths. No definite explanation has been found for the differences in records G107 and G108, which were recorded within 1000 feet of each other on the Caltech campus. The main differences in amplitude spectra of the two records occur between 3 and 6 Hz, with Millikan Library (G108) spectra being stronger. A possible, simple explanation is that standing surface waves were formed in the soil between the Library basement and the deep basements of the adjacent buildings. Distances and wave velocities are consistent with this hypothesis.

The presence of material attenuation apparent in the peak acceleration data of Figure 2.2, was investigated further using root mean square (r.m.s.) acceleration values from the same group of accelerograms. The r.m.s. accelerations were obtained from an unpublished study of accelerogram correlation functions begun by H.-Y. Ko and R. F. Scott, and continued by the writer. R.m.s. accelerations were available from N-S, E-W, and from radial and transverse components. In order to eliminate the component orientation with respect to the source-station direction as a variable, transverse components were chosen for study rather than N-S or E-W components.

The logarithm of r.m.s. acceleration, normalized for the effect of an assumed body-wave geometric spreading (inverse of distance) are plotted against epicentral distance, s, in Figure 2.3. Although including considerable scatter, the data again show a well-defined straight-line falloff with epicentral distance, represented by the equation

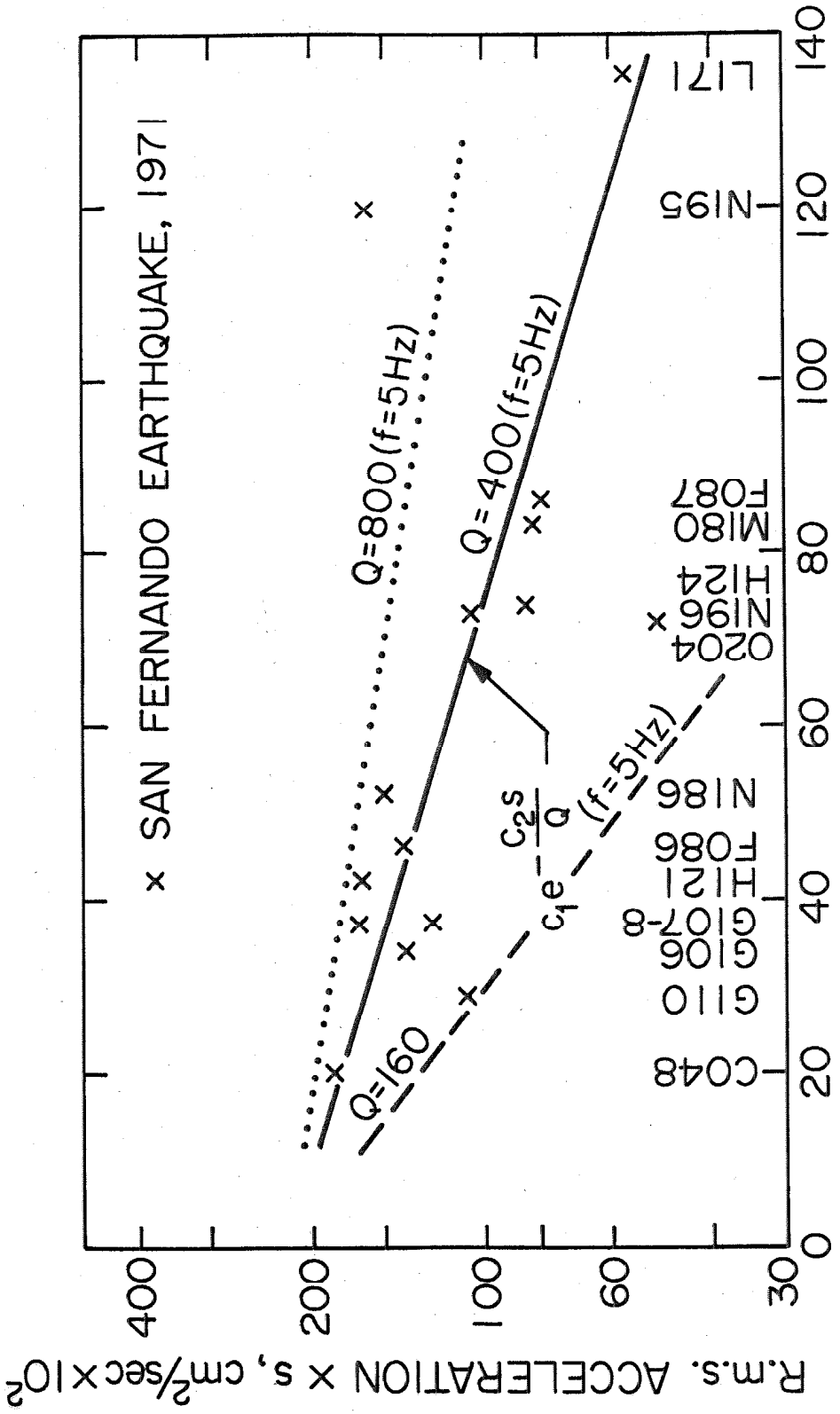

Figure 2.3. R.m.s. acceleration, normalized for effect of spherical spreading by multiplying acceleration by epicentral distance. Transverse components only.

$$\langle a \rangle s = c_1 e^{-(c_2 s/Q)} \qquad (2.2)$$

where $\langle a \rangle$ is r.m.s. acceleration and c_1 and c_2 are constants. This expression is consistent with body-wave amplitude decay expressions commonly used in seismology, where $c_2 = \pi f/\beta$ is employed, β being shear wave velocity and $1/Q$ a dimensionless constant, the specific attenuation (Knopoff, 1964).

Since the r.m.s. acceleration is a frequency-averaged quantity, it would be expected that r.m.s. accelerations are less scattered than peak accelerations. Comparing Figures 2.2 and 2.3, this is seen to be so. If it is assumed that the average frequency characterized by the r.m.s. acceleration is 5 Hz, and assuming a shear wave velocity β of 3.0 km/sec, the slope of the solid line in Figure 2.3 corresponds to a value of $Q = 400$. To show the effect of changes in the value of Q, the dotted line is drawn for a value of $Q = 800$ and the dashed line for a value of $Q = 160$ both for an assumed $f = 5$ Hz. Alternatively, for constant $Q = 400$, the dotted line corresponds to a frequency of 2.5 Hz and the dashed line to a frequency of 12.5 Hz.

The conclusions of this preliminary investigation may be summed up as follows:

1) Peak ground displacements do not show a regular pattern of attenuation with increasing epicentral distance. Their values are influenced by the development of surface waves in deep, relatively soft surficial soil layers, and they show much more scatter than peak velocities and peak accelerations. Their mean trend cannot be well described by a geometric spreading term such as the inverse of either epicentral distance or of its square root.

2) Peak ground velocities are clearly influenced by the development of surface waves but not to the same extent as peak displacement values. Surface waves do not dominate peak velocities, and with considerable scatter, their amplitude decay is proportional to the inverse of epicentral distance.

3) Peak and r. m. s. ground accelerations follow a well-defined pattern of attenuation with distance; the rate of fall-off is greater than the inverse of distance, and is consistent with an exponential material attenuation term with Q of about 400, in addition to a spherical spreading term proportional to the inverse of epicentral distance.

From this limited set of data it appears that the propagation of low frequency components of strong ground motion is dominated by generation of surface waves depending upon path geology and epicentral distance. The higher frequency components, however, which contribute to peak velocities and peak accelerations, behave in a much more regular manner, decaying steadily with distance and exhibiting less scatter; part of the scatter in these data is caused, but not dominated, by surface waves. These observations suggest that studies of strong ground motion attenuation should deal separately with the low frequency band, where surface waves are an important factor, and with the intermediate and high frequency bands, where a much more regular amplitude decay behavior is observed. The remainder of this chapter describes an empirical and much more detailed study of the amplitude decay of strong ground motion from the San Fernando earthquake, in the higher frequency band, from 0.4 to 16 Hz.

2. 2. Main study: the data set.

Of the 229 strong motion accelerograms from the San Fernando earthquake, 101 were recorded at ground level, mostly in building basements, within a radius of 200 km of the epicenter (Hudson, 1971). Of these, 95 were included in the set of corrected accelerograms published by the Earthquake Engineering Research Laboratory; the remaining six records were of very low amplitude, and were not processed to the Volume II stage. Fourier amplitudes of the horizontal components of these 95 accelerograms form the data set for this study. The recording sites, labelled by their Caltech reference numbers, are shown in Figure 2. 4 and are listed in Table 2. 1.

Two separate sets of Fourier amplitude data were derived from the set of accelerograms. One was taken directly from Volume IV which presents Fourier transforms of the corrected accelerograms given in Volume II. Details of the transform computations using the Fast Fourier Transform algorithm are given by Trifunac and Udwadia (1972) in Part A of Volume IV.

Since accelerographs are usually oriented so that the accelerogram component directions coincide with the principal axes of the building in which they are located, the horizontal accelerogram components in the Volume II data are randomly oriented with respect to the earthquake source-station direction, or azimuth. In order to eliminate component orientation as a variable, a set of rotated accelerograms was computed from the Volume II records having radial and transverse components parallel and perpendicular to the

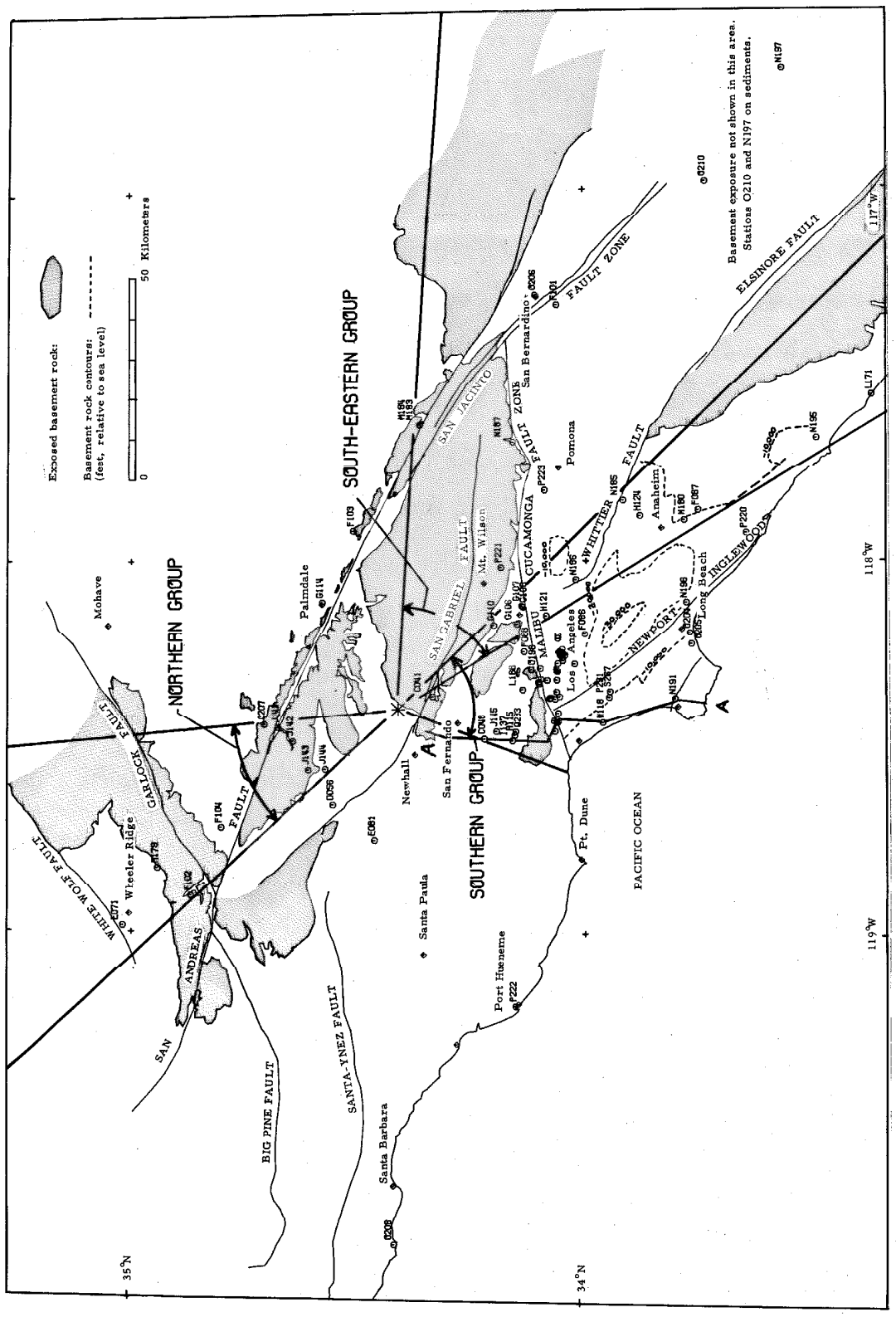

Figure 2.4. Accelerograph sites and site groupings used in study.

CALTECH REF NO.	STATION	STATION COORDINATES N	E	AZIMUTH	DISTANCE(KM)* r_e	r_h	TIME (SEC) AT S-ARRIVAL**
C041	PACOIMA DAM, CAL.	34 20 06	-118 23 48	159 36 45	9.1	15.9	1.7
C048	8244 ORION BLVD. 1ST FLOOR, LOS ANGELES, CAL.	34 13 16	-118 28 16	199 35 42	22.4	25.9	2.8
C051	250 E FIRST STREET BASEMENT, LOS ANGELES, CAL.	34 03 01	-118 14 26	159 33 03	42.8	44.7	0.0
C054	445 FIGUEROA STREET, SUB-BASEMENT, LOS ANGELES, CAL.	34 03 12	-118 15 24	161 27 22	41.9	43.9	1.8
D056	CASTAIC OLD RIDGE ROUTE, CAL.	34 33 18	-118 39 24	303 50 45	28.6	31.4	0.8
D057	HOLLYWOOD STORAGE BSMT. LOS ANGELES, CAL	34 05 00	-118 20 00	168 40 44	37.1	39.3	1.5
D058	HOLLYWOOD STORAGE P.E. LOT, LOS ANGELES, CAL.	34 05 00	-118 20 00	168 40 44	37.1	39.3	1.5
D059	1901 AVE. OF THE STARS SUBBSMT., LOS ANGELES, CAL.	34 03 14	-118 24 58	183 57 22	39.8	41.8	(-0.1)[b]
D062	1640 S. MARENGO ST. 1ST FL., LOS ANGELES, CAL.	34 03 36	-118 12 48	155 34 15	42.8	44.8	4.4
D065	3710 WILSHIRE BLVD. BASEMENT, LOS ANGELES, CAL.	34 03 42	-118 18 24	166 15 30	40.0	42.0	(-0.3)[b]
D068	7080 HOLLYWOOD BLVD. BASEMENT, LOS ANGELES, CAL.	34 06 05	-118 20 37	169 33 45	35.0	37.3	0.0[a]
E071	WHEELER RIDGE, CAL.	35 01 05	-118 59 05	321 35 31	86.0	87.0	0.0[c]
E072	4680 WILSHIRE BLVD., BASEMENT, LOS ANGELES, CAL.	34 03 41	-118 19 51	169 18 42	39.5	41.6	2.6
E075	3470 WILSHIRE BLVD., SUBBASEMENT, LOS ANGELES, CAL.	34 03 40	-118 17 58	165 54 32	40.1	42.1	1.3
E078	WATER AND POWER BUILDING, BASEMENT, LOS ANGELES, CAL.	34 03 00	-118 15 00	160 30 17	42.5	44.5	1.3[b]
E081	SANTA FELICIA DAM, CAL CUTLET WORKS	34 27 41	-118 45 02	279 45 36	32.9	35.3	(-1.9)[b]
F083	3407 6TH STREET, BASEMENT, LOS ANGELES, CAL.	34 03 45	-118 17 43	165 21 49	40.0	42.1	1.1
F086	VERNON, CMD BLDG., CAL.	34 00 00	-118 12 00	157 32 26	49.4	51.1	1.7
F087	ENGINEERING BUILDING, SANTA ANA, ORANGE COUNTY, CAL.	33 45 00	-117 52 00	145 54 30	88.5	89.4	0.0
F088	633 E BROADWAY, MUNICIPAL SERVICES BLDG, GLENDALE, CAL.	34 08 00	-118 14 50	154 53 42	34.1	36.5	1.2
F089	808 SOUTH OLIVE STREET, STREET LEVEL, LOS ANGELES, CAL.	34 02 07	-118 15 03	161 20 54	44.0	45.9	4.6
F092	2011 ZONAL AVENUE, BASEMENT, LOS ANGELES, CAL.	34 03 36	-118 12 16	154 44 33	43.1	45.0	(-0.1)[b]
F095	120 NORTH ROBERTSON BLVD., SUB-BASEMENT, LOS ANGELES, CAL.	34 04 32	-118 22 58	175 27 20	37.4	39.6	2.5
F098	646 SOUTH OLIVE AVENUE, BASEMENT, LOS ANGELES, CAL.	34 02 50	-118 15 14	161 06 21	42.7	44.6	4.9
F101	EDISON COMPANY, COLTON, CAL.	34 03 34	-117 18 45	110 56 55	107.6	108.4	1.3
F102	FT. TEJON, TEJON, CAL.	34 52 03	-118 54 09	317 44 21	68.5	69.7	0.0[c]
F103	PUMPING PLANT, PEARBLOSSOM, CAL.	34 30 30	-117 55 18	76 11 14	45.4	47.2	0.2
F104	OSO PUMPING PLANT, GORMAN, CAL.	34 48 05	-118 43 03	325 56 10	52.2	53.6	0.0[c]
F105	UCLA REACTOR LABORATORY, LOS ANGELES, CAL.	34 04 00	-118 27 00	168 16 32	38.7	40.8	2.3
G106	CALTECH SEISMOLOGICAL LAB., PASADENA, CAL.	34 08 55	-118 10 15	143 45 31	36.1	38.4	2.9
G107	CALTECH ATHENAEUM, PASADENA, CAL.	34 08 20	-118 07 17	139 26 01	39.8	41.8	5.0
G108	CALTECH MILLIKAN LIBRARY, BASEMENT, PASADENA, CAL.	34 08 12	-118 07 30	139 59 14	39.8	41.8	4.5
G110	JET PROPULSION LAB., BASEMENT, PASADENA, CAL.	34 12 01	-118 10 25	138 02 25	31.5	34.1	1.8
G112	611 WEST SIXTH STREET, BASEMENT, LOS ANGELES, CAL.	34 02 57	-118 15 16	160 53 11	42.5	44.5	2.0
G114	PALMDALE FIRE STATION, STORAGE ROOM, PALMDALE, CAL.	34 34 40	-118 06 45	55 10 15	32.3	34.8	1.1
H115	15250 VENTURA BLVD., BASEMENT, LOS ANGELES, CAL.	34 09 14	-118 27 50	193 01 52	29.3	32.1	4.1
H118	8639 LINCOLN AVE., BASEMENT, LOS ANGELES, CAL.	33 57 36	-118 25 07	183 34 29	50.2	51.9	1.0

TABLE 2.1

Listing of accelerograms in study.

CALTECH REF NO.	STATION	STATION COORDINATES N	E	AZIMUTH	DISTANCE(KM)* r_e	r_h	TIME(SEC)AT S-ARRIVAL**
H121	900 SOUTH FREMONT AVENUE, BASEMENT, ALHAMBRA, CAL.	34 05 06	-118 08 56	147 07 05	43.1	45.0	6.0
H124	2600 NUTWOOD AVENUE, BASEMENT, FULLERTON, CAL.	33 52 39	-117 52 53	140 51 30	70.2	77.3	8.8
I128	435 NORTH OAKHURST AVENUE, BASEMENT, BEVERLY HILLS, CAL.	34 04 40	-118 23 26	175 42 49	37.1	39.3	5.1
I131	450 NORTH ROXBURY DRIVE, FIRST FLOOR, BEVERLY HILLS, CAL.	34 04 07	-118 24 22	184 26 02	36.2	40.3	6.4
I134	1800 CENTURY PARK EAST, BASEMENT (P-3), LOS ANGELES, CAL.	34 03 46	-118 23 42	174 50 00	38.9	41.0	6.0
I137	15910 VENTURA BLVD., BASEMENT, LOS ANGELES, CAL.	34 09 30	-118 28 48	195 52 48	29.0	31.8	4.9
J141	LAKE HUGHES, ARRAY STATION 1, CAL.	34 40 30	-118 26 24	350 45 41	29.6	32.3	2.1
J142	LAKE HUGHES, ARRAY STATION 4, CAL.	34 38 30	-118 28 48	342 26 22	26.8	29.8	2.0
J143	LAKE HUGHES, ARRAY STATION 9, CAL.	34 36 30	-118 33 42	325 11 49	26.6	29.6	0.0
J144	LAKE HUGHES, ARRAY STATION 12, CAL.	34 34 18	-118 33 36	319 42 44	23.3	26.7	0.8
J145	15107 VANOWEN STREET, BASEMENT, LOS ANGELES, CAL.	34 11 42	-118 27 42	193 15 05	24.7	28.0	1.5
J148	616 S. NORMANDIE AVENUE, BASEMENT, LOS ANGELES, CAL.	34 03 45	-118 17 56	166 03 01	39.9	42.0	5.6
L166	3838 LANKERSHIM BLVD., BASEMENT, LOS ANGELES, CAL.	34 08 15	-118 21 39	170 51 04	30.8	33.4	1.8
L171	SOUTHERN CALIF. EDISON, NUCLEAR POWER PLANT, SAN ONOFRE, CAL.	33 22 03	-117 33 17	145 43 31	139.8	140.4	2.4[c]
M176	1150 SOUTH HILL STREET, SUB-BASEMENT, LOS ANGELES, CAL.	34 02 40	-118 15 34	161 43 44	42.9	44.8	2.5
M179	TEHACHAPI PUMPING PLANT, C.A.A. SITE, GRAPEVINE, CAL.	34 56 30	-118 49 36	326 25 04	70.7	71.9	0.0[c]
M180	4300 WEST CHAPMAN AVENUE, BASEMENT, ORANGE, CAL.	33 48 51	-117 53 33	145 58 07	84.3	85.3	1.3
M183	6074 PARK DRIVE, GROUND LEVEL, WRIGHTWOOD, CAL.	34 21 40	-117 37 58	94 19 25	70.8	72.0	6.7
M184	6074 PARK DRIVE, GROUND LEVEL, WRIGHTWOOD, CAL.	34 21 40	-117 37 58	94 19 25	70.8	72.0	4.1
N185	CARBON CANYON DAM, CAL.	33 54 52	-117 50 26	136 41 22	75.6	76.7	1.1
N186	WHITTIER NARROWS DAM, CAL.	34 01 12	-118 03 10	143 22 07	54.1	55.6	0.3
N187	SAN ANTONIO DAM, UPLAND, CAL.	34 09 26	-117 40 47	112 49 59	72.1	73.3	3.0
N188	1880 CENTURY PARK EAST, PARKING, 1ST LEVEL, LOS ANGELES, CAL.	34 03 44	-118 24 50	185 08 59	38.9	41.0	5.7
N191	2516 VIA TEJON, GROUND LEVEL, PALOS VERDES ESTATES, CAL.	33 46 02	-118 23 13	177 40 34	67.8	69.1	0.6
N192	2500 WILSHIRE BLVD., BASEMENT, LOS ANGELES, CAL.	34 03 35	-118 16 47	163 37 48	40.7	42.7	4.1
N195	SAN JUAN CAPISTRANO, CAL.	33 29 22	-117 40 14	146 22 03	122.6	123.2	9.7
N196	LONG BEACH STATE COLLEGE, GROUND LEVEL, LONG BEACH, CAL.	33 46 35	-118 06 45	159 07 03	75.4	76.5	1.4
N197	ANZA POST OFFICE, STORAGE ROOM, ANZA, CAL.	33 33 20	-116 40 25	120 16 31	185.7	186.1	8.3
0198	GRIFFITH PARK OBSERVATORY, MOON ROOM, LOS ANGELES, CAL.	34 07 06	-118 17 58	168 03 25	34.0	36.4	3.5
0199	1625 OLYMPIC BLVD., GROUND FLOOR, LOS ANGELES, CAL.	34 02 58	-118 16 26	163 10 11	42.0	43.9	6.3
0204	215 WEST BROADWAY, UTILITIES BUILDING, LONG BEACH, CAL.	33 46 10	-118 11 37	164 50 03	73.8	74.9	0.0
0205	TERMINAL ISLAND, LONG BEACH, CAL.	33 45 53	-118 13 30	167 02 33	73.6	74.8	1.8
0206	HALL OF RECORDS, SAN BERNARDINO, CAL.	34 06 20	-117 17 04	107 58 06	108.2	109.0	6.5
0207	RESERVOIR, FAIRMONT RESERVOIR, CAL.	34 42 18	-118 25 37	355 08 14	32.8	35.3	0.0[c]
0208	UNIVERSITY OF CALIFORNIA, SANTA BARBARA, CAL.	34 24 45	-119 51 00	270 26 53	133.4	134.0	2.7
0210	HOSE STORAGE ROOM, HEMET FIRE STATION, HEMET, CAL.	33 43 47	-116 58 45	119 33 56	151.4	152.0	2.2
P214	4867 SUNSET BOULEVARD, BASEMENT, LOS ANGELES, CALIFORNIA	34 05 54	-118 17 37	163 38 31	36.2	38.5	1.0

TABLE 2.1. Continued.

CALTECH REF NO.	STATION	STATION COORDINATES N	E	AZIMUTH	DISTANCE(KM)* r_e	r_h	TIME(SEC)AT S-ARRIVAL**
P217	3345 WILSHIRE BOULEVARD, BASEMENT, LOS ANGELES, CAL.	34 03 45	-118 17 43	165 21 49	40.0	42.1	1.1
P220	666 WEST 19TH STREET, GROUND FLOOR, COSTA MESA, CAL.	33 38 38	-117 55 35	152 36 54	95.8	96.7	0.0[c]
P221	SANTA ANITA RESERVOIR, ARCADIA, CAL.	34 11 06	-118 01 06	125 24 51	43.3	45.2	0.6
P222	PORT HUENEME, NAVY LABORATORY, CAL.	34 09 00	-119 12 00	248 45 09	79.3	80.3	0.5
P223	PUDDINGSTONE RESERVOIR, SAN DIMAS, CAL.	34 05 18	-117 48 48	123 20 46	65.0	66.2	2.5
P231	9841 AIRPORT BOULEVARD, BASEMENT, LOS ANGELES, CAL.	33 56 46	-118 23 09	176 33 27	51.7	53.3	0.0[c]
Q233	14724 VENTURA BOULEVARD, 1ST FLOOR, LOS ANGELES, CAL.	34 09 08	-118 27 19	191 18 47	29.3	32.1	4.9
Q236	1760 N. ORCHID AVENUE, GND FLOOR, HOLLYWOOD, CAL.	34 06 10	-118 20 20	168 51 02	34.9	37.3	4.6
Q239	9100 WILSHIRE BOULEVARD, BASEMENT, BEVERLY HILLS, CAL.	34 04 00	-118 23 22	176 10 36	36.4	40.5	4.8
Q241	800 W. FIRST STREET, 1ST FLOOR, LOS ANGELES, CAL.	34 03 26	-118 15 02	160 06 42	41.8	43.8	6.2
R244	222 FIGUEROA STREET, 1ST FLOOR, LOS ANGELES, CAL.	34 03 25	-118 15 03	160 01 51	41.9	43.8	5.2
R246	6464 SUNSET BOULEVARD, BASEMENT, LOS ANGELES, CAL.	34 05 50	-118 19 52	167 51 20	35.7	38.0	5.0
R249	1900 AVENUE OF THE STARS, BASEMENT, LOS ANGELES, CAL.	34 03 55	-118 24 56	184 40 20	39.2	41.3	5.0
R251	234 FIGUEROA STREET, BASEMENT, LOS ANGELES, CAL.	34 03 20	-118 15 25	160 52 32	41.8	43.8	2.9
R253	535 S. FREMONT AVENUE, BASEMENT, LOS ANGELES, CAL.	34 03 09	-118 15 28	161 23 20	42.0	44.0	5.9
S255	6200 WILSHIRE BOULEVARD, GROUND FLOOR, LOS ANGELES, CAL.	34 03 47	-118 21 43	173 30 56	38.9	41.0	1.0
S258	3440 UNIVERSITY AVENUE, BASEMENT, LOS ANGELES, CAL.	34 01 22	-118 16 59	163 14 34	44.6	46.5	4.8
S261	1177 BEVERLY DRIVE, BASEMENT, LOS ANGELES, CAL.	34 03 21	-118 23 43	175 21 05	39.6	41.7	0.0
S265	3411 WILSHIRE BOULEVARD, 5TH BASEMENT, LOS ANGELES, CAL.	34 03 45	-118 17 57	166 03 01	39.9	42.0	5.9
S266	3550 WILSHIRE BOULEVARD, BASEMENT, LOS ANGELES, CAL.	34 03 42	-118 18 06	165 54 15	40.0	42.1	5.6
S267	5260 CENTUARY BOULEVARD, 1ST FLOOR, LOS ANGELES, CAL.	33 56 42	-118 22 19	174 58 07	52.0	53.6	6.2

* r_e is epicentral distance; r_h is hypocentral distance.

** From beginning of accelerogram.

a Instrument triggered by S-arrival.

b Instrument triggered after S-arrival; 0.0 used in computations. Value given is inferred by comparison of ground displacement waveform with that of nearby record.

c Estimate uncertain.

TABLE 2.1. Continued.

source-station direction. To eliminate two further variables, the instrument triggering time and the record length, a 15-second length of accelerogram was taken, starting at the S-arrival. The choice of 15 seconds as the sample length was somewhat arbitrary, the main consideration being the inclusion of the duration of faulting, which has been placed at between 8 and 12 seconds (Hanks, 1974b). S-wave arrivals were read from the corrected accelerograms according to the technique described by Hanks (1974b). In a few records the S-arrival was uncertain, and the selected times have been noted as such in Table 2.1. Apart from these cases, the arrival times listed in Table 2.1 are thought to be accurate to within 0.2 seconds. As an example of a 15-second-long rotated accelerogram, the Pacoima Dam record is shown in Figure 2.5. It is interesting to note that the peak acceleration in the transverse component is 1370 cm/sec^2 (1.4g), compared with the highest peak in the original components of 1148 cm/sec^2 (1.15 g).

Fourier transforms of the 15-second accelerograms were computed by the same programs used by the EERL in the routine computations for the Volume IV series. These programs are described in detail, and listed, by Trifunac and Lee (1973). The definition of Fourier transform used throughout this work is given by the equation

$$\hat{g}(f) = \int_{-\infty}^{\infty} g(t) e^{-2\pi i f t} dt \qquad (2.3)$$

where $\hat{g}(f)$ is the transform of the function $g(t)$, $i = \sqrt{-1}$ and f is

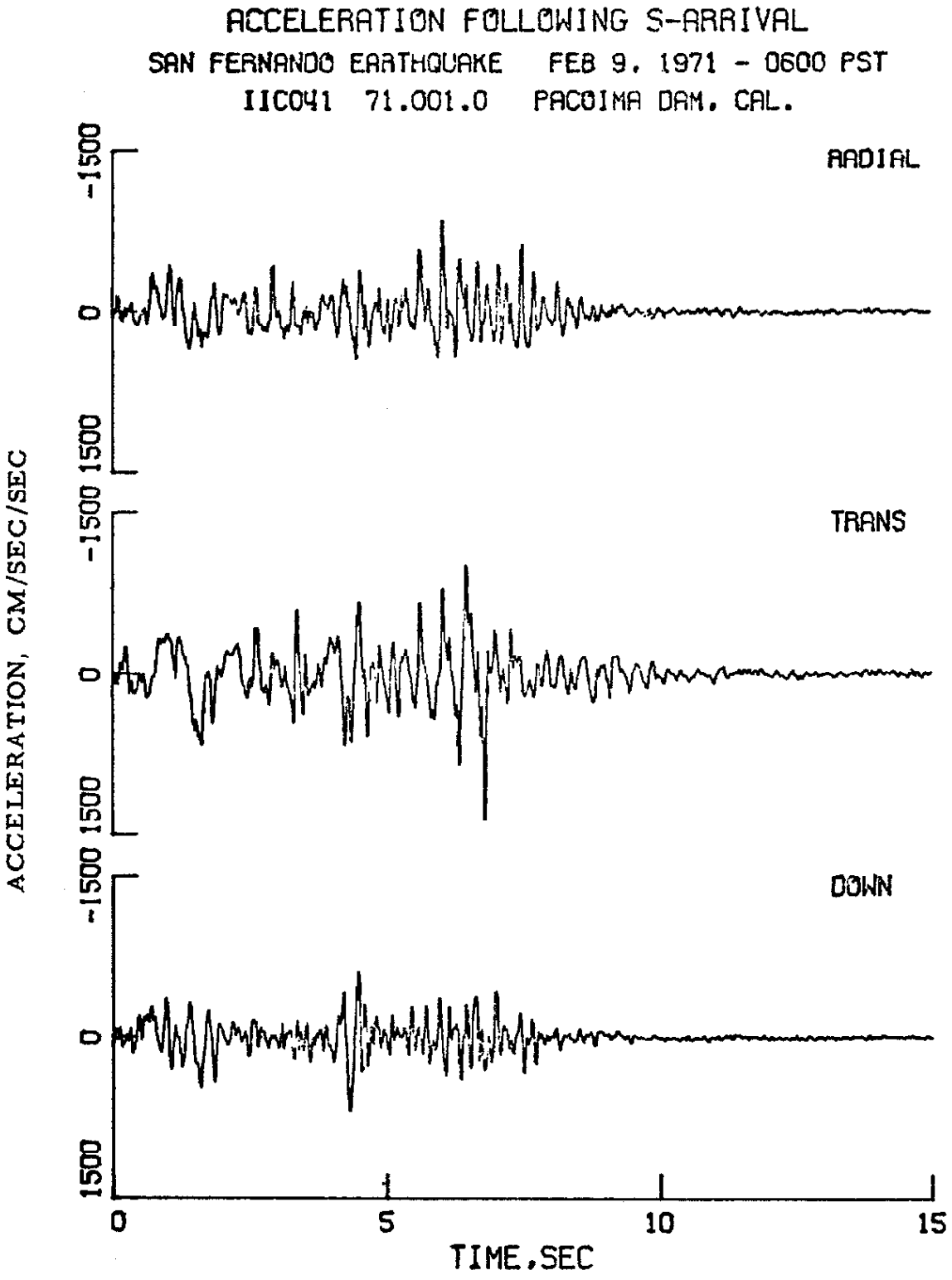

Figure 2.5. Rotated, 15-second long Pacoima Dam accelerogram.

frequency in Hertz. If $x(t)$ is an accelerogram of finite length T, such that

$$x(t) = 0 \text{ for } t < 0 \text{ and } t > T,$$

then from equation (2.3), its transform $\hat{x}(f)$, is given by the expression

$$\hat{x}(f) = \int_0^T x(t) e^{-2\pi i f t} dt \tag{2.4}$$

The computer subroutine used for numerical computation of the transform returns transform values at the discrete frequencies $n\Delta B$, $n = 0, 1, 2, \ldots, m$ where

$$\Delta B = \frac{1}{T} \tag{2.5}$$

and m is such that $m\Delta B \leq 25$ Hz.

The Fourier amplitude of acceleration $X(f)$, which is used throughout the following study, is the modulus of the complex Fourier transform, $\hat{x}(f)$. That is

$$X(f) = |\hat{x}(f)|$$

Since this chapter principally studies the decay of Fourier amplitude with hypocentral distance r, $X(f)$ will often be written with a second argument, as $X(f, r)$. To avoid the continual use of the lengthy phrase "Fourier amplitude of acceleration," "Fourier amplitude," or simply "amplitude," will be used in its place. When the time function transformed is not acceleration and this is not clear from the context, the time function will be mentioned specifically.

The Fourier amplitude spectra of the rotated, horizontal components of the Pacoima Dam accelerogram are shown in Figure 2.6.

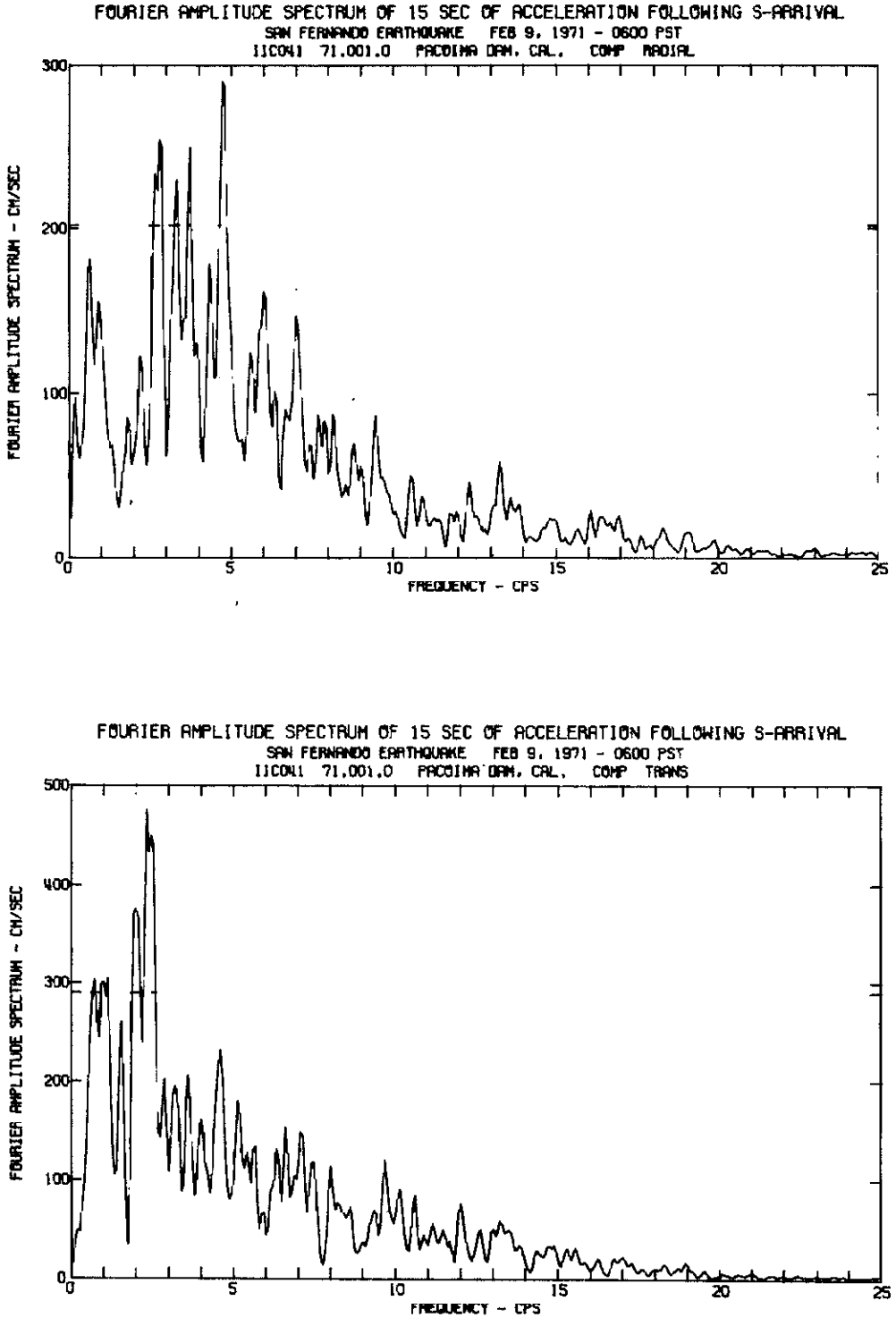

Figure 2.6. Fourier amplitude spectra of the horizontal components of the accelerogram in Figure 2.5.

2. 3. Data smoothing.

It can be seen that the Fourier amplitude spectra in Figure 2.6 consist of fairly smooth underlying functions rising to maxima between 2 and 4 Hz and then decaying with increasing frequency; superimposed upon these are apparently random, rapidly-fluctuating functions. The amplitude of the fluctuations appears to be in proportion to the amplitude of the underlying smooth function. This pattern of rapid fluctuations with frequency, superimposed on a smooth base function is observed in all Fourier amplitude spectra of earthquake ground accelerations.

An explanation for this is that the underlying shape is determined by the general features of the earthquake source and propagation path, while the rapid fluctuations result from both irregularities in the source motions, and from the inhomogeneities along the propagation path. The path inhomogeneities cause reflection, refraction and wave scattering, with the result that at any given frequency, wave components arriving by different paths, with different phase angles, interfere in a random manner, constructively at some frequencies and destructively at others. If this is indeed the explanation for the spectral fluctuations, then by the same arguments, the fluctuation should be random in space as well as in frequency.

This hypothesis suggests that the data be examined for:

(1) a simple, average attenuation behavior, that can be interpreted in terms of average behavior of crustal rocks, and

(2) a statistical description of the variation, or scatter, of individual data points about the mean behavior.

The basic data set of this study are Fourier amplitudes of accelerations sampled at six discrete frequencies: 0.4, 1.0, 2.0, 4.0, 8.0 and 16.0 Hz at 95 locations. As a measure of the average amplitude trends, smoothed samples were obtained by taking a simple unweighted average at each sampling frequency, over 2M+1 amplitude points, i.e. the central data point and M points to each side. After some experimentation, described in Appendix 1, a value of M = 5 was chosen for the 15-second records, giving the average over 11 frequency increments. From equation (2.5) it is seen that this corresponds to a resolution bandwidth, $B_e = 11/15 = 0.73$ Hz. This data set was labelled M5H15 where M5 refers to the smoothing interval discussed above, "H" implies that hypocentral distances are used in any calculations requiring source distance, and "15" refers to the 15-second sample length. In order to study the scatter, a second data set was prepared from the 15-second record amplitudes, with no smoothing. For this set, $B_e = 1/T = 0.067$. This set was labelled M0H15.

A third data set was prepared from the Volume IV Fourier amplitudes of the full-length accelerograms. After further experimentation with resolution bandwidth, it was found that smoothing over 21 amplitude data at each sampling frequency appeared to be about optimum. In this case, since T varies from record to record, M = 10 does not correspond to a constant B_e. Since most records are longer than 30 seconds, generally $B_e < 0.73$ Hz, the value for smoothing the 15-second data. This data set was labelled M10HIV.

2.4. Data groups.

In order to correlate amplitudes with transmission path geology and with source-station azimuth, three groups of sites were formed.

Most of the San Fernando earthquake data were recorded to the south of the epicenter, and the 71 sites with source-station aximuths, φ, in the range 130 to 200 degrees form the first group. These sites are shown in Figure 2.4, and are listed with amplitude data obtained from them in Tables A2.1, A2.4 and A2.5 in Appendix 2.

The general geologic features of the Los Angeles region are depicted in Figures 2.4, 2.7 and 2.8. The dominant geological features are the great depths of sediments, of up to 30,000 feet, in the Los Angeles Basin and in the San Fernando Valley. A cross-section along line A-A′ (Figure 2.4) reproduced from Duke et al. (1971), is shown in Figure 2.8. The section illustrates the complex pattern of faulting, depression and uplift of basement blocks, and highly deformed sedimentary strata. Of the 71 stations in the southern group, three are on basement rock and the remainder are on varying depths of sediments.

The second group is formed from sites north of the epicenter, with source-station azimuths in the range 310 to 360 degrees. The locations of these sites are shown in Figure 2.4. Of the 9 sites, 4 are on crystalline basement rock, one (J141) is in the San Andreas Fault zone, and the remainder are on sediments ranging in thickness from

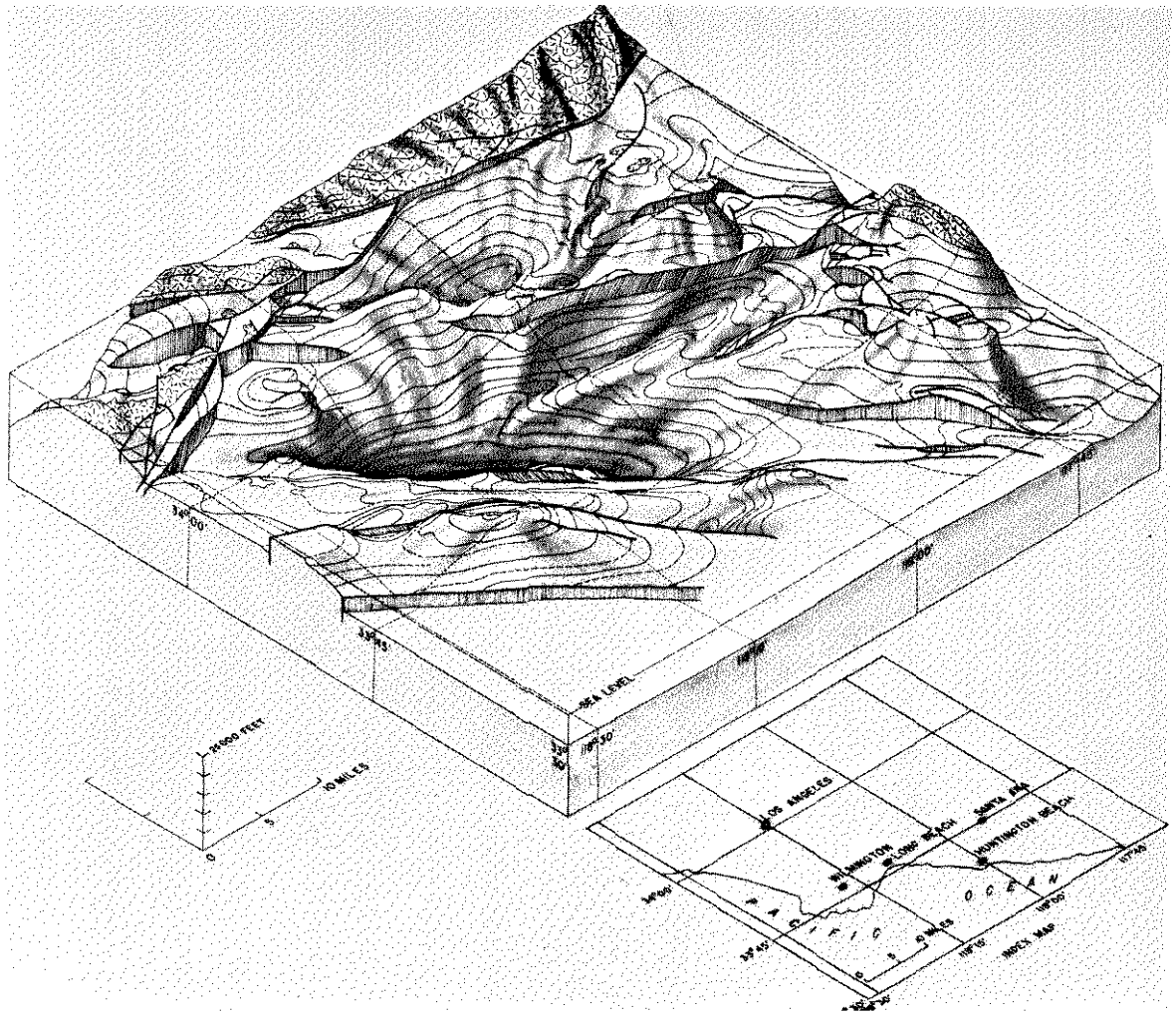

Figure 2.7. Basement rock surface in the Los Angeles Basin. Ground level of overlying sediment varies from sea level to 1000 feet (from Yerkes et. al. 1965).

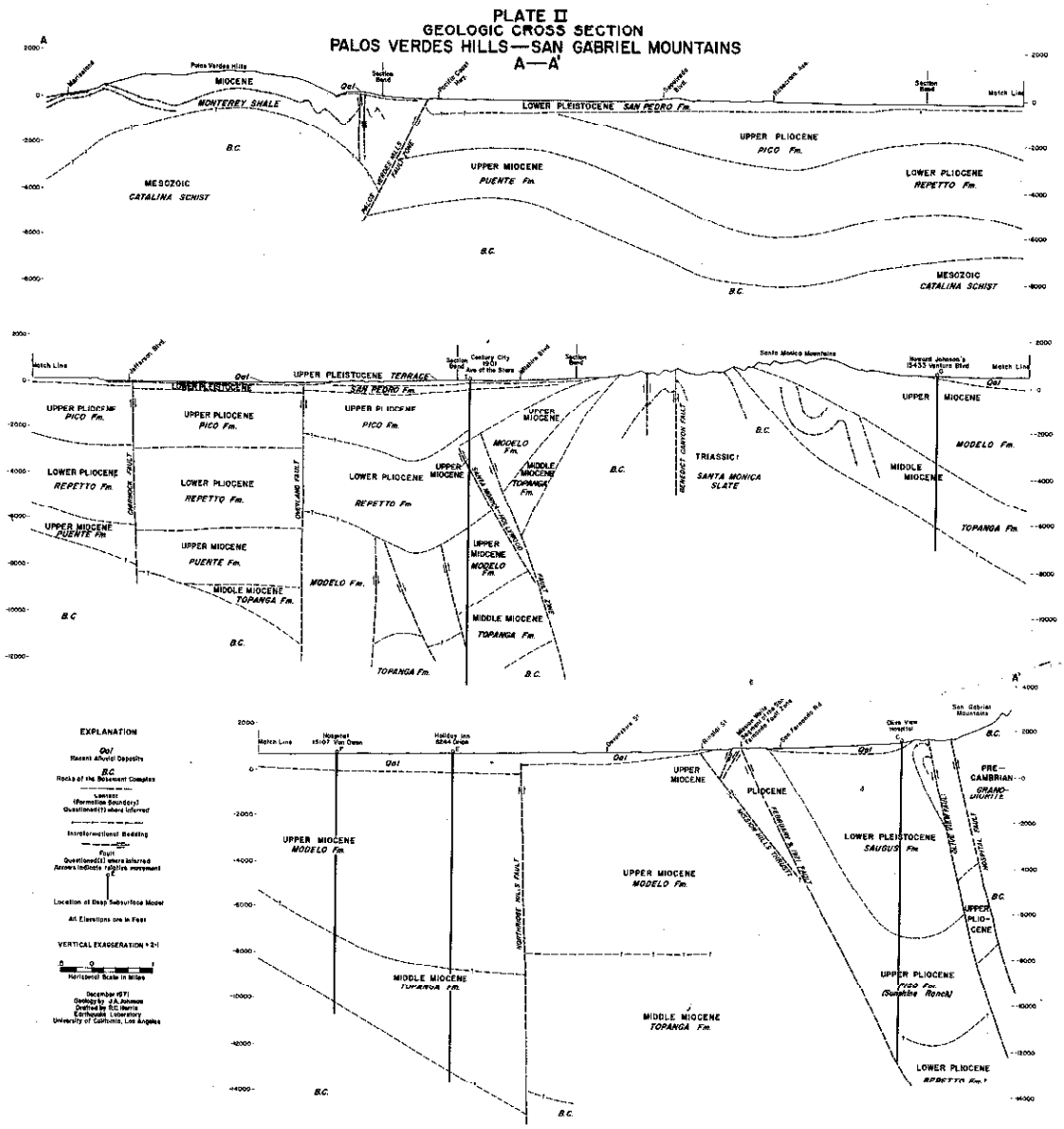

Figure 2.8. Geologic cross-section, approximately N-S, through San Fernando Valley and western side of Los Angeles Basin. Location shown by line A-A' in Figure 2.4. (Duke et. al. 1971).

15 feet (M179) to 12,000 feet (E071). The northern sites are listed in Table A2.2 of Appendix 2.

The third group is formed from sites generally to the south-east of the epicenter, with azimuths in the range of 90 to 150 degrees. Twelve sites from the southern group were also placed in this group, in order to include the basement rock sites G106. This gives a more even distribution of basement sites with distance, making a better study of attenuation along crystalline rock paths possible. These sites are listed in Table A2.3 of Appendix 2.

2.5. The southern data.

The following general observations can be made from Figures 2.9(a) through (f) showing the southern group M5H15 data plotted against r at each sampling frequency:

(1) The data, with the exception of the labelled data points discussed separately, in each figure fall within fairly well defined bands, which decrease monotonically with increasing distance.

(2) The rate of decay in amplitude increases with increasing frequency.

(3) The amount of scatter in the data is nearly constant with respect to changes in both frequency and distance.

(4) There is no consistent difference between transverse and radial amplitudes.

Viewing these data as a whole, they give the general impression of quite regular behavior even allowing for the nonuniform

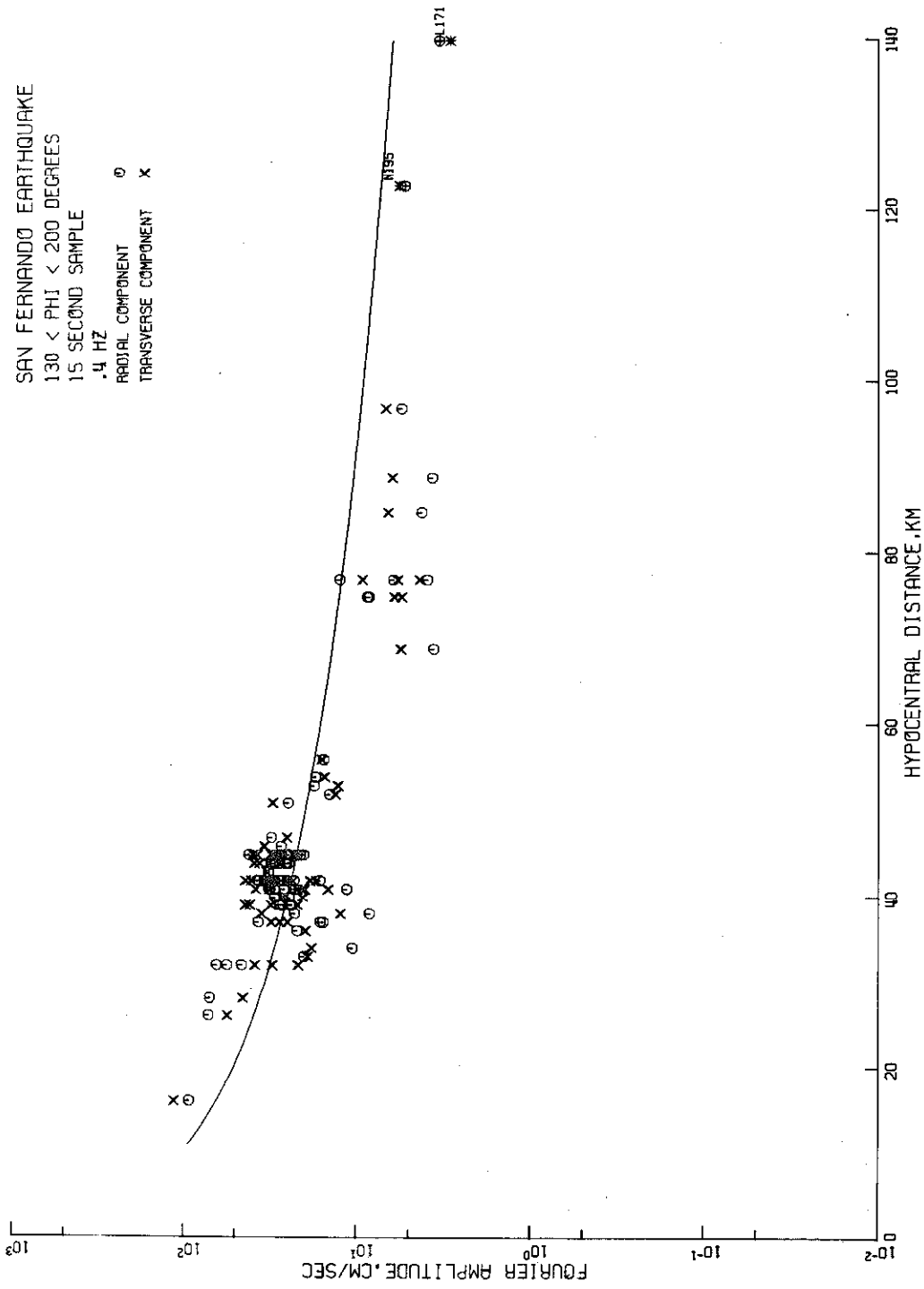

Figure 2.9(a). Fourier amplitudes of acceleration from southern, smoothed, 15-second (M5H15) data. The curve is drawn from equation (2.6) with Q = 330 and A(0.4) = 1050 cm/sec.

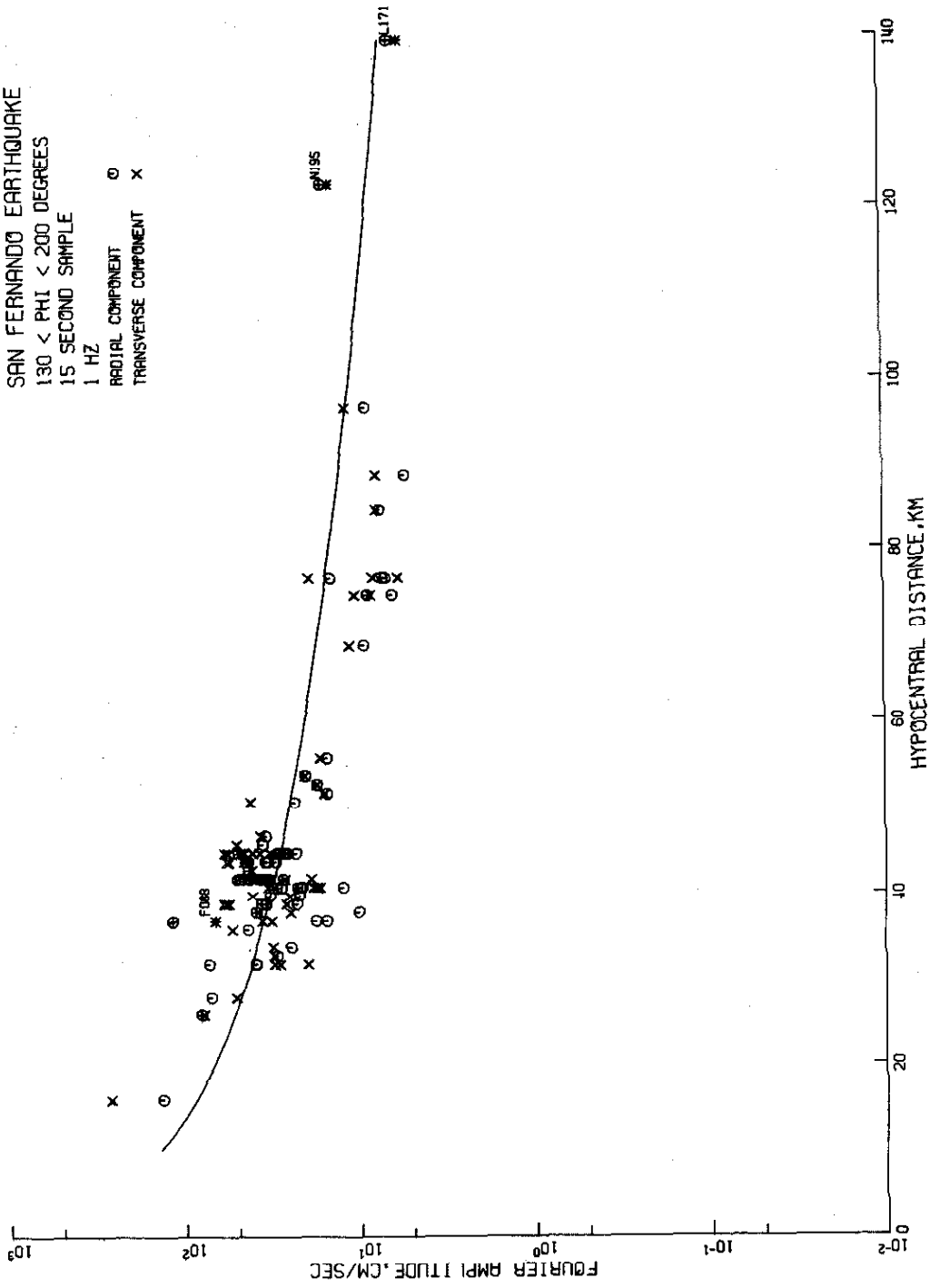

Figure 2.9(b). Q = 330, A(1) = 1440 cm/sec.

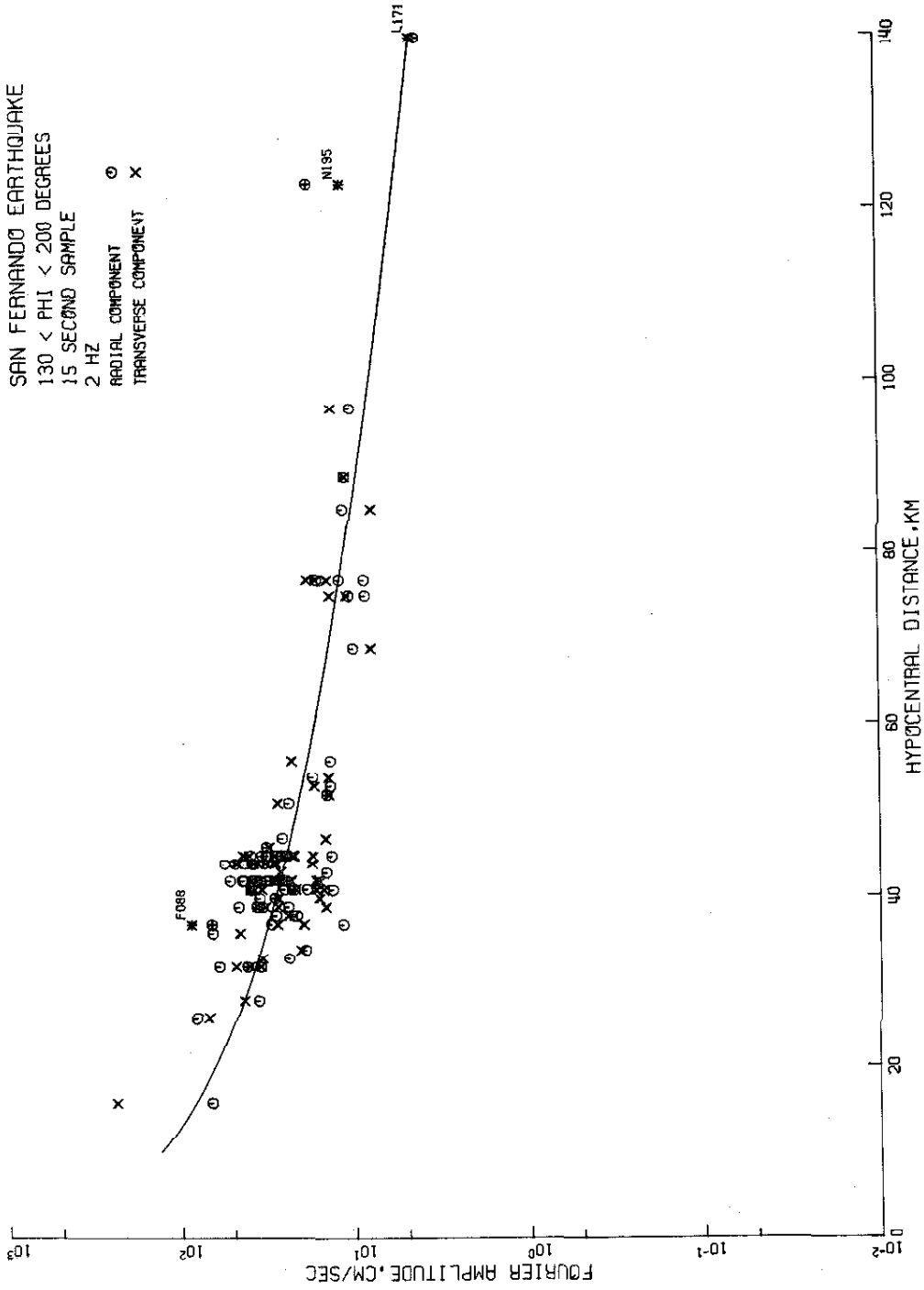

Figure 2.9(c). Q = 330, A(2) = 1490 cm/sec.

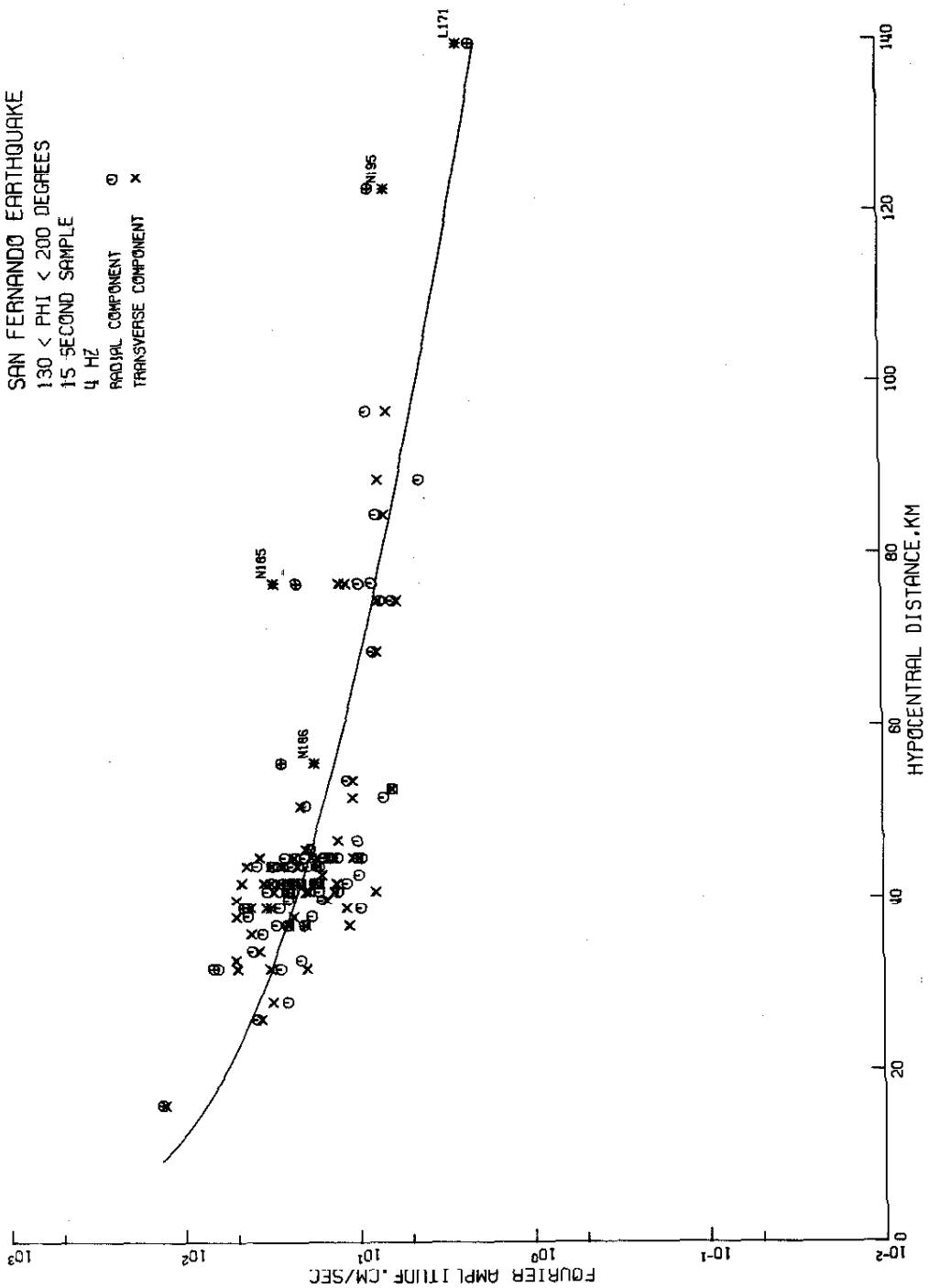

Figure 2.9(d). Q = 330, A(4) = 1440 cm/sec.

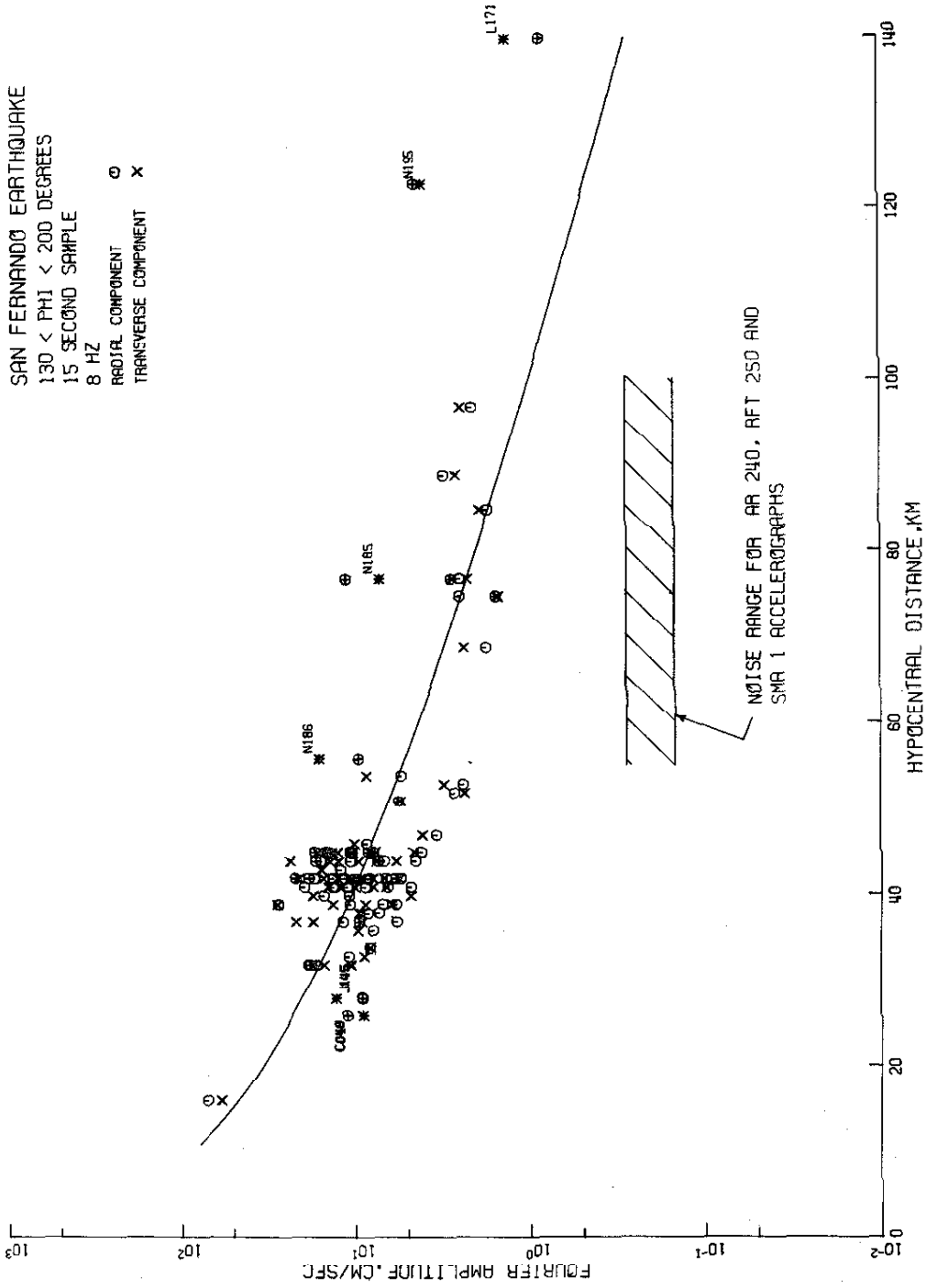

Figure 2.9(e). Q = 330, A(8) = 1100 cm/sec.

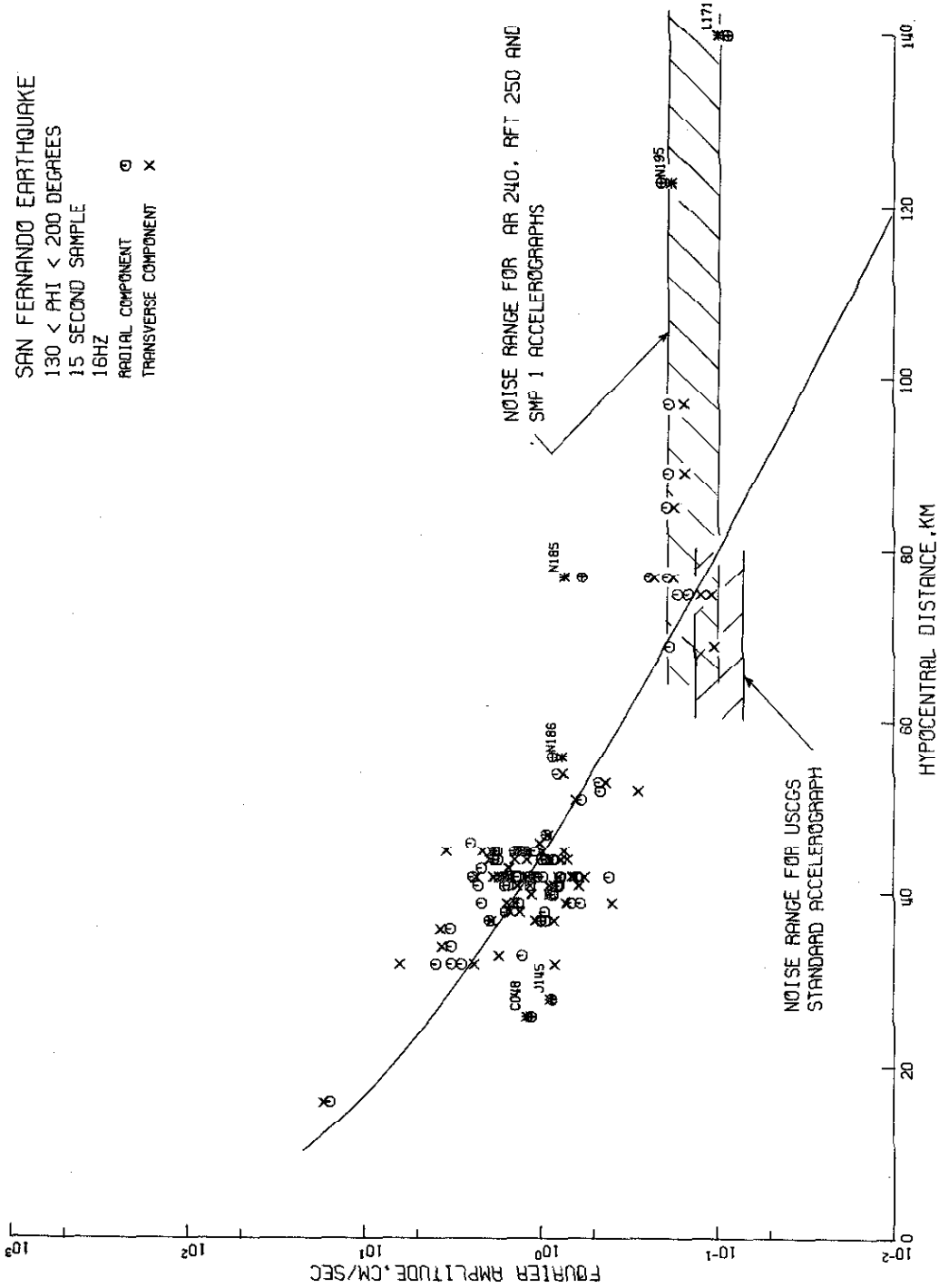

Figure 2.9(f). Q = 330, A(16) = 370 cm/sec.

distribution of recording sites with distance. The suggestions made in Section 2.3, that propagation of strong motion might be described by an underlying, simple and regular pattern of behavior, upon which is superimposed a random pattern of scatter, do seem to hold.

2.5.1. Data winnowing.

There is considerable scatter in these data, and records giving extreme amplitudes were investigated to determine if they had been modified by any extraneous processes. As a result, the points marked in the figures by a superimposed cross and labelled, e.g. N195 Figure 2.9(a), were excluded, or winnowed, from the data used in determining attenuation parameters, and in analyses of the scatter. The excluded data are listed in Table 2.2.

With the large number of data points – 852, from the six frequency samples from both components at 71 sites – removal of these 31 data has little effect on the overall trends in the data group as a whole, but it does affect the statistics of the scatter, since most of the winnowed data have extremely high amplitudes. All of the winnowing can be justified on physical grounds, except perhaps for F088, where some judgment was required.

Fourier spectra of the horizontal components of record F088, from the Glendale Municipal Services Building, are shown in Figure 2.10. The narrow band peaks between 1 to 1.5 Hz are far more pronounced than those in any other record among the 95 ground-level accelerograms studied. More typical ground level spectra, recorded at approximately the same epicentral distance, and on

TABLE 2.2.

Data winnowed from southern group

Record	Frequency	Reason
F088	1, 2 Hz	Apparently influenced by building response
N185	4, 8, 16 Hz	Instrument on crest of earth dam with fundamental frequency $f_o \approx 3.0$ Hz.
N186	8, 16 Hz	Instrument on crest of earth dam with fundamental frequency $f_o \approx 5.5$ Hz.
C048 J145	8, 16 Hz	Exceptionally high ratio of sediment to basement path caused unusually high attenuation.
F087 H124 M180 N191 N196 O124 O205 P220	16 Hz	Data at digitization noise level.
L171 N195	All frequencies	S_n-arrival dominates.

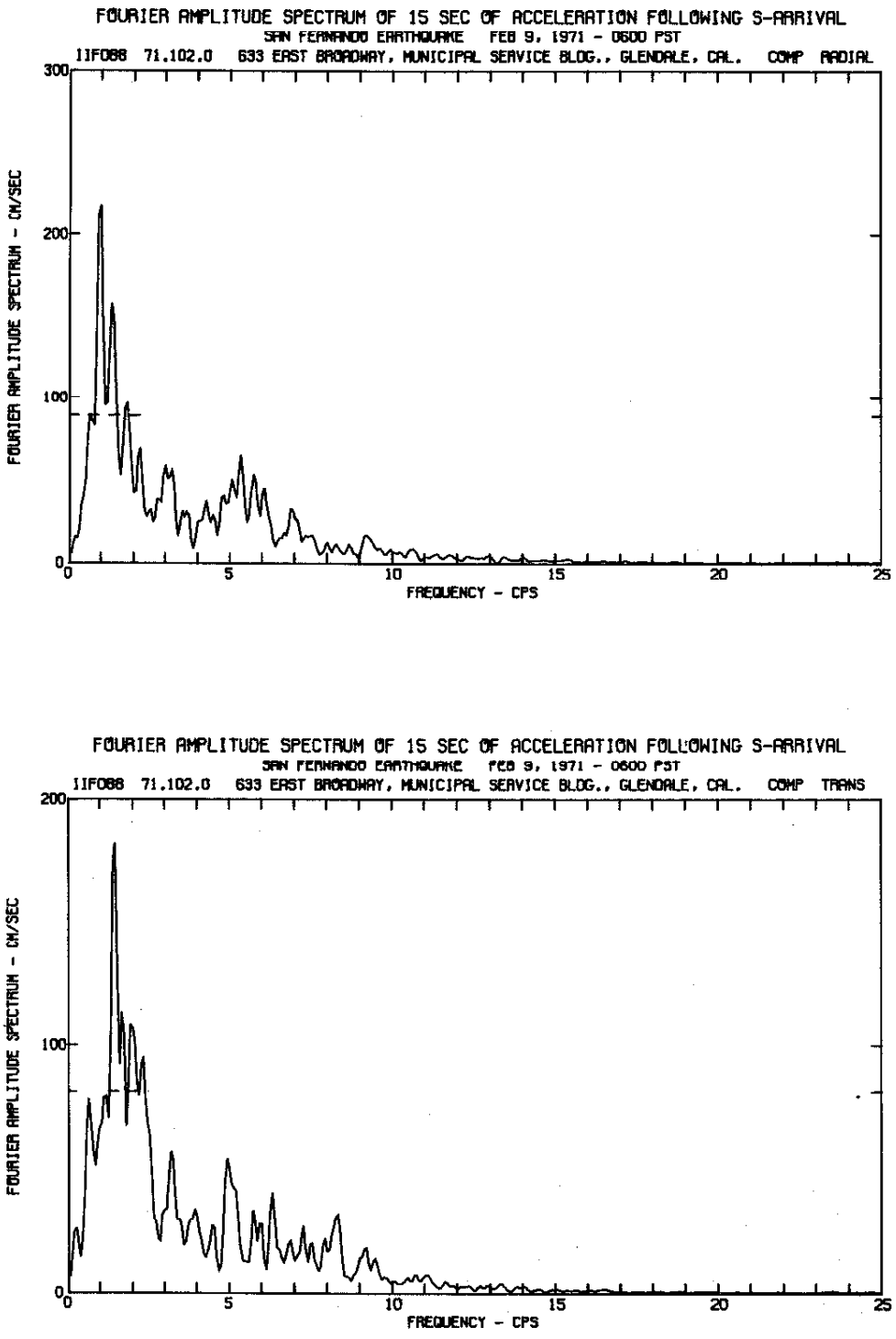

Figure 2.10. Note unusually high spectral peaks for a building basement record.

similar depths of sediment (about 4000 feet) are shown in Figure 2.11. Peaks such as those seen in the F088 spectra are more typical of records made on upper floors of tall buildings, where resonant response of the structure causes amplification or a narrow band, or bands of frequency components. A typical upper story spectrum is shown in Figure 2.12. The Glendale building has three stories in the form of an open square supported on four steel columns above an open courtyard. Thus the lateral stiffness is relatively low, and the center of gravity relatively high. Although no detailed analysis has been made, a fundamental frequency of around 1 Hz would be possible for such a structure. Soil-structure interaction is unlikely, however, in view of the flexibility of the superstructure, so that the influence of the building's own response on the recording in the basement should be minimal. A tentative explanation has been given by Lord (1974). He suggested that motion of an adjacent, massive, concrete shear-wall structure—the Public Services Building—was transmitted to the basement floor of the Municipal Services Building to which the accelerograph is fixed. Since the adjacent building has a basement which abuts on (but is not in rigid contact with) the basement in which the instrument is situated, transfer of motion is quite possible. It is Lord's opinion that resonant motion at about 1 to 2 Hz in a rocking mode would be consistent with the physical characteristics of the adjacent building. Because of the atypical appearance of the spectra, and because of Lord's explanation, it is assumed that the high spectral peaks do not have a geophysical origin, and consequently data at 1 and 2 Hz from F088 were taken out of the set.

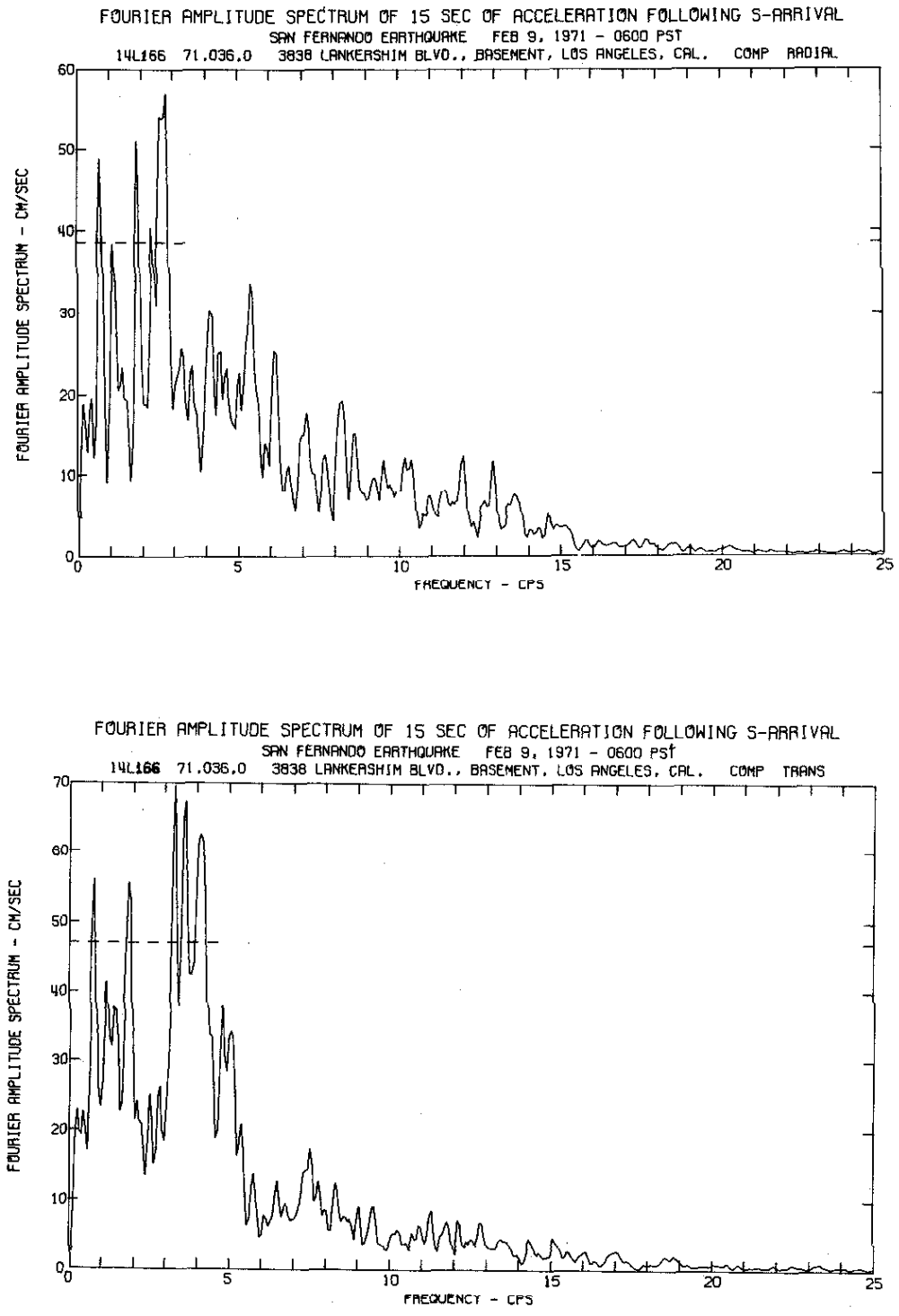

Figure 2.11. Typical ground level spectra, recorded at a similar distance and on a similar depth of sediment to F088 in Figure 2.10.

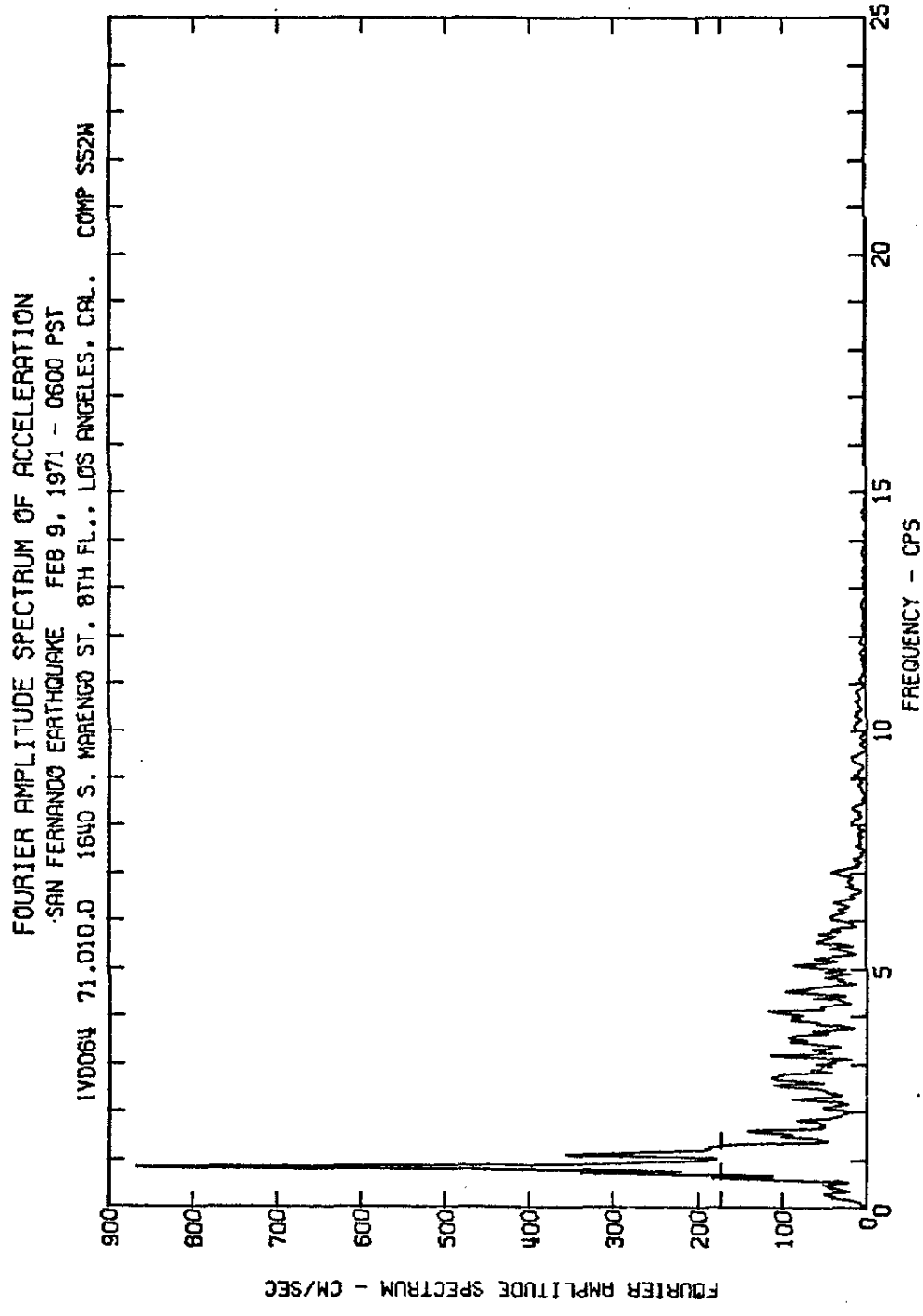

Figure 2.12. Amplitude spectrum from roof record of an 8-story, reinforced concrete building. The peak is better developed than in most roof-record spectra.

Records N185 and N186 were made on the crests of long earth dams. The Whittier Narrows Dam, N186, is 56 feet high and several thousand feet long. Using Ambraseys' (1960) shear wedge model and assuming a shear wave velocity of 800 ft/sec, the computed fundamental frequency of the dam is 5.5 Hz. As the estimate of shear wave velocity may be considerably in error, 4 Hz data and above were deleted. Similarly, the fundamental frequency of the 99 feet high, 2610 feet long, Carbon Canyon Dam, N185, was computed to be 3.1 Hz. Spectra of this record have several strong peaks at frequencies above 2.5 Hz. Data from 4 Hz and above were deleted.

At 16 Hz, and to a lesser extent at 8 Hz, the amplitude data at the two sites on deep sediments in the San Fernando Valley, C048 and J145, were well below the average trends in amplitude. The upper trace of the fault causing the San Fernando earthquake is shown in Figure 2.8. The hypocenter has been placed at between 8 and 13 km deep by various investigators (Hanks, 1974a), and therefore about one third to half of the ruptured fault is shown in Figure 2.8. Regardless of the true value of hypocentral depth, it is seen that a large part of the propagation path to these sites (C048 and J145) is through sediments. With the exception of C048 and J145, typical propagation paths for southern group sites pass through crystalline basement rock for distances of a few to many tens of kilometers, followed by a few kilometers or less through sediments. The average attenuation behavior, and the parameters estimated to describe it, reflect the response expected from mixed-geology paths where the major part

of the path is through crystalline rock. Since greater material attenuation is expected in sediments, and because this will be more marked at high frequencies, the 8 and 16 Hz data from C048 and J145 were deleted.

The sudden flattening of the amplitude data in Figure 2.9(f) at hypocentral distances greater than 60 km suggests the presence of noise. The noise ranges shown in Figure 2.9(f) have been obtained by Berrill and Hanks (1974) from the results of an experiment by Trifunac et al. (1973) who measured digitization errors in the routine data processing. It was found that the principal source of high frequency errors in the EERL digitized accelerograms was operator error in positioning the digitizing machine cross-hairs. When the results of the experiment are scaled according to the digitization rates of the 15-second accelerograms, the noise levels shown in Figures 2.9(e) and (f) are obtained. In view of the agreement between the 16 Hz data at $r > 60$ km and the experimental noise levels, it was assumed that these data were due principally to noise. Accordingly, 16 Hz data from the group of records, F087 through P220 in Table 2.2, were taken out of the set.

At hypocentral distances of between 110 km and 130 km, strong phases reflected from the Mohorovičić discontinuity have recently been observed by seismologists and in some cases,

these phases dominate the record at the time of the direct shear wave arrivals. This may account for the anomalously high values at N195 and also at L171 which fall within these distances. Accordingly, data from these sites were excluded from the set.

2.6. An amplitude decay expression.

The regular trends observed in Figure 2.9 together with the results of the preliminary study, suggested that an attempt be made to match the general trends in the amplitude data with a decay expression including a $1/r$ geometric spreading term, together with an exponential material attenuation term of the form given in equation (2.2). The curves in Figure 2.9 are drawn from the following equation incorporating these spreading and material absorption terms:

$$\overline{X}(f, r) = \frac{A(f)}{r} e^{-(\pi f r / Q\beta)} \qquad (2.6)$$

where

$\overline{X}(f, r)$ is Fourier amplitude of acceleration,

f is frequency in Hertz,

r is hypocentral distance,

$A(f)$ is a measure of source excitation strength,

$1/Q$ is the apparent specific attenuation, and

β is shear wave velocity.

Values of Q and of A(f) at the six sampling frequencies, used in drawing the curves from equation (2. 6), will be obtained from the data by a least-squares parameter estimation technique.

Except for the points at $r \geq 60$ km at 0. 4 and 1 Hz, it is seen that the curves follow the underlying trends in the data as well as they can be defined in the presence of the considerable scatter. Furthermore, the low values of the 0. 4 and 1 Hz data beyond 60 km are found to be caused by waves at these frequencies dispersing outside the 15-second sampling window. When the full-length record amplitudes are used, their average levels follow the attenuation curves well throughout the distance range.

Expressions such as equation (2. 6) are widely used in seismology (Bullen, 1963; Knopoff, 1964) to account for amplitude losses. The geometric spreading and material absorption terms are now discussed in more detail.

2. 6. 1. Geometrical attenuation.

An earthquake source, buried in an infinite homogeneous, isotropic linearly elastic solid gives rise to two sets of body waves; one set travelling outward with dilatational, or P-wave, velocity α,

the other travelling outward with shear wave or S-wave velocity β. These waves are the so-called far-field radiation of the earthquake; their amplitudes decay as $1/r$ and dominate the displacement field for distances such that

$$Kr \gg 1 \tag{2.7}$$

where $K = 2\pi f/c$ is the wave number, and c is either α or β depending on whether P or S-waves are being considered. Conversely, when $Kr \ll 1$, the near-field components of the displacement field, the "static" displacements, dominate. These amplitudes decay in proportion to $1/r^2$ (Haskell, 1964).

In our case, we are considering wave components with frequencies at or above 0.4 Hz. If we assume a shear wave velocity in crystalline rock of 3.2 km/sec, then from inequality (2.7), the $1/r$-shear wave components will govern when $r \gg 1$ km. Similarly, assuming $\alpha = 5.5$ km/sec, $r \gg 2$ km assures dominance of the $1/r$-dilatational wave components. Since at the closest recording site, the Pacoima Dam (C041), has $r = 15.9$ km, these conditions should both be satisfied, at least for the initial rupture, to which the hypocentral distance r is referred. As the rupture of the San Fernando source progressed upwards on the fault, it passed within about 4 km of the Pacoima Dam (Hanks, 1974a), and it is likely that $1/r^2$ decaying components contribute at least partially to the recorded ground motion at the dam. Furthermore, it is unlikely that in these circumstances the idealization of the rupture surface as a point source implicit in equation (2.6), is valid. In the particular case of the San Fernando earthquake, the assumption of a point source is perhaps

not unrealistic even for the Pacoima Dam, since Hanks (1974a) has found that approximately 80 percent of the energy release occurred in the immediate hypocentral region. In general, the assumption of a point source is considered valid for r greater than dimensions of the earthquake source.

Returning to the general discussion of geometric spreading, body waves reaching a free surface interact with the surface giving rise to surface waves. Since surface waves only exist close to a surface, they spread in two dimensions; hence at large distances from the source their amplitudes decay in proportion to $1/r^{\frac{1}{2}}$ (see, for example, Bullen, 1963; Tolstoy, 1973).

From the way in which the curves drawn with a $1/r$ geometric spreading term in Figures 2.9, match the trend of the data, it appears that surface waves with their much smaller rate of decay, do not make a major contribution to acceleration amplitudes at the frequencies considered.

2.6.2. Material attenuation.

Wave propagation in real media is accompanied by a dissipation of energy which cannot be explained by geometric spreading, or radiation losses alone. In solids, it is considered that the dissipation mechanism is principally frictional (Bradley and Fort, 1966) but viscous effects must also be present. Knopoff (1964) reviews the topic of material attenuation, and reports that experimental data from a large number of tests on different materials show that material dissipation in solids, including rocks, can be described mathematically

over a wide range of frequencies, by a constant specific attenuation, $1/Q$. He notes, however, that no simple rheological model has been found corresponding to constant specific attenuation.

The specific attenuation may be defined as follows. Let ΔE be the energy dissipated per cycle of oscillation in a unit volume of material, and let E denote the peak energy stored in that volume during a cycle. Then Q is defined by the relationship

$$\frac{2\pi}{Q} = \frac{\Delta E}{E} \quad . \tag{2.8}$$

That is, $1/Q$ is the ratio of energy dissipated per radian to the peak energy stored during a cycle of vibration. Let the phase angle of the motion be ϕ. Then from equation (2.8),

$$\frac{dE}{d\phi} = -\frac{1}{Q} E \quad . \tag{2.9}$$

Consider a harmonic wave with wave number κ propagating at velocity c, and with space coordinate s, then $d\phi/ds = \kappa$. Using this relationship, equation (2.9) may be integrated to obtain

$$E(s) = E_0 e^{-(\kappa s/Q)} = E_0 e^{-(2\pi f s/Qc)} \tag{2.10}$$

where E_0 is the peak energy of the wave at distance $s = 0$. Since the peak energy stored is proportional to the square of the amplitude, $a(s)$, of the motion, amplitude attenuation is given by the equation

$$a(s) = a_0 e^{-(\pi f s/Qc)} \quad , \tag{2.11}$$

where a_0 is the amplitude at distance $s = 0$.

Bradley and Fort (1966) summarize from the literature the following observed properties of material attenuation in rocks:

(1) Dissipation is less for a single crystal than for an aggregate of crystals.

(2) The rate of energy dissipation decreases with increasing pressure, suggesting that dissipation is related to the proportion of voids in the rock.

(3) On the basis of only a small amount of data, it appears that attenuation is insensitive to temperature.

(4) The limited amount of investigation on the effect of strain-amplitude on dissipation suggests that dissipation is virtually independent of amplitude for strains less than 10^{-4} (Mason, 1958).

Some idea of the shear strain dependence of dissipation in granular sediments can be obtained from Figure 10 of Seed and Idriss, (1970) which summarizes test data from several sources for sands and for mixed sands and gravels. The damping ratio, which is proportional to $1/Q$ (Knopoff, 1964), for dense sands and gravels appears to be strain-independent for strains less than about 5×10^{-3}. For looser materials (sands with a 40% relative density, for example), damping exhibits strain dependence for strains above 5×10^{-4}. Since it is improbable that rock behavior becomes nonlinear at lower strains than for soils, it is assumed that the 10^{-4} criterion for rock given in item (4) is conservative.

Since granular materials in the Los Angeles region generally are dense, a strain of 10^{-4} appears to be a good criterion for the onset of the influence of strain level on dissipation for sediments and, recalling item (4), also for crystalline basement rock.

Estimates of peak strains ϵ_{max}, during the San Fernando earthquake for eight sites with a wide range of hypocentral distances are given in Table 2.3. The peak strain values shown were computed from peak displacement data taken from the integrated displacement records in Volume II of the EERL series Strong Motion Earthquake Accelerograms (Hudson et al., 1971). In the computations, it was assumed that the displacement peaks resulted from a single harmonic wave travelling with a velocity of 3.2 km/sec in basement rock and 1 km/sec in sediments. The period of the actual displacement waveform at the peak displacement was measured between three adjacent zero crossings of the integrated displacement curves. These periods are shown in the third column of Table 2.3, and since all were close to 5 seconds, that value was used throughout the computations. At distant stations, the peak displacement occurred outside the 15-second time window following the S-arrival. In these cases, peak strain levels were computed for both the 15-second window and for the entire record. The second to last column in Table 2.3 shows the average, $\bar{d}_{max}$, of all displacement peaks occurring during the 15 seconds following the S-arrival. The last column shows the resulting strains, $\bar{\epsilon}_{max}$. Since it is unlikely that peak displacements are the result of a single harmonic wave, it is, therefore also unlikely that peak strains will occur at a single point in the medium. Hence, the strain levels given in the table, based upon this assumption, should overestimate actual values.

Alternatively, peak strain estimates may be obtained by considering them to be caused by a single travelling wave u(t, r) such that

TABLE 2.3.

Peak strain estimates at selected stations

Record	Hypocentral distance, km.	Period at d_{max}	During 15 sec. window		During complete record*		Average during 15 sec. window	
			d_{max}, cm	$\varepsilon_{max}(10^{-4})$	d_{max}, cm	$\varepsilon_{max}(10^{-4})$	$\bar{d}_{max}$, cm	$\bar{\varepsilon}_{max}(10^{-4})$
Rock Sites								
C041 (S14W)	15.9	5.5	38	1.5			22	0.9
O198 (S00W)	36.4	5.0	7.3	0.3			3.6	0.14
G106 (S90W)	38.4	5.0	5.0	0.2			3.2	0.13
N191 (S25E)	69.1	5.0	1.0	0.04	3.4	0.14	1.2	0.04
Sedimentary Sites								
C048 (N00W)	25.9	5.0	14.9	1.9			9.6	1.2
G107 (N90E)	41.8	5.5	7.3	0.9			3.5	0.4
O204 (N00E)	74.9	5.0	5.0	0.6	5.8	0.7	3.5	0.4
F087 (S86W)	89.4	5.5	4.0	0.5	5.7	0.7	2.7	0.3

*Shown only where different from values in the 15 second window.

$$u(t, r) = g(r-ct) \qquad (2.12)$$

where c is wave velocity. Peak strain, ϵ_{max}, may be obtained by differentiation as follows:

$$\epsilon_{max} = \left|\frac{\partial u}{\partial r}\right|_{max} = \frac{1}{2}\left|\frac{\partial u}{\partial t}\right|_{max} = \frac{v}{c}$$

where v is again peak ground velocity. Taking values of peak ground velocity from the Volume II series and using the same wave velocities as in Table 2.3, peak strains of about twice the values given in the table are obtained. For example, $\epsilon_{max} = 3\times10^{-4}$, 3×10^{-4} and 1.4×10^{-4} are obtained for sites C041, C048 and G107 respectively.

Except at the two closest stations, Pacoima Dam (C041) on crystalline basement rock and the Holiday Inn (C048) on deep sediments, the computed strains are below the 10^{-4} criterion. Thus the effects of material nonlinearity should be confined to the immediate focal region, and comparisons in the majority of the data should be unaffected by material nonlinearity. It is seen in Figures 2.9(e) and (f) that the amplitudes at 8 and 16 Hz are relatively low at the two sites, C048 and J145, on the deep sediments of the San Fernando Valley within 25 km of the epicenter. This may be due to higher specific attenuation (lower Q) due to material nonlinearity, or it may simply be caused by the greater than usual ratio of sedimentary path length to basement rock path length, with the sediments and basement having different, but constant Q's. The latter cause was assumed in excluding the data at these frequencies.

However even these data (C048 and J145) show no extreme departures from the behavior of the data set as a whole. From this

observation, and from the computed strain levels, it can be concluded that while material nonlinearity may be very important close to the focus, at hypocentral distances of 20 km or more it does not appear to be a major factor.

2.6.3. Least-squares estimation of parameters.

Let X_{ij} denote an observed Fourier amplitude value at frequency f_i and hypocentral distance r_j, taken from the data set. Let $\overline{X}(f_i, r_j)$ denote the corresponding value predicted by equation (2.6). As in Chapter 1, let the uncertainty factor k be defined by

$$k_{ij} = \frac{X_{ij}}{\overline{X}(f_i, r_j)} \tag{2.13}$$

The pattern of scatter in the semi-log plots in Figures 2.9 together with Davenport's (1972) observation that the scatter in peak acceleration data has a lognormal distribution, suggests that the distribution of $\log_e k$ for this data may also be approximately Gaussian. In that case, the best estimate of the parameter Q and the values of A(f) at the six discrete sampling frequencies in equation (2.6) will be those which minimize

$$\Phi = \sum_{i=1}^{6} \sum_{j=1}^{n} (\log_e k_{ij})^2 \tag{2.14}$$

over the data set (Tukey, 1965), where 6n is the number of data. In effect, this minimization scheme puts equal weight on each data point. Since clearly anomalous data have been winnowed, and because the

scatter appears fairly constant with respect to variations in distance and frequency, equal weighting of data is a reasonable practice. Substituting from equations (2.6) and (2.13) into equation (2.14), we get

$$\Phi = \sum_{i=1}^{6} \sum_{j=1}^{n} [\log_e X_{ij} - \log_e \overline{X}(f_i, r_j)]^2$$

$$= \sum_{i=1}^{6} \sum_{j=1}^{n} \left[\log_e X_{ij} - \left(\log_e A_i - \log_e r_j - \frac{\pi f_i r_j}{Q\beta}\right)\right]^2 \qquad (2.15)$$

where $A_i = A(f_i)$ and f_i takes the values: 0.4, 1, 2, 4, 8 and 16 Hz for $i = 1, 2, \ldots, 6$ respectively. The values of Q and A_i to minimize Φ for the various data sets were found using a standard least squares technique.

2.7. Attenuation parameters for southern data.

In this section an empirical description of the average amplitude attenuation is obtained by estimating the parameters which "best fit" the relationship of equation (2.6) to the southern group data. Statistics of the scatter about this average will be examined. Estimates of the source strength function A(f) will also be obtained from the parameter estimation procedure, and will be discussed separately in Chapter 3.

2.7.1. Average attenuation.

Using the method described in Section 2.6.3, the values of Q and A_i shown in Table 2.4 were obtained for M5H15 data from the southern sites. A value for shear wave velocity β of 3.2 km/sec has

TABLE 2.4.

Attenuation parameter estimates, M5H15 data, southern group.

Parameter	Value	90% confidence interval
Q	330	310-360
A_1**	1050 cm/sec	910-1200 cm/sec
A_2	1440	1240- -*
A_3	1490	1280-1700
A_4	1440	1230-1630
A_5	1100	920-1230
A_6	370	300-410

*None found.

**The subscripts 1, 2, ...,6 refer to the frequencies 0.4, 1, 2, 4, 8 and 16 Hz respectively.

been assumed. The method of confidence interval computation is described by Marquardt (1964). The curves shown in Figures 2.9 result from the substitution of these values into equation (2.6)

It has already been noted that, particularly at high frequencies, the curves fit the trend of the data closely. It would be difficult to improve on the fit at frequencies of 2 Hz and above, either by free-hand sketching or by using a higher order attenuation expression, and further complexity would not be justified by the amount of scatter.

Agreement between the 1Hz data (Figure 2.9(b)) and the curve is not as good as at higher frequencies. At this frequency, data recorded at hypocentral distances beyond 60 km is generally overestimated by about a factor of two. But these discrepancies are still within the general pattern of scatter.

At 0.4 Hz (Figure 2.9(a)) the differences between data and curve are more pronounced. An explanation may be found in the dispersion of waves outside the 15-second window. This supposition is supported by observing that Fourier amplitudes from sites beyond 60 km computed from the full-length records do not fall below the attenuation curves as we see here. This is seen in Section 2.7.7. Since simple surface wave dispersion leads to a retardation of the high frequency components, and not the low frequency components (Bolt, 1970a), surface wave dispersion by itself is not the mechanism that is seen in Figure 2.9(a) and 2.9(b). However, the presence of surface waves at low frequencies only is consistent with the observations here, since, because of their lower velocities in general and particularly in sediments, they will arrive later than body waves.

2.7.2. Scatter in the smoothed data.

The uncertainty factor k, defined by equation (2.13), is used as a measure of scatter. Histograms showing the frequency distribution (using "frequency" in the statistical sense) of k at each sampling frequency for the smoothed data of the southern group are given in Figure 2.13. The arithmetic mean $\bar{k}$, standard deviation σ_k and third moment m_k for each sampling frequency are given in Table 2.5. They are based on the attenuation parameters given in Table 2.4. The shapes of the distributions are fairly constant, but the 8 and 16 Hz data show a slightly wider spread about their mean values, which in each case are approximately unity.

It is seen in Table 2.5 that $\bar{k}$ is not equal to unity. The reason for this is found in the least-squares estimation of the attenuation curves obtained by the minimization of $\Sigma(\log k)^2$. This results in the average value of log k tending to zero, which is equivalent to the geometric mean k_G, of k tending to unity. Since from the properties of mean values, $\bar{k} \geq k_G$, with equality only if all k's are equal, values of $\bar{k}$ greater than one are expected.

It was noted earlier that higher-frequency components of seismic waves should be more susceptible to wave scattering by virtue of their shorter wavelengths, and that this was expected to be one of the causes of scatter in Fourier amplitude data. In view of the forty-fold increase in frequency from 0.4 to 16 Hz, the increased spread in the distributions of k at higher frequencies is remarkably small.

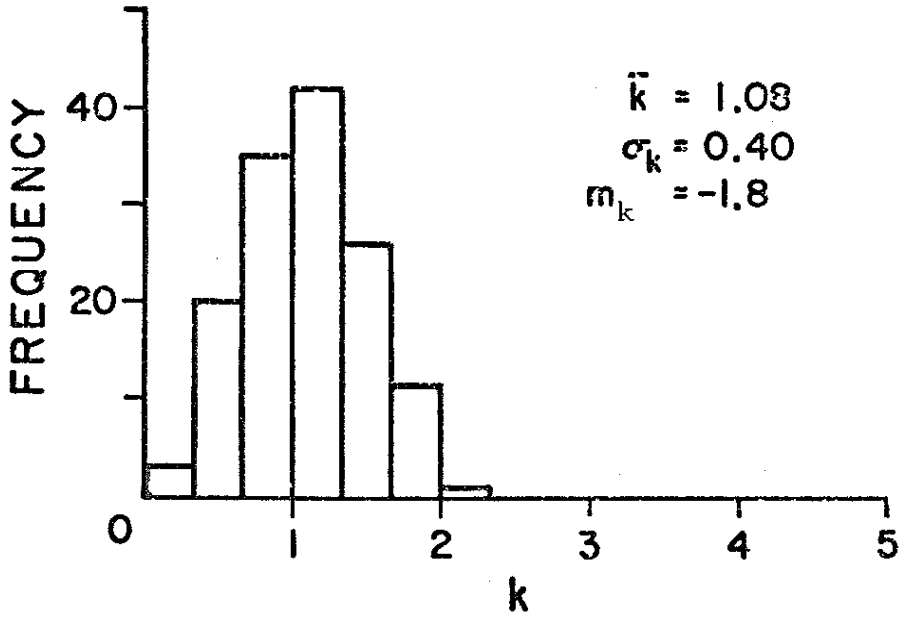

(a) 0.4 Hz

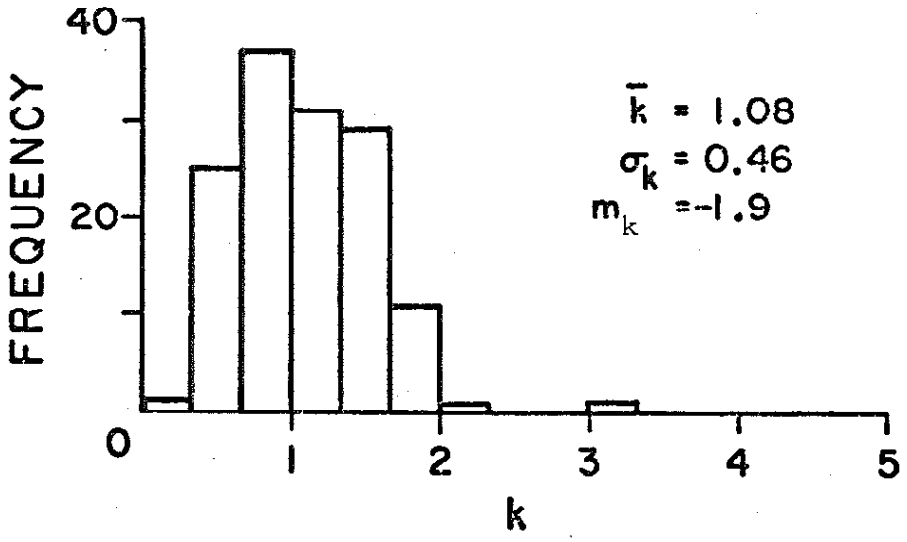

(b) 1 Hz

Figure 2.13. Scatter in southern M5H15 data shown by distribution of k.

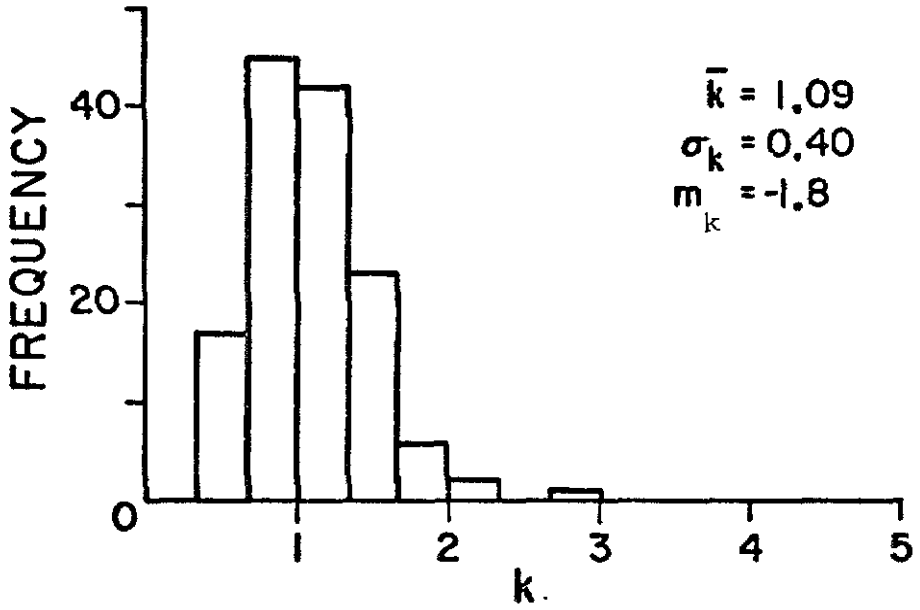

(c) 2.0 Hz

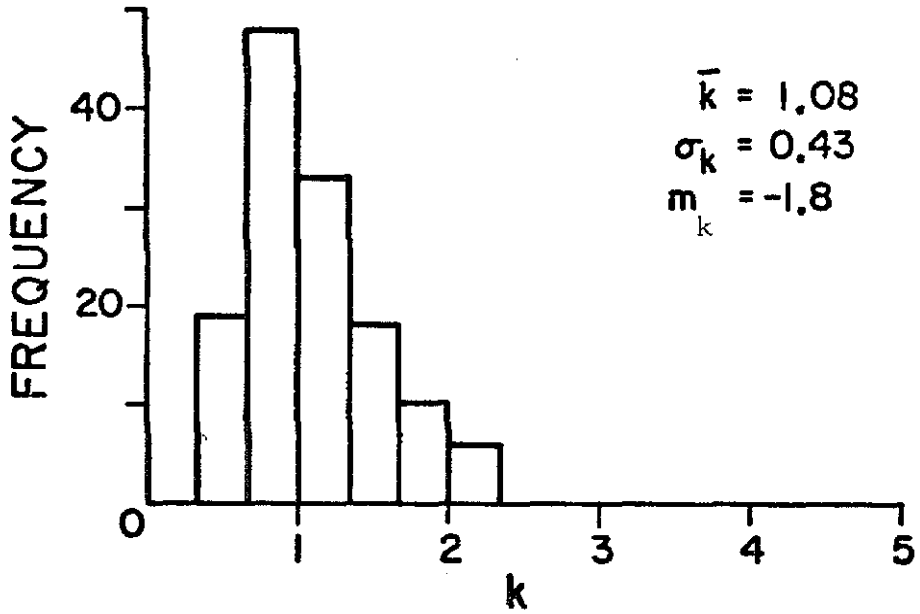

(d) 4.0 Hz

Figure 2.13. Continued.

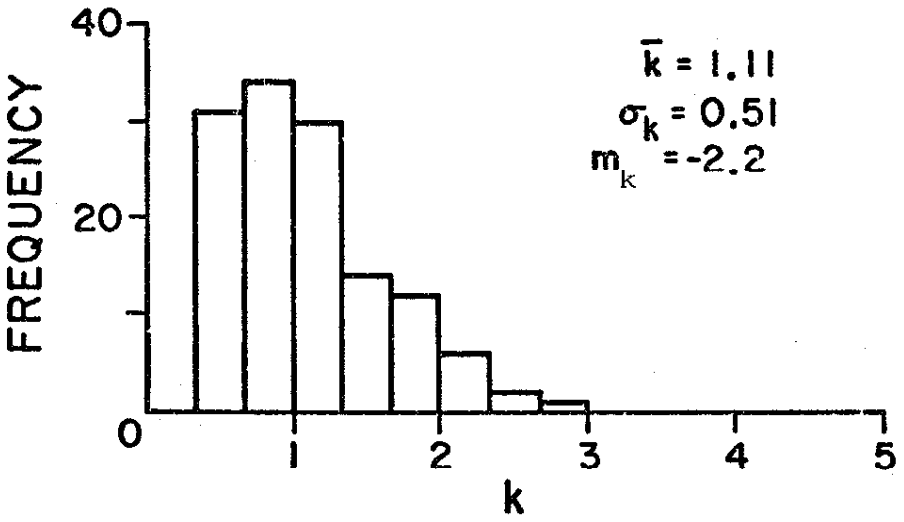

(e) 8.0 Hz

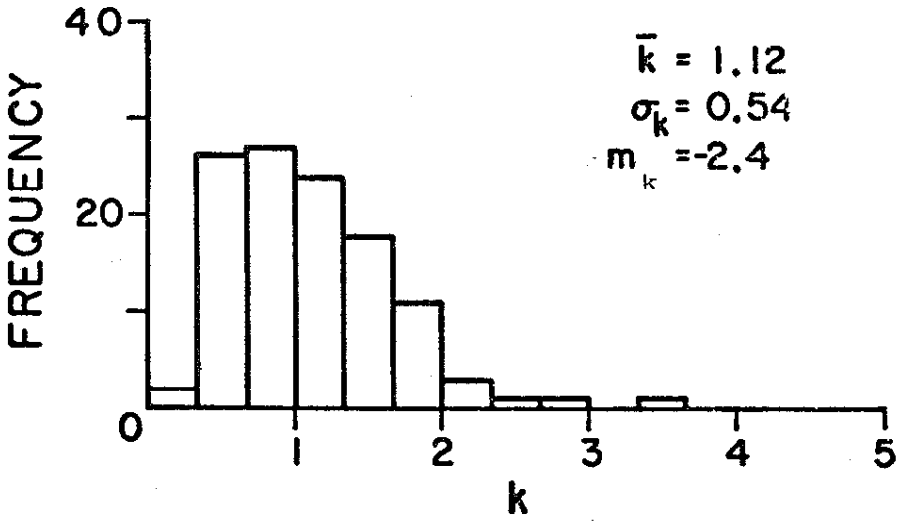

(f) 16.0 Hz

Figure 2.13. Continued.

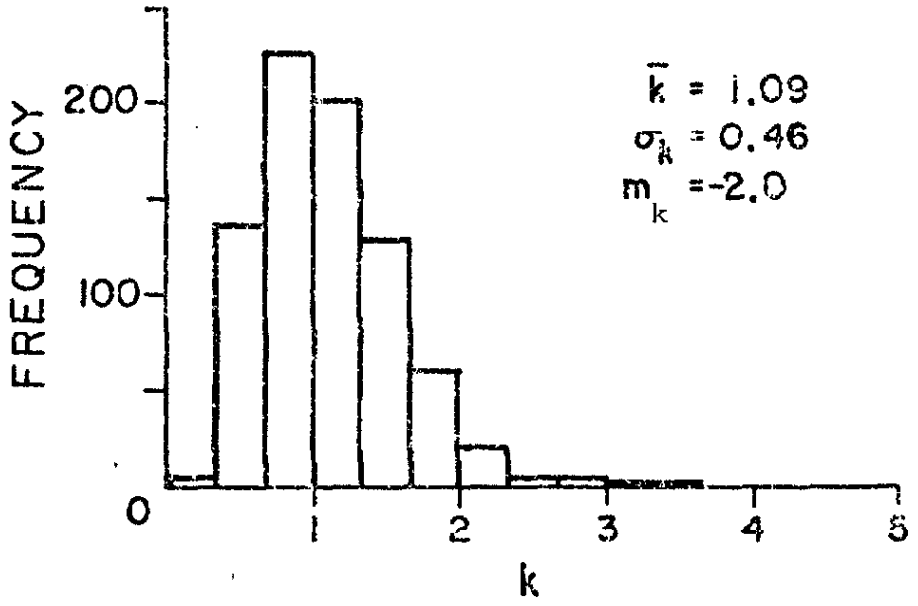

(g) Combined frequency samples, M5H15 data.

Figure 2.13. Continued.

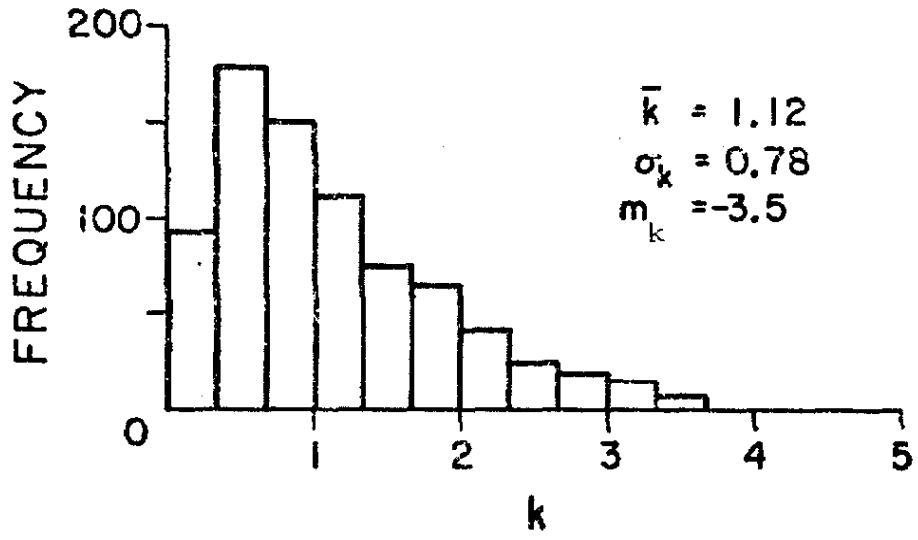

Figure 2.16(g). Combined frequency samples, M0H15 data.

TABLE 2.5.

k-factor statistics for the three sets of data from the southern group of sites

f (Hz)	M5H15 smoothed, 15-second accelerograms			M0H15 unsmoothed, 15-second accelerograms			M10HIV smoothed, full length accelerograms		
	$\bar{k}$	σ_k	m_k	$\bar{k}$	σ_k	m_k	$\bar{k}$	σ_k	m_k
0.4	1.08	0.40	-1.8	1.24	0.89	-4.9	1.03	0.39	-1.6
1	1.08	0.46	-1.9	1.18	0.81	-3.9	1.08	0.41	-1.8
2	1.09	0.40	-1.8	1.06	0.79	-3.2	1.08	0.41	-1.8
4	1.08	0.43	-1.8	1.05	0.69	-2.4	1.09	0.47	-1.9
8	1.11	0.51	-2.2	1.10	0.74	-3.1	1.10	0.56	-2.3
16	1.12	0.54	-2.4	1.10	0.75	-3.1	1.13	0.55	-2.4
Combined samples	1.09	0.46	-2.0	1.12	0.78	-3.5	1.08	0.47	-2.0

The histogram in Figure 2.13(g) shows the frequency distribution of k for data from all sampling frequencies taken together. It is seen that this histogram is a good approximation to any of those from individual frequency samples. (Note that Figure 2.13(g) is the upper figure on the page.)

2.7.3. Relative amplitudes of radial and transverse components.

It was observed in Section 2.5.2. that there is no apparent systematic difference in amplitude between radial and transverse components. This observation is confirmed by the statistics of the k-factor distribution for the two components of smooth, 15-second amplitude data shown in Table 2.6. The transverse amplitudes are stronger on the average by less than 5 percent. They are also more scattered, as seen in a 10 percent higher average standard deviation. These differences are small and about the same as those that occur between different frequency samples. For engineering purposes, in view of the much greater uncertainties in estimating design earthquakes (for example, in predicting the earthquake recurrence and source parameters) these differences are not considered significant. No separation of components will be made henceforth.

Possible reasons for this are (a) that the San Fernando rupture mechanism had almost equal components of strike- and dip-slip dislocation, and (b) that scattering by propagation path inhomogeneities further reduced differences between components.

2.7.4. Engineering significance of resolution bandwidth.

The foregoing discussion of scatter in Fourier amplitude ordinates has been concerned with the M5H15 amplitude data, which is smoothed over a bandwidth of 0.73 Hz.

TABLE 2.6.

k-factor statistics for radial and transverse components separately, for smoothed, southern 15-second data

f (Hz)	Radial component			Transverse component		
	$\bar{k}$	σ_k	m_k	$\bar{k}$	σ_k	m_k
0.4	1.06	0.40	-1.7	1.01	0.40	-1.9
1	1.00	0.37	-1.4	1.17	0.51	-2.5
2	1.13	0.40	-2.0	1.06	0.39	-1.6
4	1.05	0.42	-1.6	1.11	0.45	-2.0
8	1.08	0.51	-2.0	1.14	0.52	-2.2
16	1.13	0.49	-2.2	1.11	0.60	-2.5
Combined samples	1.07	0.43	-1.8	1.12	0.48	-2.1

It is obvious from the appearance of an unsmoothed Fourier amplitude spectrum (Figure 2.6, for example) that the distribution of scatter in Fourier amplitude data is highly dependent upon the resolution bandwidth. Hence, for a statistical distribution of scatter to be of use in structural design, the smoothing bandwidth used in obtaining the statistics should be equivalent to the range of frequency components making the principal contribution to the response of the structure.

The half-power bandwidth, Δf, is a commonly used measure of the bandwidth making the chief contribution to the response of a structure. Let y be the amplitude of response of a structure, and y_{max} be the amplitude of a resonance peak at frequency f_n, as shown in Figure 2.14; then Δf is defined as the width of the resonance peak at the half-power points where $y = y_{max}/\sqrt{2}$. In the case of a viscously-damped structure, it can be shown (e.g. Thomson, 1965) that

$$\frac{\Delta f}{f_n} = 2\zeta \qquad (2.16)$$

where ζ is the fraction of critical viscous damping.

Since ζ is fairly constant for many structures, the effect of change in natural frequency is to change the width of frequency band sampled. It is seen from equation (2.16) that for a given value of ζ, the half-power width increases in direct proportion to natural frequency. Hence, structures with high natural frequencies should be less susceptible to spectral peaks and troughs, since from equation (2.16) they respond to a wider frequency band and because scatter is nearly

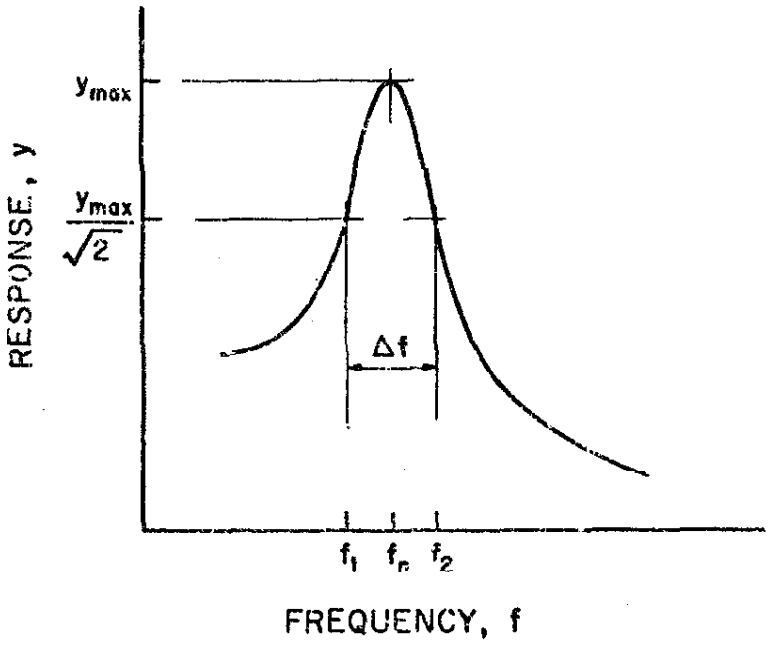

Figure 2.14. Δf defined as the width of the resonance curve at the half-power points, $y_{max}/\sqrt{2}$.

independent of frequency for a constant smoothing bandwidth. Values of ζ, computed from equation (2.16) and corresponding to a Δf of 0.73 Hz, equal to the smoothing bandwidth of the M5H15 data, are shown in Table 2.7. Values of ζ for $\Delta f = 0.067$ Hz, the bandwidth resolution of the raw Fourier amplitudes from the 15-second data before smoothing, are also shown in Table 2.7. Since equivalent viscous damping of 2 to 5 percent of critical is typical for many structures, it can be seen that only at higher frequencies do typically damped structures respond to as wide a bandwidth as the resolution width of the smoothed data. Thus, the distributions of scatter found for the smoothed data are applicable to structures with 2 to 5 percent critical damping only at frequencies of about 8 to 16 Hz. From Table 2.7 it is seen that structures with natural frequencies of about 1 Hz and levels of damping in the typical 2 to 5 percent range will respond to a frequency band of about 0.07 Hz, which is near the bandwidth resolution of the M0H15 data. Structures with natural frequencies near 1 Hz, therefore, will be subject to the scatter seen in the unsmoothed Fourier amplitudes, examined below.

2.7.5. Unsmoothed Fourier amplitude data.

Unsmoothed Fourier amplitude data from the southern group of 15-second accelerograms are listed in Table A2.4, Appendix 2, and are plotted against hypocentral distance in Figures 2.15. These data, labeled M0H15, are considerably more scattered than their smoothed counterparts, but they do show the same general attenuation trends observed in the smoothed data. The attenuation curves shown have the same parameters as those in the plots of smoothed data. The parameters A_i and Q estimated by the least-squares method from

TABLE 2.7.

Fraction of critical damping for single-degree-of-freedom oscillator with natural frequency f_o and half-power bandwidth Δf

f_o (Hz)	Fraction of critical damping, ζ	
	$\Delta f = 0.73$ Hz	$\Delta f = 0.067$ Hz
0.4	0.91	0.084
1.0	0.37	0.034
2.0	0.18	0.017
4.0	0.09	0.008
8.0	0.045	0.004
16.0	0.023	0.002

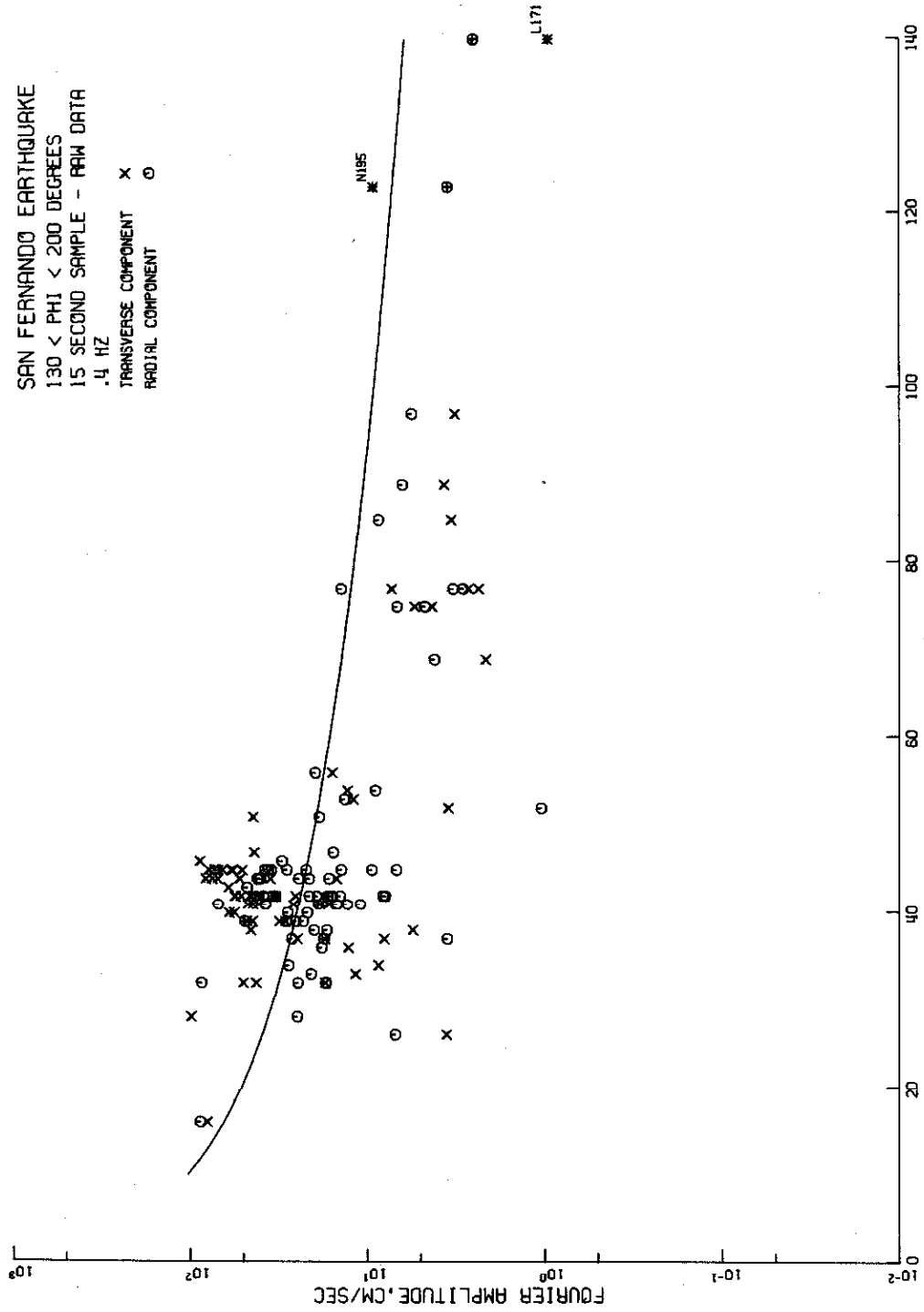

Figure 2.15(a). Unsmoothed Fourier amplitudes of acceleration from 15-second accelerograms of southern group. [Curve drawn from equation (2.6) with Q = 330 and A(0.4) = 1050 cm/sec].

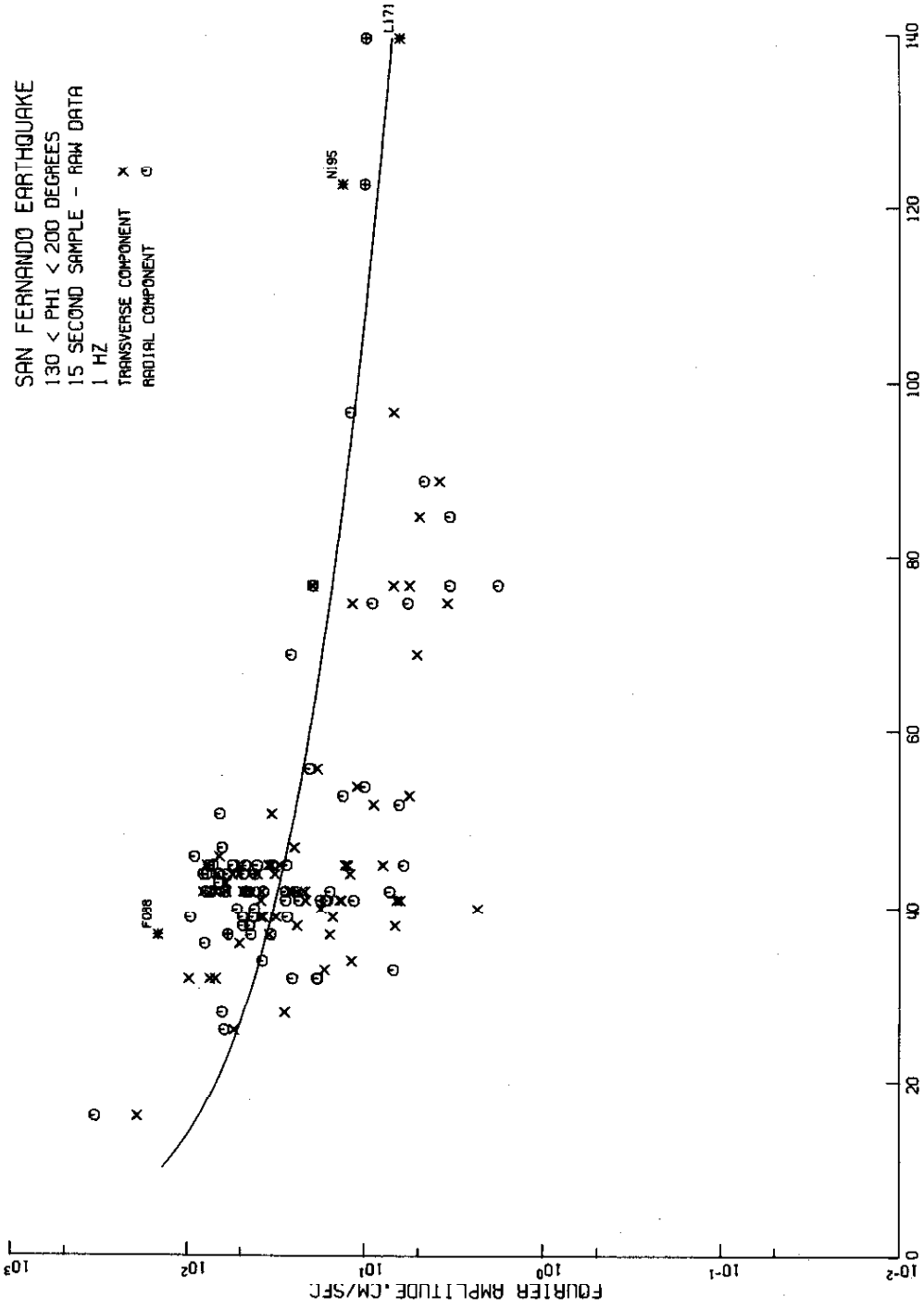

Figure 2.15(b). Q = 330, A(1) = 1440 cm/sec.

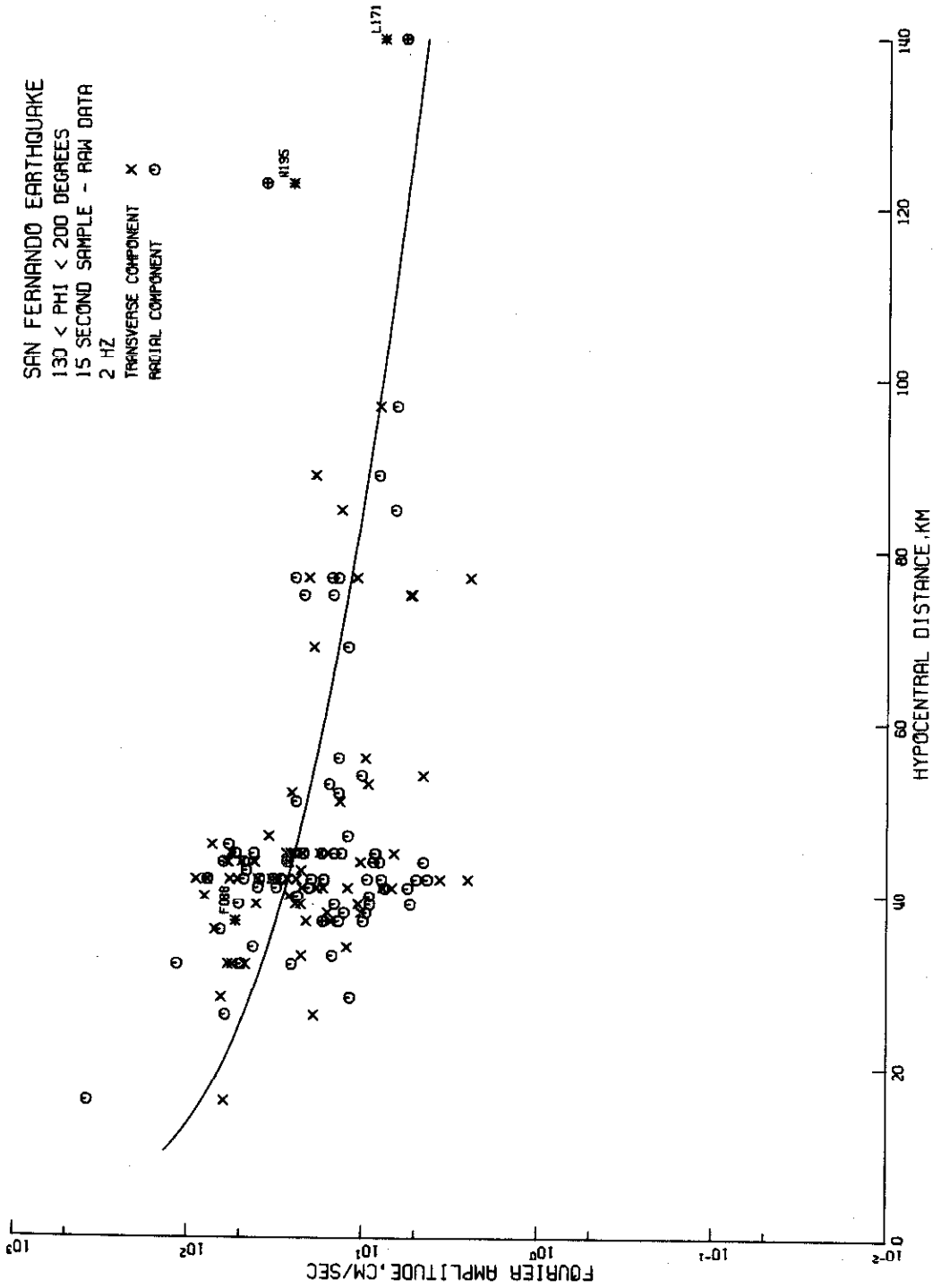

Figure 2.15(c). Q = 330, A(2) = 1490 cm/sec.

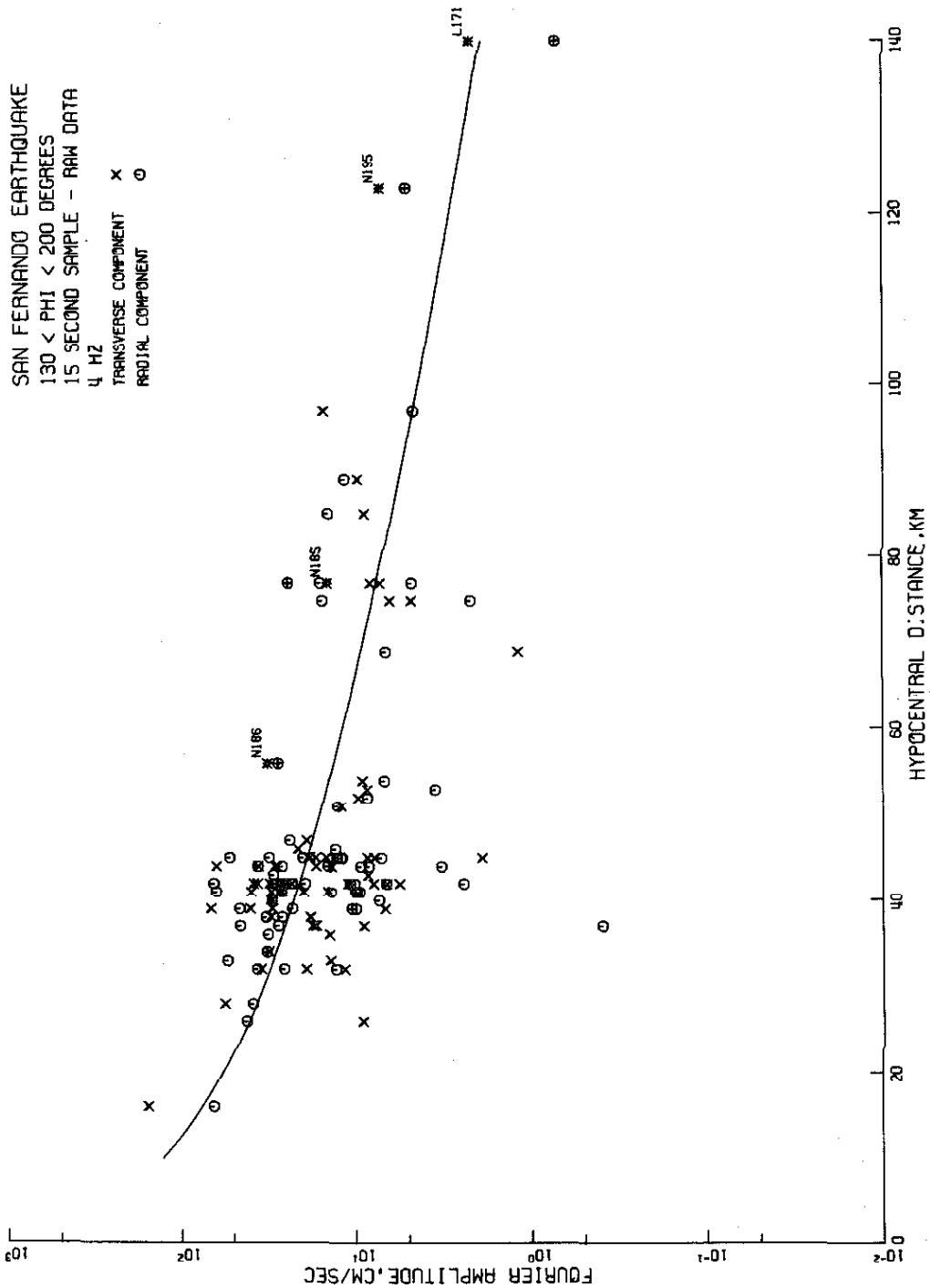

Figure 2.15(d). Q = 330, A(4) = 1440 cm/sec.

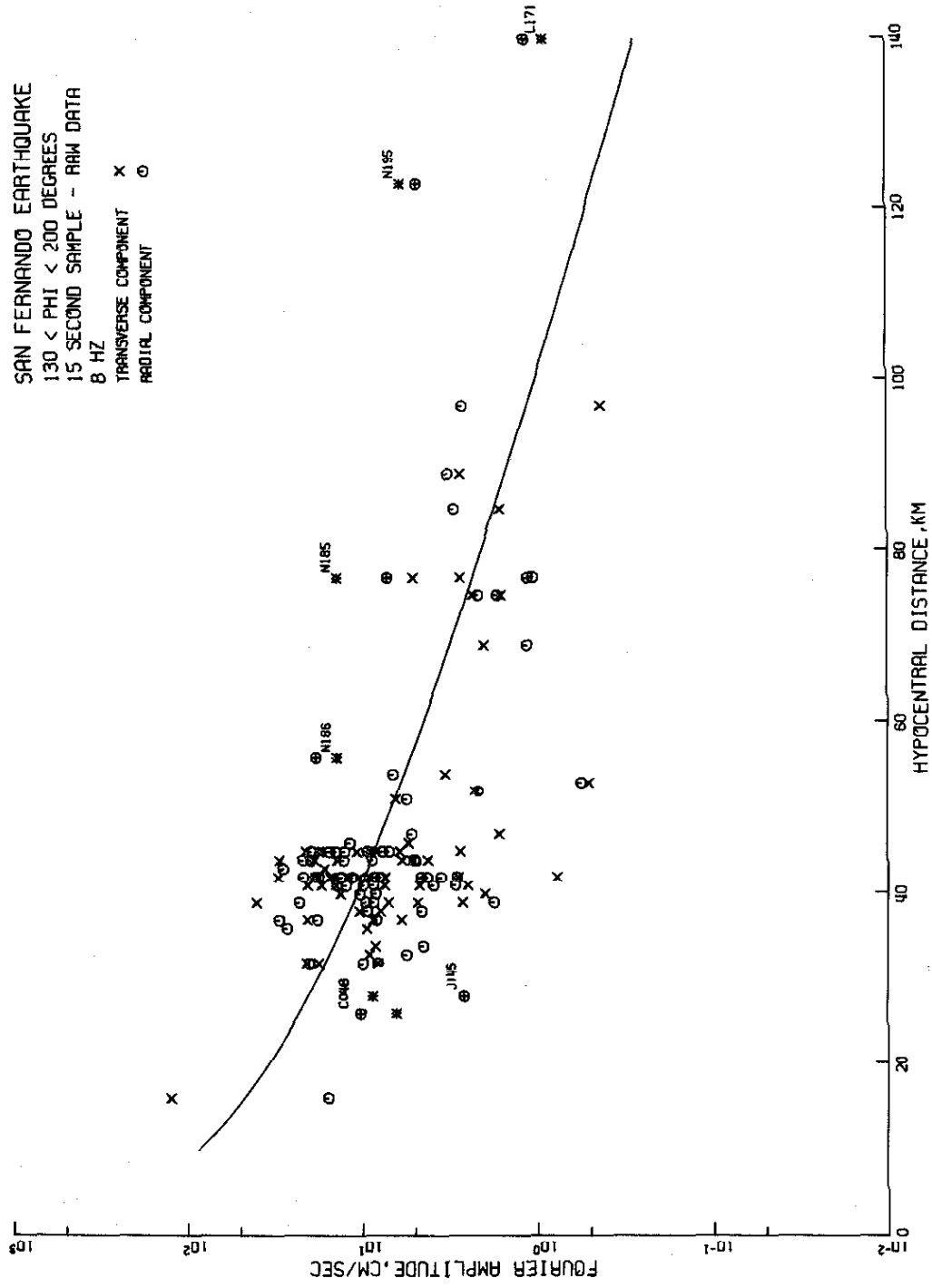

Figure 2.15(e). $Q = 330$, $A(8) = 1100$ cm/sec.

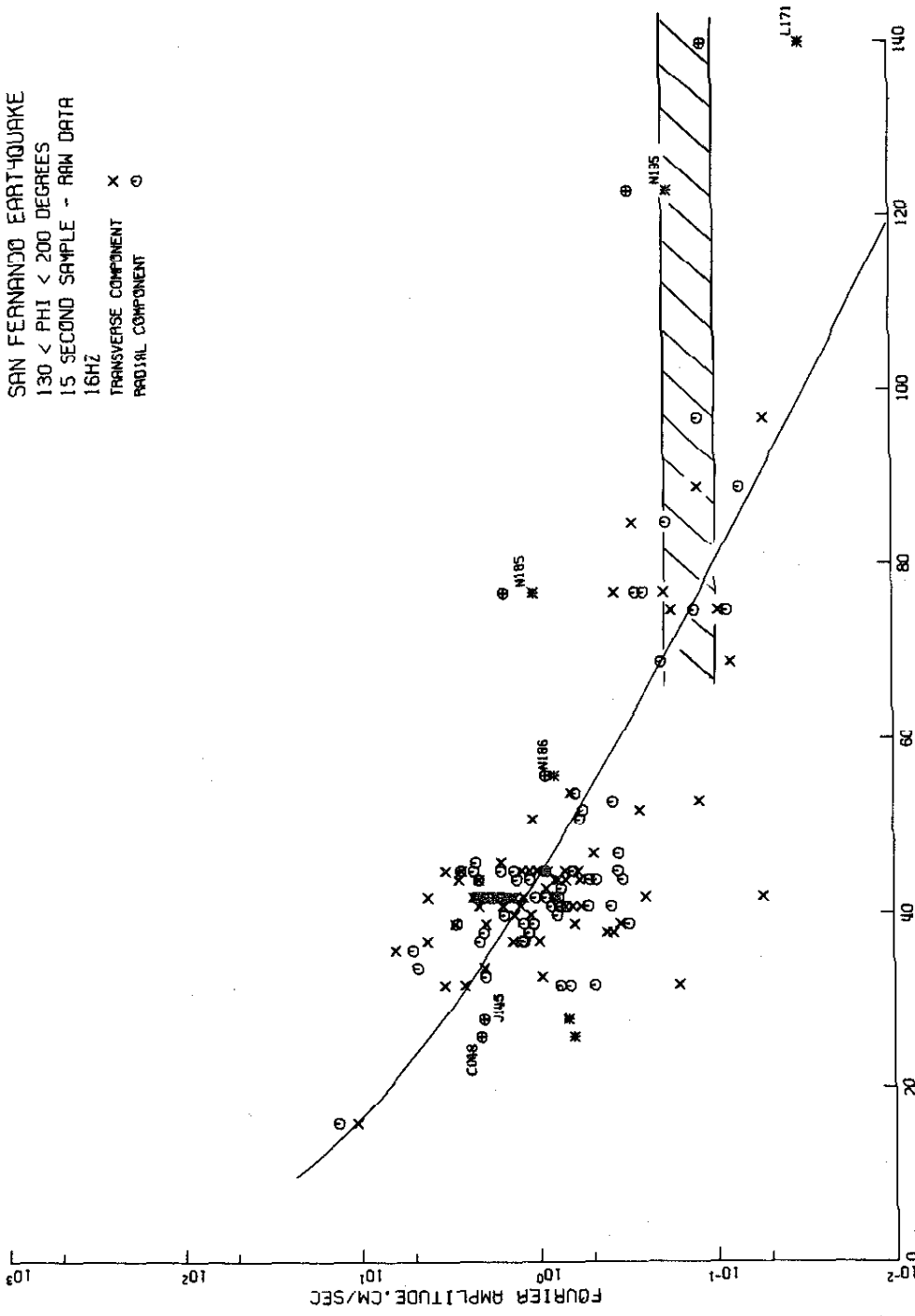

Figure 2.15(f). Q = 330, A(16) = 370 cm/sec. Hatched area shows noise range. Smoothing in the original noise level determination leaves range too narrow for the unsmoothed amplitudes shown in this figure.

the unsmoothed M0H15 data are shown in Table 2.8. These values are fairly close to those from the M5H15 data shown in Table 2.4, but their confidence intervals are considerably wider. The resulting k-values for the M0H15 amplitudes are not greatly different when computed from the parameters in Table 2.4 or from those in Table 2.8. Since it is considered that the smoothed amplitudes (M5H15) give more reliable estimates of Q and A_i, the values from Table 2.4 were used in computing the k-values for the M0H15 amplitudes. Histograms showing the frequency distributions of k for the M0H15 data are given in Figures 2.16, and the individual k-values are listed in Appendix 3. The greater scatter is reflected in flatter, more widely-spread distributions, and is shown quantitatively in the standard deviations of k. Again, the distributions at different frequencies are quite similar, as can be seen from the statistics given in Table 2.5. For comparison, the histogram of k for the six frequency samples combined is shown as Figure 2.16(g) on the same page as the corresponding histogram from the M5H15 data, Figure 2.13(g).

2.7.6. Effect of resolution bandwidth on scatter in Fourier amplitudes.

The effect of resolution bandwidth on scatter of Fourier amplitude data is seen in Figure 2.17, in which accumulated relative frequency ("frequency" being used in the statistical sense) is shown for both the smoothed and unsmoothed data.

In view of the large number of data, these curves should closely approximate the cumulative probability distributions for k corresponding to the two resolution bandwidths. They can, therefore

TABLE 2.8.

Estimated parameters from M0H15, southern data

Parameter	Value	90% confidence interval
Q	370	330 - 430
A_1*	960 cm/sec	750 - -**
A_2	1280	990 - -**
A_3	1130	870 - 1460
A_4	1120	870 - 1460
A_5	830	630 - 1070
A_6	250	190 - 330

*The subscripts 1, 2, ..., 6 refer to the frequencies 0.4, 1, 2, 4, 8 and 16 Hz respectively.

**None found.

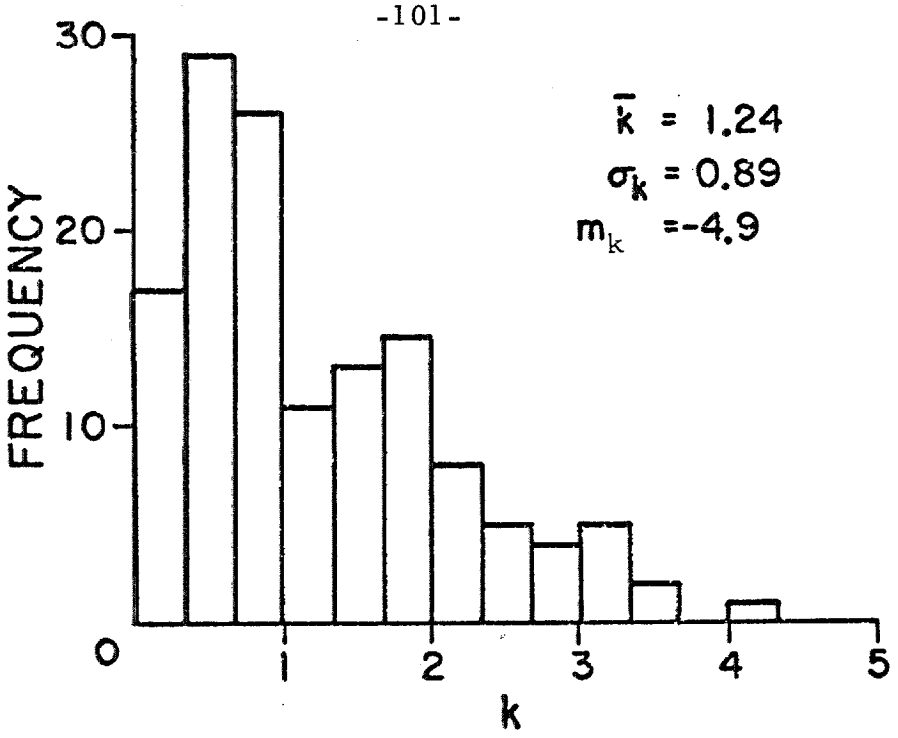

(a) 0.4 Hz

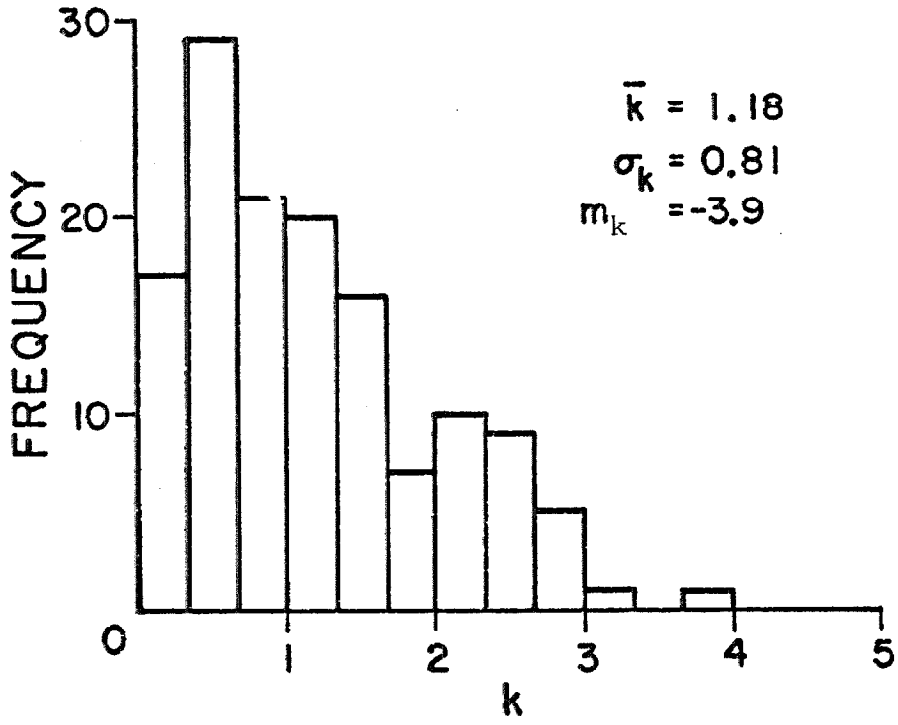

(b) 1.0 Hz

Figure 2.16. Scatter in southern M0H15 data shown by distribution of k.

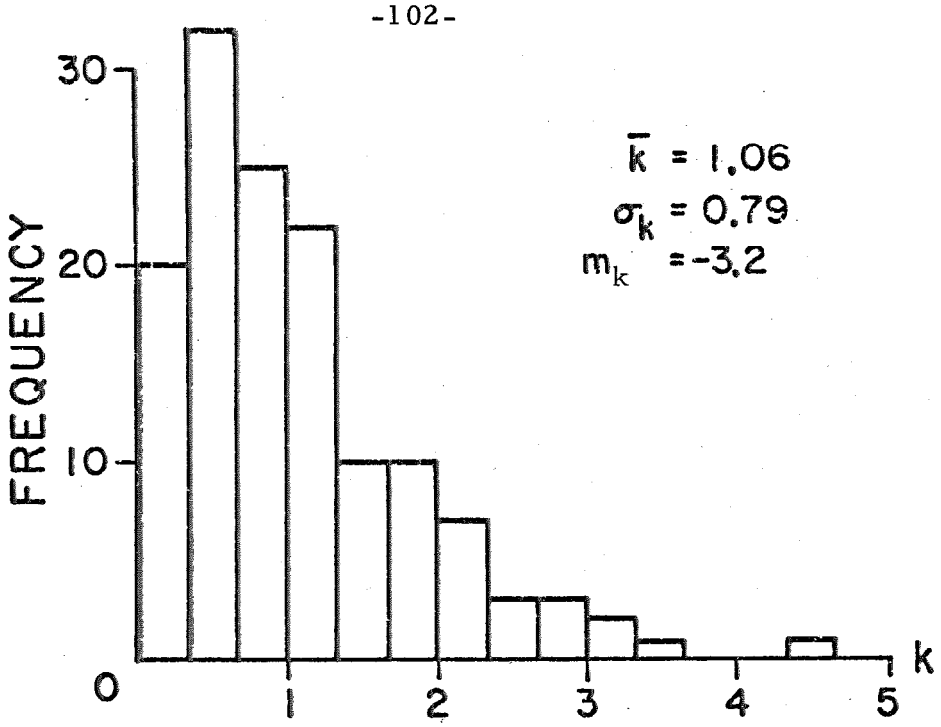

(c) 2.0 Hz

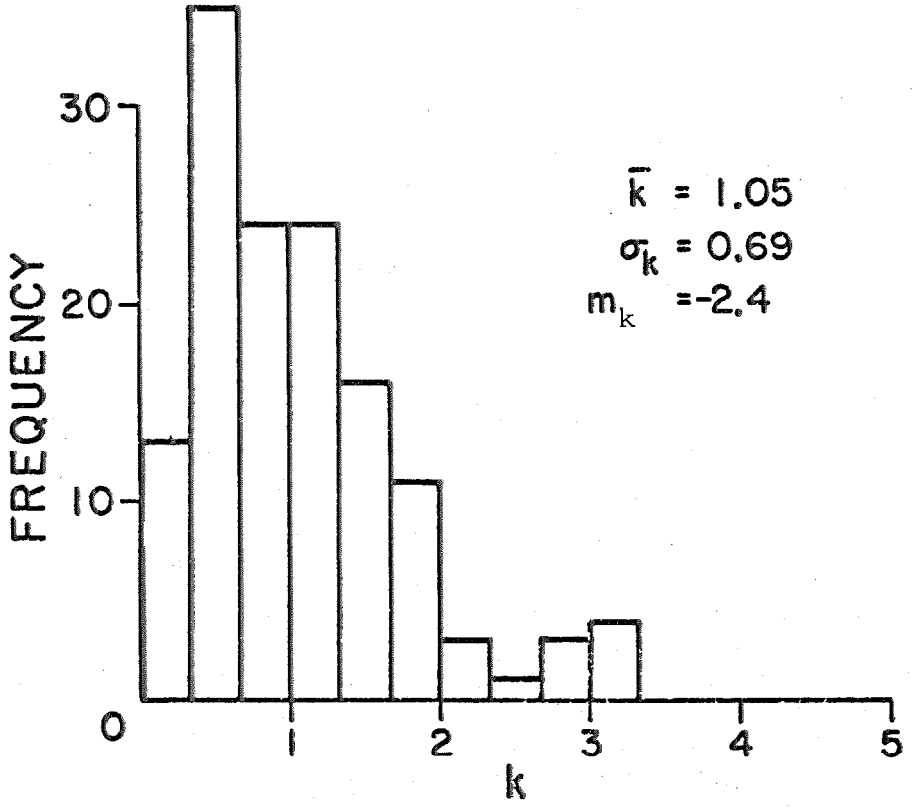

(d) 4.0 Hz

Figure 2.16. Continued.

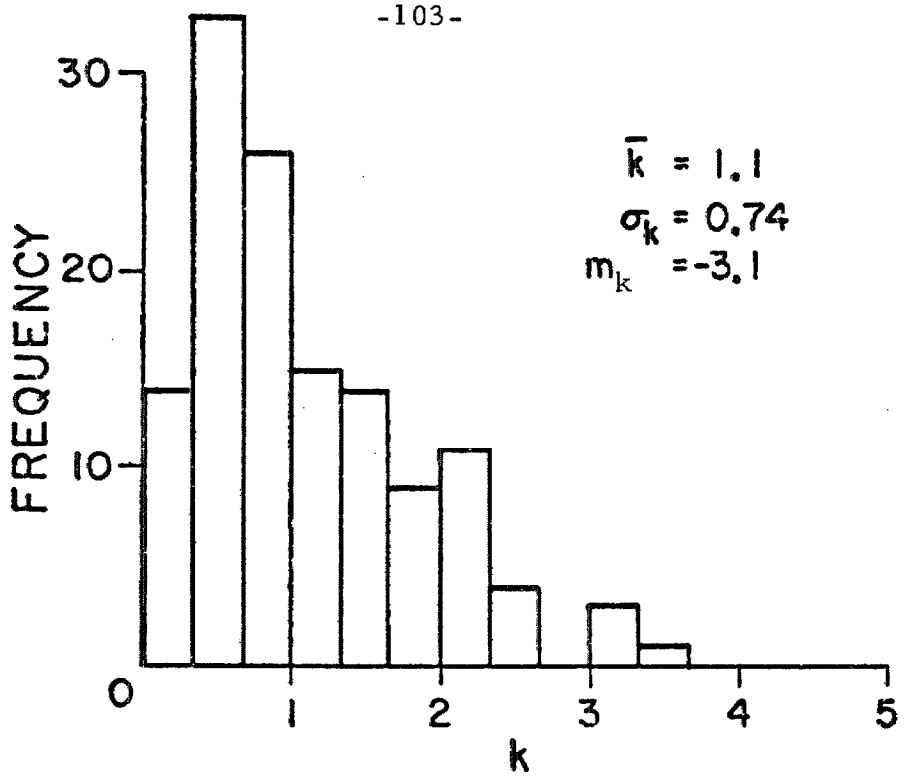

(e) 8.0 Hz

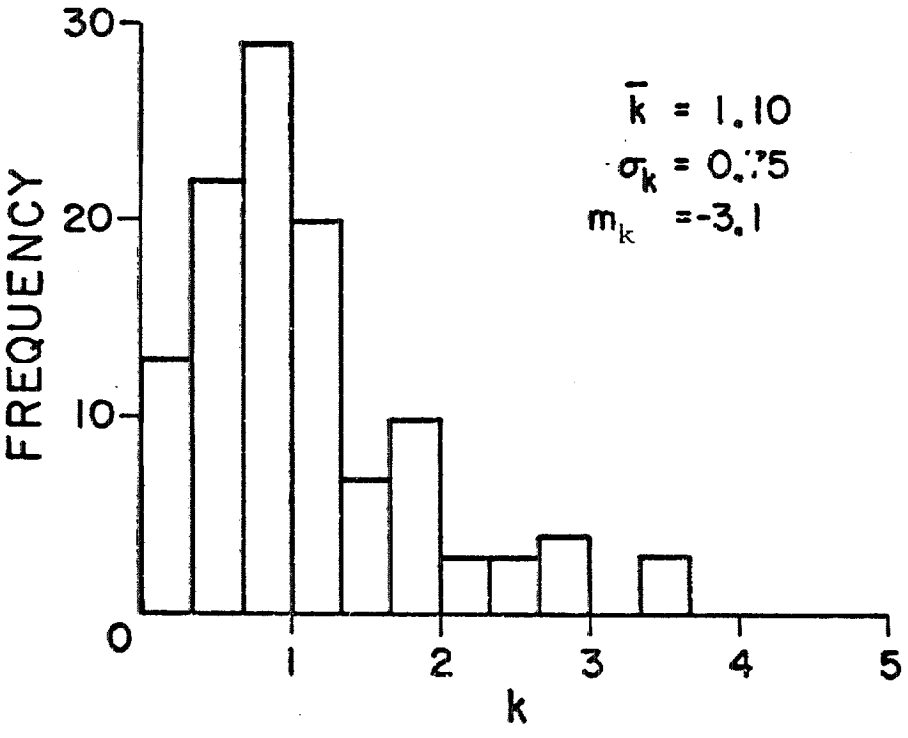

(f) 16.0 Hz

Figure 2.16. Continued.

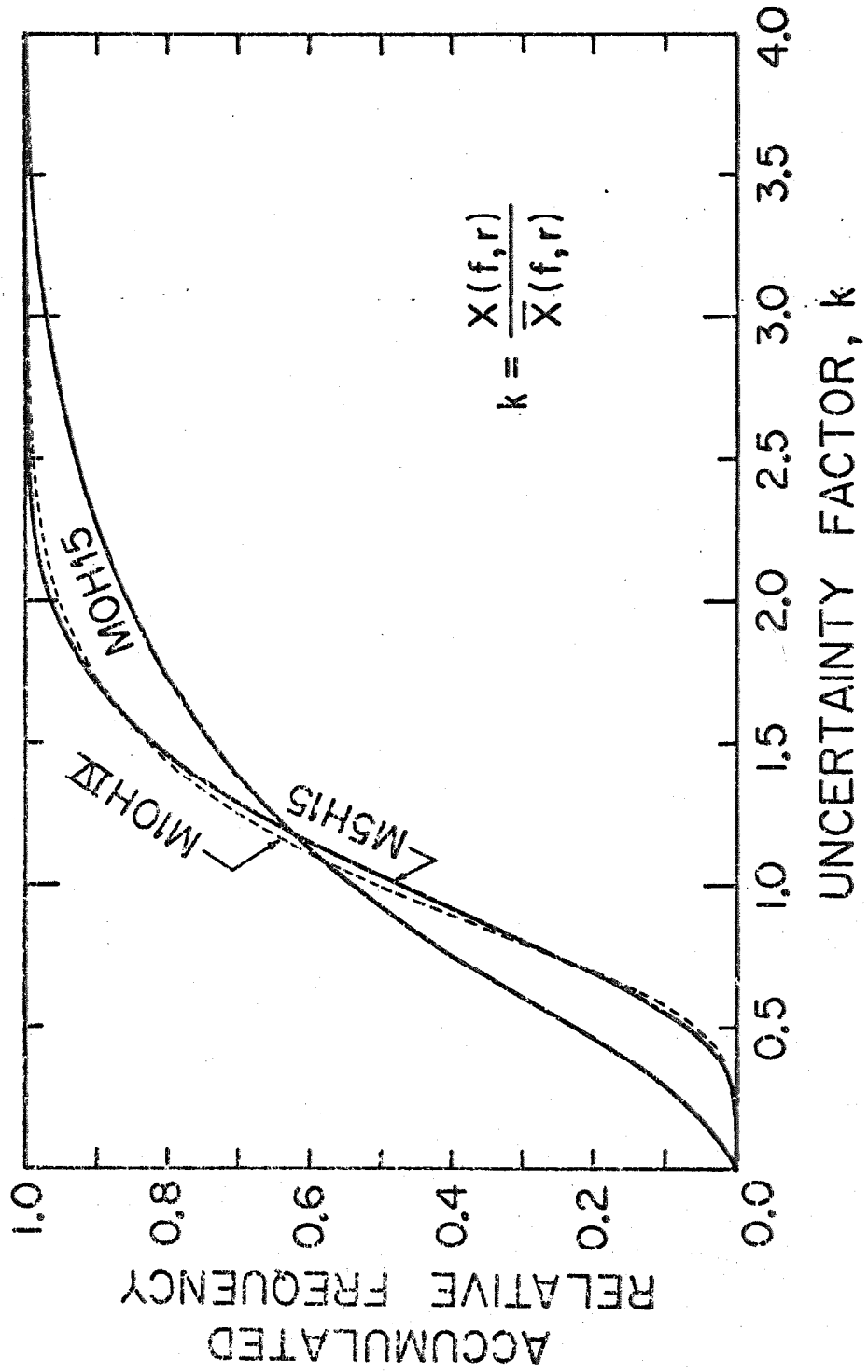
ACCUMULATED RELATIVE FREQUENCY
1.0
0.8
0.6
0.4
0.2
0.0
0.5
1.0
1.5
2.0
2.5
3.0
3.5
4.0
UNCERTAINTY FACTOR, k
$k = \frac{X(f,r)}{\overline{X}(f,r)}$
M10H15
M5H15
M10H1X

Figure 2.17.

be used to compute confidence limits for Fourier amplitude estimates obtained from equation (2.6).

For example, consider a given earthquake specified by its source strength function A(f). Suppose a value of Fourier amplitude of ground acceleration $X_{0.90}(f, r)$ is sought at hypocentral distance r and frequency f, for which the probability is 90 percent that this value will not be exceeded during the earthquake. That is, $\overline{X}_{0.90}(f, r)$ is sought such that

$$\text{Prob}[X(f, r) < \overline{X}_{0.90}(f, r)] = 0.90 \qquad (2.17)$$

Suppose further, that the value should correspond to a half-power bandwidth of 0.73 Hz. The value of $X_{0.90}(f, r)$ can be obtained by first finding the expected value $\overline{X}(f, r)$ from equation (2.6). Then from Figure 2.17, the uncertainty factor k is found, corresponding to the accumulated relative frequency of 0.90. From the M5H15 curve for which $B_e = 0.73$ Hz, the value of $k_{0.90}$ is 1.7. Then from equation (2.13) defining k, we find

$$X_{0.90}(f, r) = 1.7\,\overline{X}(f, r)\,, \qquad (2.18)$$

the value required. In a real situation the source strength would not be known precisely, and uncertainties associated with it should also be considered.

For engineering use, scatter distributions for several values of f and $\Delta f/f$ are presented in Appendix 4. A worked example is presented in Chapter 4 using the results of this study to arrive at a design earthquake.

2. 7. 7. Attenuation of full-length accelerogram amplitudes.

So far amplitude data from the rotated, 15-second samples have been studied. It is of interest to compare the attenuation of Fourier amplitudes computed from the full-length records with that of the 15-second data. These data are available directly from the EERL, on a master tape of Volume IV data.

Smoothed Fourier amplitudes of the full-length accelerograms from the southern sites are listed in Table A2. 5, Appendix 2, and are shown in Figure 2. 18, where they are plotted against hypocentral distance. The smoothing procedure which results in variable resolution bandwidths has been described in Section 2. 3. Estimates of the parameters Q and A_i obtained from the M10HIV data by the least-squares procedures of Section 2. 6. 3 are listed in Table 2. 9 below. The solid curves plotted in the figures result from the substitution of these parameter values into equation (2. 6). The attenuation curves from the M5H15 data are shown by dashed lines, for comparison.

The value of $Q = 330$ is the same as that obtained from the 15-second record data. Only at 0. 4 and 1 Hz is there any difference in the values of A_i. It can be concluded from this that essentially all the energy in components with frequencies at and above 2 Hz is contained within the 15-second window following the S-arrival. This implies that these components are not dispersed outside the 15-second window and also that the energy content of the P waves coming in before the S-arrival is small.

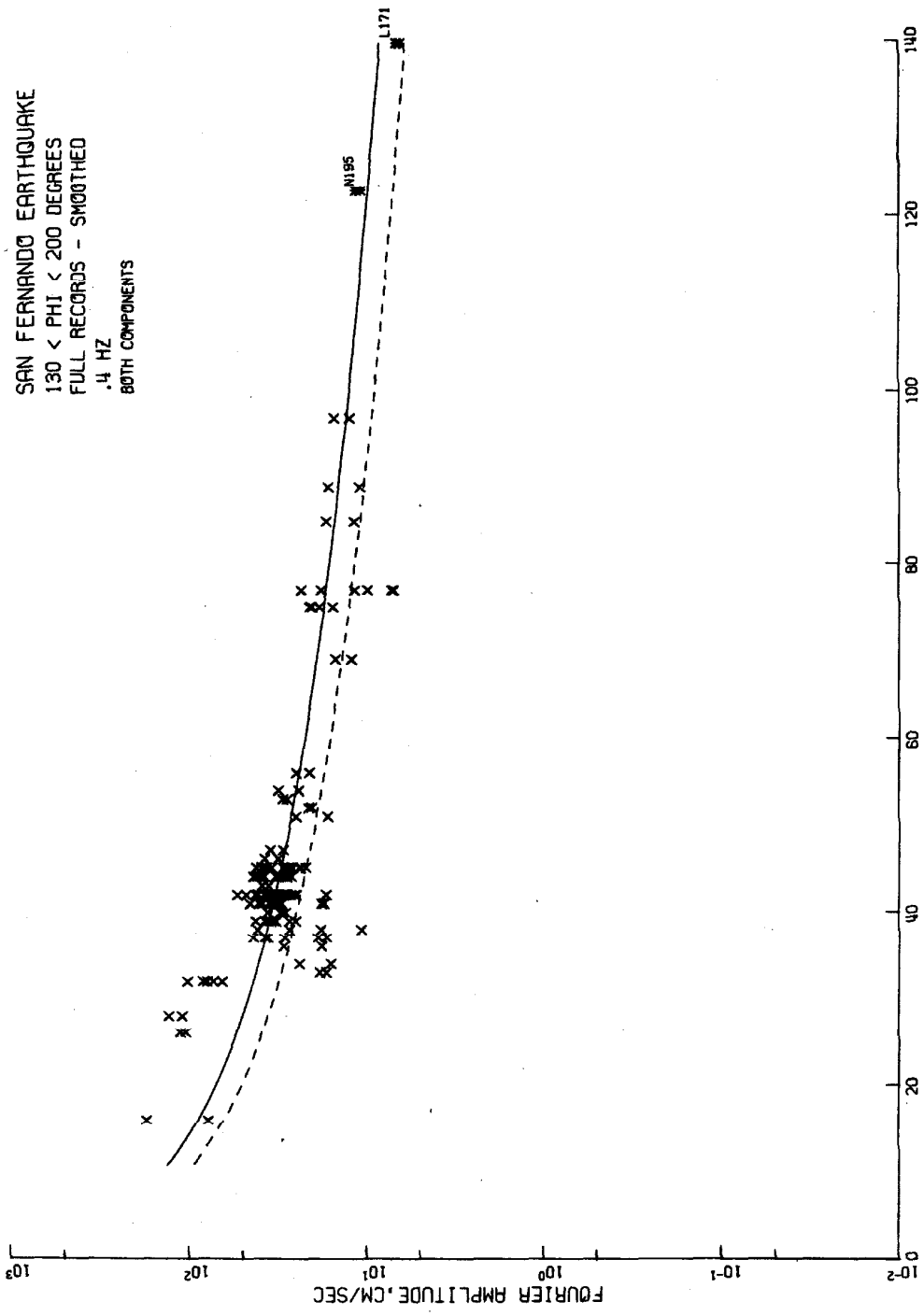

Figure 2.18(a). Fourier amplitudes of acceleration from southern smoothed, full-length accelerograms (M10H10 data). The full-line curve is drawn from the parameters in Table 2.9 ($Q = 330$, $A(0.4) = 1460$ cm/sec)

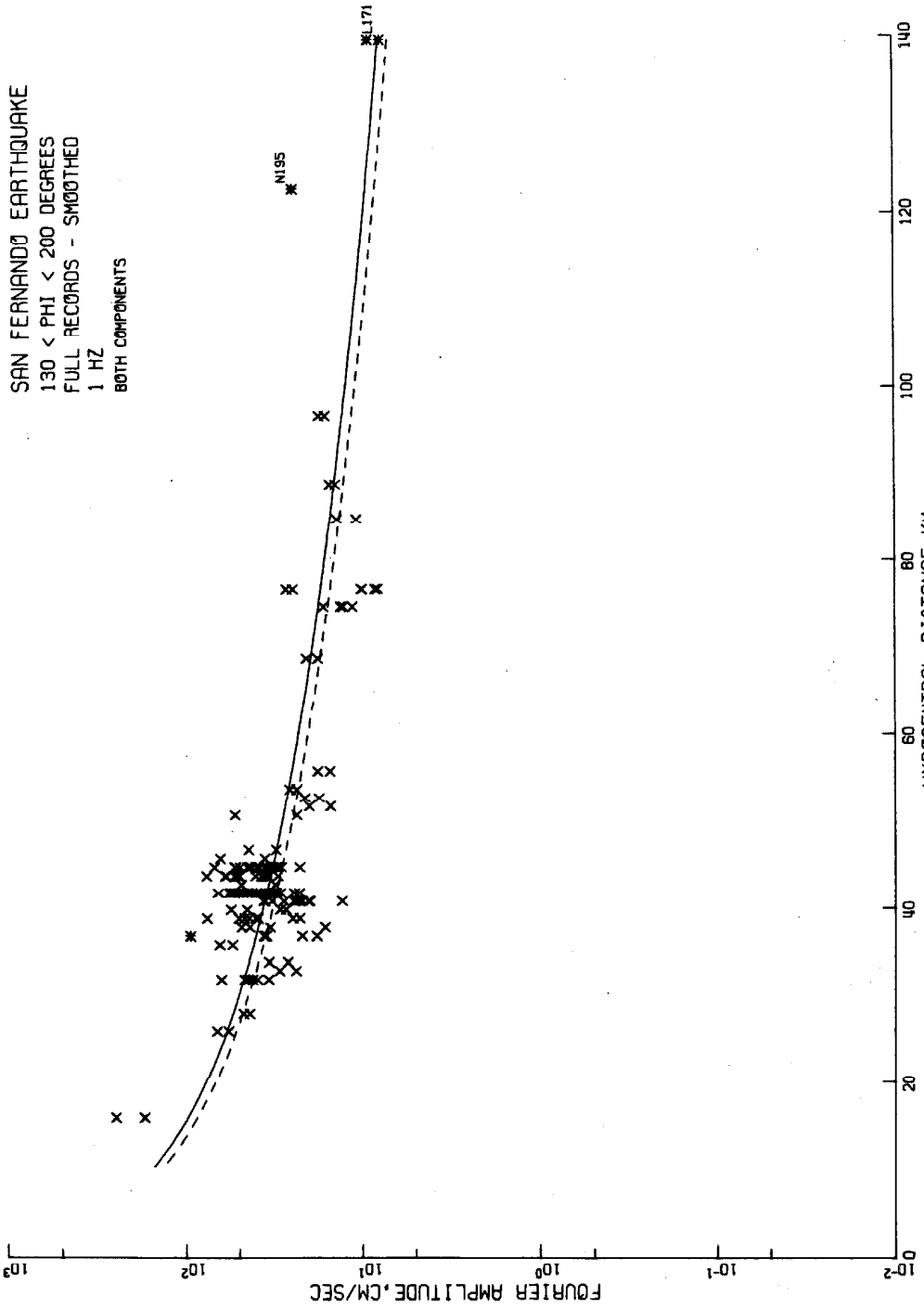

Figure 2.18(b). Solid line has Q = 330, A(1) = 1640 cm/sec.

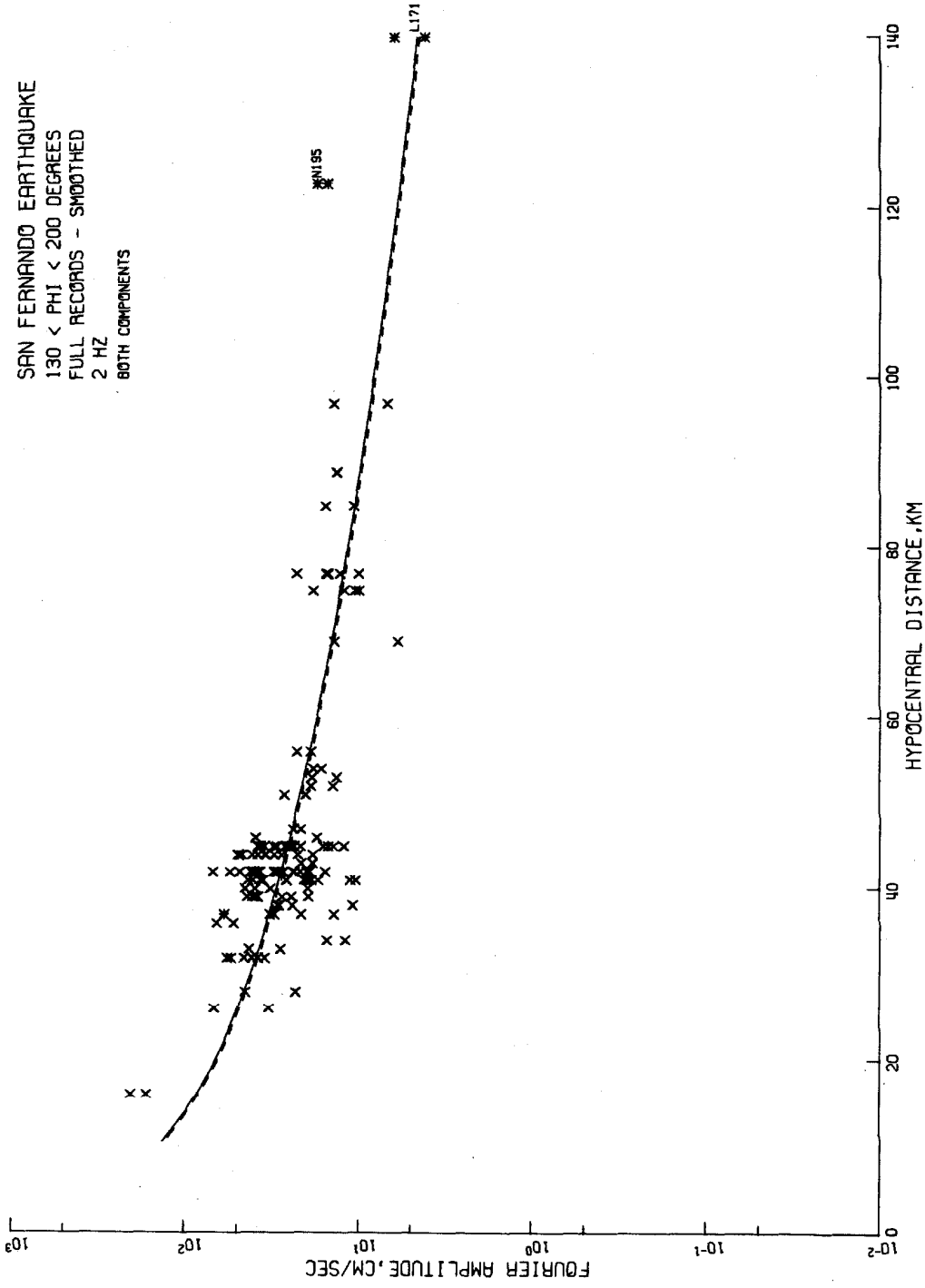

Figure 2.18(c). Solid line Q = 330, A(2) = 1490 cm/sec.

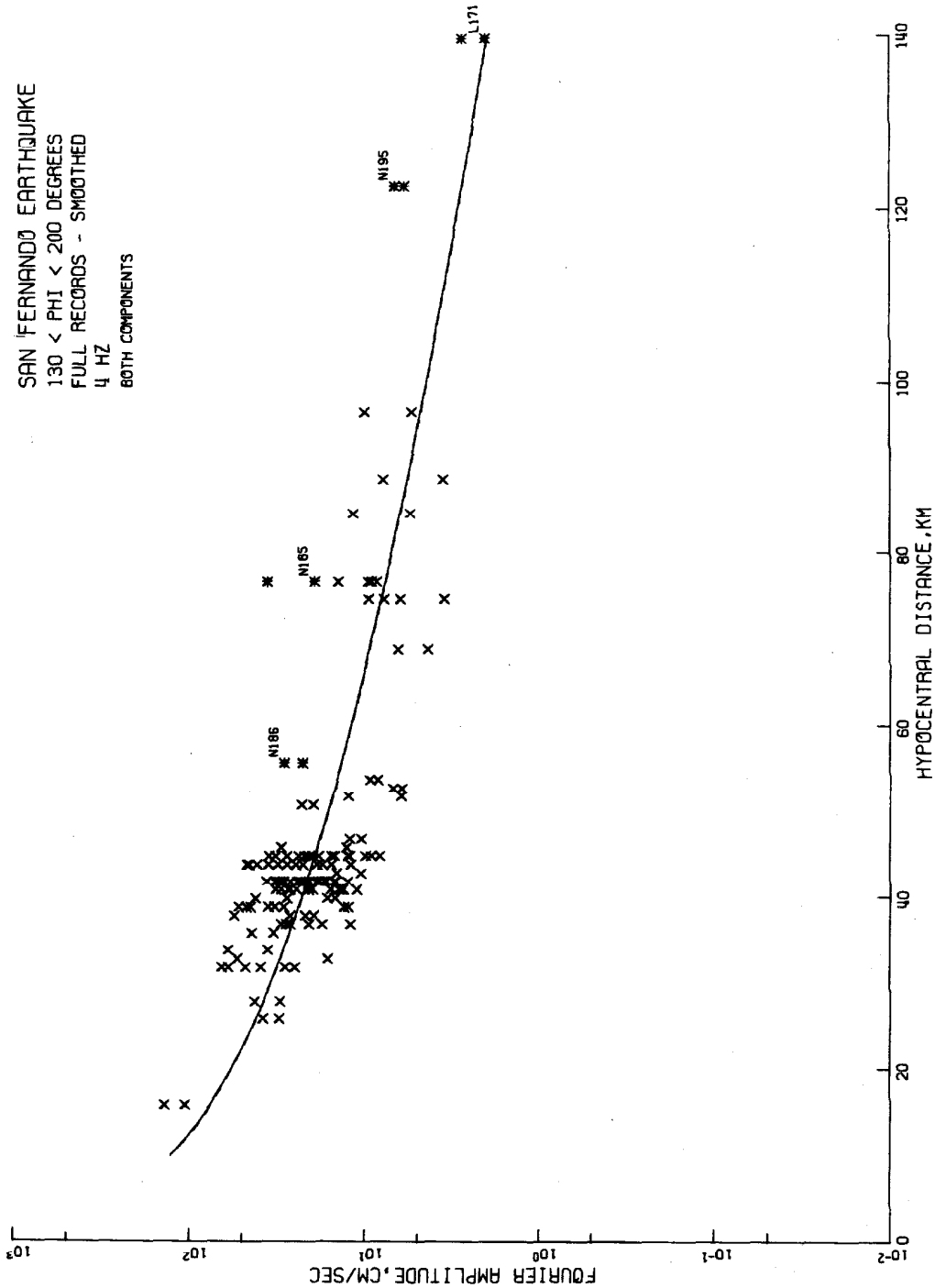

Figure 2.18(d). Solid line Q = 330, A(4) = 1460 cm/sec.

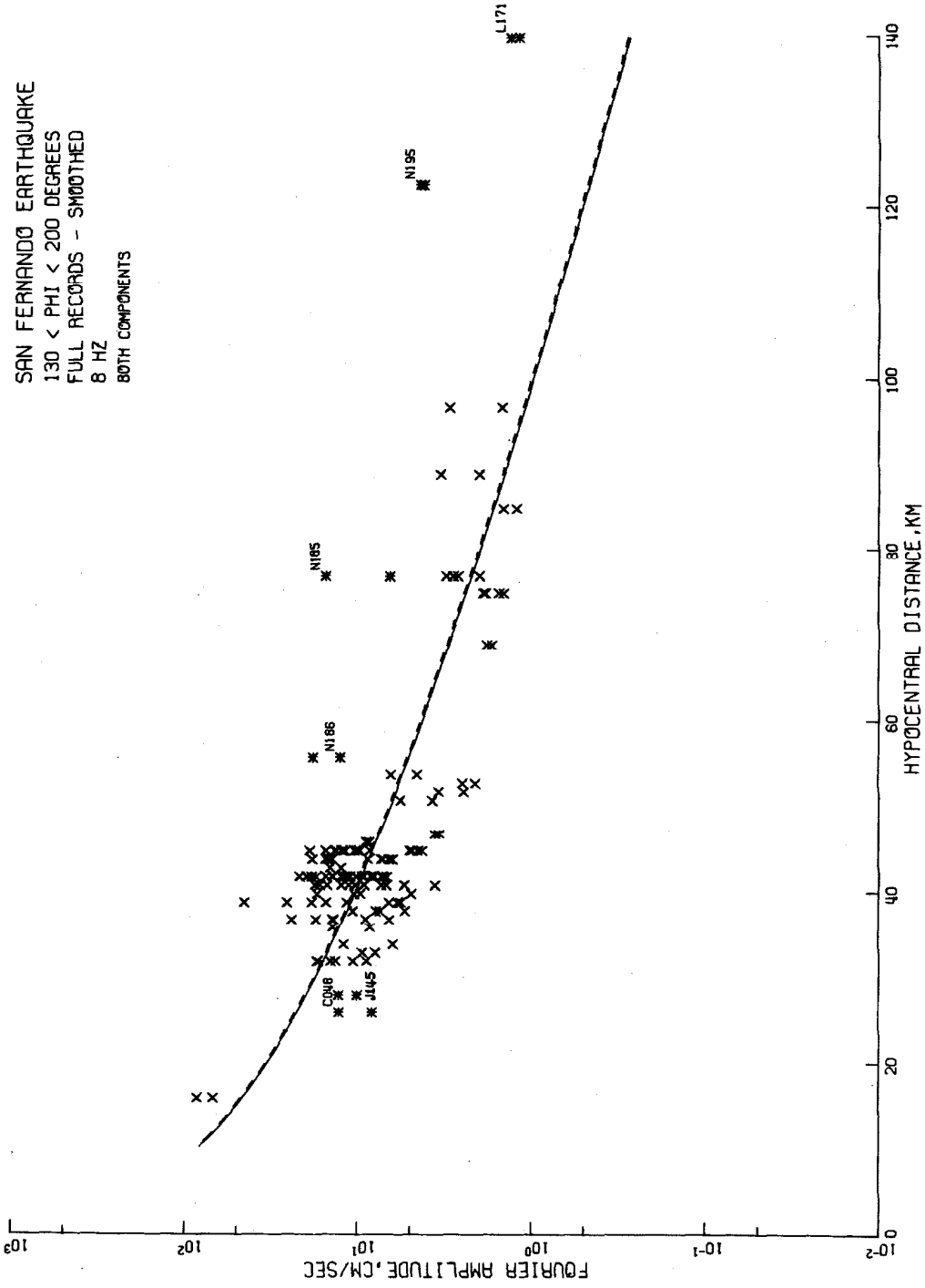

Figure 2.18(e). Solid line Q = 330, A(8) = 1070 cm/sec.

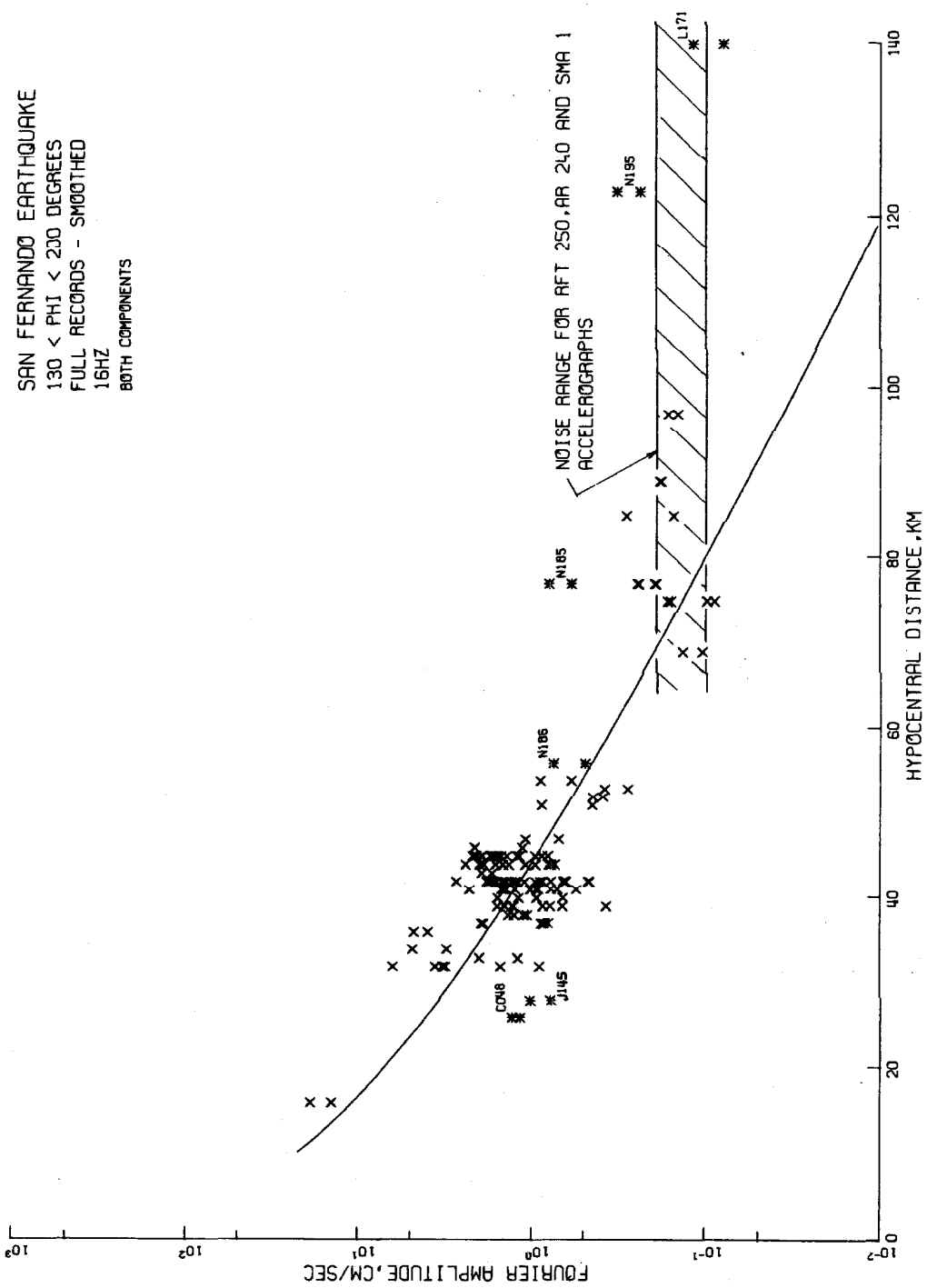

Figure 2.18(f). Q = 330, A(16) = 370 cm/sec.

TABLE 2.9.

Estimated parameters for smoothed,

Volume IV data, southern group

Parameter	Value	90% confidence interval
Q	330	310-360
A_1 **	1460 (1050)* cm/sec	1260-1700
A_2	1640 (1440)*	1460- none found
A_3	1490	1270-1730
A_4	1460	1240-1680
A_5	1070	900-1220
A_6	370	310-440

*Value for 15-second data (from Table 2.4).

**The subscripts 1, 2, ..., 6 refer to the frequencies 0.4, 1, 2, 4, 8 and 16 Hz respectively.

At 1 Hz and below the situation is different. Comparing Figures 2.9(a) and 2.18(a) it is seen that:

(1) data points from the full-length records at these frequencies are generally higher than those from the 15-second records,

(2) they follow a simple attenuation curve given by equation (2.6) much more closely than do the 15-second data, and

(3) they do not have the relatively low amplitudes found in the 15-second data at large focal distances.

From these observations it is concluded that (1) even though surface waves are apparently contributing to ground motions in the 0.4-1 Hz range, geometric attenuation can be described by a $1/r$ term throughout the 0.4-16 Hz frequency band; and (2) low amplitudes noted at 0.4 and 1 Hz in the 15-second data at large hypocentral distances are due to part of the wave motion at these frequencies being dispersed and arriving outside the 15-second sampling window.

The scatter in these (M10HIV) data is quite similar to that of the smoothed, 15-second amplitudes. This can be seen from the values of $\bar{k}$, σ_k and m_k in Table 2.5, and from the accumulated relative frequency of k, which shows the distribution of k from the six sampling frequencies combined, plotted in Figure 2.17.

2.8. Attenuation of the northern data.

Unlike the southern group of sites in which almost all sites have sedimentary surface geology, nearly half the accelerograph sites in the northern group are on crystalline basement rock, and it is possible to estimate a value of Q for propagation paths entirely

in the basement. However, since there are only 9 sites in the group, estimates of parameters cannot be made with nearly as much confidence as they were from the southern group. The 9 stations are listed in Table 2.10 together with a brief description of site geology, taken from Hudson (1971), a Woodward-Lundgren (1973) report and USGS Map OM-125. An additional record, D056, Castaic, is included in the table and the attenuation plots for comparison, but is not used in estimating parameters for the group, since it lies at an azimuth well separated from the rest of the group.

It is interesting to correlate features of the amplitude spectra from the rotated, 15-second records, shown in Figure 2.20, with propagation path geology. The general amplitude level at site J144, Figure 2.20(a), on several thousand feet of sediments and at a hypocentral distance of 27 km is about twice that of the next further site, J143 (Figure 2.20(b)) on basement rock at a distance of 30 km. While the spectra of J143 and nearby J142 on weathered basement rock differ in the frequencies at which individual peaks occur, their average levels are quite similar. Note the strongly fluctuating peaks even in these spectra from basement rock sites. Both components have similar strengths. The following site, J141 at a distance of 32 km has quite different spectra which are dominated by strong peaks at 1-2 Hz. Above 2.5 Hz, the general spectral levels are similar to those at the preceding sites, but the peaks below 2.5 Hz are more than 100 percent higher than peaks near these frequencies, in spectra from nearby sites. Since this site is located on the San Andreas Fault, these peaks are quite probably due to the presence of waves trapped

TABLE 2.10.

Sites in northern group

Record	Hypocentral distance (km)	Site-station azimuth (degrees)	Site geology
J144	26.7	320	10 feet of landslide debris over several thousand feet of marine sandstone
J143	29.6	325	Gneiss
J142	29.8	342	Weathered granite
D056*	31.4	304	Several thousand feet of Miocene shale
J141	32.3	351	In fracture zone of San Andreas Fault. Log from nearby well in fracture zone records 3000 ft of sands and clays. Granite on either side of fault.
O207	35.3	353	Granite
F104	53.8	326	Approximately 2000 ft of sediments
F102	69.7	318	Granite
M179	71.9	326	15 feet of recent alluvium over gneiss
E071	87.0	322	12,000 feet of sediments

*Not used in estimating parameters.

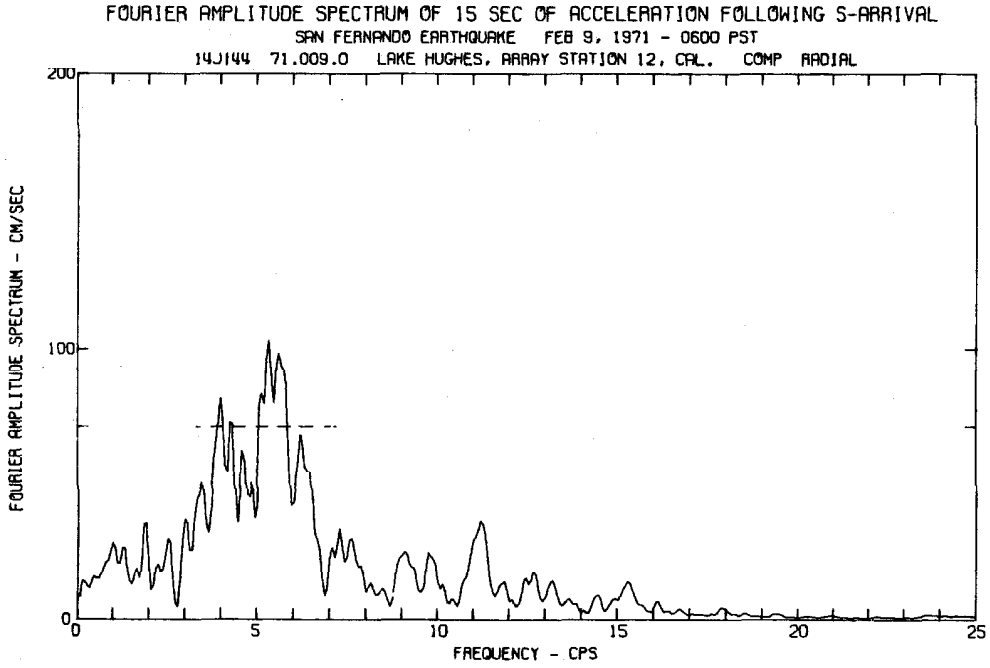
FOURIER AMPLITUDE SPECTRUM OF 15 SEC OF ACCELERATION FOLLOWING S-ARRIVAL
SAN FERNANDO EARTHQUAKE FEB 9, 1971 - 0600 PST
14J144 71.009.0 LAKE HUGHES, ARRAY STATION 12, CAL. COMP RADIAL
FOURIER AMPLITUDE SPECTRUM - CM/SEC
200
100
0
0
5
10
15
20
25
FREQUENCY - CPS

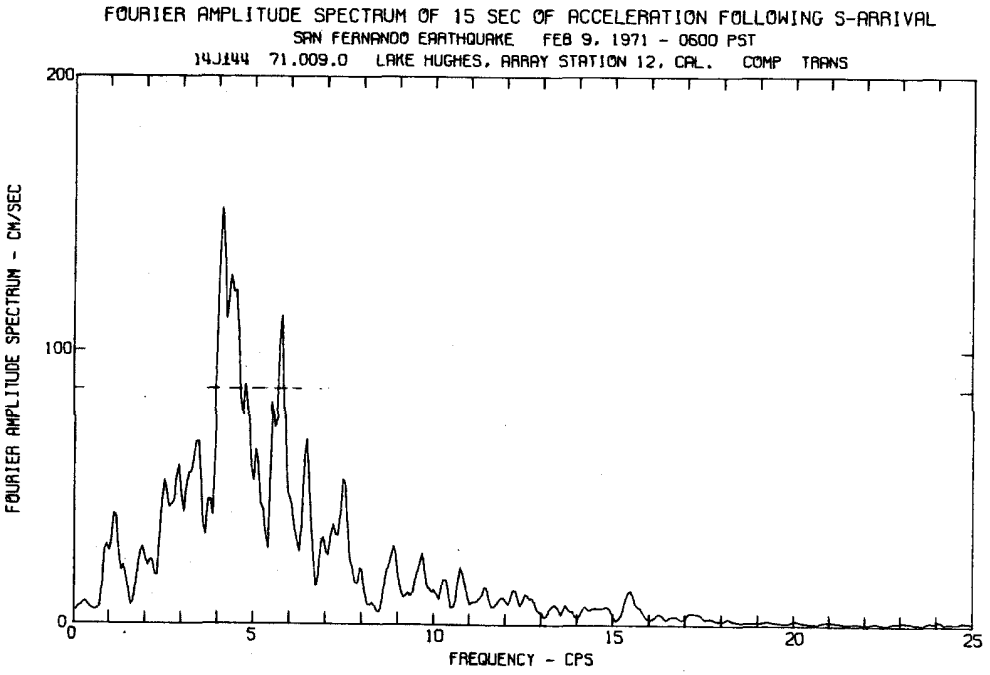
FOURIER AMPLITUDE SPECTRUM OF 15 SEC OF ACCELERATION FOLLOWING S-ARRIVAL
SAN FERNANDO EARTHQUAKE FEB 9, 1971 - 0600 PST
14J144 71.009.0 LAKE HUGHES, ARRAY STATION 12, CAL. COMP TRANS
FOURIER AMPLITUDE SPECTRUM - CM/SEC
200
100
0
0
5
10
15
20
25
FREQUENCY - CPS

Figure 2.20(a)

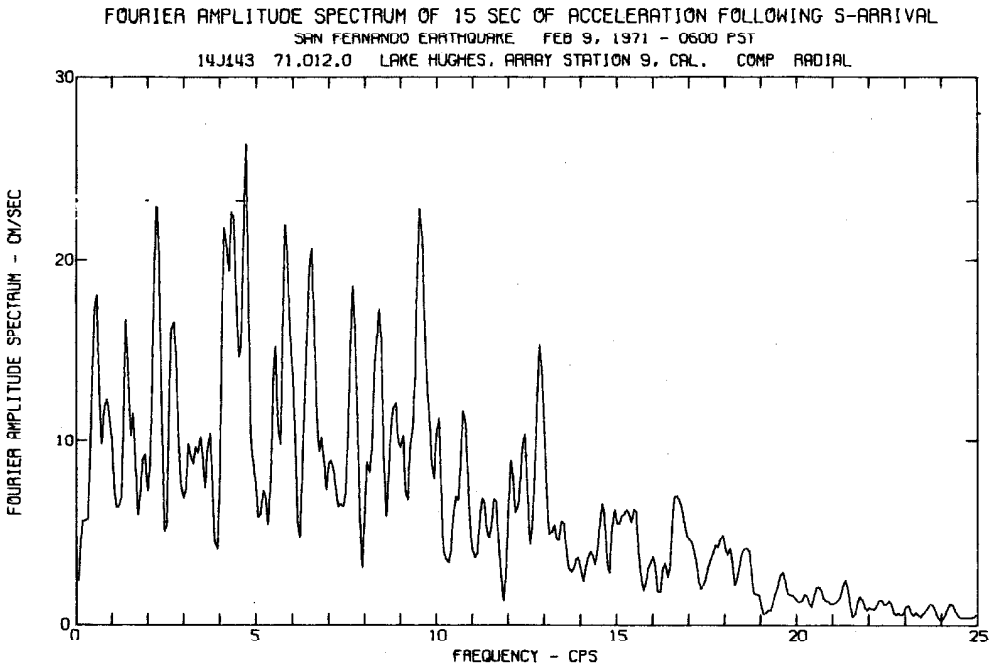
FOURIER AMPLITUDE SPECTRUM OF 15 SEC OF ACCELERATION FOLLOWING S-ARRIVAL
SAN FERNANDO EARTHQUAKE FEB 9, 1971 - 0600 PST
14J143 71.012.0 LAKE HUGHES, ARRAY STATION 9, CAL. COMP RADIAL
FOURIER AMPLITUDE SPECTRUM - CM/SEC
FREQUENCY - CPS
0
10
20
30
0
5
10
15
20
25

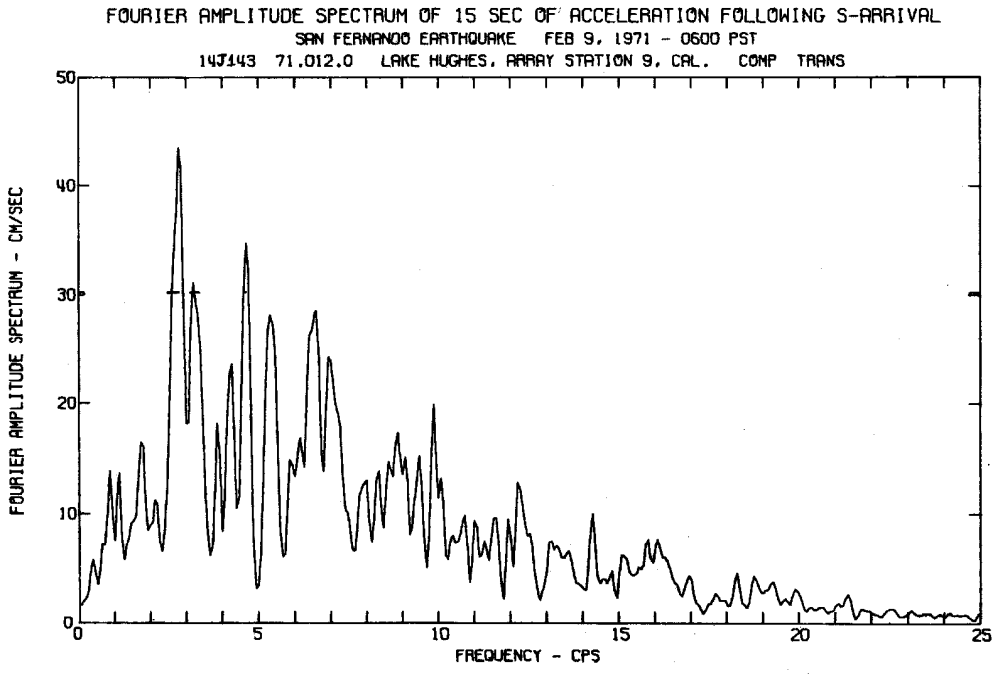
FOURIER AMPLITUDE SPECTRUM OF 15 SEC OF ACCELERATION FOLLOWING S-ARRIVAL
SAN FERNANDO EARTHQUAKE FEB 9, 1971 - 0600 PST
14J143 71.012.0 LAKE HUGHES, ARRAY STATION 9, CAL. COMP TRANS
FOURIER AMPLITUDE SPECTRUM - CM/SEC
FREQUENCY - CPS
0
10
20
30
40
50
0
5
10
15
20
25

Figure 2.20(b).

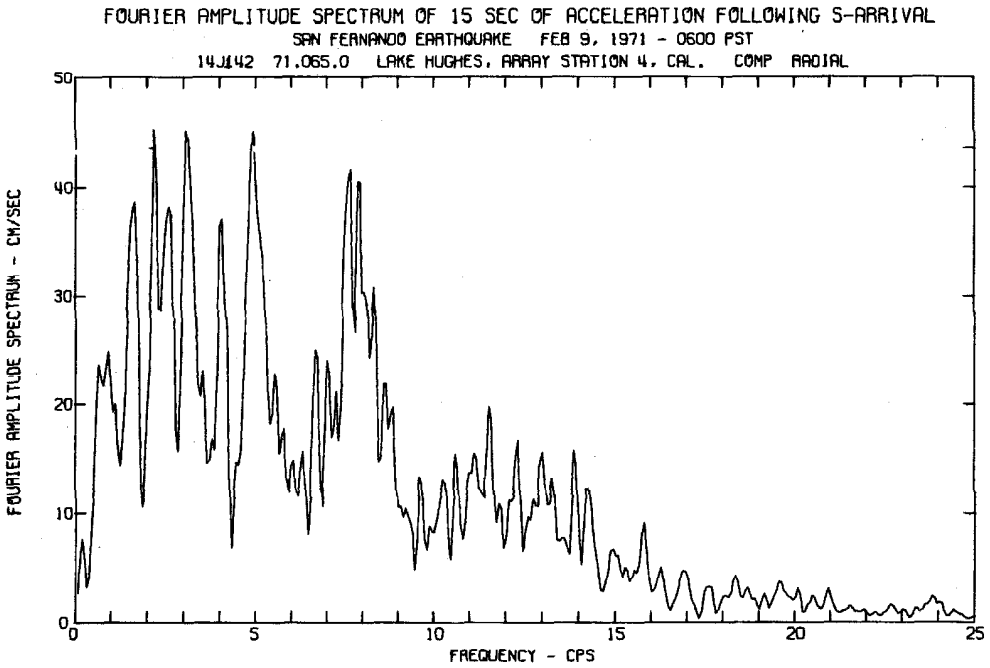
FOURIER AMPLITUDE SPECTRUM OF 15 SEC OF ACCELERATION FOLLOWING S-ARRIVAL
SAN FERNANDO EARTHQUAKE FEB 9, 1971 - 0600 PST
14J142 71.065.0 LAKE HUGHES, ARRAY STATION 4, CAL. COMP RADIAL
FOURIER AMPLITUDE SPECTRUM - CM/SEC
FREQUENCY - CPS
0
10
20
30
40
50
0
5
10
15
20
25

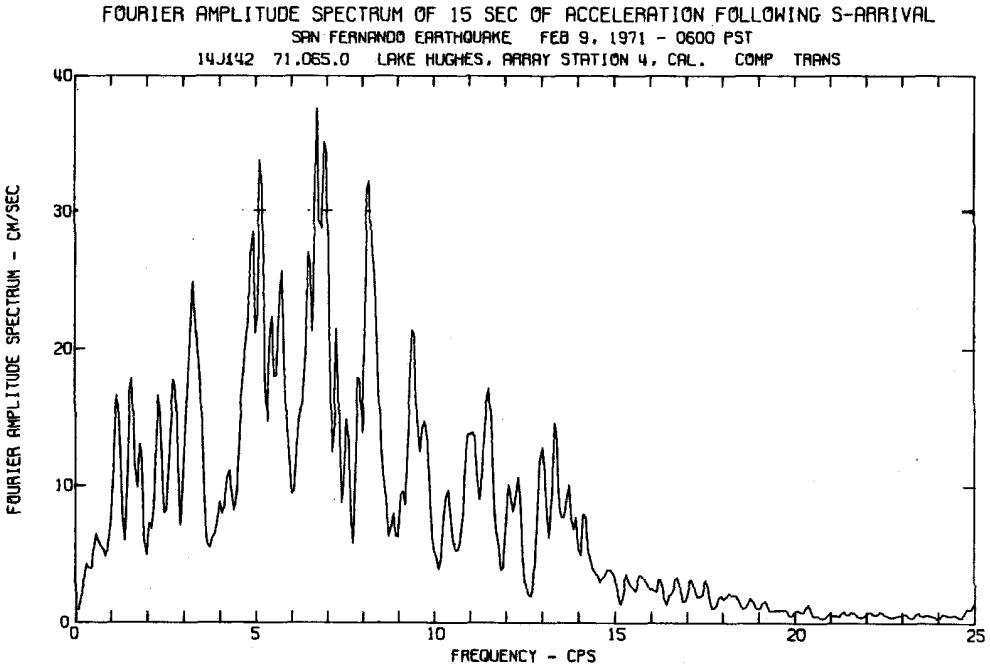
FOURIER AMPLITUDE SPECTRUM OF 15 SEC OF ACCELERATION FOLLOWING S-ARRIVAL
SAN FERNANDO EARTHQUAKE FEB 9, 1971 - 0600 PST
14J142 71.065.0 LAKE HUGHES, ARRAY STATION 4, CAL. COMP TRANS
FOURIER AMPLITUDE SPECTRUM - CM/SEC
FREQUENCY - CPS
0
10
20
30
40
0
5
10
15
20
25

Figure 2.20(c).

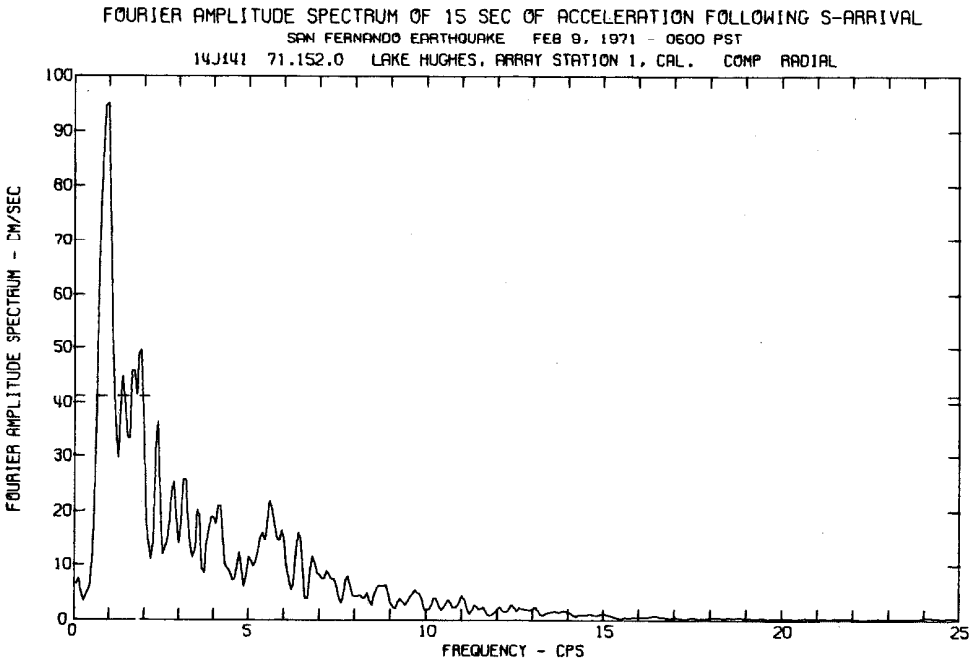
FOURIER AMPLITUDE SPECTRUM OF 15 SEC OF ACCELERATION FOLLOWING S-ARRIVAL
SAN FERNANDO EARTHQUAKE FEB 9, 1971 - 0600 PST
14J141 71.152.0 LAKE HUGHES, ARRAY STATION 1, CAL. COMP RADIAL
FOURIER AMPLITUDE SPECTRUM - CM/SEC
FREQUENCY - CPS
0
10
20
30
40
50
60
70
80
90
100
5
15
25

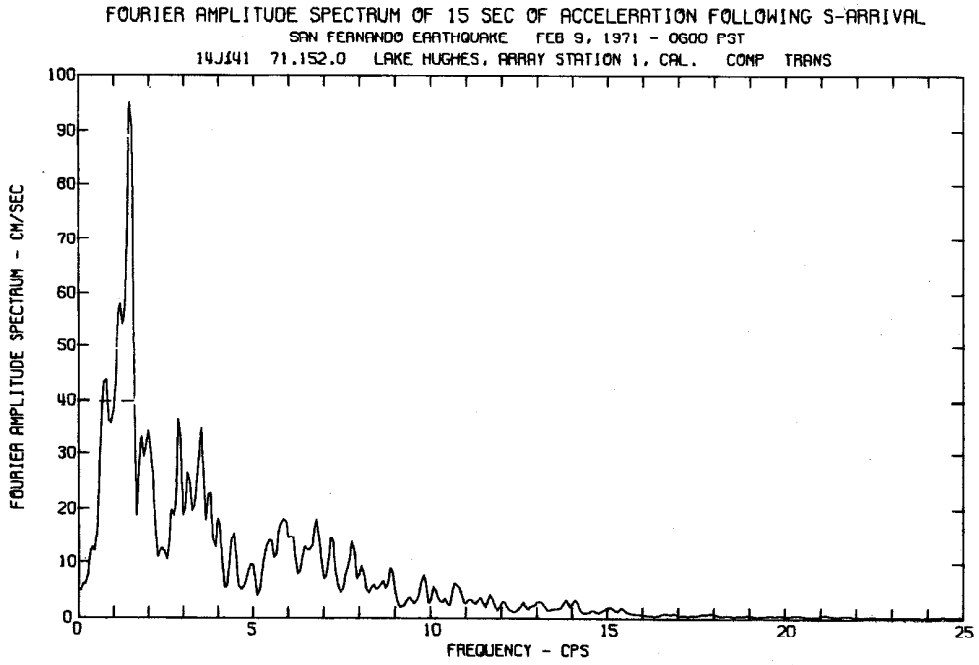
FOURIER AMPLITUDE SPECTRUM OF 15 SEC OF ACCELERATION FOLLOWING S-ARRIVAL
SAN FERNANDO EARTHQUAKE FEB 9, 1971 - 0600 PST
14J141 71.152.0 LAKE HUGHES, ARRAY STATION 1, CAL. COMP TRANS
FOURIER AMPLITUDE SPECTRUM - CM/SEC
FREQUENCY - CPS
0
10
20
30
40
50
60
70
80
90
100
5
15
25

Figure 2.20(d).

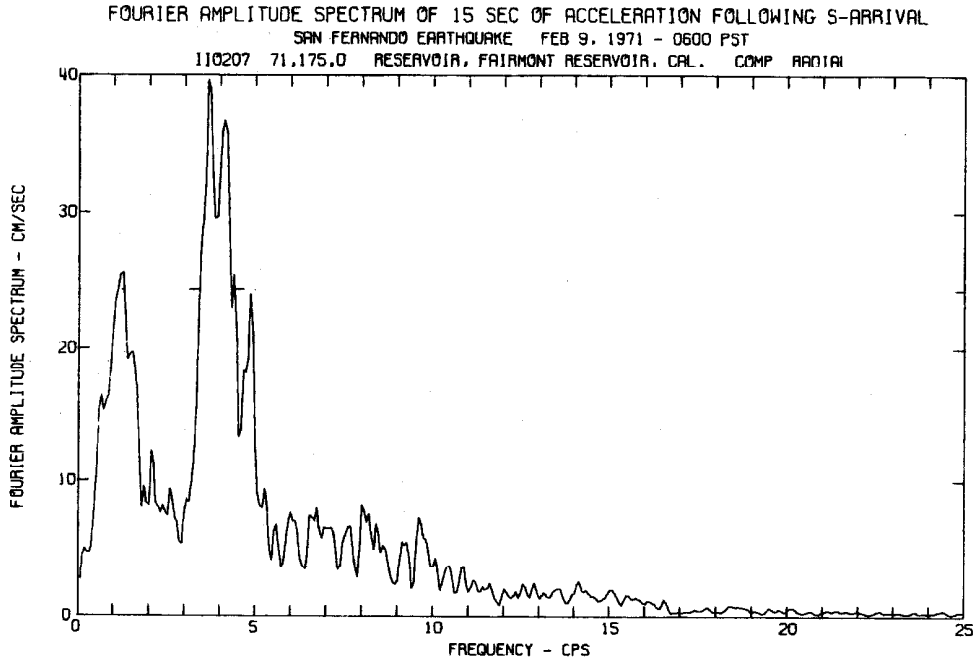
FOURIER AMPLITUDE SPECTRUM OF 15 SEC OF ACCELERATION FOLLOWING S-ARRIVAL
SAN FERNANDO EARTHQUAKE FEB 9, 1971 - 0600 PST
110207 71,175,0 RESERVOIR, FAIRMONT RESERVOIR, CAL. COMP RADIAL
FOURIER AMPLITUDE SPECTRUM - CM/SEC
FREQUENCY - CPS
0
10
20
30
40
5
15
25

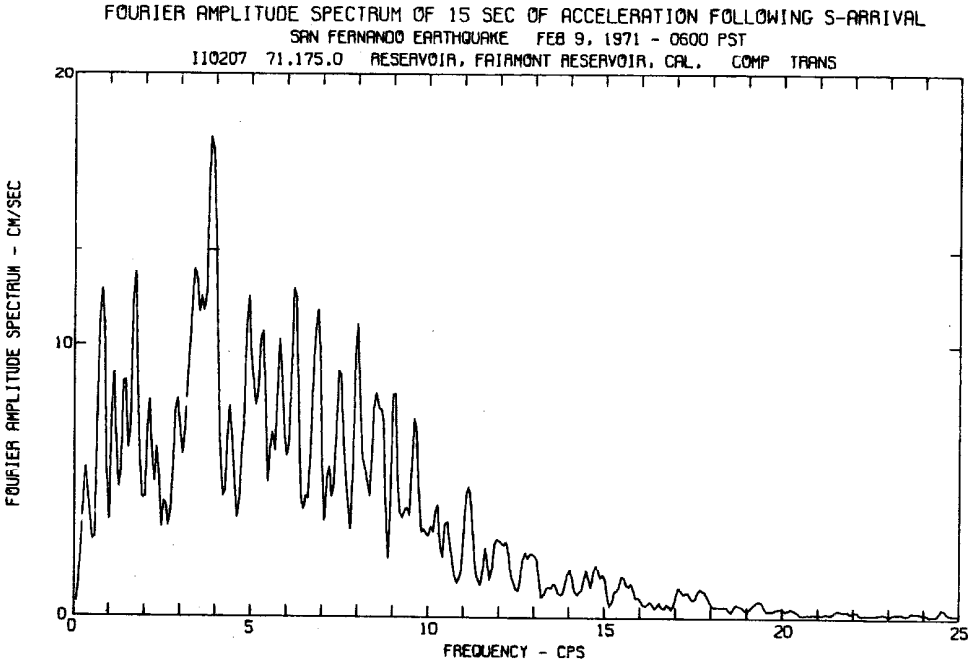
FOURIER AMPLITUDE SPECTRUM OF 15 SEC OF ACCELERATION FOLLOWING S-ARRIVAL
SAN FERNANDO EARTHQUAKE FEB 9, 1971 - 0600 PST
110207 71,175,0 RESERVOIR, FAIRMONT RESERVOIR, CAL. COMP TRANS
FOURIER AMPLITUDE SPECTRUM - CM/SEC
FREQUENCY - CPS
0
10
20
5
15
25

Figure 2.20(e).

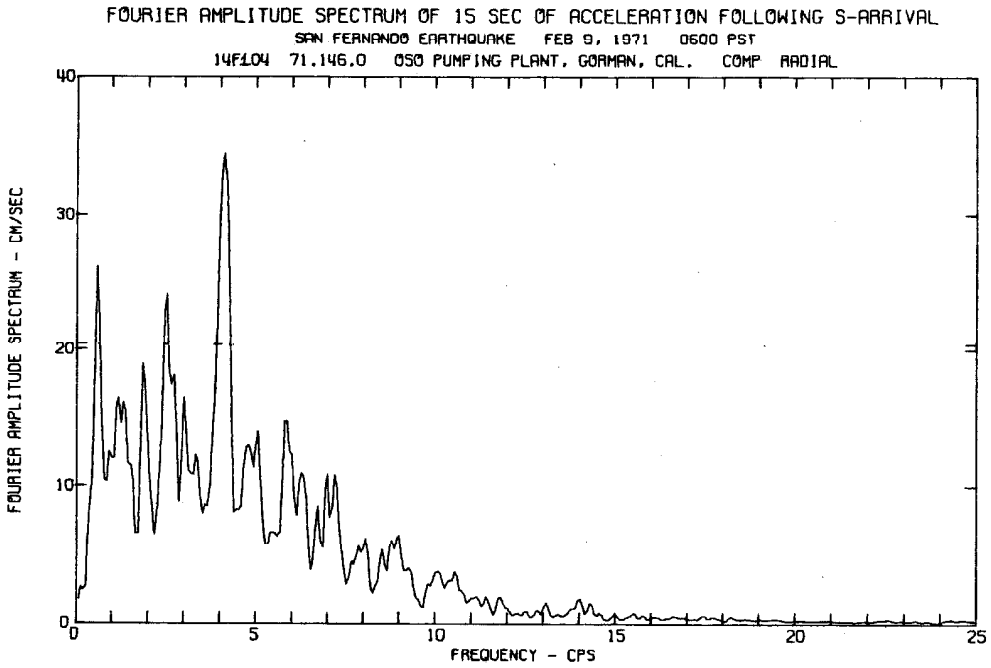
FOURIER AMPLITUDE SPECTRUM OF 15 SEC OF ACCELERATION FOLLOWING S-ARRIVAL
SAN FERNANDO EARTHQUAKE FEB 9, 1971 0600 PST
14F104 71.146.0 OSO PUMPING PLANT, GORMAN, CAL. COMP RADIAL
FOURIER AMPLITUDE SPECTRUM - CM/SEC
FREQUENCY - CPS
0
10
20
30
40
0
5
10
15
20
25

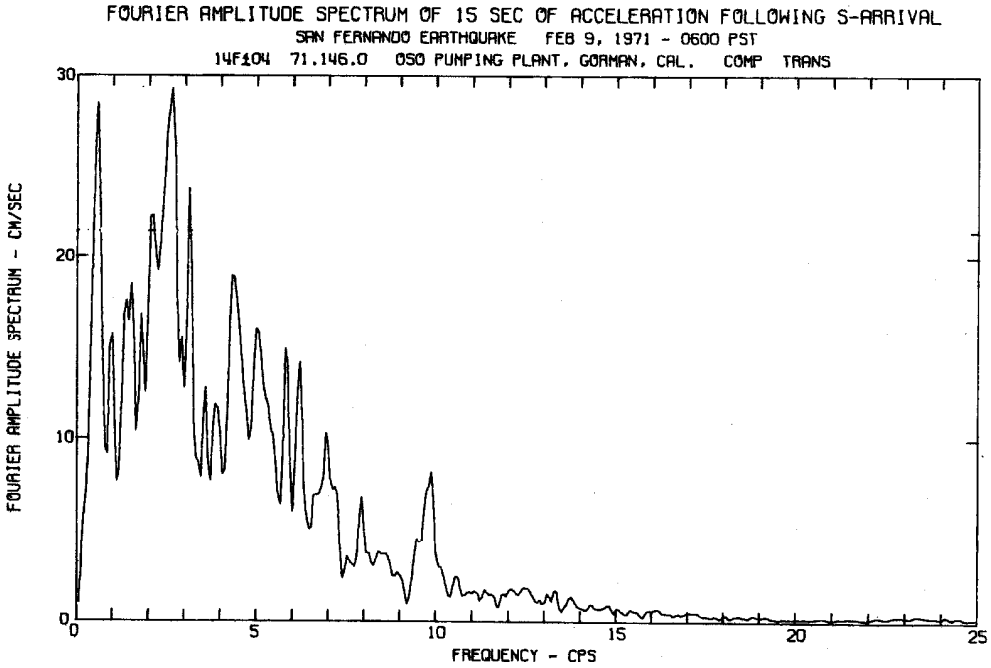
FOURIER AMPLITUDE SPECTRUM OF 15 SEC OF ACCELERATION FOLLOWING S-ARRIVAL
SAN FERNANDO EARTHQUAKE FEB 9, 1971 - 0600 PST
14F104 71.146.0 OSO PUMPING PLANT, GORMAN, CAL. COMP TRANS
FOURIER AMPLITUDE SPECTRUM - CM/SEC
FREQUENCY - CPS
0
10
20
30
0
5
10
15
20
25

Figure 2.20(f).

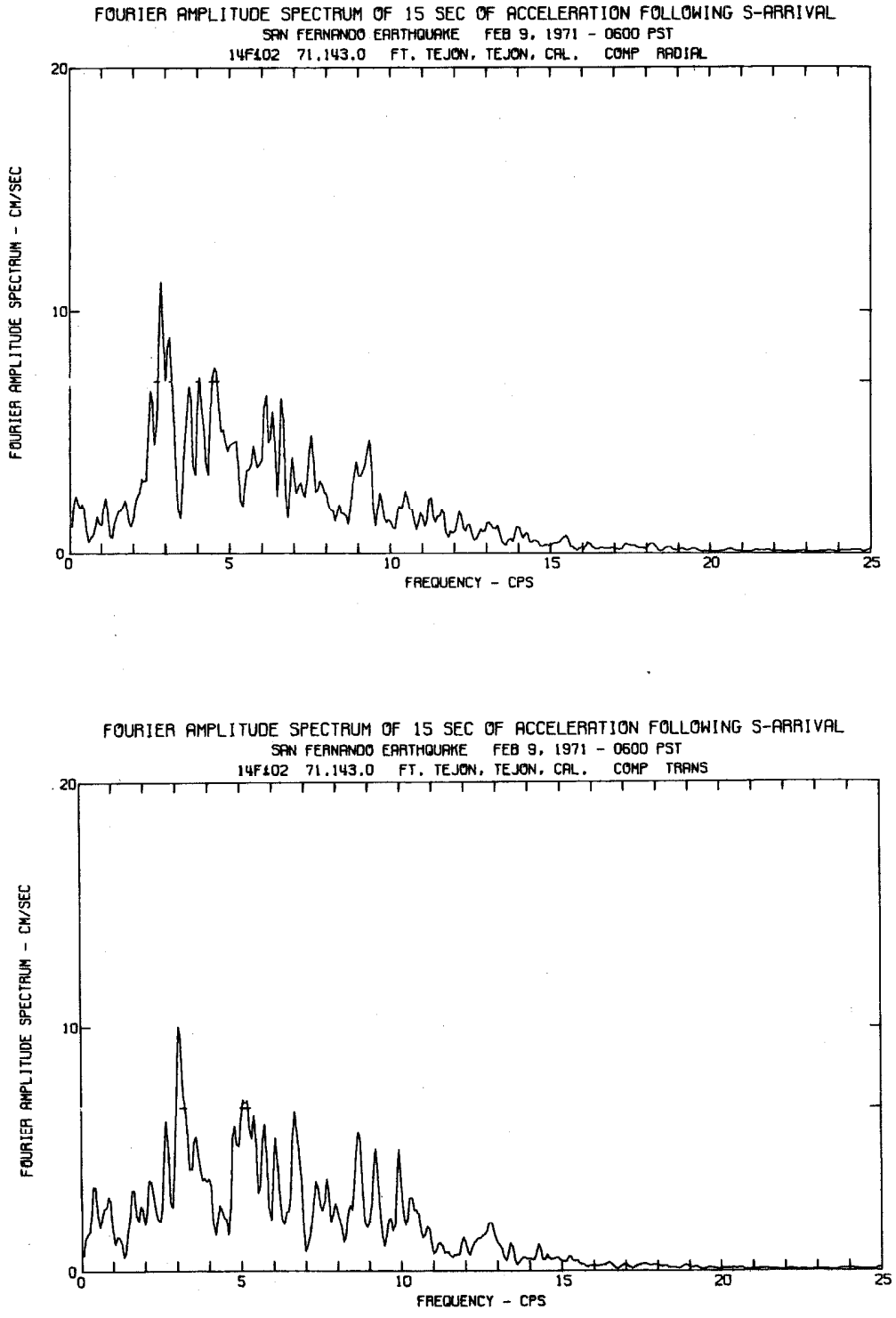
FOURIER AMPLITUDE SPECTRUM OF 15 SEC OF ACCELERATION FOLLOWING S-ARRIVAL
SAN FERNANDO EARTHQUAKE FEB 9, 1971 - 0600 PST
14F102 71.143.0 FT. TEJON, TEJON, CAL. COMP RADIAL
FOURIER AMPLITUDE SPECTRUM - CM/SEC
FREQUENCY - CPS
0
5
10
15
20
25
FOURIER AMPLITUDE SPECTRUM OF 15 SEC OF ACCELERATION FOLLOWING S-ARRIVAL
SAN FERNANDO EARTHQUAKE FEB 9, 1971 - 0600 PST
14F102 71.143.0 FT. TEJON, TEJON, CAL. COMP TRANS
FOURIER AMPLITUDE SPECTRUM - CM/SEC
FREQUENCY - CPS

Figure 2.20(g).

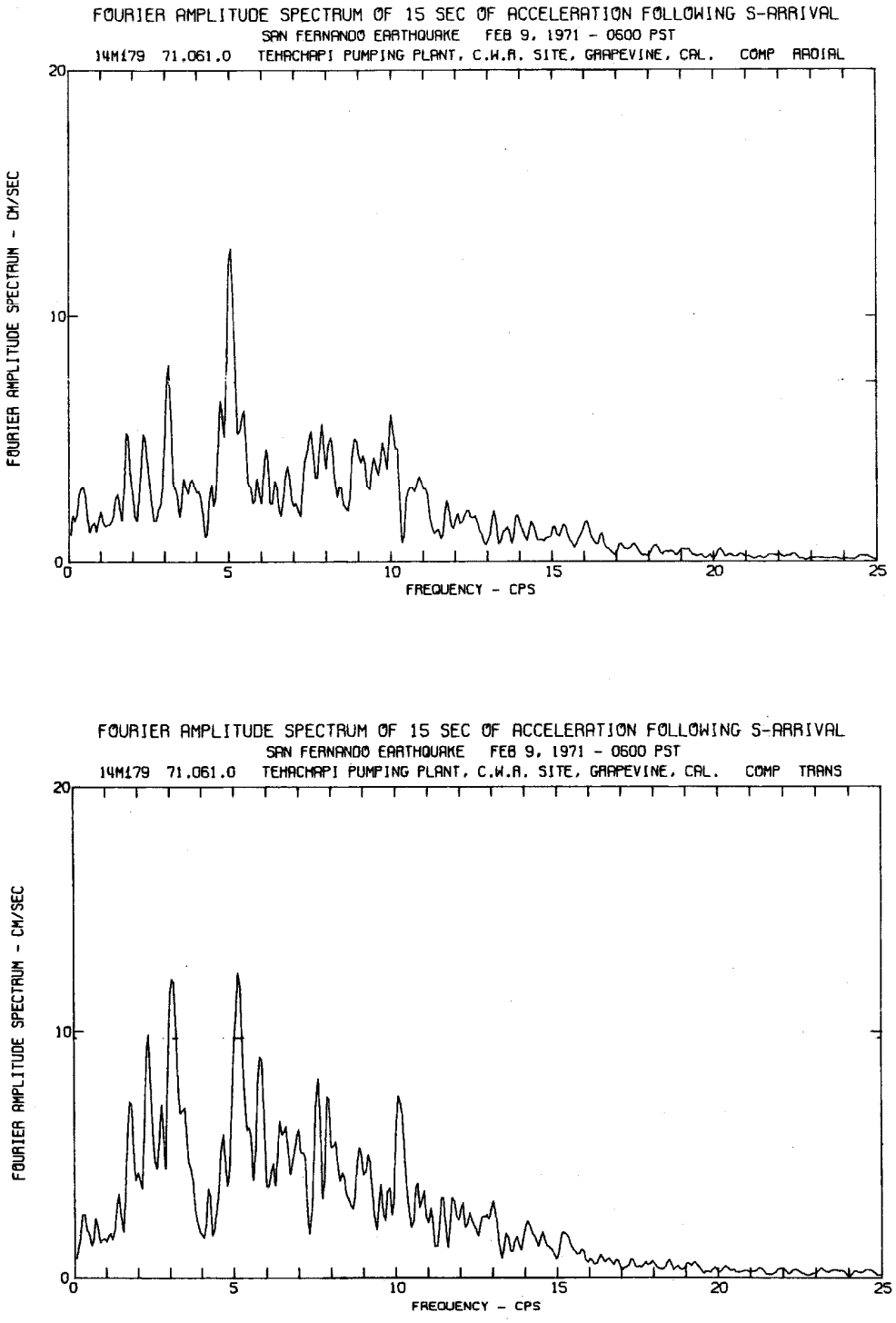
FOURIER AMPLITUDE SPECTRUM OF 15 SEC OF ACCELERATION FOLLOWING S-ARRIVAL
SAN FERNANDO EARTHQUAKE FEB 9, 1971 - 0600 PST
14M179 71.061.0 TEHACHAPI PUMPING PLANT, C.W.A. SITE, GRAPEVINE, CAL. COMP RADIAL
FOURIER AMPLITUDE SPECTRUM - CM/SEC
FREQUENCY - CPS
FOURIER AMPLITUDE SPECTRUM OF 15 SEC OF ACCELERATION FOLLOWING S-ARRIVAL
SAN FERNANDO EARTHQUAKE FEB 9, 1971 - 0600 PST
14M179 71.061.0 TEHACHAPI PUMPING PLANT, C.W.A. SITE, GRAPEVINE, CAL. COMP TRANS
FOURIER AMPLITUDE SPECTRUM - CM/SEC
FREQUENCY - CPS

Figure 2.20(h).

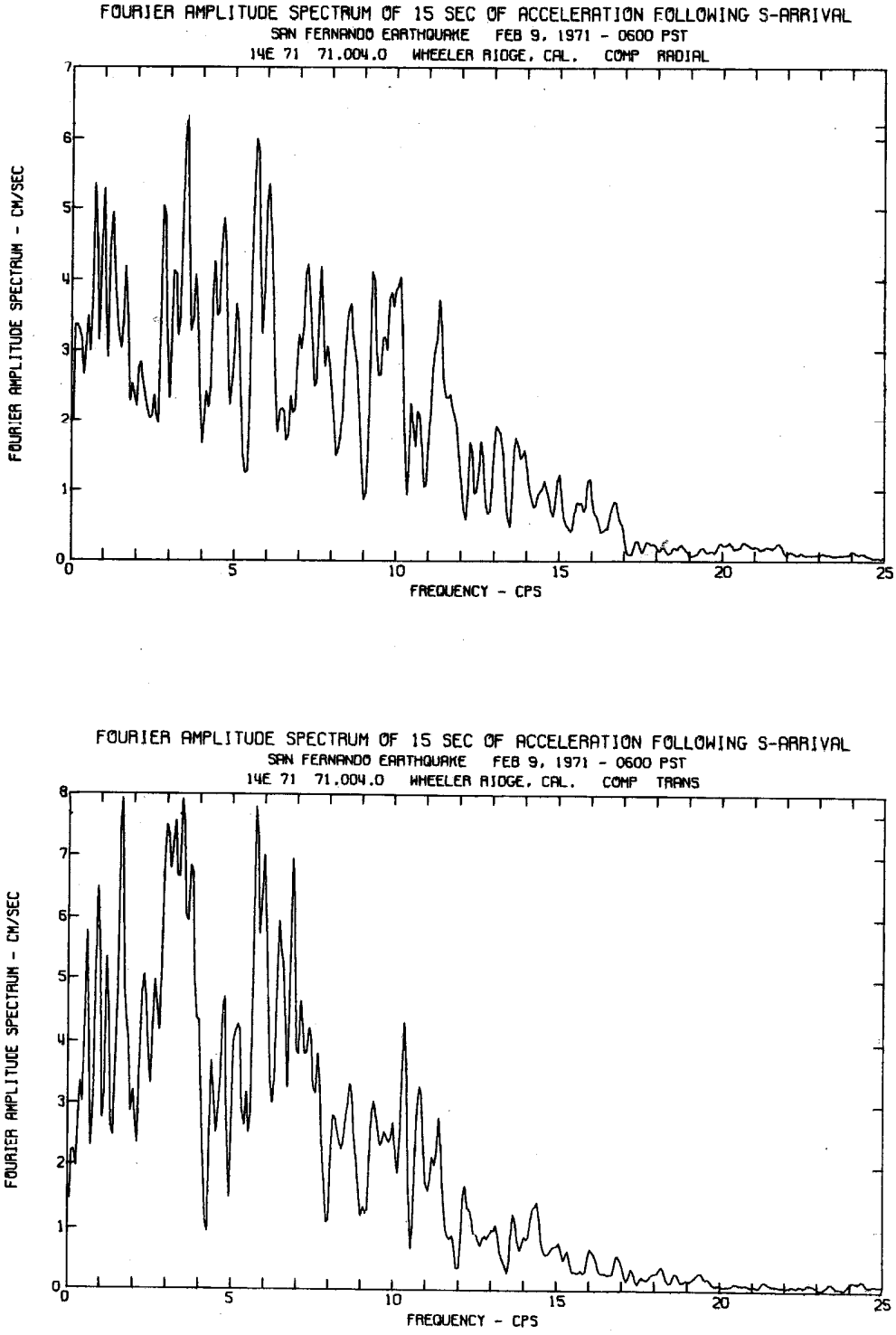
FOURIER AMPLITUDE SPECTRUM OF 15 SEC OF ACCELERATION FOLLOWING S-ARRIVAL
SAN FERNANDO EARTHQUAKE FEB 9, 1971 - 0600 PST
14E 71 71.004.0 WHEELER RIDGE, CAL. COMP RADIAL
FOURIER AMPLITUDE SPECTRUM - CM/SEC
FREQUENCY - CPS
FOURIER AMPLITUDE SPECTRUM OF 15 SEC OF ACCELERATION FOLLOWING S-ARRIVAL
SAN FERNANDO EARTHQUAKE FEB 9, 1971 - 0600 PST
14E 71 71.004.0 WHEELER RIDGE, CAL. COMP TRANS
FOURIER AMPLITUDE SPECTRUM - CM/SEC
FREQUENCY - CPS

Figure 2.20(i).

in the fault fracture zone. Continuing to the next site, O207, the Fairmont reservoir, the spectrum of the transverse component is similar to those of the closer, basement rock sites, but with a generally lower level of amplitude consistent with its greater focal distance. The radial component, however, shows two broad spikes centered around 1 Hz and 4 Hz. Since the instrument is located on basement rock and not on the dam, no explanation can be found for these peaks, which are 2.5 to 4 times the height of the general level of the spectrum.

The general pattern of higher spectral amplitudes at sedimentary sites than at basement rock sites of comparable focal distance continues to be evident in the remaining four sites of the group. These are F104 and E071 on deep sediments, and F102 on crystalline basement rock. Site M179 has a 15 foot layer of alluvium overlying basement rock. This should affect only high frequencies, since for example, assuming a shear velocity of 600 feet/sec, the fundamental natural frequency of shear vibration of the alluvial layer is 10 Hz. Since 600 feet/sec is a low, but not unreasonable value for recent alluvium, it is quite likely that the relatively high spectral level above about 7 Hz is caused by local amplification. However, below this frequency, the record should reflect essentially basement rock behavior.

2.8.1. Winnowing the northern data.

Let us first examine J141, site No. 1 in the Lake Hughes accelerograph array, to see if an explanation can be found for the high spectral peaks between 0.5 and 2 Hz in both components. The

accelerograph is located in the Lake Hughes Township Post Office. The town is situated on the floor of a south-eastward trending valley which coincides with the San Andreas Fault, and which has been formed by it. At Lake Hughes, topographical maps show the width of the valley ranging from approximately 600 to 1000 feet, and this is probably the approximate width of the fracture zone of the fault at this point. A geologic cross-section through the fault some miles to the south-east (Woodward-Lundgren, 1973) shows the fault zone to be approximately 1000 feet wide, containing fracture material between vertical faces of sound granitic basement rock. It is probable that a similar configuration exists at Lake Hughes. The log of a water well drilled in the fault zone approximately 200 feet west of the accelerograph site and included in the Woodward-Lundgren (1973) report sheds light on the nature of the fault zone material. It records an 860 feet thick layer of sands and clay over harder sand layers. Duke et al. (1971) conducted a seismic survey of the surficial soils at the site and found $\alpha = 1870$ ft/sec and $\beta = 1070$ ft/sec for these soils.

Assuming that the sides of the fault fracture zone are, in fact, vertical and consist of sound rock and that the base of the 860 foot softer layer is horizontal and that material below this level is substantially stiffer than that above it, the upper layer of the fracture zone may be approximated by a long, rectangular elastic body with three rigid boundaries and a free surface. Wood (1973) has solved the plane strain vibration problem for such a body. As noted above, the width of the valley floor at Lake Hughes lies between

about 700 and 1000 feet. Since the presence of the fault has created the valley, it is reasonable to assume that the fault zone width at Lake Hughes is also in this range. Assuming for convenience a width equal to the depth of the soft fault-zone layer, that is 860 feet, and assuming elastic constants corresponding to the wave velocities noted above,the lower several natural frequencies of the fracture zone calculated from Wood's results are shown in Table 2. 11. The amplitude spectrum of the N21E accelerogram component which is approximately transverse to the fault at Lake Hughes, is shown in Figure 2. 21 with the natural frequencies from Table 2. 11 superimposed. The agreement between spectral peaks and the computed natural frequencies is remarkably good and it suggests that the anomalously high peaks at J141 were, indeed, caused by resonant response of the soft, crushed material in the fault shatter zone. Because of the nonlinearity of soil materials, it is probable that the response of higher modes would be severely damped, and this appears to be the case, since the spectral peaks are much less pronounced at frequencies above about 2 Hz.

While it is probable that the actual fault zone width is within the range defined by the valley topography, the assumed value of 860 feet may well be incorrect, thus the effect of an error in the assumption should be examined. If the actual width were greater, it can be seen from Wood's Figure 3. 2, that the fundamental frequency $f_{1,1}$ would decrease slowly to a limiting value of nearly half that shown in Table 2. 10, i. e. to about 0. 31 Hz. Thus the effect on our

TABLE 2.11.

Estimated lower natural frequencies of San Andreas Fault fracture zone at Lake Hughes

Mode number	Frequency $f_{n,m}$, Hz							
n \ m	1	2	3	4	5	6	7	8
1	0.65	1.0	1.4	1.5	2.2	2.3	2.9	3.1
2	1.1	1.6	2.0	2.3	2.7	2.7	3.2	3.4

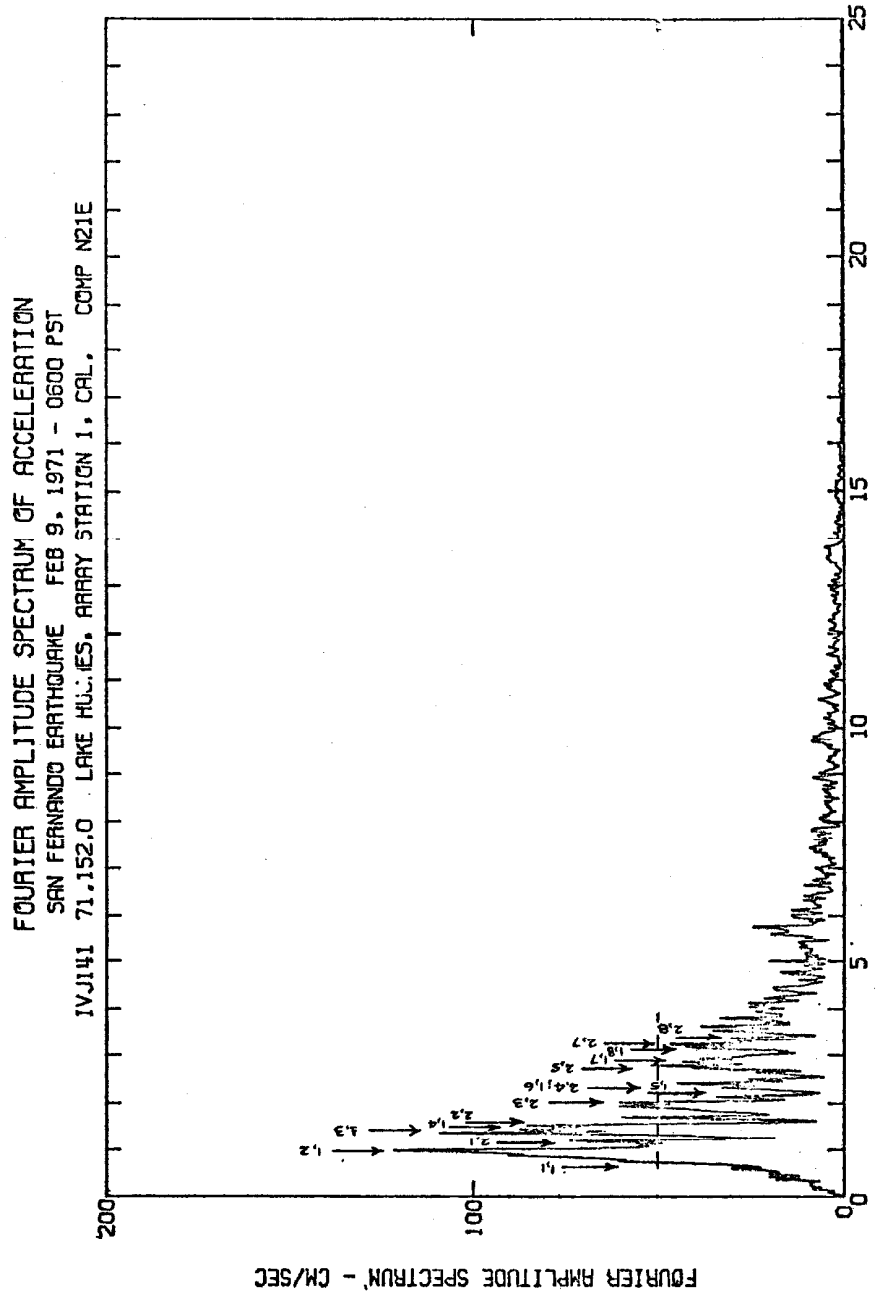

Figure 2.21. Natural frequencies computed from Wood's solution, for the San Andreas fault zone at Lake Hughes.

argument of underestimating the fracture zone width is not great. However, widths less than the assumed value may cause large increases in the fundamental frequency. A width of 500 feet, for example, gives $f_{1,1} = 1$ Hz. At smaller values, fault width becomes the governing dimension, and $f_{1,1}$ tends to increase in inverse proportion to fault width.

From this analysis, it is reasonable to assume that the relatively high spectral peaks below about 3-5 Hz are caused by the unusual site conditions, and accordingly 0.4, 1, and 2 Hz data were taken out of the northern set.

Anomalous peaks in the spectra of O207 and M179 were noted in the previous section. Some data from these records were also removed during parameter estimation. All data eliminated from the northern set are shown in Table 2.12.

2.8.2. Attenuation of northern data.

Smoothed Fourier amplitudes at 0.4, 1, 2, 4, 8, and 16 Hz from the northern group of 15-second accelerograms are plotted against hypocentral distance in Figure 2.22. Data points from basement rock sites are marked by a shaded background. Points excluded from the set are plotted but are labeled and have a cross drawn over them.

Several observations can be made from these figures. As before, the data show an overall pattern of attenuation with increasing distance and increasing frequency. With fewer data, the trends are not as regular, but they are present.

TABLE 2.12.

Data winnowed from northern group

Record	Frequency	Component
J141	0.5, 1, 2 Hz	both
O207	0.5, 1, 4 Hz	radial only
M179	8, 16 Hz	both

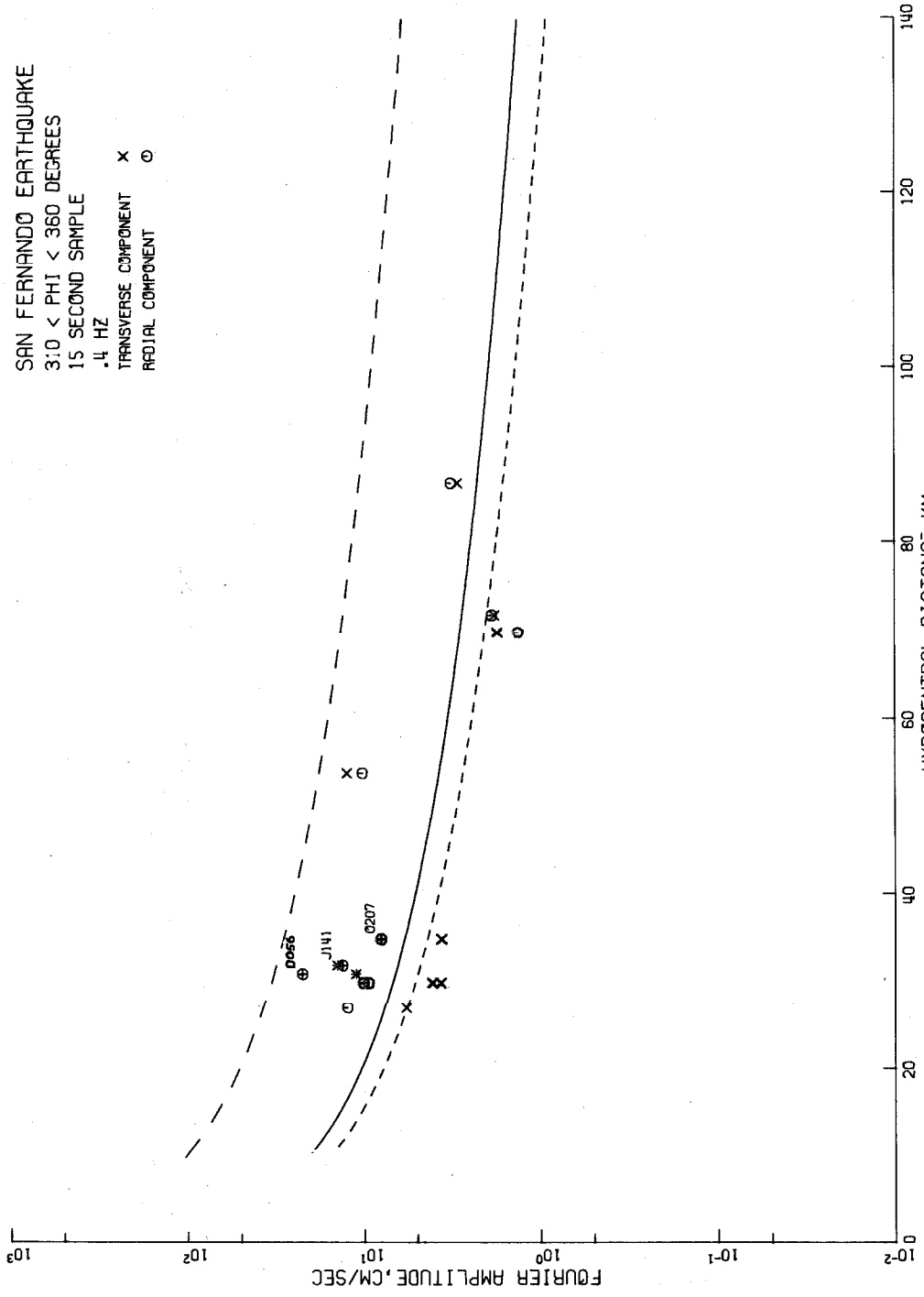

Figure 2.22(a) Fourier amplitudes of acceleration, northern, M5H15 data. Solid line shows "best fit" to all data ($Q = 700$ and $A = 210$ cm/sec); short-dashed line, "best fit" to basement site data only, which are shown with a shaded background; long-dashed line from southern M5H15 data.

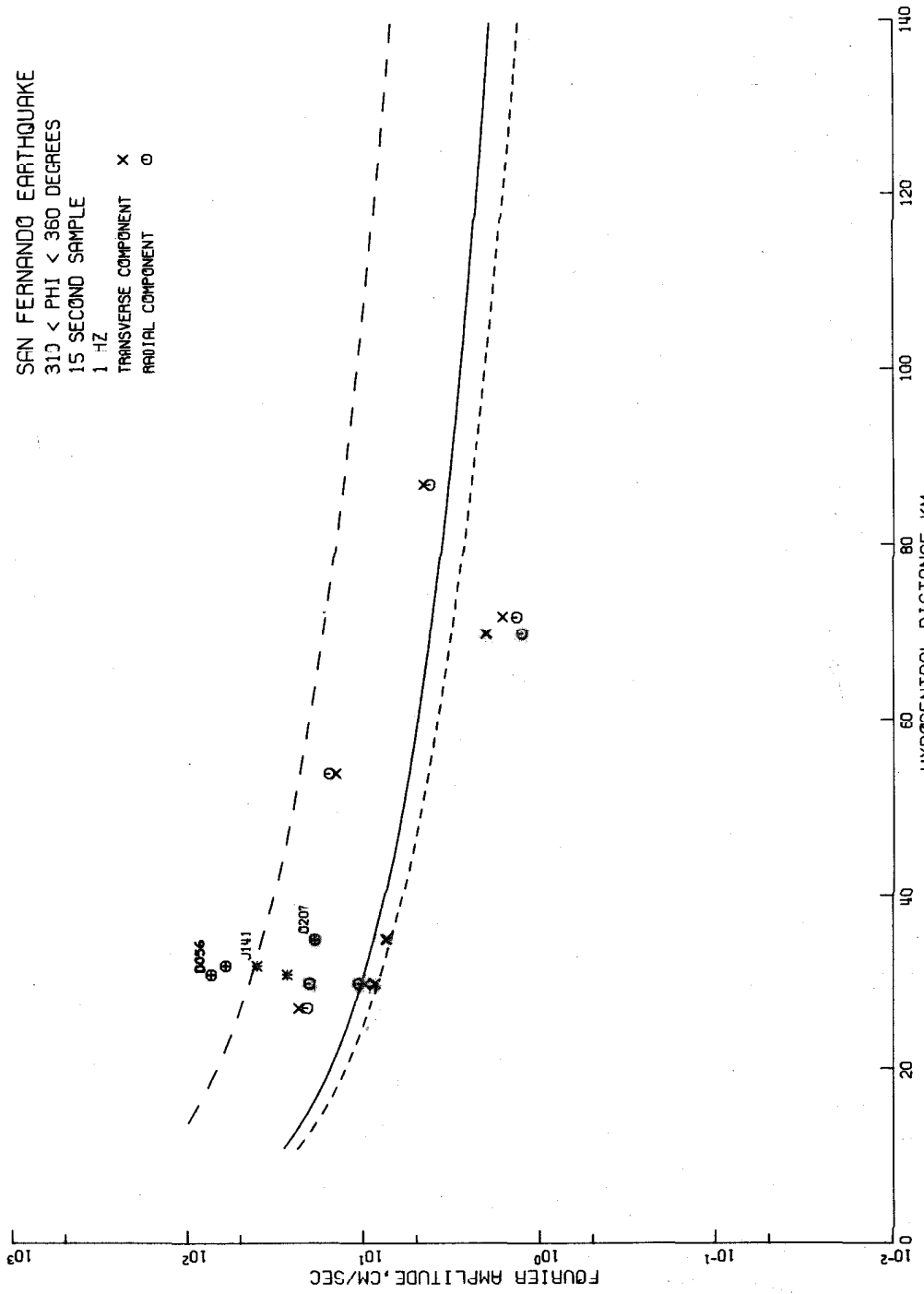

Figure 2.22(b). A = 320 for solid line.

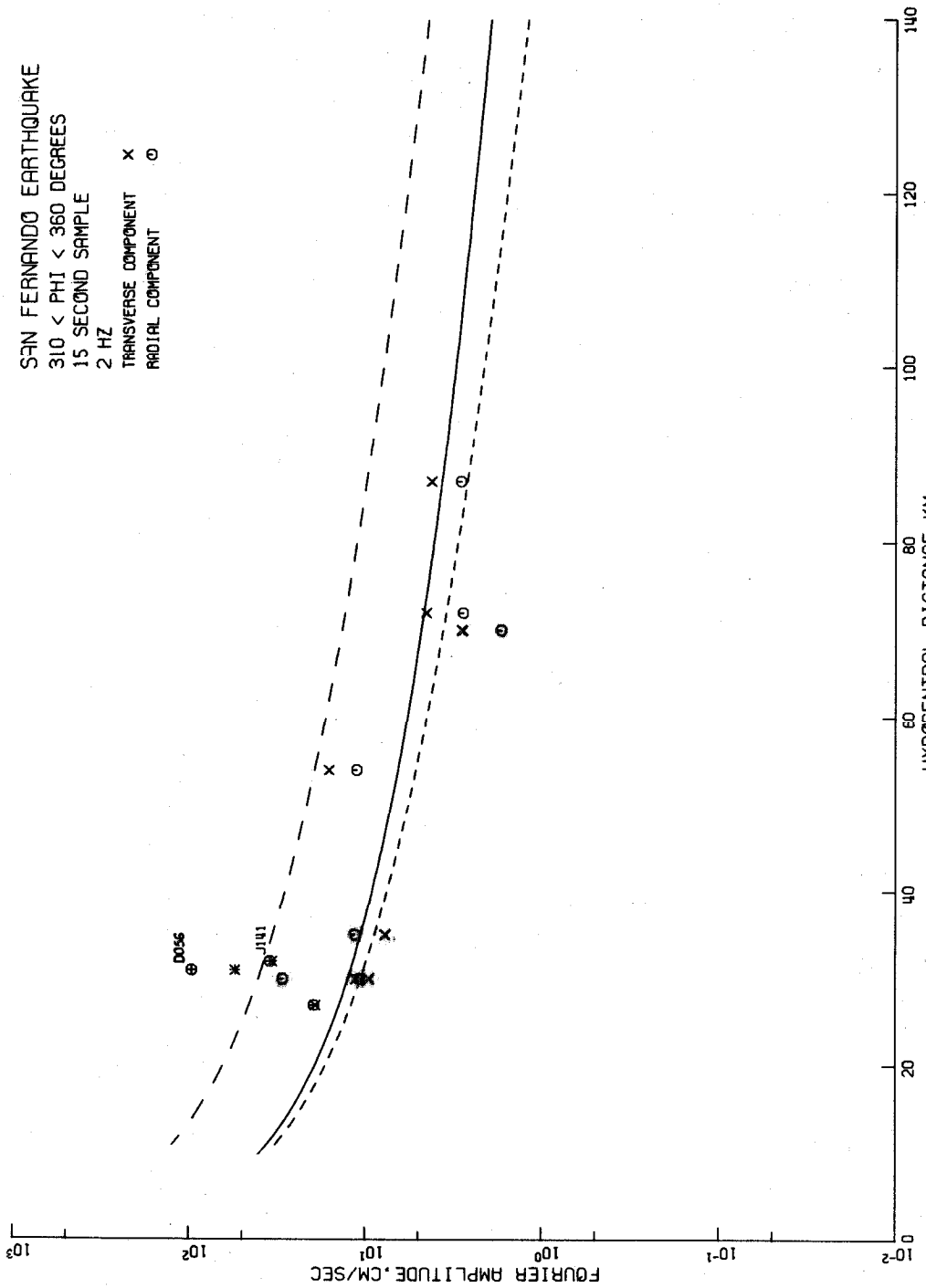

Figure 2.22(c). A = 410 for solid line.

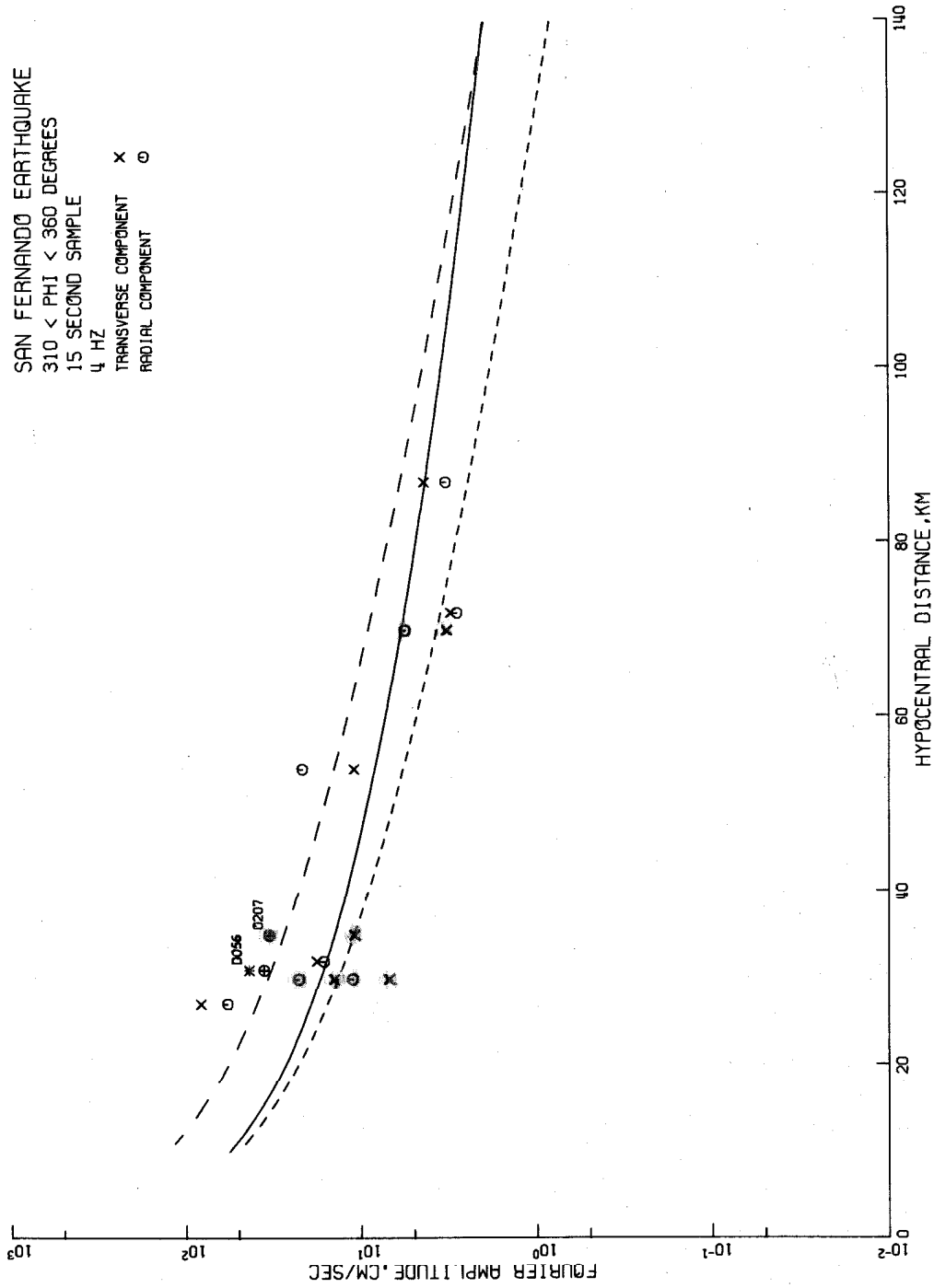

Figure 2.22(d). A = 600 for solid line.

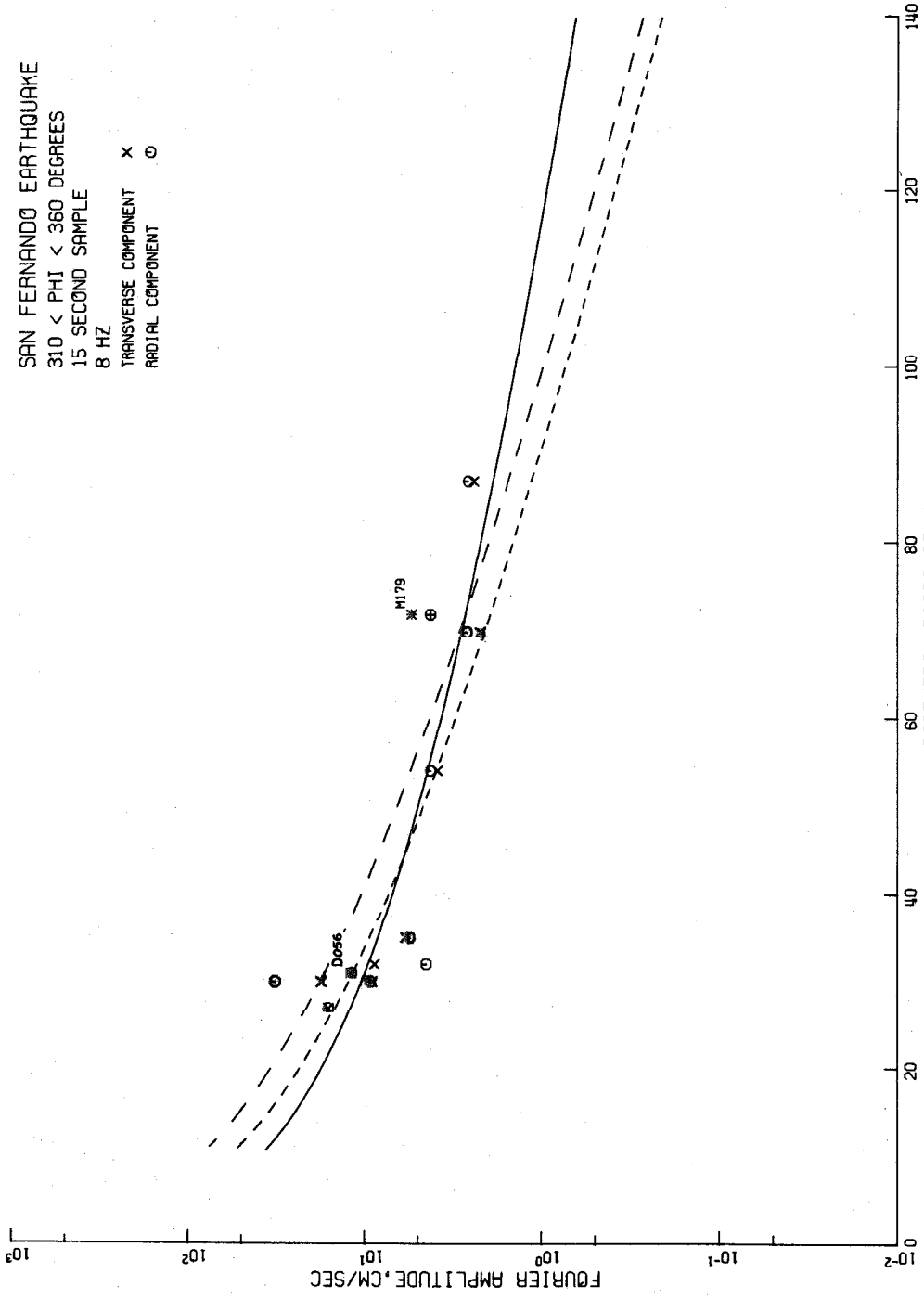

Figure 2.22(e). A = 440 for solid line.

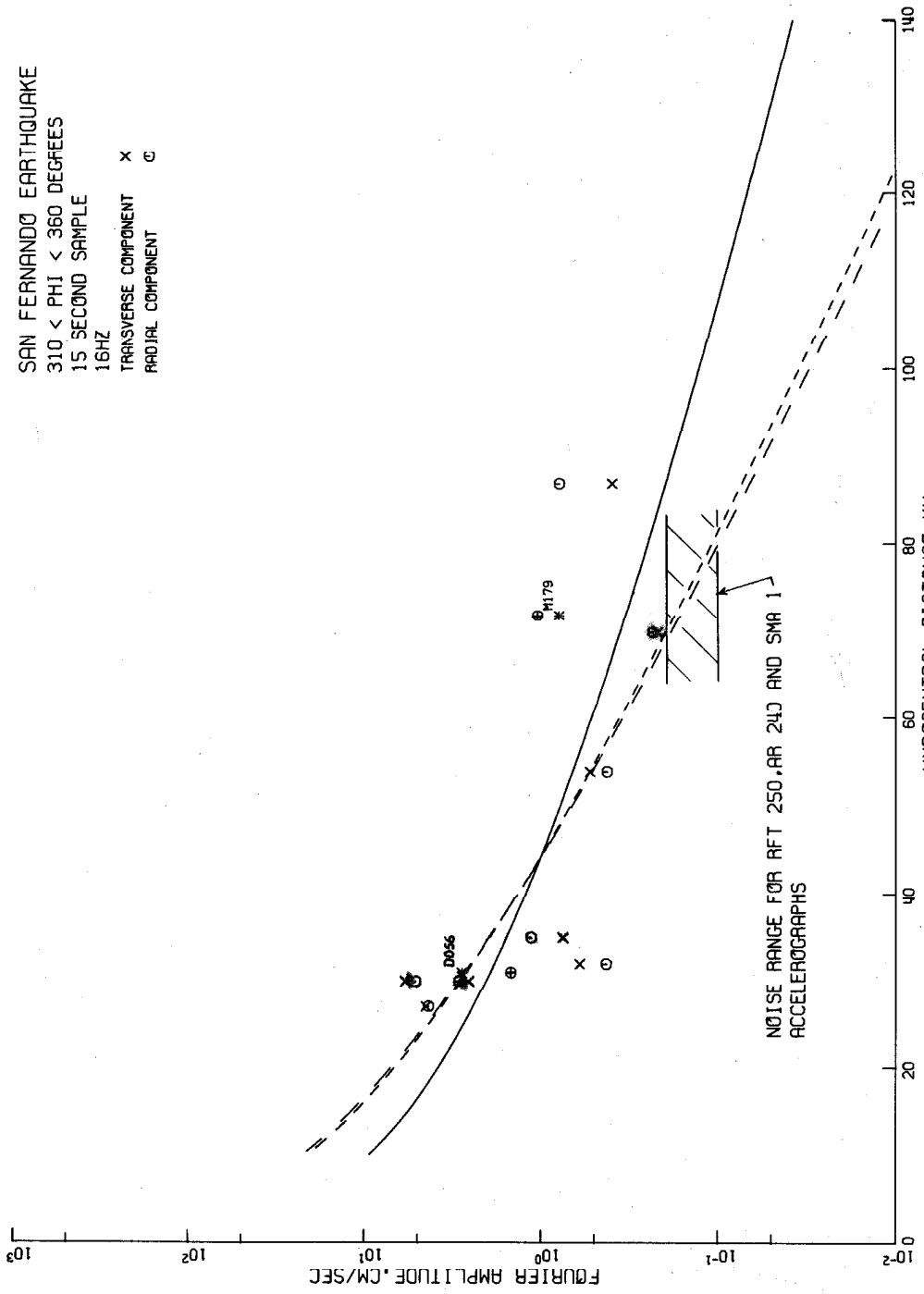

Figure 2.22(f). A = 120 for solid line.

At the lower frequencies, 0.4 to 4 Hz, sites on sediments show consistently higher spectral amplitudes than those on basement rock. At 8 and 16 Hz there is little apparent distinction, but values of $\overline{k}$ in Table 2.14 do show that on the average, the sediment site amplitudes are higher. From these diagrams, and from the corresponding spectra in Figure 2.20, it appears that propagation through sedimentary paths in this region results in a broad-band amplification of ground motion, which is particularly marked in frequency components below about 8 Hz. At higher frequencies this is not so apparent, possibly due to greater material attenuation of the high frequency components [note that f occurs as a multiplier in the attenuation exponent of equation (2.6).]

The attenuation curves from the southern group M5H15 data are shown in Figure 2.22 by the broken lines with long segments. These are the same as the solid line curves plotted in Figure 2.9. Generally the data, even from sedimentary sites, fall below these curves, indicating that less energy was radiated to the north than to the south. This point is investigated further in Chapter 3.

Because of the small number of data, it is difficult to compare the scatter with that of the southern data. However, excluding D056 which may be influenced by its different source-station azimuth, the amount of scatter appears comparable to that of the southern M5H15 data.

Using the least-squares parameter estimation procedure described in Section 2.6.3, the parameters given in Table 2.13 were

TABLE 2.13.

Attenuation parameters from M5H15 data of northern group

Parameter	Basement rock sites only		Complete group	
	Value	90% confidence interval	Value	90% confidence interval
Q	350	270 - 500	700	500 - 1500
A_1*	160	70 - none found	210 cm/sec	100 - none found
A_2	270	120 - none found	320	160 - none found
A_3	380	180 - none found	410	210 - none found
A_4	570	260 - none found	600	310 - none found
A_5	740	330 - 1520	440	220 - 820
A_6	340	170 - 710	120	60 - 220

*The subscripts 1, 2, . . . , 6 refer to the frequencies 0.4, 1, 2, 4, 8 and 16 Hz respectively.

obtained from the M5H15 data of the northern group. Two estimations were made, one from the basement rock sites alone, and the second from the complete group. The solid lines in Figure 2.22 are given by parameters obtained from the entire group, and the broken line with short segments, is from the basement rock parameters.

Note that the solid curve representing the average amplitude of all sites in the group is generally higher than the curve for basement sites alone, by a factor of about 1.5 to 2. This implies that on the average, the sediment sites are accelerated more strongly.

The significance of the A_i's being smaller than for the southern group is discussed in terms of a propagating rupture, in Chapter 3.

It is seen in the following section that the basement data are much less scattered than the complete group. On the assumption, then, that the A_i's from basement groups are a better estimate of the true A(f), the value of Q for the complete group was estimated again by the least-squares procedure, with the A_i's held fixed at their basement rock values. A Q of 400 was found; but the scatter was greater, with $\sigma_k = 1.05$ for the combined frequency samples, compared with $\sigma_k = 0.84$ for the entire group (see Table 2.14).

When weighing the reliability of these results, the small number of data should be kept in mind. In such a small set, a few extreme points can change the results quite significantly. As an illustration of this, consider the data from E071, Wheeler Ridge at r = 87 km. From Figure 2.22(e) and (f) it is clear that the high amplitudes from E071 at 8 and 16 Hz are the reason for the lower rate of attenuation, and thus large Q value, of the solid curve. If it

TABLE 2.14.

Statistics of k for northern M5H15 data

f (Hz)	All N sites			Basement sites only			Sedimentary sites* w.r.t. basement attenuation curve			All N sites w.r.t. Q=400, $\tilde{A}$ for basement		
	$\bar{k}$	σ_k	m_k	$\bar{k}$	σ_k	m_k	$\bar{k}$	σ_k	m_k	$\bar{k}$	σ_k	m_k
0.4	1.25	0.86	-4.4	1.14	0.60	-2.4	2.14	1.35	-19.0	1.69	1.16	-10.6
1	1.31	0.84	-4.6	1.16	0.71	-3.0	2.03	1.16	-15.0	1.63	1.04	-8.8
2	1.13	0.60	-2.6	1.14	0.70	-2.9	1.66	0.72	-6.6	1.34	0.71	-4.2
4	1.30	1.07	-6.4	1.07	0.44	-1.6	2.42	1.61	-30.4	1.64	1.24	-11.4
8	1.13	0.61	-2.5	1.13	0.67	-2.6	1.43	0.58	-2.2	0.98	0.50	-1.3
16	1.38	1.06	-3.0	1.12	0.56	-2.2	3.39	4.0	-32.2	1.16	1.36	-3.5
Combined samples	1.25	0.84	-3.9	1.13	0.58	-2.5	2.16	1.81	-2.49	1.39	1.05	-5.3

*E071, F104, J144, M179.

were not for these high values, the solid curve representing the overall attenuation of the group would be much closer to the broken line representing basement rock site behavior. In a larger data set, such as the southern group, extreme values in a few data are outweighed by the regular behavior of the majority of data. (This can be demonstrated with the southern data by leaving in the winnowed points – but not the noisy ones – during the least-squares run. The resulting parameters are hardly changed at all.)

2.8.3. Scatter in the northern data.

Statistics of k describing scatter in four subdivisions of the northern data group are given in Table 2.14. Histograms depicting the distribution of scatter for the combined frequency samples are shown for each subdivision in Figures 2.23. The following conclusions can be drawn from the distribution of the k-values:

(1) Data from basement sites only is much less scattered, with $\sigma_k = 0.58$, than the entire group of data, for which $\sigma_k = 0.84$.

(2) However, even the basement sites alone show more scatter than the southern M5H15 data as a whole, for which $\sigma_k = 0.46$. Comparing the standard deviation of the basement k's in Table 2.14 with those of the M5H15 southern data in Table 2.5 at each sampling frequency, it is seen that while the northern basement σ_k's are fairly constant with respect to frequency, the southern group σ_k's increase with increasing frequency. At 16 Hz, both values are about the same, with the lower frequency components of the southern group being less

scattered than their northern, basement counterparts. This cannot be simply related to overall path geology, since the northern sedimentary data are much more scattered again.

(3) The high average value of $\bar{k} = 2.16$ for sedimentary sites alone with respect to the basement attenuation curves indicates that, in this group at least, but probably in general, sedimentary sites were more strongly accelerated than basement sites. From Table 2.13, it is seen that this effect is greatest at low frequencies and decreases, but is still present, at higher frequencies. The high values of k, σ_k and m_3 at 16 Hz are caused almost entirely by data from site E071, which are anomalously high, but no reason could be found for their exclusion.

2.9. South-eastern group.

The other area in which several records were obtained from the San Fernando earthquake within a narrow range of source-station azimuths, is to the south-east of the epicenter. Seven stations have source-station azimuths between 90 and 125 degrees and hypocentral distances ranging from 45 to 109 km. Five of these stations are on basement rock, one (N187) on the crest of an earth dam, and two on sediments of about 1000 feet thick. In order to include a further basement site, G106, closer to the epicenter, the south-eastern boundary of the group was extended to a line from the epicenter with an azimuth of 150 degrees. This added several sites in the easternmost part of the southern group, bring the total number of sites in this

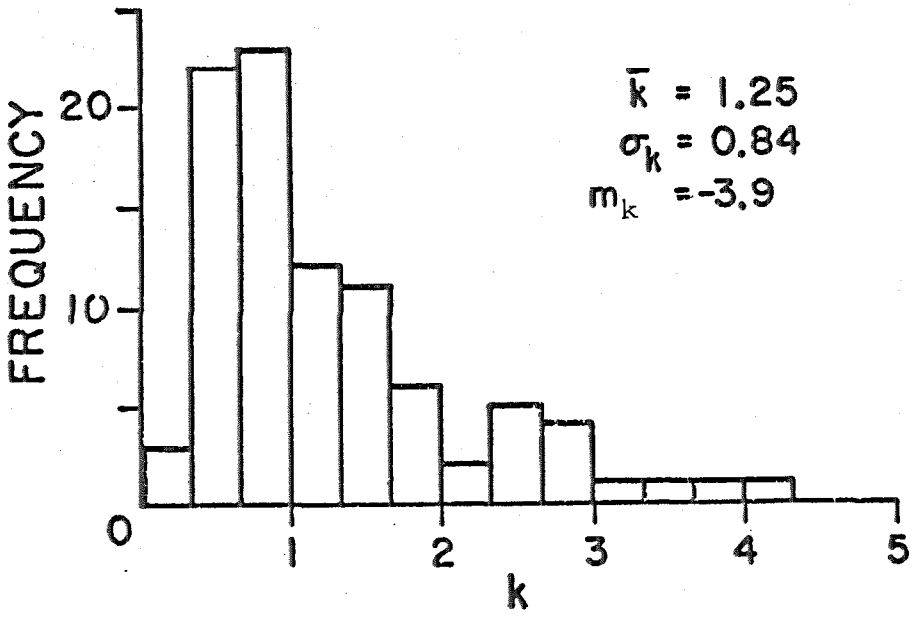

(a) Complete group.

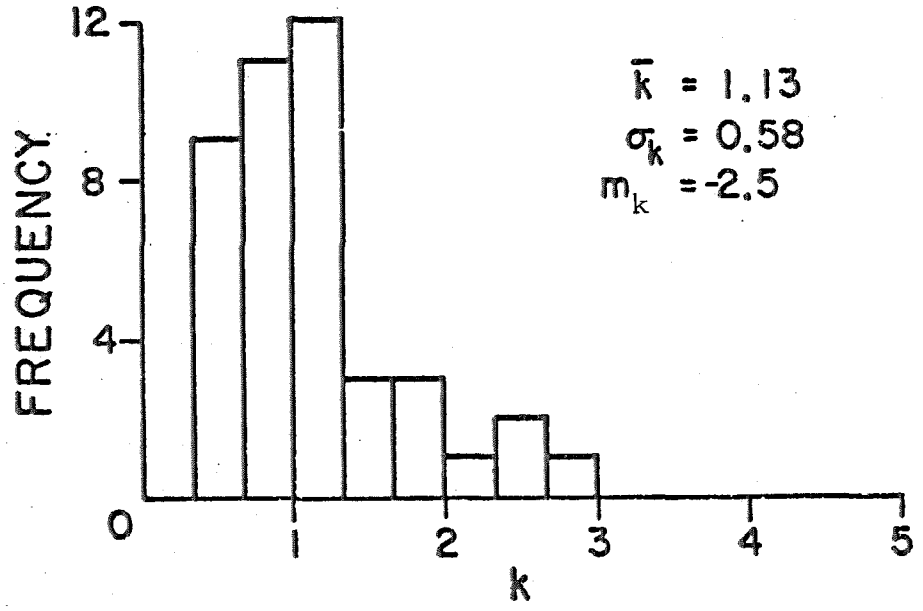

(b) Basement rock sites only.

Figure 2.23. Scatter in northern M5H15 data, shown by distribution of k, for the six frequency samples taken together.

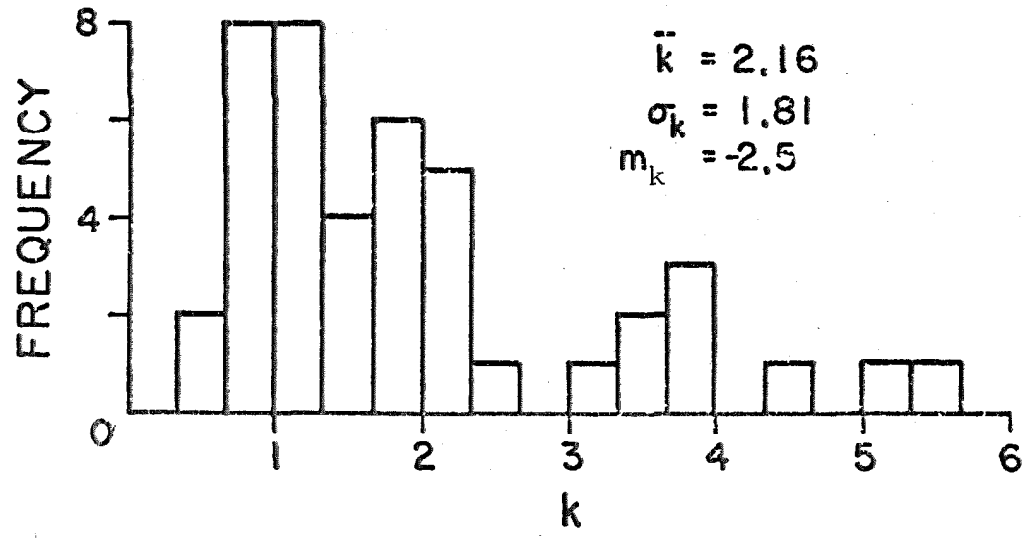

(c) Sediment sites w. r. t. basement attenuation curve

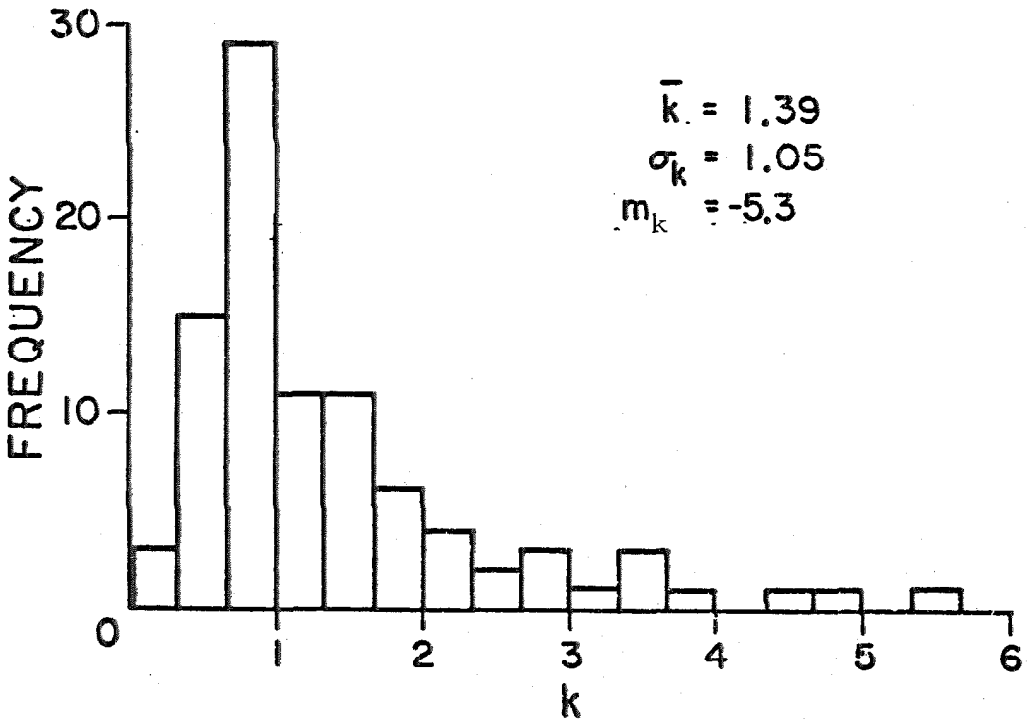

(d) Complete group, w. r. t. basement A_i's and Q = 400.

Figure 2. 23. Continued.

group to 17. The sites included, and the amount of overlap among the groups can be seen in Figure 2. 4. The sites are listed in Table 2. 15 with a brief description of site geology. The M5H15 Fourier amplitudes of acceleration studied in this section are listed in Table A2. 3 of Appendix 2.

2. 9. 1. Winnowing the south-eastern data.

Some Fourier amplitude data obtained from records N185, N186, H124, M180 and F087 were excluded from the southern data group and are also excluded from this group. Reasons for this have been given in Section 2. 5. 1. In addition, some data points from other accelerograms were excluded.

The first, N187, the San Antonio Dam, shows several pronounced spectral peaks at 2. 5 Hz and above. Assuming $\beta = 1000$ ft/sec, a fundamental frequency of 2. 5 Hz was computed using Ambrasey's (1960) shear wedge model. This suggests that the peaks are caused by resonant vibration of the dam. Accordingly, the 4, 8 and 16 Hz components of N187 were deleted from the data set.

The 0. 4 and 1 Hz amplitude data were excluded from both components of record H121, The Sears Building, Alhambra. There are pronounced peaks in the 12th floor record spectra near 0. 4 and from 1-2 Hz, and these show up in both radial and transverse components of the rotated basement record. Because of the coincidence of roof and basement peaks, it was suspected that some structural response was recorded by the basement instrument. However, as Crouse (1973) points out, even in relatively simple situations it is

TABLE 2.15.

South-eastern sites

Record	Hypocentral distance (km)	Site-station azimuth (degrees)	Site geology
G110	34.1	138	200-300 ft alluvium over basement rock
G106	38.4	144	Granitic basement
G108	41.8	140	1000 ft alluvium
G107	41.8	139	1000 ft alluvium
H121	45.0	147	4000 ft sediments
P221	45.2	125	Basement rock (instrument near dam abutment)
N186	55.6	137	8000 ft of sediments. Instrument on crest of 56 ft high earth dam
P223	66.2	123	Volcanic inclusions and shale
M183	72.0	94	Alluvium veneer over basement
M184	72.0	94	Alluvium veneer over basement
N187	73.3	113	Approx. 150 ft alluvium over basement. Instrument on top of 160 ft high earth dam.
N185	76.7	137	18,000 ft of sediment. Instrument on 99 ft high earth dam.
H124	77.3	141	16,000 ft of sediments
M180	85.3	146	10,000 ft of sediments
F087	89.4	146	9,000 ft of sediments
F101	108.4	111	Approx. 1000 ft of sediments
O206	109.0	108	Approx. 1000 ft of sediments

difficult to identify the existence of soil-structure interaction effects, let alone estimate their magnitude. In the southern group, only in clear-cut cases of external modification were data winnowed. However, in smaller groups like this, extreme values such as those in H121 have much greater influence on the general trend, and it was judged prudent to exclude them.

The data winnowed from the south-eastern group are listed in Table 2.16.

2.9.2. Attenuation in south-eastern group.

Smoothed Fourier amplitudes from the south-eastern group of 15 second accelerograms are shown in Figure 2.24 plotted as a function of frequency and hypocentral distance. As with the two previous data groups, it can be seen that amplitude attenuates with increasing propagation distance, and that the rate of attenuation increases with frequency. The attenuation curves shown in the figures were obtained, as before, from least-squares estimates of the attenuation parameters which are listed in Table 2.17. The solid line is drawn from the parameters obtained from the group as a whole, and the broken line with short dashes from basement rock site data only. Average amplitude from the southern group is shown by the broken line with long dashes. Again, it is seen that the general trend in amplitude attenuation is adequately predicted by the attenuation expression of equation (2.6).

As found in the northern data, amplitudes recorded on sedimentary sites tend to be higher than those from basement rock sites

TABLE 2.16.

Data winnowed from south-eastern group

Record	Frequency	Component	Reason
H121	0.4, 1	both	Influenced by structural vibration
N185	4, 8, 16	both	Influenced by dam response
N186	4, 8, 16	both	Influenced by dam response
N187	4, 8, 16	both	Influenced by dam response
F087	16	both	Digitization noise
H124	16	both	Digitization noise
M180	16	both	Digitization noise

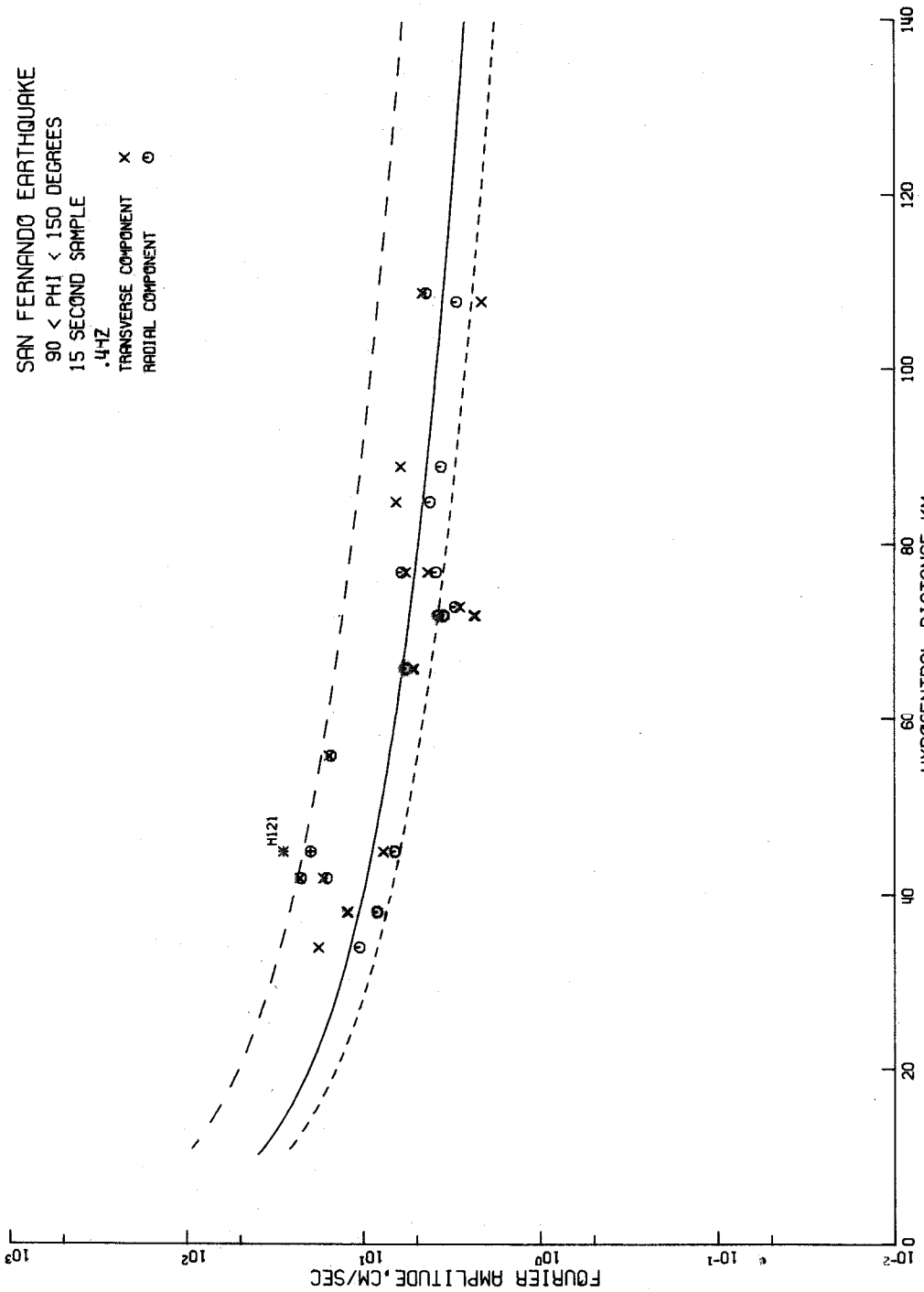

Figure 2.24(a). The solid line shows the "best fit" to all data in the south-eastern group; the short-dashed line is for the basement rock sites only; and the long-dashed line shows the average amplitude of the southern M5H15 data.

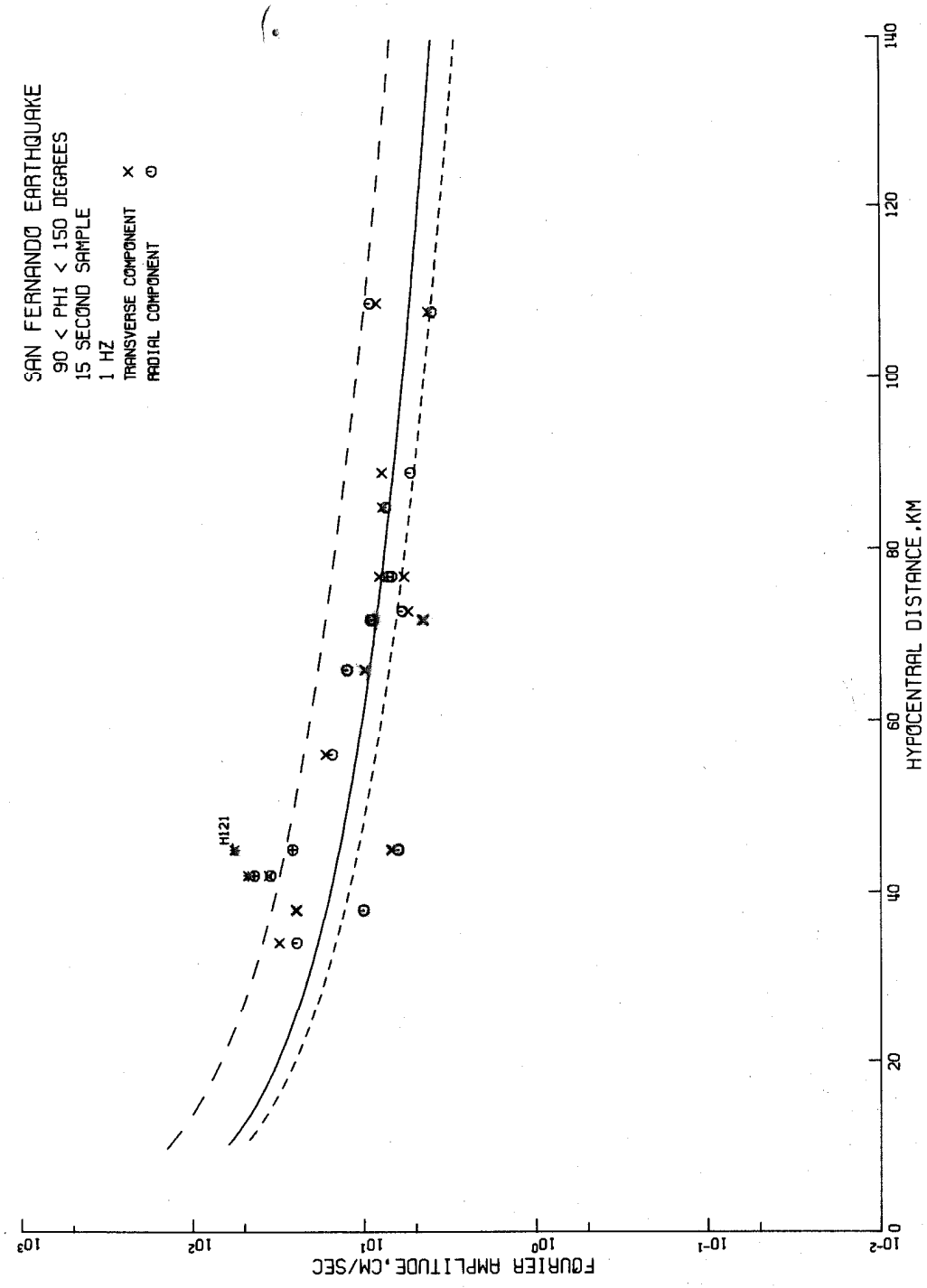
SAN FERNANDO EARTHQUAKE
90 < PHI < 150 DEGREES
15 SECOND SAMPLE
1 HZ
TRANSVERSE COMPONENT ×
RADIAL COMPONENT ⊙
H121
FOURIER AMPLITUDE,CM/SEC
HYPOCENTRAL DISTANCE,KM
10-2
10-1
10⁰
10¹
10²
10³
0
20
40
60
80
100
120
140

Figure 2.24(b)

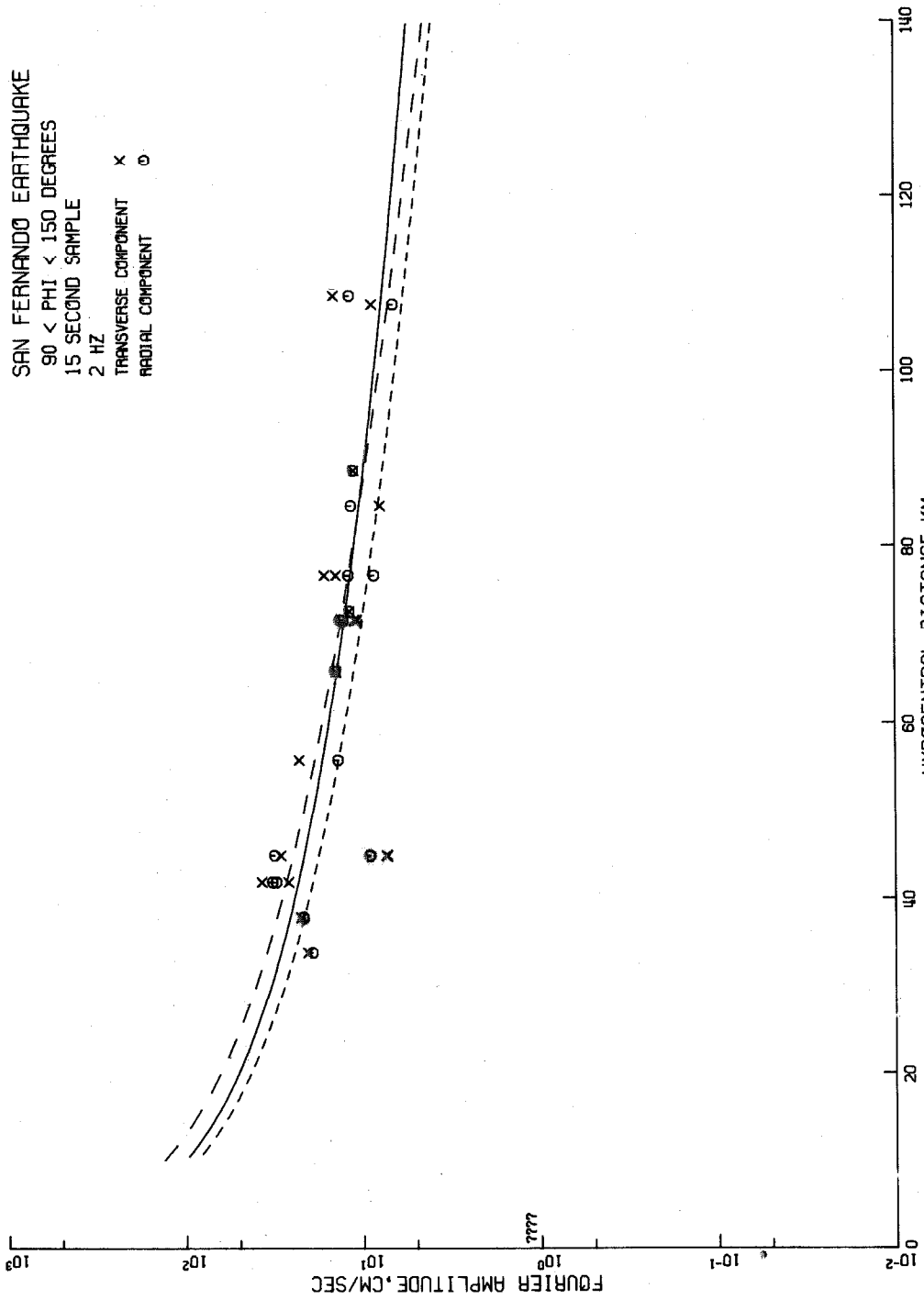
SAN FERNANDO EARTHQUAKE
90 < PHI < 150 DEGREES
15 SECOND SAMPLE
2 HZ
TRANSVERSE COMPONENT x
RADIAL COMPONENT o
FOURIER AMPLITUDE,CM/SEC
HYPOCENTRAL DISTANCE,KM
10-2
10-1
10⁰
10¹
10²
10³
???
0
20
40
60
80
100
120
140

Figure 2.24(c).

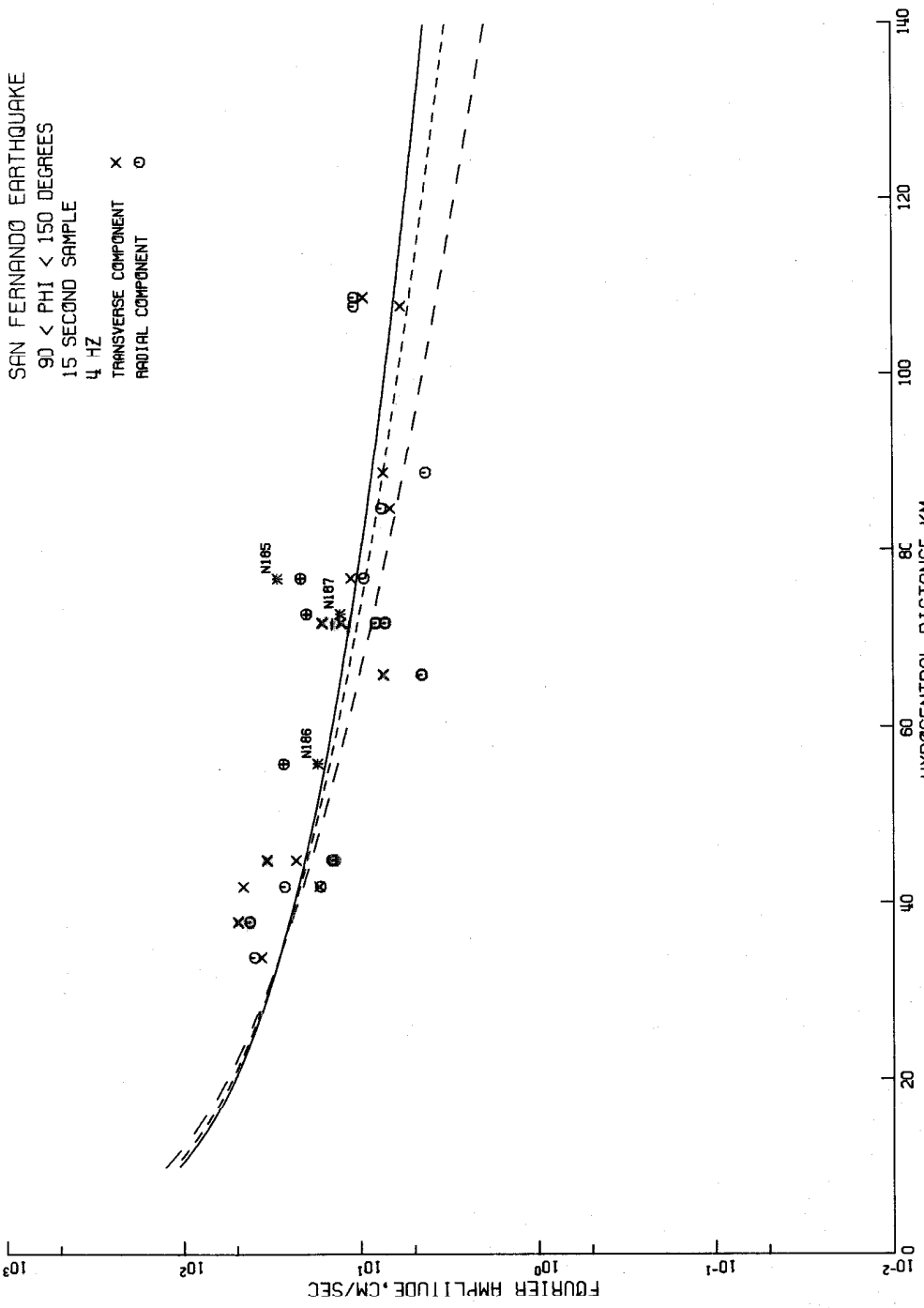
SAN FERNANDO EARTHQUAKE
90 < PHI < 150 DEGREES
15 SECOND SAMPLE
4 HZ
TRANSVERSE COMPONENT ×
RADIAL COMPONENT ⊙
N185
N187
N186
FOURIER AMPLITUDE,CM/SEC
HYPOCENTRAL DISTANCE,KM
10-2
10-1
10⁰
10¹
10²
10³
0
20
40
60
80
100
120
140

Figure 2.24(d).

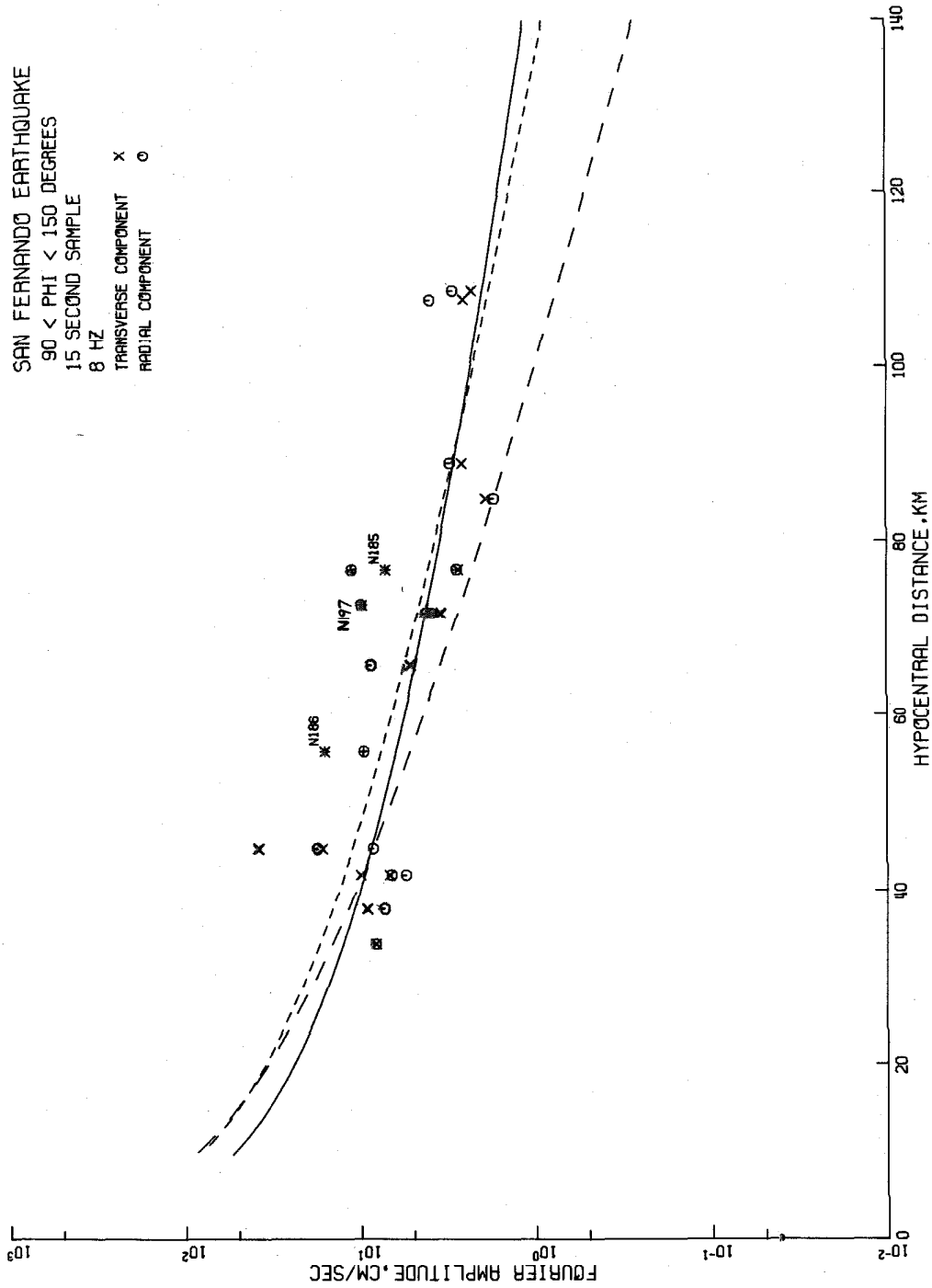
SAN FERNANDO EARTHQUAKE
90 < PHI < 150 DEGREES
15 SECOND SAMPLE
8 HZ
TRANSVERSE COMPONENT X
RADIAL COMPONENT O
N185
N187
N186
FOURIER AMPLITUDE,CM/SEC
HYPOCENTRAL DISTANCE,KM

Figure 2.24(e).

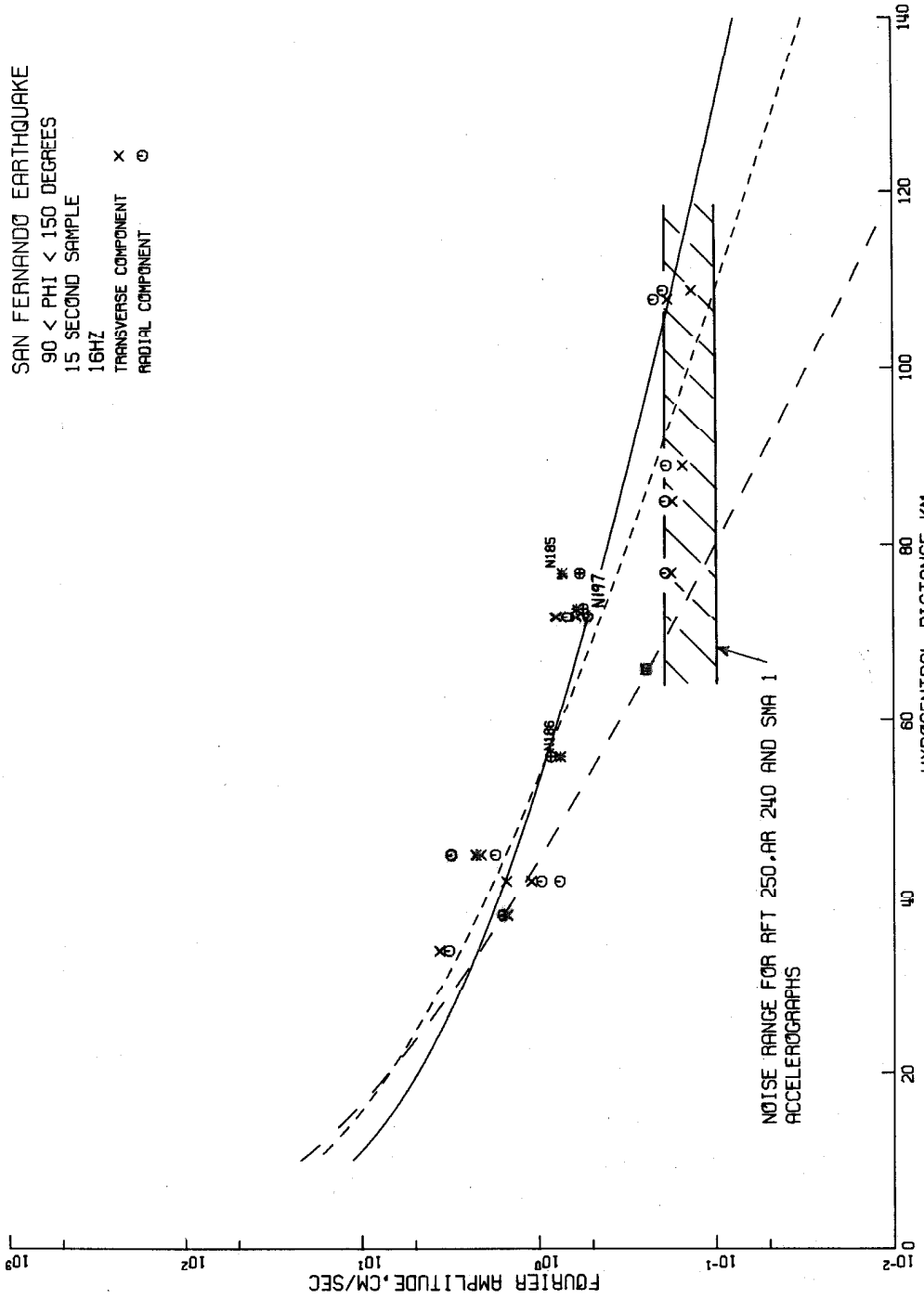
SAN FERNANDO EARTHQUAKE
90 < PHI < 150 DEGREES
15 SECOND SAMPLE
16HZ
TRANSVERSE COMPONENT ×
RADIAL COMPONENT ⊖
FOURIER AMPLITUDE,CM/SEC
HYPOCENTRAL DISTANCE,KM
NOISE RANGE FOR AFT 250,AR 240 AND SNA 1
ACCELEROGRAPHS
N185
N197
N186

Figure 2.24(f).

TABLE 2.17.

Parameters from smoothed, 15-second records in south-eastern group

Parameter	Basement rock sites only		Complete group	
	Value	90% confidence interval	Value	90% confidence interval
Q	550	450 - 800	860	700 - 1150
A_1	290 cm/sec	160 - none found	410 cm/sec	300 - 560
A_2	520	290 - none found	650	480 - none found
A_3	930	520 - none found	1070	790 - 1430
A_4	1230	690 - 2200	1130	810 - 1560
A_5	930	510 - 1690	580	420 - 800
A_6	250	150 - 450	140	100 - 200

at low frequencies (see Figures 2.24(a) and (b)) and in general, little different from basement rock amplitudes at high frequencies (see Figures 2.22(c), (d), (e) and (f)).

In view of the wide confidence intervals reflecting a small number of scattered data, the difference between the Q of 350 from the northern data and Q of 550 found here is not surprising. In fact, there are not enough data in either group to determine a basement Q very precisely. However, in view of the smaller confidence interval of the value from the northern group (270 to 500 vs. 450 to 800), and the better agreement of the northern value with $Q = 330$ for the southern data whose propagation paths are largely through basement rock, more reliance should be placed upon the northern value of $Q = 350$.

The higher values of A_1, A_2, and A_3 determined from the complete group of sites, together with a higher Q, implies that sedimentary sites are accelerated more strongly than basement sites in the 0.4 - 2 Hz frequency band. In fact, sedimentary sites were shaken more strongly than basement sites throughout the frequency range; this can be seen from Table 2.18 showing statistics of k for various sub-groups. The value of $\bar{k}$ for the six sampling frequencies combined is 30 percent higher for sedimentary sites than for basement rock sites when both are computed relative to the basement attenuation curve. The difference is greatest at 0.4 Hz where $\bar{k}$ is 90 percent larger for sedimentary sites; the difference decreases with increasing frequency until at 16 Hz the two $\bar{k}$ values are nearly equal. The low k values for

TABLE 2.18.

Statistics of k for M5H15 data from the south-eastern group

f (Hz)	All S-E sites			Basement sites only**			Sedimentary sites w.r.t. basement attenuation curve		
	$\bar{k}$	σ_k	m_k	$\bar{k}$	σ_k	m_k	$\bar{k}$	σ_k	m_k
0.4	1.13	0.56	-2.4	1.04	0.32	-1.4	1.98	0.80	-11.1
1	1.10	0.50	-2.0	1.08	0.46	-1.9	1.67	0.65	-6.0
2	1.05	0.33	-1.3	1.06	0.30	-1.3	1.47	0.42	-3.5
4	1.10	0.46	-1.9	1.13	0.56	-2.4	1.22	0.47	-2.1
8*	1.15	0.77	-3.4	1.19	0.86	-4.0	0.90	0.47	-1.1
16	1.10	0.47	-2.0	1.14	0.56	-2.1	1.18	0.52	-2.0
Combined samples	1.10	0.52	-2.2	1.10	0.51	-2.1	1.43	0.66	-4.7

*High values at this frequency caused by spectral peak in transverse component of P221 at 8 Hz.

**G106, M183-4, P221, P222.

sedimentary sites at 8 Hz and correspondingly high values for basement sites are caused by spectral peaks at 8 Hz in record P221. This also causes the high value of k = 3.5 in histogram (b), Figure 2.25. Since the record was made on basement rock some distance away from an abutment of the Santa Anita dam, Arcadia, California, its exclusion from the set is difficult to justify. However, the 8 Hz component does appear to be anomalously high, possibly due to vibration of the concrete arch dam being transmitted to the accelerograph. Consequently, there is reason to doubt the statistics at 8 Hz and we may say that in general, sedimentary sites were shaken more strongly throughout the frequency band of 0.4 to 16 Hz.

Scatter, as measured by σ_k, and seen in the histograms in Figures 2.25, does not exhibit the large increase from basement rock sites to sedimentary sites that was seen in the northern data. Values of 0.51, 0.52, 0.66 for the combined frequency samples were found for the basement sites alone, the complete set, and the sedimentary sites alone, respectively; these values indicate much less scatter in the south-eastern group than the corresponding values of 0.58, 0.84 and 1.81 from northern data. No explanation has been found for these quite different behaviors.

2.10. Relationship between site geology and ground motion intensity.

It was noted in Chapter 1 that, in general, incoming wave motion tends to be amplified by the presence of soft surface layers, but that this tendency is opposed by greater energy dissipation in softer soils. Analysis of the effects expected at a particular

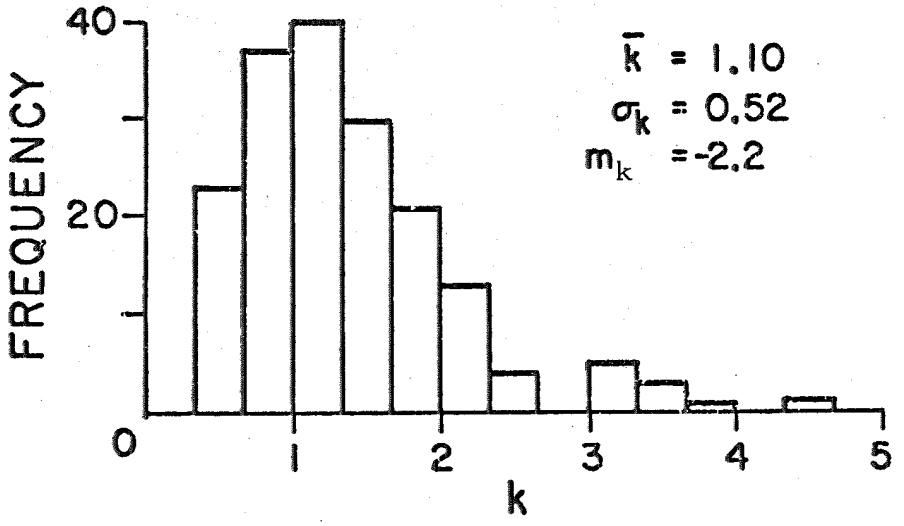

(a) Complete group.

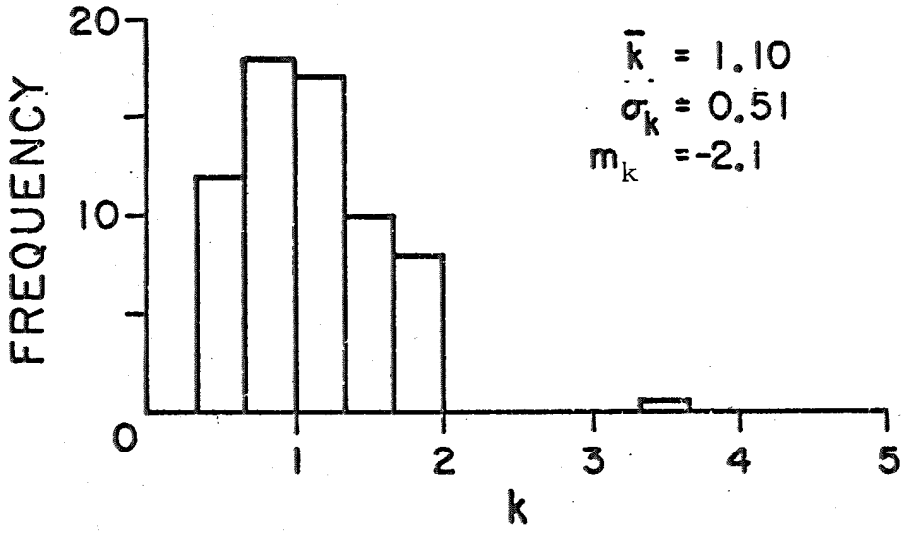

(b) Basement rock sites only.

Figure 2.25. Scatter in south-eastern M5H15 data shown by distribution of k. Distributions are for the six frequency samples taken together.

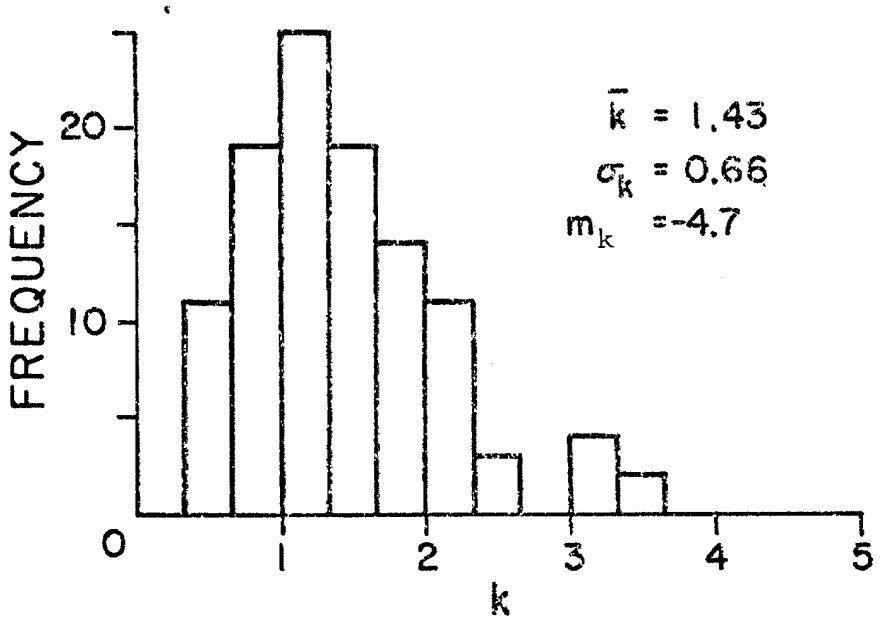

(c) Sediment sites, w. r. t. basement attenuation curve.

Figure 2.25. Continued.

site is normally not practicable due to the complications caused by material inhomogeneities and irregular geometric configurations of the site soils. Obtaining values of the material properties of the soils adds a further difficulty, which is compounded by evidence that the behavior of large masses of soil is quite different to that of a small laboratory sample. Thus it is not clear if, under strong ground motions, we should expect

(a) Sedimentary sites to record stronger accelerations than similarly located basement rock sites, and

(b) Marked differences in recorded amplitudes of acceleration to exist among sedimentary sites of different soil stiffnesses.

Clearly these are questions of considerable importance in earthquake engineering. Some answers are indicated in the present study as follows.

The large number of sites recording the San Fernando earthquake allows correlations to be made between recorded amplitudes and surface geology at the site. With average levels of Fourier amplitude defined by the attenuation curves, any correlation between ground-motion intensity and geology should be reflected in the k-values.

Trifunac and Brady (1975) have compiled a list of descriptions of local geology at a large number of strong-motion accelerograph sites, and have correlated peak ground motion values and Modified Mercalli intensities with geologic type. They have classified local geology into three broad groups: "soft" sites, in the Los Angeles region usually recent alluvium, as class 0; sites of "intermediate" soil stiffness, usually sedimentary rock, as class 1; and "hard" basement rock sites as class 2. While this is not a fine division, and

the classification of any individual site may be in error, over the large number of data we have, average geologic properties should be well-defined, and any correlations between intensity of motion and site geology should emerge.

The unsmoothed, M0H15 amplitude data from the southern sites were sorted according to site classification, and values of k computed for each site. Statistics describing the distribution of k in each class are shown in Table 2.19. It is seen that the "medium" sites were accelerated slightly more strongly, by 5 percent, than the "soft" sites; the medium data are also slightly more scattered than the "soft" site data. Thus in answer to question (b) above, it does not appear that sediment type, classified according to stiffness, has any net effect on strong ground motion amplitudes.

The answer to question (a) is much more complicated, since the behavior of individual sites appears to be strongly influenced by topography. We have observed that, in general, sedimentary sites in the northern and south-eastern groups recorded higher amplitudes of acceleration than corresponding basement rock sites. From Tables 2.14 and 2.18 it is seen that, averaged over the entire frequency range, amplitudes on sediments to the north were 60 percent higher than on basement rock, and to the south-east they were 30 percent higher. The differences between these two values cautions against too much generalization; but it does appear that, on the average, sediments recorded stronger motion than hard rock sites.

TABLE 2.19.

Statistics of k for southern data grouped according to Trifunac and Brady's site soil classification (M0H15 data)

frequency (Hz)	Class 0 "soft" soils (550 data)			Class 1 "medium" soils (202 data)			Class 2 "hard" soils (36 data)		
	$\bar{k}$	σ_k	m_k	$\bar{k}$	σ_k	m_k	$\bar{k}$	σ_k	m_k
0.4	1.23	0.87	-4.6	1.36	0.99	-6.4	0.76	0.45	-0.8
1	1.15	0.77	-3.5	1.15	0.78	-3.6	1.88	1.22	-13.2
2	1.03	0.75	-2.7	1.05	0.70	-2.6	1.69	1.62	-15.9
4	0.99	0.65	-2.2	1.21	0.80	-3.0	1.17	0.51	-2.1
8	1.10	0.75	-3.1	1.10	0.68	-2.8	1.16	0.95	-4.2
16	1.08	0.72	-2.9	1.07	0.70	-1.3	1.54	1.23	-9.4
Combined samples	1.10	0.76	-3.2	1.16	0.79	-3.5	1.37	1.07	-7.1

However, this is not the impression given by the data for "hard" sites in Table 2.18. The average amplitudes at the three sites in this group (C041, G106 and O198) are higher, and more scattered than those of the two sedimentary groups. Table 2.20 shows the individual k-values for these sites. The two sites, C041 and O198, which show average k's above the general level of the southern group, are both situated in mountainous terrain. Several authors have investigated the effect of high topographic relief on the Pacoima Dam record, C041, and have concluded that the mountain and canyon topography did modify the record in a complex manner (Wong and Jennings, 1975). This is reflected in the k-values, which suggest constructive interference resulting in amplification of motion at some frequencies and destructive interference at others. In general, topography affects components with wavelengths equal to or less than the dimensions of the topographic object. Since record O198, Griffith Park Observatory, was recorded at the crest of a mountain with a base width of several kilometers, it is probable that it, too, underwent modification resulting from irregular site topography and this view is reinforced by an average k of 1.44. On the other hand, G106, the Caltech Seismological Laboratory which is sited on a low hill without the extremes of relief found at the other sites, recorded much lower amplitudes, with $\bar{k} = 0.53$. The relatively mild topographic relief is suggested as the reason for the low amplitudes, which are well below the general trend in southern amplitudes. However, even a relatively regular site such as this is not free from pronounced spectral peaks

TABLE 2.20.

k-values from M0H15 data at basement rock sites of the southern group

f (Hz)	C041		G106		O198	
	R	T	R	T	R	T
0.4	1.24	1.35	0.21	0.64	0.46	0.64
1	2.23	3.87	0.20	1.42	1.39	2.20
2	0.75	4.55	0.34	0.32	2.16	2.01
4	2.06	0.86	1.26	1.08	0.54	1.21
8	2.62	0.33	0.88	0.38	0.72	2.05
16	0.96	1.24	0.26	0.70	3.39	2.70
Average	1.65	2.03	0.53	0.76	1.44	1.80

as is seen from Figure 2.26. Since outcrops of basement rock are usually accompanied by high topographic relief, for purposes of assessing seismic risk the behavior of site O198 should be taken as normal in the absence of further data. (Because of its proximity to the source, and extreme relief, C041 cannot be considered typical.)

To sum up these observations on the effect of site geology, it appears that, in general, sedimentary sites were accelerated more strongly than basement rock sites, particularly at lower frequencies, say below 2 Hz, and that within the range of generally coarse-grained sediments found in the Los Angeles region, no marked difference in intensity of shaking can be seen between sites on recent alluvium and those on sedimentary rock. However, all records obtained on the three basement rock sites available for comparison have pronounced spectral peaks, which can be as high as those expected on sediments at comparable distances. From the point of view of engineering risk, therefore, any distinction on the basis of the geologic types found in the Southern California area does not seem justified.

2.11. Conclusions from Chapter 2.

The principal conclusion of this chapter is that, while there is considerable scatter in the Fourier amplitudes of acceleration studied, their average amplitude decay can be described very well, throughout the 0.4 - 16 Hz band considered, by a simple body-wave decay expression, with geometrical spreading accounted for by employing the reciprocal of distance and with a constant Q material attenuation term. Furthermore, when the amplitude data are smoothed over a constant

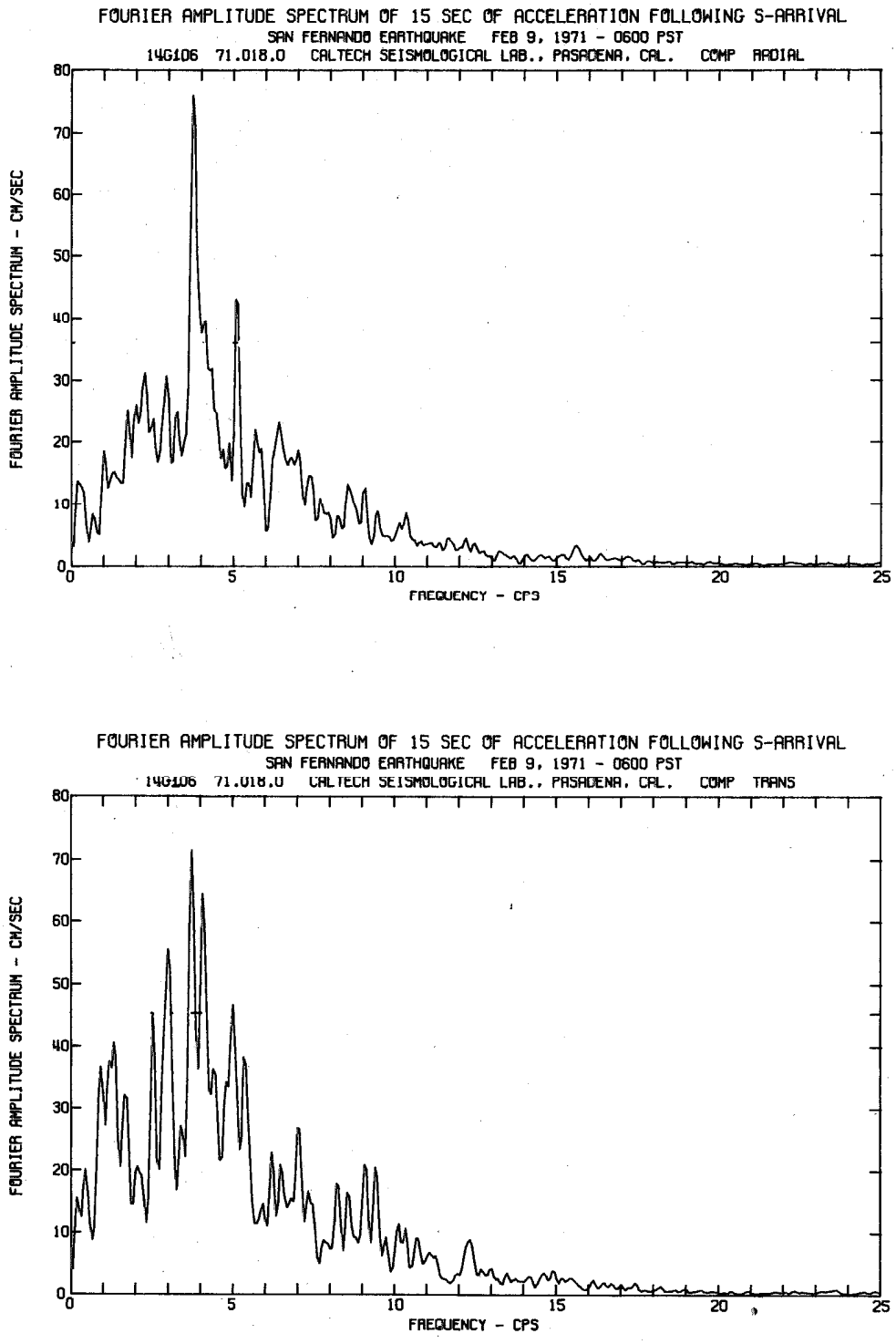

Figure 2.26. Notice spectral fluctuations and high peak near 4 Hz.

bandwidth at each sampling frequency, the scatter distribution does not change markedly with either frequency or distance.

The following specific conclusions may be stated:

(1) the average Fourier amplitude can be described by the expression

$$\overline{X}(f, r) = \frac{A(f)}{r} e^{-(\pi f r / Q\beta)} \qquad (2.6)$$

(2) No significant difference could be seen between amplitudes of radial and transverse components.

(3) For the southern group, in which most of the data lie, a Q of 330 was found, with the 90 percent confidence interval of 310-360. (β was assumed equal to 3.2 km/sec throughout.)

(4) The much smaller numbers of data in northern and south-eastern groups did not allow such a precise determination of Q. Also, both these groups contain several basement rock sites, whereas the southern group has only three basement sites in a total of 71 sites. For the complete northern set, Q = 700 with a 90 percent confidence interval of 500-1500. For the complete south-eastern set, Q - 860, with a 90 percent confidence interval of 700-1150.

(5) For basement rock sites only, the following values of Q were found for the northern and south-eastern data groups:

Q	90 percent confidence interval	
350	270-500	(N)
550	450-800	(S-E)

The paucity of data and the fairly large amount of scatter show in the difference between the values, and in the wide confidence intervals.

(6) Scatter in the data is conveniently measured by an uncertainty factor k, given by equation (2. 13), where

$$k = \frac{X(f, r)}{\overline{X}(f, r)}$$

X being a data point at frequency f and focal distance r, and $\overline{X}(f, r)$ the value predicted by the decay expression rule at (f, r). The statistical distribution of k is fairly constant with respect to frequency; for unsmoothed southern data from the 15-second accelerograms, the standard deviation of k, $\sigma_k = 0.78$, and the distribution tapers off much more quickly at high values than does the corresponding lognormal distribution. With smoothing over a band of 0. 73 Hz, the distribution is much tighter, with $\sigma_k = 0.46$.

(7) Amplitudes at 0. 4 and 1 Hz computed from the 15 second records are lower than those from full length accelerograms, indicating that for $f \leq 1$ Hz there is dispersion of energy outside the 15 second sampling window. No indication of this was found in the 2 Hz and higher frequency samples.

(8) The average intensity of ground motion was stronger to the south of the epicenter than at a comparable distance to the north. Intensities to the south-east were between those to the north or south.

(9) There appears to be no justification for saying that soft sedimentary sites in the Los Angeles region are shaken more strongly than sedimentary sites of intermediate soil stiffness.

(10) The average spectral level of accelerations recorded on a few crystalline rock stations does appear to be lower than that recorded at similar focal distances on sediments. However, the peaks of the few basement rock spectra available are relatively high, and peak amplitudes from basement sites are often comparable to those recorded on sediments at similar distances. This suggests that the seismic risk on basement sites, particularly those with high topographic relief, is no less than on sedimentary sites.

3. THE SAN FERNANDO EARTHQUAKE SOURCE

In Chapter 2 the decay of $\overline{X}(f, r)$ was the primary concern, given some particular source excitation A(f). In this chapter, A(f) is considered in more detail, particularly how observed A(f) agrees with A(f) predicted by simple source models of the San Fernando earthquake.

The discussion draws upon the results of geophysical investigations of earthquake rupture mechanisms, and since some of these are not well-known in the engineering literature, a brief summary is considered to be in order.

3.1. Seismic source models.

Recent, intensive research into the nature of the earthquake source has resulted in several different models relating the radiated seismic wave field to details of the rupture mechanism. Since detailed knowledge of the failure mechanism leading to crustal earthquakes is presently not available, all source models are to some degree approximate. In this section, some results providing exact solutions to assumed, and in some cases quite specialized, rupture conditions are first summarized; then approximate models are discussed with emphasis upon the intuitively derived, but very successful, two-parameter source model introduced by Brune (1970).

Maruyama (1963) and Haskell (1964) have presented exact solutions for the dynamic displacement field resulting from the sudden appearance of an arbitrary dislocation in an infinite, homogeneous, isotropic, linearly elastic solid. Haskell goes on to specialize his solution to

the case of a propagating, ramp-function dislocation, and uses this example to discuss the amplitude spectrum of radiated seismic waves. He demonstrates that above a certain "corner frequency" f_o, which is proportional to the inverse of fault length, Fourier amplitude spectra of far-field displacement waves exhibit a rapid fall-off of amplitude with increasing frequency which, in the case of the ramp-function dislocation, is asymptotic to cf^{-2}, where f is frequency and c is some constant. This is illustrated schematically in Figure 3.1. [Hanks and Wyss (1972) show that for the radiated energy to be bounded, the exponent of f must be less than -1.5.] From the data of Thatcher and Hanks (1973) it is seen that frequencies of interest in engineering (say, 0.05 to 20 Hz) are near or, more often, above the corner frequency for M7 earthquakes. Thus details of the spectrum for $f \geq f_o$ are of prime interest to earthquake engineers.

Haskell also demonstrates that coherent, or uniform, propagation of rupture has the effect of focusing energy in the direction of rupture propagation, and he provides an alternative derivation of the classical work of Ben-Menahem (1961) on this topic. Since, as we shall see, focusing of energy by rupture propagation had a marked effect on the strength of ground motions recorded south of the San Fernando epicenter, this well-known seismological phenomenon deserves consideration in earthquake engineering.

The focusing effect of a propagating rupture is superimposed upon the four-lobed radiation pattern, usually denoted by $\mathcal{R}_{\theta\varphi}$, expected from a dislocation source, and serves to modify it by increasing the

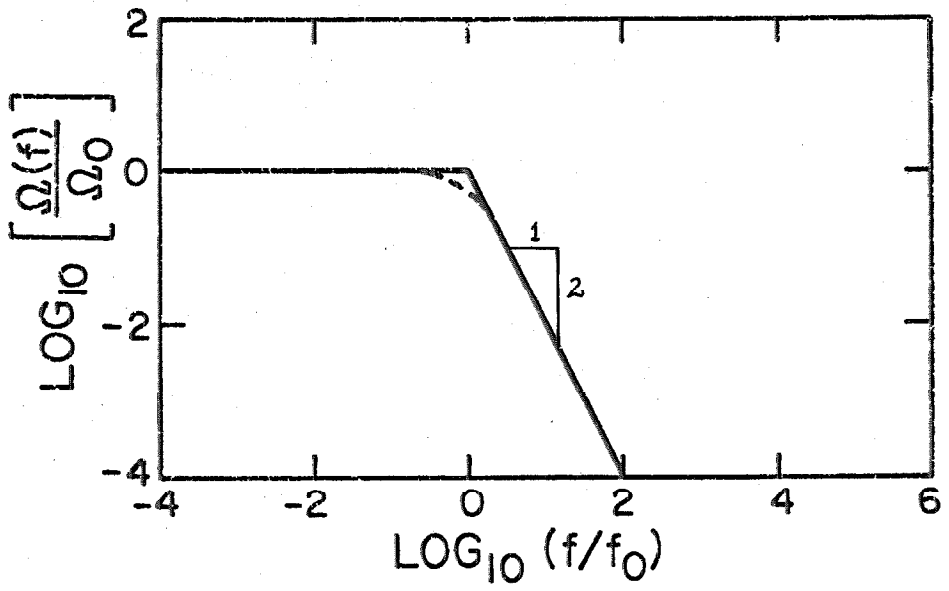

Figure 3.1. Displacement amplitude spectrum of far-field shear waves. Brune's expression (equation (3.1)) shown by the broken line.

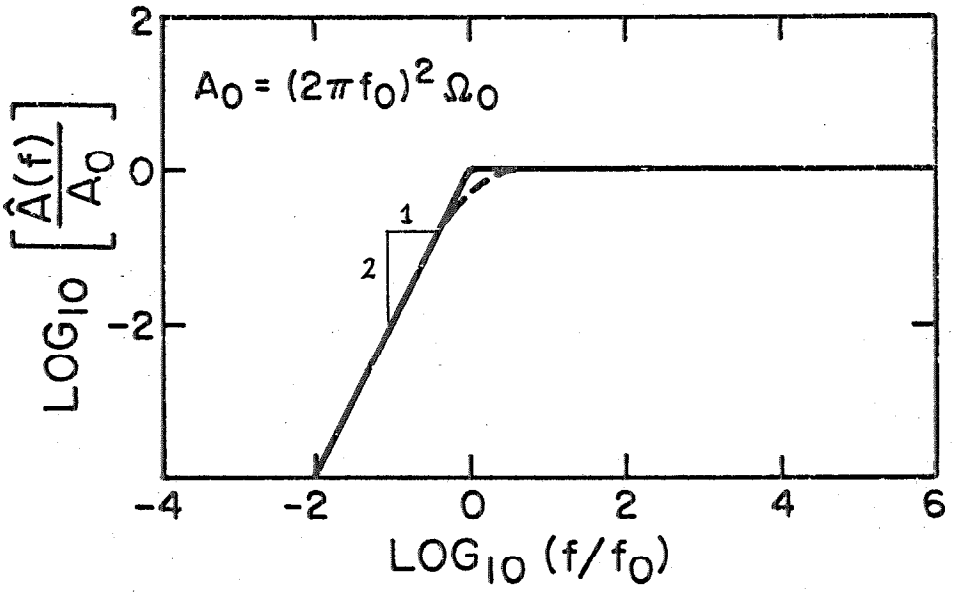

Figure 3.2. Far-field amplitude of acceleration spectrum corresponding to Figure 3.1.

amount of energy emitted in the direction of rupture propagation, at the expense of that emitted in the opposite direction. An explicit expression for $R_{\theta\varphi}$ can be found, for example, in Randall (1973a). It has been observed that the classical radiation pattern $R_{\theta\varphi}$ is often not well-developed, particularly near its nodes where it is very sensitive to variations in direction. This is physically reasonable, since a fault is unlikely to be perfectly planar and $R_{\theta\varphi}$ is based on an assumed point source. This problem is further discussed by Hanks and Wyss (1972). In the case of the data used in this study, no well-defined pattern emerged in a plot of individual, decay-corrected Fourier amplitudes of acceleration from the southern set. By averaging amplitudes within smaller ranges of azimuth than those of the three groups employed in this study, some details of a radiation pattern modulated by rupture propagation effects may be found.

Randall (1966) and Archambeau (1968) present exact solutions for the elastic radiation in an idealized, infinite elastic solid resulting from the sudden relaxation of stress within a finite-volume source region in a pre-existing stress field. Because precise details of the real rupture mechanism are not known, assumptions are again necessary. In Archambeau's solution, assumptions are made about the shape and size, as functions of time, of the region in which stress relaxation has occurred.

Because detailed understanding of the rupture mechanism is lacking, and because of the complexity of the mathematics in the exact solutions for the idealized rupture mechanisms discussed above, many

attempts have been made to relate the principal features of the radiated seismic wave field to a few parameters describing the average properties of the rupture process. Brune (1971b) and Aki (1972a) review the considerable number of investigations made into simple source models, and consequently a general review is not attempted here. Instead, the principal results of a simple two-parameter model are presented.

Brune (1970, 1971a) proposed a simple model relating the Fourier amplitude spectrum of far-field shear wave displacement, $\Omega(f)$, in an infinite, homogeneous, isotropic elastic solid to two independent parameters of the dislocation source. The asymptotic form of Brune's spectrum provides a close approximation to the exact solution of Randall (1966) for a spherical relaxation source.

Brune's expression for the far-field Fourier amplitude of shear displacement, $\Omega(f)$, is as follows:

$$\Omega(f) = \frac{\Omega_o}{1+(f/f_o)^2} \qquad (3.1)$$

where Ω_o is the displacement spectrum ordinate at zero frequency, f is frequency, and f_o is the spectral corner frequency considered in more detail below. Equation (3.1) is plotted in Figure 3.1, together with its asymptotes.

The low frequency asymptote, given by the constant value of Ω_o in Figure 3.1, is related to the source parameter seismic moment M_o (note that M_o is not magnitude, for which the symbol M, without subscript, has been used) by the expression (Keilis-Borok, 1960):

$$\Omega_o = \frac{1}{4\pi r} \frac{M_o}{\mu} \frac{1}{\beta} \Re_{\theta\varphi} \tag{3.2}$$

where r is the hypocentral distance, μ is the shear modulus, β is the shear wave velocity, and $\Re_{\theta\varphi}$ is the radiation pattern. Seismic moment is defined in terms of the average dislocation $\bar{u}$, or fault offset, and fault area S (of arbitrary shape) by the expression (Aki, 1966):

$$M_o = \mu \bar{u} S \tag{3.3}$$

Randall (1973b) points out that when motions at the source are uni-directional toward the position of final equilibrium, a physical condition expected of a relaxation or dislocation source,

$$\Omega(f) \leq \Omega_o \tag{3.4}$$

Thus the spectrum is bounded by its low-frequency asymptote.

The corner frequency, f_o, marking the intersection of the low- and high-frequency asymptotes, is proportional to the inverse of the fault dimension R, which, in the simple model, is taken to be the radius of the equivalent circular area. With a conservation of energy argument, Brune (1970) (corrected by Brune, 1971a) determines the constant of proportionality, obtaining an expression for f_o in terms of R as follows:

$$2\pi f_o = \frac{2.34\beta}{R} \tag{3.5}$$

By physical arguments, Brune obtained a high-frequency asymptote proportional to $f^{-\gamma}$, with $\gamma = 2$, as shown in Figure 3.1. Randall (1973a) notes that the exponent γ is related to the nature of the highest order singularity in the dislocation time function, and that, in general, instantaneous relaxation sources should have the value of $\gamma = 2$. However, the value of $\gamma = 2$ applies only to instantaneous rupture. A coherently propagating rupture, in addition to focusing energy in the direction of propagation as discussed above, introduces a further factor of f^{-1} into the high-frequency amplitudes. For an instantaneous relaxation source, the resulting high frequency spectral asymptote is thus proportional to f^{-3}.

A further parameter, the static stress drop $\Delta\sigma$, is often used in seismological studies, and it is related to M_o and R through Keilis-Borok's (1959) result for a plane circular fault on which shear traction drops from some value σ_o to $(\sigma_o - \Delta\sigma)$. Namely,

$$M_o = \frac{16}{7} \Delta\sigma R^3 \qquad (3.6)$$

Five separate source parameters have been introduced above in the discussion of the two-parameter source model; only two of which (excluding one or other of the equivalent pair R and S) are independent:

$\bar{u}$	average fault dislocation
S	fault area
M_o	seismic moment ($M_o = \mu \bar{u} S$)
R	(equivalent) source dimension
$\Delta\sigma$	static stress drop

The spectral parameters:

Ω_o • the zero-frequency limit of the displacement amplitude spectrum

f_o corner frequency

may be expressed in terms of any independent pair of source parameters. In addition, shear modulus μ and the shear wave velocity β enter as physical constants.

Rupture propagation was also discussed, but it is not considered in the simple model. Parameters describing the direction and velocity of rupture should be included in a more comprehensive model. Similarly, the spectral parameter γ depends sensitively on further details of the faulting model, and is generally not well defined by observations (see, for example Thatcher and Hanks, 1973).

Seismic moment, M_o, being related directly to Ω_o is a convenient choice for the low-frequency parameter and can be determined from field observations of fault area and offset (Hanks, 1974a) or from teleseismic records (for example, Wyss and Hanks, 1972).

Determination of the high frequency end of the spectrum is less certain, since it depends more upon fine details or dynamics of the rupture process (Haskell, 1964). Brune's model points to high frequency amplitudes determined by Ω_o, $\gamma = 2$, and f_o, obtained from R by equation (3.5). However, both f_o and γ also depend upon the further variables of direction and

coherence of rupture propagation (Haskell, 1964), the shape of the fault plane (Savage, 1972), and details of the dislocation time-function (Haskell, 1964; Randall, 1973a). Thus until the rupture process is better understood, specification of high frequency spectral amplitudes by the two-parameter model is essentially empirical. In contrast to the pessimistic picture given by this caveat, it has been found that predictions by the two-parameter model agree well with observations of earthquakes whose parameters vary over a large range of values.

For large earthquakes with $6.4 < M < 7.2$, Hanks and Wyss (1972) and Wyss and Hanks (1972) have found agreement to within a factor of 2 to 3 between values of M_o and R from field observations and those predicted by the two-parameter model from teleseismic observations. Randall (1973a) cites similar agreement for smaller earthquakes.

Source parameter determinations for southern California earthquakes have been made by Hanks and Wyss (1972), Thatcher and Hanks (1973), Tucker and Brune (1973), Hanks et al. (1975), Trifunac (1972) and Thatcher (1972). Within the framework of the two-parameter model, Hanks and Thatcher (1972) and Thatcher and Hanks (1973) explore the relationships between M_o and f_o, and several other, commonly-used source parameters, including local magnitude M_L. [M_L is also related to R and $\Delta\sigma$ by Randall (1973a).] In their second paper, Thatcher and Hanks examine 138 recordings of California shocks in the magnitude range of 2 to 7. Although data are sparse for larger earthquakes, the larger shocks had stress drops, $\Delta\sigma$, in the range of 1 to 100 bars. From equation (3.6) it can be

seen that this observation presents a strong argument against the practice of scaling earthquake sources by a single parameter.

In an engineering context, application of Brune's (1970) theory to strong-motion problems has been discussed by Trifunac (1973), and it has been used by Hanks (1975) to estimate long-period ground motions in the Los Angeles Basin from a great earthquake on the San Andreas fault.

Fourier amplitudes of displacement have been considered in the preceding discussion, following the custom of the seismological literature. However, since the strong-motion data are in units of amplitude of acceleration, it is appropriate to consider the corresponding acceleration amplitude spectrum.

Let $\overline{A}(f)$ denote the Fourier amplitude of acceleration of the simple source model, corresponding to a given $\Omega(f)$. (As with $\overline{X}$, the bar above the A signifies that $\overline{A}(f)$ is predicted by a model, rather than obtained from observed data.) Then an expression for $\overline{A}(f)$ in terms of Ω_o and f_o may be obtained from equation (3.1) using the identity

$$\overline{A}(f) = (2\pi f)^2 \Omega(f) \quad . \tag{3.7}$$

Substituting from equation (3.1) into equation (3.7) yields

$$\overline{A}(f) = \frac{\Omega_o (2\pi f_o)^2}{1+(f_o/f)^2} \tag{3.8}$$

From equation (3.8) it can be seen that $\overline{A}(f)$ has a constant high frequency asymptote A_o given by the expression

$$A_o = (2\pi f_o)^2 \Omega_o \tag{3.9}$$

and a low frequency asymptote proportional to f^2. The acceleration spectrum and its asymptotes are shown in Figure 3.2.

Substituting from equations (3.2), (3.3), and (3.5) into Equation (3.9) yields

$$A_o = \frac{(2.34)^2}{4} \frac{S}{\pi R^2} \frac{\bar{u}\beta}{r} \Re_{\theta\varphi} .$$

Since $S = \pi R^2$, A_o is a function of the single source parameter $\bar{u}$, and is given by the expression

$$A_o = 1.37 \frac{\beta \bar{u}}{r} \Re_{\theta\varphi} . \qquad (3.10)$$

Thus, within the framework of this simple theory, the high-frequency asymptote is related to the single source parameter $\bar{u}$. This presents the immediate question of how can the high-frequency, or "most-dynamic", components of the spectrum depend solely on the static dislocation, $\bar{u}$? The answer to this apparent discrepancy is found in the implicit assumption in the model, that the static stress drop $\Delta\sigma$, which is related to $\bar{u}$ (Knopoff, 1958), is equal to the effective stress σ_e, acting during fault movement. Effective stress, which is related to the dynamics of faulting (Kanamori, 1972) and thus to the non-zero frequency components of motion, is defined as the difference between the initial shear stress σ_o acting on the fault before rupture and the functional shear stress σ_f resisting motion during faulting. Thus $\sigma_e = \sigma_o - \sigma_f$. It is not necessary that $\sigma_e = \Delta\sigma$. However, within the uncertainties in their determination, $\Delta\sigma \approx \sigma_e$ has been found for the San Fernando earthquake by Trifunac (1972) and for the 1943 Tottori, Japan, earthquake by Kanamori (1972).

The empirical nature of the simple model is well illustrated by equation (3.10). Consider, for example, two rupture events, one consisting of five independent dislocations of adjacent fault segments, each of area 20 km^2 and each with offset $\bar{u}$. From equation (3.10) the total high frequency amplitude from this multiple event should be five times that of a second event, consisting of a single, coherent rupture of $\bar{u}$ over a fault area of 100 km^2. This essentially empirical nature of the simple model should be kept in mind, particularly in the engineering applications suggested in the following chapter.

From equation (3.5) and the relationship between magnitude M and source dimension R of Randall (1973a) or from the data of Thatcher and Hanks (1973) it can be seen that for $M \geq 5$, it is likely that the corner frequency f_o will be below 0.4 Hz. In the case of the M = 6.4, San Fernando earthquake, $f_o \simeq 0.1$ Hz, and the frequencies considered in this study are well above the corner frequency. Thus an expression in terms of A_o for Fourier amplitudes of acceleration, $\overline{A}(f)$, predicted by the source model should be useful. Substituting from equation (3.9) into (3.8) yields

$$\overline{A}(f) = \frac{A_o}{1+(f_o/f)^2} \qquad (3.11)$$

In conclusion, the following expressions for f_o and A_o are repeated here for completeness:

$$f_o = \frac{2.34\beta}{2\pi R} \qquad (3.5)$$

$$A_o = \frac{1.37\beta\bar{u}}{r} \mathcal{R}_{\theta\phi} \qquad (3.10)$$

3.2. Comparison between predicted and observed acceleration spectral amplitudes.

The physical significance of A(f) can be seen from equation (2.6)

when $\overline{X}(f, r)$ is evaluated at a hypocentral distance of $r = 1$. In this case

$$A(f) \approx \overline{X}(f, r) \quad . \tag{3.19}$$

Expression (3.19) would be exact if the material attenuation term $e^{-(\pi f r/Q\beta)}$ were exactly equal to 1 at $r = 1$ km. The greatest error occurs at $f = 16$ Hz, in which case, for $r = 1$, $Q = 330$ and $\beta = 3.2$ km/sec, $e^{-(\pi f r/Q\beta)} = 0.95$. This error is small compared with the other uncertainties in determining A(f). Thus, physically, A(f) determined from a set of data is the average Fourier amplitude of acceleration of the data, corrected for material attenuation and geometric spreading, and referred to an imaginary focal sphere of radius 1 km.

Estimates of A(f) for each data group have been obtained at the six sampling frequencies during the least-squares estimation of attenuation curve parameters. These estimates, taken from Tables 2.4, 2.9, 2.13 and 2.17 are plotted in Figures 3.3, 3.4 and 3.5.

The reason for the difference between the two curves from the southern M5H15 and M10HIV data in Figure 3.3 has been discussed in Chapter 2, where it was attributed to dispersion of long period wave components outside the 15-second sampling window. The difference is not great, but since some energy is lost from the 15-second records, the trace from the full-length records will be used in the comparisons that follow.

Estimates of A(f) for the northern data are shown in Figure 3.4. The apparently higher average amplitude values for basement rock site data compared with the group as a whole, at 8 and 16 Hz, are a result of the parameter estimation process, rather than an indication of any real difference. This can be seen from Figures 2.19(c) and (f). If anything, the basement amplitudes are lower at these frequencies, but the group as a whole is better fitted in the least-squares sense

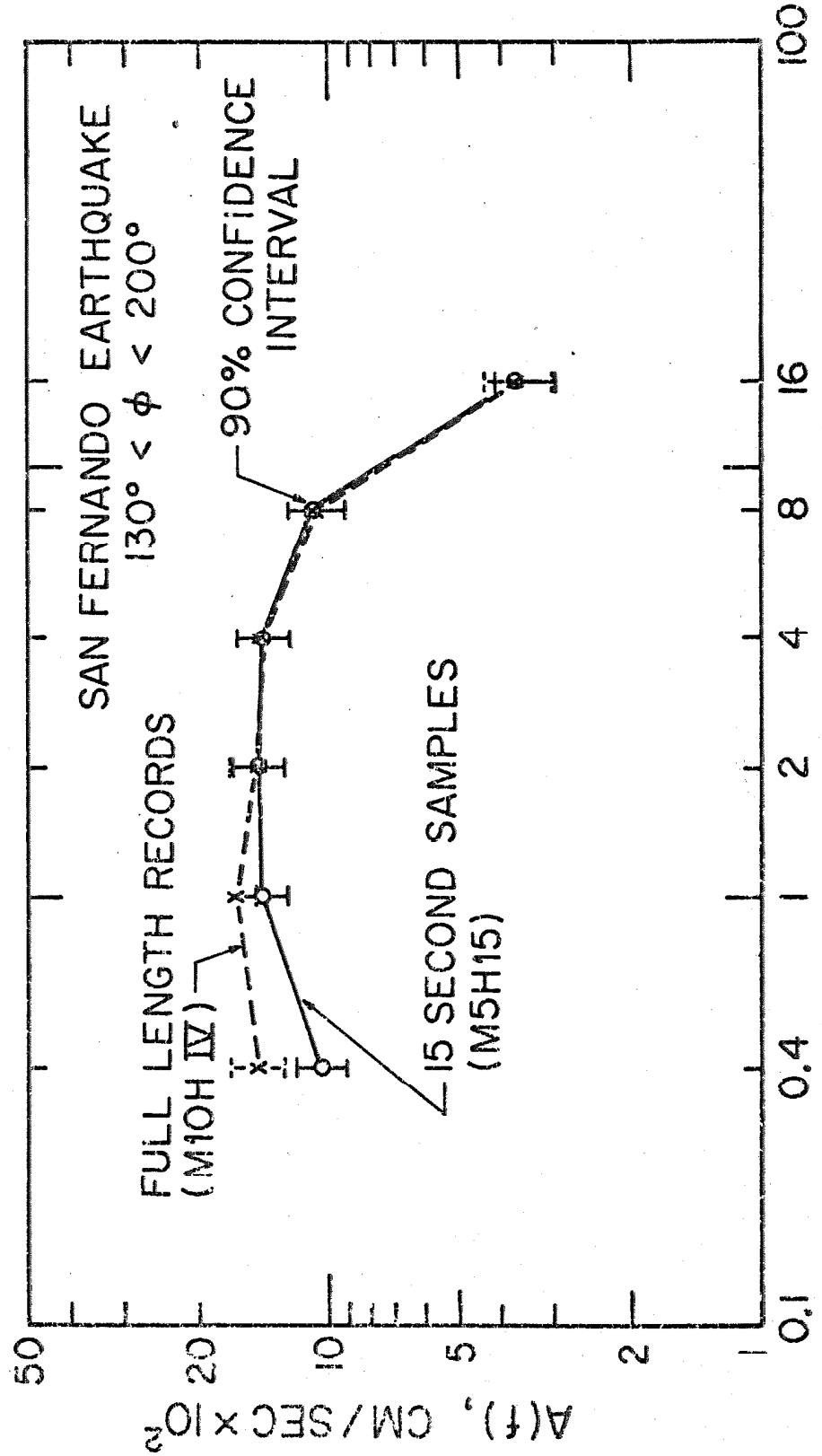

Figure 3.3. The source excitation function, A(f), estimated from southern data.

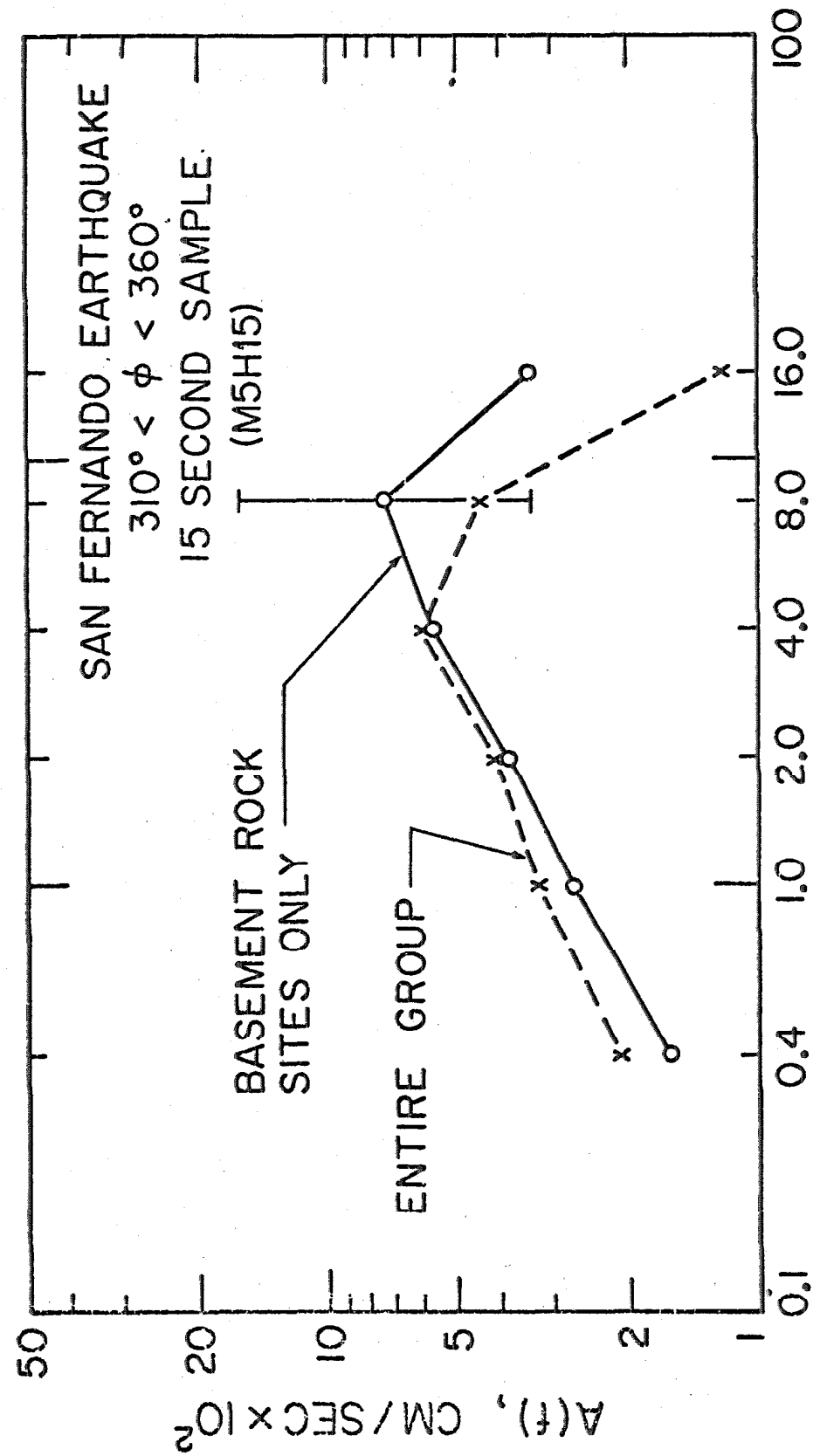

Figure 3.4. Estimates of A(f) from northern M5H15 data. The error bar at 8 Hz shows the 90% confidence interval for A_5 and is indicative of the large uncertainty in the A(f) determination. Confidence intervals for the remaining points are found in Table 2.13.

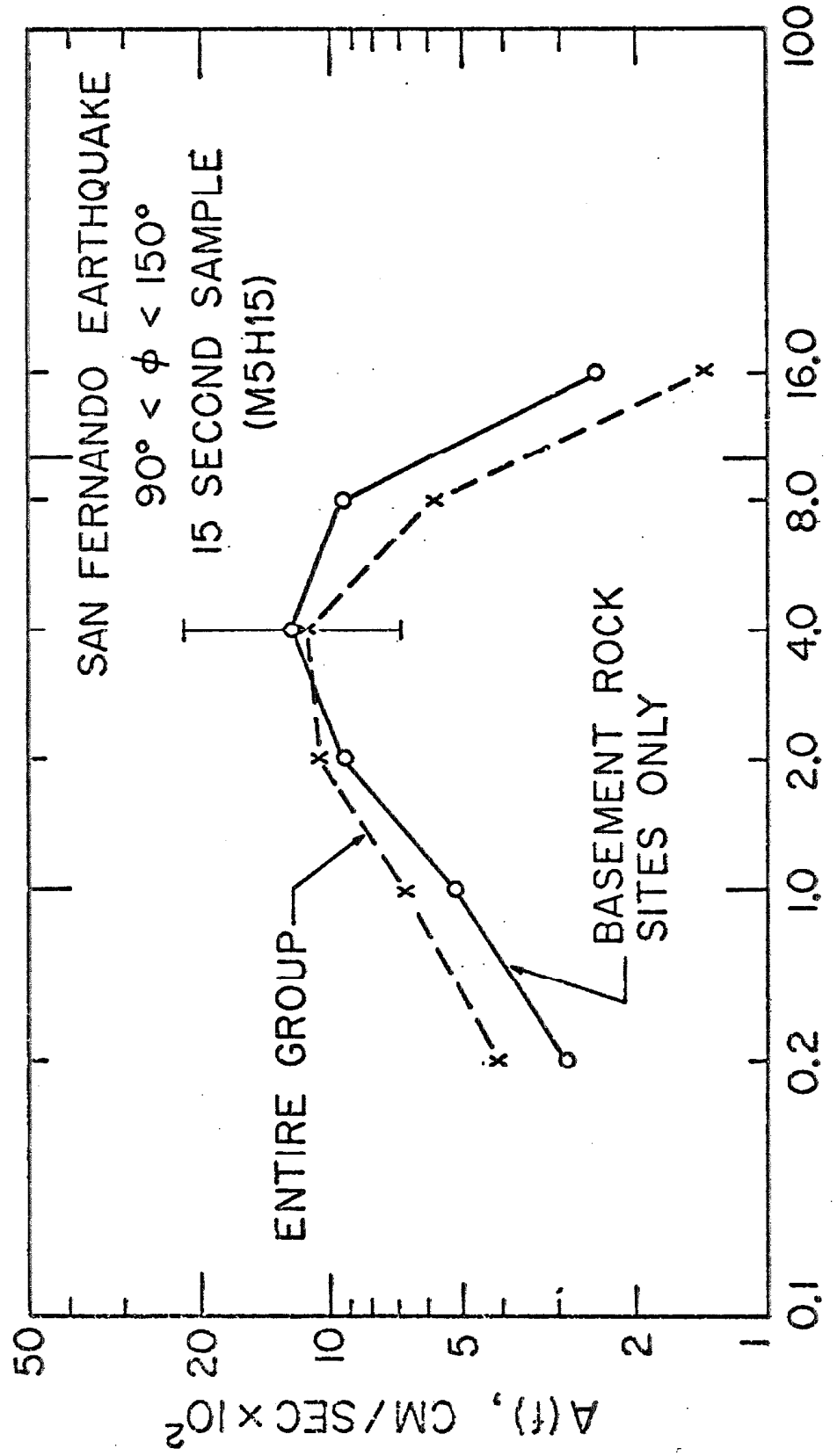

Figure 3.5. Estimates of A(f) from south-eastern M5H15 data. Error bar shows 90% confidence interval for A_4. (See Table 2.17 for intervals at other points).

by a higher value of Q and lower values of A_5 and A_6 (recall that $A_5 = A(8)$ and $A_6 = A(16)$). At the lower frequencies, the effect of material attenuation is not so great, and for $f \leq 4$ Hz the A(f) curves shown in Figure 3.4 should reflect the relative amplitudes faithfully. To a lesser extent the same effect is seen in the south-eastern data in Figure 3.5. Little, if any, real difference can be found between the amplitudes at basement rock sites and those of the group as a whole, in Figures 2.18(e) and (f). Yet in Figure 3.5 at 8 Hz and above, there is a 70 percent difference between the basement rock curve and the curve for the complete group shown in Figure 3.5.

Since basement rock amplitudes show much less scatter than amplitudes from the complete northern and south-eastern groups of data, estimates of A(f) from basement rock data only are considered to be more reliable than those from the complete data groups. The basement-rock only estimates of A(f) will be used for these two groups in the comparisons that follow.

Independent estimates of the source parameters of the San Fernando earthquake are available from (a) teleseismic observations, (b) field observations of the surface trace of the fault and (c) the distribution of aftershocks. These data are summarized by Wyss and Hanks (1972). Choosing from their summary, seismic moment, $M_o = 10^{26}$ dyne-cm and rupture region radius R = 12 km as representative values of two parameters, (we may equally as well have chosen the fault area, and average displacement, for example) Ω_o and f_o can be calculated from equations (3.2) and (3.5) respectively. Assuming $\beta = 3.2$ km/sec and $\mu = 3 \times 10^{11}$ dynes/cm^2, equation (3.2)

gives $\Omega_o = 830\ R_{\theta\varphi}$ cm-sec at r = 1 km. Substituting R = 12 km into equation (3.5) yields a corner frequency of $f_o = 0.10$ Hz, which is below the 0.4 to 16 Hz range of our data. Thus the flat A(f) acceleration spectrum seen in Figure 3.3, out to 8 Hz which corresponds to f^{-2} behavior in a displacement spectrum, is consistent with the f^{-2} high frequency asymptote of Brune's model.

Substituting for Ω_o and f_o in equation (3.8) and approximating the effect of the free surface by multiplying by a factor of two yields the source model estimate of $\overline{A}(f) \simeq 670$ cm/sec for $f \geq 0.4$ Hz and r = 1 km. In obtaining this value, the further assumption of $R_{\theta\varphi} = 1$ was made. In the case of the southern group this is a good assumption since the maximum of $R_{\theta\varphi}$ modulated by rupture propagation does lie to the south. The difference between emission of energy to the north and to the south is discussed further below. The approximation for the free-surface effect by multiplying by a factor of two is a commonly-used one (e.g. Trifunac, 1972) but is rigorous only in the case of SH-waves.

Thus values of $\overline{A}(f)$, predicted by the asymptotes to equation (3.8), are shown by a solid line in Figure 3.6 which is compared with estimates of A(f) from the strong-motion data. Two points requiring discussion arise from Figure 3.6. First, there are differences among the three A(f) functions themselves estimated from the three groups of strong motion data. Second, is their relationship to the source model prediction $\overline{A}(f)$.

On the first point, the question arises of whether the differences at low frequencies reflect a greater propagation of energy to the south

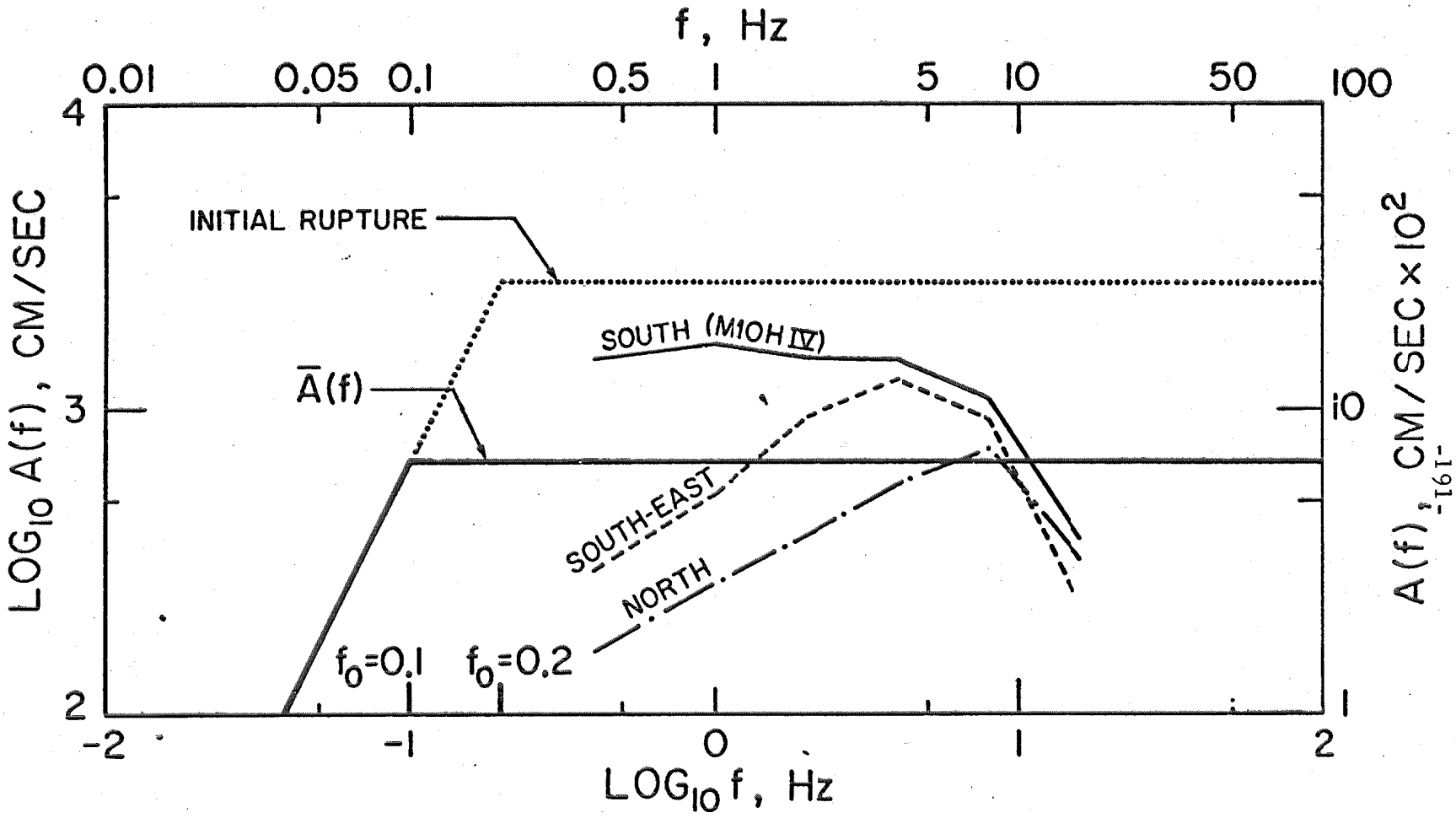

Figure 3.6. Comparative plot of A(f) estimated from southern M10HIV data and northern and south-eastern M5H15 data from basement rock sites. The spectrum labeled $\bar{A}(f)$ has the source parameters $M_o = 10^{26}$ dyne-cm and R = 12 km. The dotted spectrum corresponds to the hypothesis of massive initial rupture over a much smaller area, with $M_o = 10^{26}$ dyne-cm also, but R = 6 km.

of the epicenter by the rupture mechanism, or the difference is a consequence of wave amplification by the deep sedimentary deposits in the Los Angeles Basin. While it is impossible to resolve this question beyond any doubt, there are reasons, given below, to suppose that the San Fernando source did, in fact, radiate more energy to the south than to the north. The pattern seen in Figure 3.6 is consistent with rupture initiating at depth at the northern end of the northward dipping fault and then propagating upward and southward along the fault, focusing energy to the south. Southward propagation of the San Fernando rupture has been postulated by others (e.g. Trifunac, 1974). Such a focusing effect requires coherent propagation of rupture for the constructive and destructive wave interference responsible for focusing to take place. Bearing this in mind, the following explanation can be given for the converging curves in Figure 3.6 showing the observed A(f) from the three data groups.

If the rupture propagation velocity appears constant when it is averaged over a certain length of fault, then waves of that length (or greater) should interfere and give rise to a definite focusing pattern. But if, when viewed over shorter distances, the rupture propagation appears quite erratic, interference can not take place. From the curves in Figure 3.6 showing the three values of A(f), it appears that for wavelengths corresponding to 0.4 Hz, the San Fernando rupture propagated quite coherently, and a definite focusing of energy to the south took place. However, as frequency increases, and in effect the "smoothing distance" decreases, the rupture appears to propagate less and less

coherently with the result that less interference takes place, until at f = 8 Hz rupture appears to be quite incoherent, and nearly equal amounts of energy are radiated in the three directions studied.

Evidence that amplification by sediments was not the major cause of the higher average level of accelerations recorded to the south can be found in Table 2.14. Here it is seen that sedimentary sites in the northern group were accelerated, on the average, 2.2 times more strongly than the basement rock sites of that group. Yet there is a factor of 10 difference between the southern and northern curves at 0.4 Hz in Figure 3.6; thus a difference by a factor of nearly five remains. It is not until f > 4 Hz that the two curves come to within a factor of 2 of one another and amplification by sediments of the Los Angeles Basin can be invoked as a likely cause of the differences in A(f).

A comparison between amplitudes recorded on rock to the north and to the south of the epicenter supports the assertion that more energy was radiated to the south. Figures 3.7 show amplitude data points from basement rock sites to the south of the epicenter and also the attenuation curves for the basement rock sites of the northern data group (short dashes) and for the south-eastern group (long dashes). The solid line shows the average amplitudes of the M5H15 southern group as a whole. In the range 0.4 to 4 Hz, all the southern data (P221 and P223 from the south-eastern group are included, as are G110 and N191 which are sited on relatively shallow depths of sediment) are above the average amplitudes of the northern basement sites, by

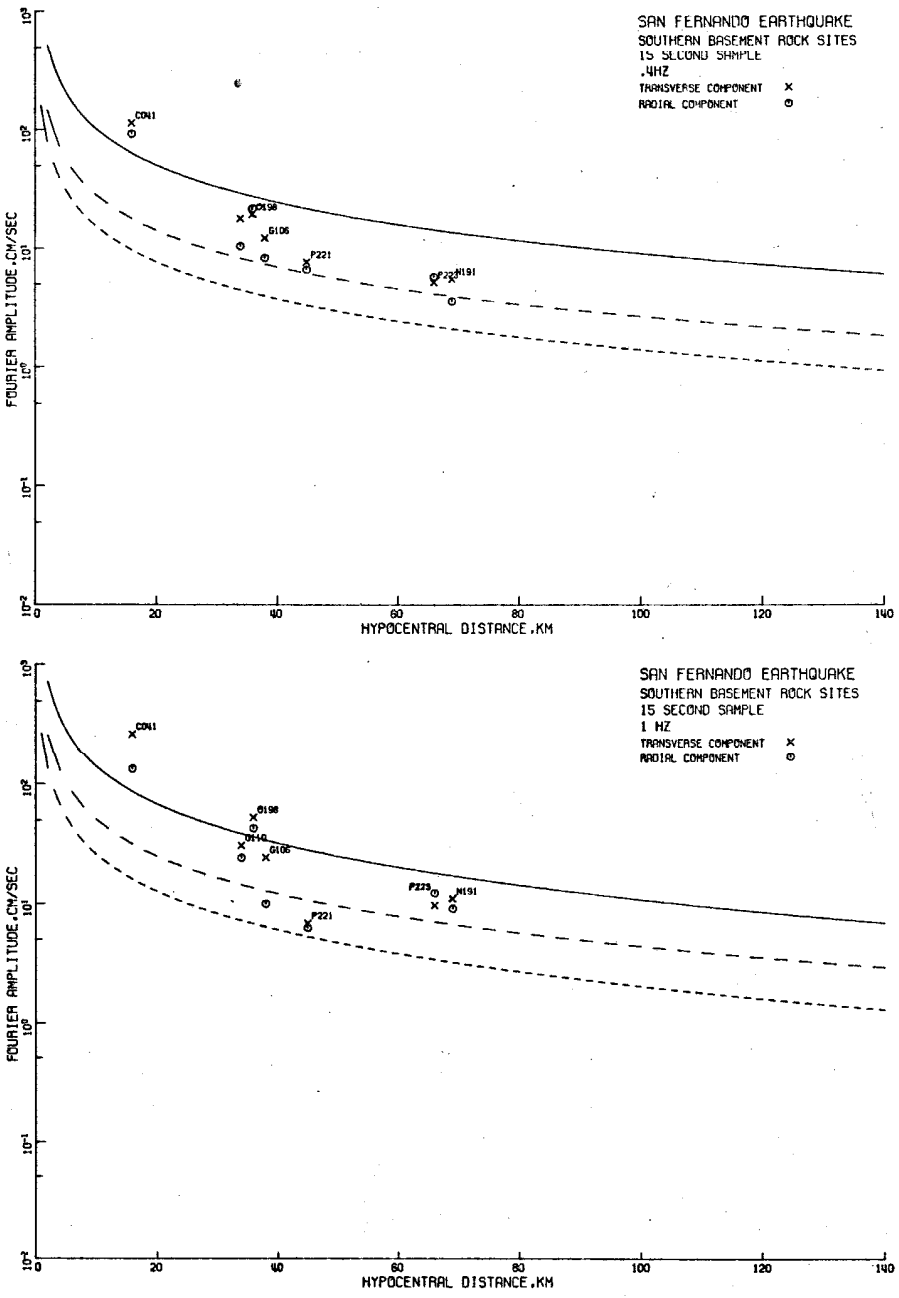

Figure 3.7. Comparison between basement rock amplitudes at different azimuths. Points show southern M5H15 data; short-dashed line, the average northern M5H15 basement amplitudes; long-dashed is from S-E M5H15 basement data. The solid curve shows the average of all southern M5H15 amplitudes.

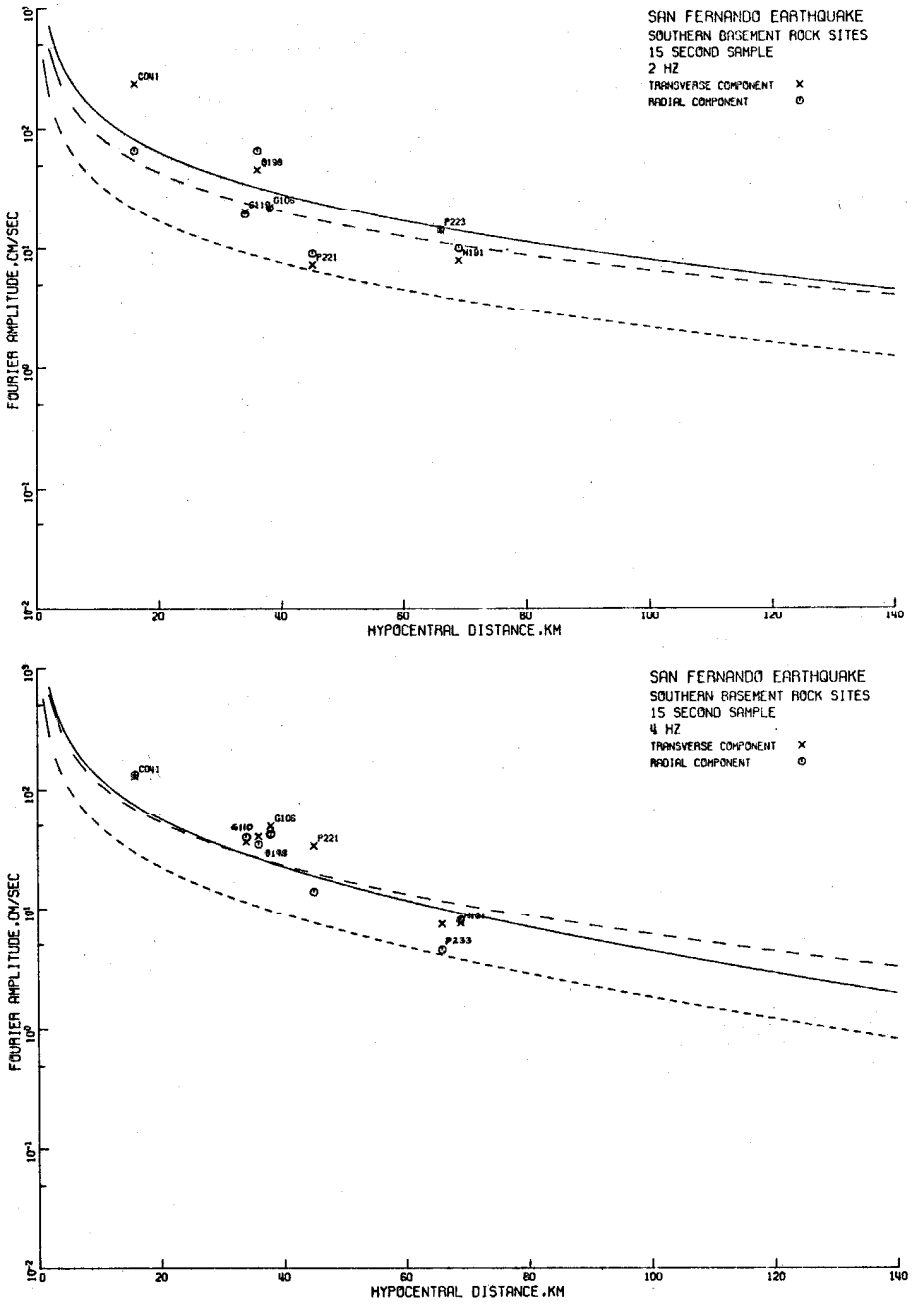

Figure 3.7. Continued.

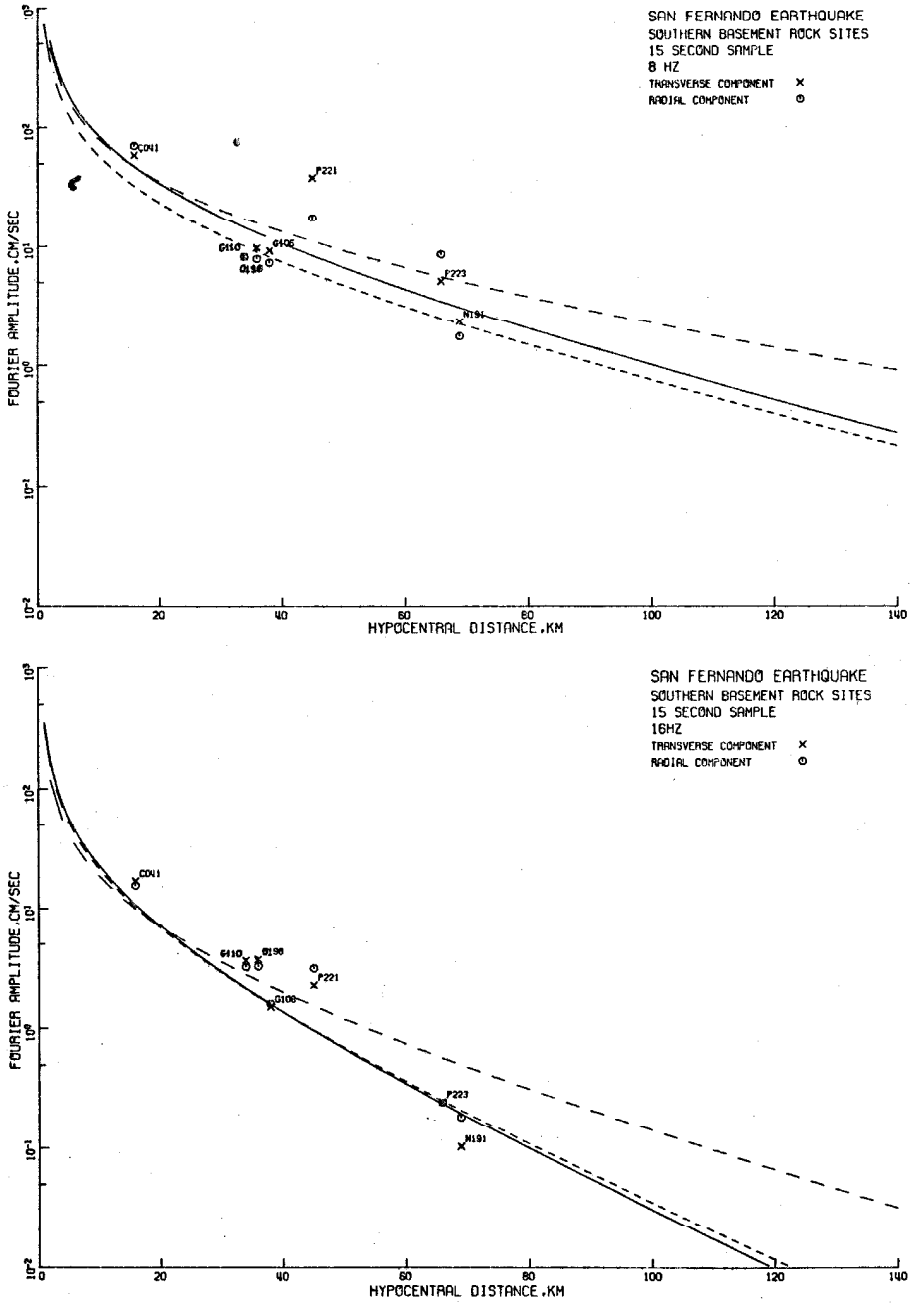

Figure 3.7. Continued.

an average factor of about 3. Thus at these frequencies, radiation was apparently stronger to the south. At 8 and 16 Hz little if any difference can be seen between the southern and northern basement sites. This is consistent with the hypothesis that coherence of rupture is lost at 8 Hz and above.

It is interesting to note that except at 0.4 Hz, and to a lesser extent at 1 Hz, the basement-site amplitudes are evenly scattered above and below the solid line in Figure 3.7, depicting the average behavior of the southern group as a whole. This suggests that high frequency components are less sensitive to geologic structure than low frequency (0.4 to 1 Hz) components.

Returning to Figure 3.6, it is seen that $\overline{A}(f)$ estimated by the source model from equation (3.8) falls below A(f) from the southern group of strong motion data by a factor of nearly 2.2. Considering the approximations involved in the model, together with the scatter in the strong-motion data, this is, however, close agreement.

Further evidence that the $A(f)_{south}$ curve in Figure 3.6 faithfully represents the strength of the seismic energy radiated to the south can be found in a comparison between this curve, and the amplitude of ground displacement spectrum from a Wood-Anderson seismograph at Pasadena, shown in Figure 4 of Wyss and Hanks (1972). Making appropriate conversions between displacement and acceleration spectra and scaling to a common distance r, it is found that the southern A(f) from the strong-motion data agrees closely with the amplitude spectrum from the Pasadena Wood-Anderson record, which was obtained on sound crystalline rock.

An explanation for the high value of A(f) may lie in the suggestion of Hanks (1974a), that the San Fernando faulting was initiated by an extremely energetic, but localized rupture in the hypocentral region. He estimates the following source parameters for this initial event:

M_o 0.85 to 1.7×10^{26} dyne/cm

R 3 to 6 km

Taking the source parameters of the initial event as $M_o = 1 \times 10^{26}$ dyne/cm and R = 6 km, for example, leads to the same low-frequency asymptote as before, but extended upward, now to a corner frequency of 0.2 Hz. The corresponding spectrum, which for $f > 0.2$ Hz is about 50 percent higher than before, is shown by the dotted line in Figure 3.7. Hanks attributes the occurrence of the highly energetic initial rupture to a very non-uniform distribution of strain energy in the fault region.

A third point to note from Figure 3.6 is the marked fall-off in amplitudes with frequency for f above about 8 Hz. In the exact solution of Randall (1966) for a spherical relaxation source, there are periodic windows in the high-frequency spectral amplitudes, where amplitudes go to zero. This may be the effect seen in the A(f) values above 8 Hz although the fall-off in Figure 3.6 is not consistent with the spectrum from Randall's model when corrected to the corner frequency of this study. However, the San Fernando earthquake clearly did not have a spherical source, and given a more realistic model of faulting, the observed fall-off in the A(f) values may contain useful seismological information. It should be noted that Crouse (1973)

observed the same phenomenon. He suggested that it might be caused in part by the fact that most strong-motion accelerographs are situated in building basements which often have dimensions of the order of the wavelength of 8 Hz components, and thus the rigidity of the basement floor would tend to impede transmission of these and higher frequency components. However, he rejected this idea as the complete cause of the spectral fall-off since it was also evident in free-field record spectra.

It is encouraging that the two estimates for $\overline{A}(f)$ enclose the observed spectral levels, but their difference is indicative of the lack of precision inherent in the two-parameter model. The strong initial rupture hypothesis serves to further illustrate the complexity of actual rupture mechanisms, and indicates the detail required in any model that is to predict seismic radiation accurately. Clearly more than two parameters are required, and with the amount of research now being made into tectonic processes in general, and rupture mechanisms and material behavior of rock in particular, there is considerable hope that better understanding and more comprehensive models will be forthcoming. In the meantime, it is heartening that the simple two-parameter model has been able to recover the overall spectral features at both teleseismic and strong-motion distances. From the results of this study, and those cited above, it appears that, given two independent source parameters, A(f) can be predicted to within a factor of about two to three.

An example is given in Chapter 4 of the use of the simple source model, together with the attenuation expression and scatter statistics of Chapter 2, to predict a design earthquake.

3.3. Conclusions from Chapter 3.

The conclusions of the previous section may be summed up as follows.

(1) The nearly flat Fourier amplitude of acceleration "reference" spectra A(f) obtained from the strong-motion data in the frequency band 0.4 - 8 Hz correspond to high frequency asymptotes proportional to f^{-2} in an amplitude of displacement spectrum. This in turn suggests a rupture mechanism involving a sudden drop in (shear) traction (Brune, 1970; Randall, 1973a).

(2) The two-parameter far-field shear wave model estimated the average strong-motion amplitude spectrum to within a factor of 2 to 3. As a corollary, stations at 10 km (Pacoima Dam) or more from the San Fernando earthquake epicenter may be considered to be effectively in the far-field.

(3) Stronger "reference" spectral amplitudes, A(f), were recorded to the south of the epicenter than to the north. The main cause of this was attributed to propagation of the rupture mechanism from north to south, causing focusing of energy southward. However, some contribution from amplification by the Los Angeles Basin sediments cannot be ruled out.

(4) The divergence at frequencies below 8 Hz of A(f) from the three different data groups, and their near-coincidence at frequencies

above 8 Hz, suggest that the rupture propagation became coherent when viewed over distances larger than the wavelength of 8 Hz components. On the other hand, it was incoherent when viewed over distances equal to the wavelength of components with frequencies greater than 8 Hz.

(5) The magnitude of the uncertainties involved in spectral predictions – and hence in design earthquake estimates – should be emphasized. At present, uncertainties in the source model alone of the order of two to three are apparent. These are large by the standards of engineering where safety factors of generally much less than two are normal. Even when more comprehensive models incorporating a larger number of source parameters are avilable, accurate estimates of seismic radiation will still be difficult. It is hard to see, for example, how the massive, localized initial rupture proposed for the San Fernando earthquake could be predicted in advance.

4. AN EXAMPLE OF DESIGN EARTHQUAKE ESTIMATION

In this chapter, the practical engineering problem of estimating a design earthquake is considered. In Chapter 1 some discussion was made of the shortcomings of presently used procedures. The method proposed here, using the results of the previous two chapters, offers an alternative to them. While it still models the physics underlying the generation and the propagation of strong earthquake motion very approximately, it is considered to be an improvement on the previous, completely empirical, methods.

The specific problem addressed is to estimate the Fourier amplitude of ground accelerations at a known distance from a fault rupture, given estimates of the faulted area and average surface offset. The method is to use the simple two-parameter source model discussed in Chapter 3 to estimate the source excitation strength A(f), and then to use the amplitude decay expression and scatter statistics of Chapter 2 to obtain expected amplitudes of ground acceleration at the site. The procedure is explained by way of an example.

The largest earthquake against which the two-parameter model has been tested is the M = 7.2 Dasht-e-Bayāz, Iran, earthquake of August 31, 1968 (Hanks and Wyss, 1972). Since the model is essentially empirical, it may not be appropriate for larger earthquakes. Difficulties may arise from (a) the elongated rupture area of larger earthquakes which violates the assumption of a circular fault surface, (b) the assumption of a point source implicit in equation (2.6) (this does not, apparently,

cause difficulties for $r \geq 16$ km in the case of the San Fernando earthquake), and (c) the effect of rupture propagation. Further discussion of these problems is beyond the scope of this study. However, the point that geophysical source models have much to offer earthquake engineering remains valid, and it is expected that realistic source models applicable also to $M > 7$ earthquakes will one day be available to engineers.

The wave propagation link in the design earthquake estimation chain, given by the amplitude decay expression of equation (2.6) is, of course, quite general, provided appropriate values of Q are known. For larger earthquakes, the decay expression can be incorporated into integral representations of moving ruptures as well as to large fault areas in a straightforward manner. In this case, for $r \leqslant R$, the geometric spreading factor will be more complicated than the simple $1/r$ term of equation (2.6), with details coming from the integration. Scott (1972) has suggested a way in which the effect of finite fault size may be accounted for and yet a simple geometric spreading expression retained.

For the San Fernando earthquake, the amplitude decay expression of equation (2.6) appears to be valid for $r \geq 16$ km (the Pacoima Dam hypocentral distance). Since the source dimension R has been estimated as 12 km a tentative simple criterion of $r > 1.5$ R for the validity of equation (2.6) for near-circular faults is suggested.

A further question normally considered in design earthquake estimates is that of the effect of the surface geology at the site. The

statistical studies of Chapter 2 show that for practical purposes, within the range of surface geologies found in the Los Angeles region, there was no difference in intensity of recorded strong ground shaking among sites with "soft", "intermediate" or "hard" surficial geology. It is considered that this conclusion may be generalized to other geographical regions with coarse-grained, generally dense, sediments or stiffer surface formations. How far these conclusions may be applied to softer sediments is, for the present, a matter for speculation. The soft clay formations at Mexico City and the San Francisco bay muds are clear exceptions. Because of the number of variables involved, it is likely that this question will remain open until a sufficient number of strong-motion accelerograms are recorded on a wide variety of geologic formations.

4.1. Worked example.

It should be noted at the outset that the procedure below applies only to the frequency range of this study, i.e. to $0.4 \leq f \leq 16$ Hz, and to ground motion effectively in the far-field, i.e. $r > 1.5$ R, say. For prediction of low-frequency ($f < 0.4$ Hz) components of ground motion and of motions in the near-field, the reader is referred to Hanks (1975) and Trifunac (1973) respectively.

Suppose that an estimate is sought for a design earthquake resulting from rupture on a fault passing within 50 km (the perpendicular distance from site to fault) of a building site. Suppose, furthermore, that the fault has a history of strike-slip movement and that conservative estimates of the expected length L, and depth of rupture h, and

surface offset u_{max} are available as follows:

$$L = 40 \text{ km}$$

$$h = 12 \text{ km}$$

$$u_{max} = 40 \text{ cm.}$$

The average dislocation $\bar{u}$ is obtained from Knopoff's (1958) result for strike-slip dislocation as

$$\bar{u} = \frac{\pi}{4} u_{max} \approx 30 \text{ cm} .$$

(In the case of a thrust fault, Starr's (1928) result of $\bar{u} \approx 3/4\ u_{max}$ should be used.) These parameters correspond roughly to an $M_o = 4.3 \times 10^{25}$ dyne-cm or $M_L = 6.5$ shock.

Assume that the site is situated in a coarse-grained, sediment-filled valley in Southern California. A value of specific attenuation Q of 330 is chosen from the results of this study.

Following Hanks and Wyss (1972), the source dimension for a rectangular fault is taken to be

$$R = L/2 = 20 \text{ km.}$$

rather than the radius of the equivalent circle. Assuming the normally-used values of β and μ for the upper crust, the computations commence with the following information:

(a) Source parameters

$R = 20$ km

$\bar{u} = 30$ cm

(b) Specific attenuation

$Q = 330$

(c) Physical constants

$$\mu = 3 \times 10^{11} \text{ dyne/cm}$$

$$\beta = 3.2 \text{ km/sec.}$$

I. Determination of $\overline{A}(f)$.

The corner frequency f_o is found from equation (3.5) as follows

$$f_o = \frac{2.34}{2\pi R}\beta = 0.060 \text{ Hz} .$$

From Figure 3.1 it is seen that $\overline{A}(f)$ is essentially constant for values of $f/f_o > 5$, say, and is given by A_o. Since this procedure is limited to $f \geq 0.4$ Hz, we have for this earthquake $f/f_o \approx 7$. Thus to a good approximation, $\overline{A}(f) = A_o$, for all $f > 0.4$ Hz. Using equation (3.10), and incorporating a factor of two to account for the effect of the free surface, and evaluating A_o at $r = 1$ km we obtain

$$A_o = \frac{2.72\beta\overline{u}}{r} \Re_{\theta\varphi}$$

$$A_o\Big|_{r=1\,\text{km}} = \frac{2.72(3.2 \text{ km/sec})(30 \text{ cm})}{(1 \text{ km})} \Re_{\theta\varphi}$$

$$A_o\Big|_{r=1\,\text{km}} = 260\, \Re_{\theta\varphi} \text{ cm/sec.}$$

Since it has been assumed that the fault break occurs on the section of fault nearest to the site, $\Re_{\theta\varphi} = 1$ exactly. (See e.g. Randall, 1973a for an explicit expression for $\Re_{\theta\varphi}$.) However it is not known how well $\Re_{\theta\varphi}$ is developed in strong ground motion, and until more information is available, the use of $\Re_{\theta\varphi} = 1$ in all circumstances is recommended.

In Chapter 3 it was noted that agreement has been found by several investigators between model predictions and independent

observations of A(f) to within a factor of two to three. Thus a factor of, say, three should be applied to the predicted $\overline{A}(f)$ to account for uncertainties in the model. (It should be noted that an even greater uncertainty factor should be applied to currently used magnitude to peak acceleration correlations, since their physical basis is weaker than that of even the two-parameter model.)

Thus the final estimate of $\overline{A}(f) = A_o$ evaluated at $r = 1$ km is

$$\overline{A}(f) = 780 \text{ cm/sec}, \quad \text{for } 0.4 \text{ Hz} \leq f \leq 16 \text{ Hz}.$$

II. Allowance for amplitude decay during propagation.

Recall equation (2.6):

$$\overline{X}(f, r) = \frac{A(f)}{r} e^{-(\pi f r / Q\beta)} \qquad (2.6)$$

Substituting for $\overline{A}(f)$, β and Q and r into equation (2.6) yields the following expression for expected Fourier amplitudes at the site

$$\overline{X}(f, 50) = \frac{780}{50} e^{-(50f/330\beta)}$$

which gives

$$\overline{X}(f, 50) = 15.6\ e^{-0.047f} \text{ cm/sec for } 0.4 \text{ Hz} \leq f \leq 16 \text{ Hz}.$$

This expression is shown in Figure 4.1.

III. Allowance for the uncertainties in the wave propagation.

At this point we have an expression for the expected, or average, Fourier amplitude of ground acceleration as a function of f, at the site. This does not, however, allow for the random nature of wave propagation through the earth's crust. The randomness in propagation is expressed in the scatter seen in the Fourier amplitudes plotted in Chapter 2. The statistical character of the scatter has been described

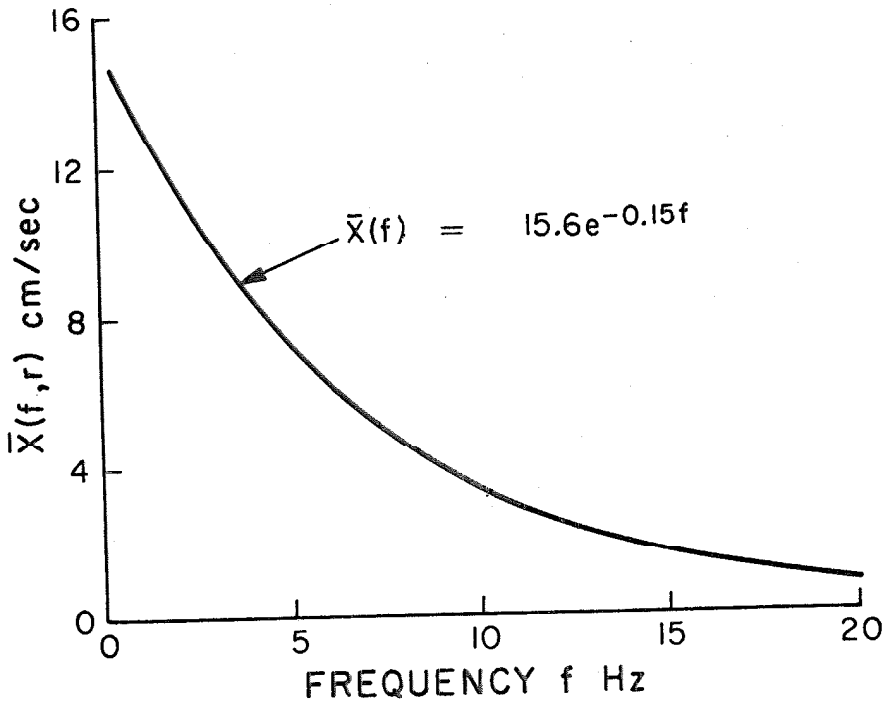

Figure 4. 1. Expected value of Fourier amplitude of ground acceleration at site considered in the example.

by the distribution of k-values, which in turn depends upon the smoothing effect of structural damping. The accumulated relative frequency curves are recomputed in a convenient form for engineering use and are given in Appendix 4. In effect, they provide the probability of occurrence of a given value of k [denoted in the plots in Appendix 4 by F(k).].

Thus, depending upon the risk of earthquake damage considered acceptable, a value of F(k) is chosen and the corresponding value of k read from the appropriate curve in Appendix 4. The expected amplitude, $\overline{X}(f, r)$, is then multiplied by k to obtain an estimate of Fourier amplitude which has the probability F(k) of not being exceeded during the earthquake. Since frequency f and the amount of damping in the structure enter as parameters in the k-value distributions, they must be known for this final step in estimating the design earthquake to be performed.

For example, suppose we are interested in the response of a structure in the n^{th} mode with natural frequency $f_n = 1$ Hz, say, and with equivalent viscous damping ζ equal to 2 percent. From equation (2.16), namely,

$$\frac{\Delta f}{f_n} = 2\zeta \qquad (2.16)$$

where Δf is the half-power bandwidth of the resonance peak at f_n, we find that

$$\frac{\Delta f}{f_n} = 0.04$$

Suppose further that we wish to have 90 percent confidence that our

amplitude estimate $\overline{X}_{90}(1, 50)$ will not be exceeded. From the curve in Figure A4.2 corresponding to $\gamma = 0.04$ (the assumption of $\gamma = \Delta f/f_n$ is discussed in Appendix 4) and $f_n = 1$ Hz, we find that $k_{90} = 2.1$. From equation (2.13) defining k, we find that

$$X_{90}(1, 50) = k_{90}\overline{X}(1, 50)$$

$$= 2.1 \times 15.6\, e^{-0.047}$$

$$= \underline{31.3 \text{ cm/sec}} .$$

Thus, given values of the fault parameters, an estimate of amplitude of ground acceleration specifying the design earthquake has been made, and the random nature of the propagation path has been considered. Recalling that the study of high frequency components of ground motion was confined to Fourier amplitudes rather than using accelerograms themselves in the time domain, or amplitudes and phases in the frequency domain, this is strictly as far as the ground motion estimating process can be taken. Improved source modelling in particular, may improve the quality of these estimates, but as long as phase information is random at the frequencies considered, a more complete description of ground motion than that given by Fourier amplitude is not possible. Thus the geophysical problem of estimating a design earthquake has been solved, albeit in an approximate manner.

4.2. Suggestions for the step from amplitude of ground motion to structural analysis.

Since the specification of design earthquakes by their Fourier amplitudes is not customary in earthquake engineering, some suggestions of how they might be applied to structural analysis will be given.

The now fairly extensive compilation of existing accelerograms could be searched for one, or preferably several records meeting the estimated Fourier amplitude requirements. This might be done by searching for suitable Fourier spectra in Volume IV of the Caltech EERL series (Hudson, ed., 1972) and then using either the accelerograms themselves as input to the structural analysis or using the response spectra computed from the accelerograms and available in Volume III of the EERL series.

To obtain estimates of structural response analytically from Fourier amplitudes of ground acceleration, the theory of random vibrations (Crandall and Mark, 1963; Lin, 1967) is required. It is customary in random vibration theory to use one-sided power spectral density G(f), rather than Fourier amplitude, and estimates of G(f) may be obtained from Fourier amplitude by the relationship (Bendat and Piersol, 1971):

$$G(f, r) = \frac{2}{T_e} \left| X(f, r) \right|^2 \qquad (4.1)$$

where T_e is the time length of record from which X(f, r) is computed. In the case of earthquake amplitudes, some care is required in selecting T_e. Equation (4.1) assumes that the time function, in this case acceleration, from which X(f, r) is computed is stationary and ergodic and that it is computed from a sample of length T_e. In an earthquake, the principal contribution to X(f, r) comes from a finite duration of strong acceleration following the S-arrival, which has a fairly uniform overall amplitude. Given the hypothesis that the length of this period of strong acceleration corresponds to the duration of fault rupture,

rupture duration is an appropriate choice for the value of T_e. If it is further assumed that the rupture is unilateral and proceeds at near the shear wave velocity,

$$T_e = \frac{2R}{\beta} \quad . \tag{4.2}$$

Thus power spectral density of acceleration may be estimated from

$$G(f, r) = \frac{\beta}{R} \left| X(f, r) \right|^2 \tag{4.3}$$

obtained by substituting equation (4.2) into (4.1).

Caughey and Stumpf (1961) solved the problem of the transient response of a damped, single-degree-of-freedom oscillator to stationary, Gaussian random input, given its power spectral density. Thus, knowing $G(f, r)$ and T_e, and making the assumption that the ground motion is Gaussian, in effect a response spectrum ordinate is obtained.

Jennings et al. (1968) generated artificial accelerograms from sections of stationary, Gaussian random processes with a specified power spectral density. Using the same procedures, a single accelerogram or an ensemble of artificial accelerograms could be generated, with power spectral density appropriate to the particular site and fault rupture.

5. CONCLUSIONS AND RECOMMENDATIONS FOR FURTHER RESEARCH

5.1. Summary and conclusions.

This investigation has examined the high frequency components ($0.4\ \text{Hz} \leq f \leq 16\ \text{Hz}$) of strong ground motion from the 1971 $M = 6.4$ San Fernando, California earthquake. The study was confined to the high-frequency components since there is an essential difference in complexity between high- and low-frequency components of strong ground motion in both their generation and their propagation. It has been observed elsewhere that at low frequencies, relatively simple waveforms are generated, and that these may propagate coherently for tens of kilometers. On the other hand, the high-frequency components considered here do not possess simple waveforms and do not propagate coherently over any significant distance. This is attributed to (a) the more complex emission of high-frequency components by the source and to (b) the sensitivity of the high-frequency components to propagation path inhomogeneities. Since these complexities result in a loss of phase coherence, the study was confined to Fourier amplitudes of ground acceleration. Samples at frequencies of 0.4, 1, 2, 4, 8 and 16 Hz were studied.

It was found that, with considerable scatter, the amplitudes follow a simple body-wave decay rule, and that the pattern of scatter is well-defined by the large number of data in the study. Azimuthal variations in average amplitudes were found, and these are attributed chiefly to the focusing effect of the southward propagation of rupture

during the San Fernando earthquake. This observation has important implications for earthquake engineering. Neglect of possible focusing effects may lead to greater realized ground motions than expected, and conversely, high amplitudes caused by rupture propagation in observed data may erroneously be attributed to other effects. This could happen with the San Fernando data, with the generally higher amplitudes recorded in the Los Angeles Basin sediments being cited as proof of the existence of large site amplification effects.

In fact, a statistical study of the relative intensities of ground motion at the 71 sites studied south of the epicenter generally in the Los Angeles Basin revealed essentially no difference in behavior between soft, generally alluvial sites and stiffer sites, generally on sedimentary rock. Furthermore, scatter in the few data available from basement rock sites showed that, from the point of view of seismic hazard, basement rock sites need not be treated differently from sedimentary sites.

Estimates of source excitation obtained from the strong-motion data agree well with (a) estimates from teleseismic observations, and (b) a prediction made by the simple two-parameter source model. This is a useful result for earthquake engineering, since the simple source models offer an alternative to the presently used and far from ideal practice of scaling design earthquakes according to magnitude. An example was worked predicting a design earthquake, using the two-parameter model, the amplitude decay rule, and the amplitude scatter statistics.

The following specific conclusions may be stated:

1. In the frequency range $0.4 \leq f \leq 16$ Hz and for hypocentral distances r in the range of the study, $16 \leq r \leq 120$ km, with considerable scatter Fourier amplitudes of acceleration X(f, r) from the San Fernando earthquake show a monotonic decay with both increasing distance and increasing frequency. This decay may be described by the expression, equation (2.6)

$$\overline{X}(f, r) = \frac{A(f)}{r} e^{-(\pi f r / Q\beta)} \qquad (2.6)$$

where $\overline{X}(f, r)$ denotes average Fourier amplitude of acceleration at frequency f and hypocentral distance r, A(f) is a measure of the source excitation, $1/Q$ is specific attenuation, and β is shear wave velocity.

2. For the mixed basement rock-sediment propagation paths of the southern group of sites, $Q = 330$ was found using a least-squares parameter estimation procedure, within a 90 percent confidence interval of 310 to 360.

3. The scatter about the mean amplitude given by equation (2.6) was measured by an uncertainty factor, k, defined by

$$k = \frac{X}{\overline{X}} \qquad (2.13)$$

where X is an amplitude data point, and $\overline{X}$ is the corresponding average value predicted by equation (2.6). The distribution of k was found to depend strongly upon the resolution bandwidth B_e of the amplitude sample. For constant B_e at each sampling frequency, the scatter distribution was nearly independent of frequency. For

$B_e = 0.73$ Hz, the k-values from the southern group of data had the following statistics:

arithmetic mean,	$\bar{k} = 1.09$
standard deviation,	$\sigma_k = 0.46$, and
third moment,	$m_k = -2.0$.

In view of the large variations in the depth of sediments upon which these data were recorded, the scatter is remarkably consistent, and indicates that sediment depth had little effect on the records.

4. Much smaller groups of data north and also south-east of the epicenter were studied. Because of the small number of records in these groups, results from them do not have the same statistical significance as those from the large southern group. Nevertheless, these groups also showed a regular decay in amplitude with both distance and frequency. Determinations of Q were not as certain as in the case of the southern group. Both groups contained fair distributions of basement rock sites, and values of Q for propagation paths entirely in basement rock were determined. For basement rock sites of the northern and south-eastern groups, $Q = 350$ and $Q = 550$ were found respectively. The 90 percent confidence intervals for these values were wide, being 270 to 500 and 450 to 800 respectively.

5. The source excitation term A(f) in equation (2.6) was also estimated from the strong-motion Fourier amplitude data. At 0.4 Hz, the value of $A(f)_{south}$ was about ten times stronger than that of $A(f)_{north}$, with the south-eastern value being in between. The differences among the A(f) values determined from the three groups

diminished with increasing frequency, until, at frequencies of 8 Hz and above, they were almost identical. This behavior is consistent with the fault rupture initiating at depth on the northward dipping fault, and propagating southward (and upward), with the velocity of propagation being sufficiently coherent for interference to take place between wave components with frequencies below 8 Hz, resulting in the focusing of energy toward the south. However, the progress of rupture was, apparently, sufficiently incoherent or erratic, so that for components with frequencies greater than 8 Hz, interference did not occur.

6. In the northern and south-eastern groups, amplitudes recorded on sediments were generally higher than those recorded on basement rock by a factor of about two. This effect was more marked in the 0.4 and 1 Hz components, and decreased with increasing frequency. In the larger southern group, with only three basement rock sites, no difference in amplitude was found between sedimentary sites with "soft" surface geology and "intermediate" site geology as classified by Trifunac and Brady (1975). Furthermore, spectral peaks in the three basement rock sites were generally as high as or above the average amplitude level of the southern group as a whole. This suggests that amplification by irregular, but well-defined, surface topography typical of basement rock outcrops poses as much of an engineering problem as does amplification caused by stiffness contrasts in sediments. On the basis of this study, no grounds could be found for treating sites on alluvium, sedimentary rock, and basement rock differently in estimating design earthquakes.

7. Values of source excitation A(f) estimated by a simple two-parameter source model agreed with those observed from the strong motion amplitudes, to within a factor of about two to three. This offers considerable promise for a more rational design earthquake estimation procedure than those currently used. A worked example showed how this might be done. However, the empirical nature of the two-parameter model should be kept in mind in engineering applications.

8. The considerable scatter in the data, and the uncertainties involved in source strength estimations deserve mention. The prediction of earthquake ground motions cannot be done precisely, and this should be borne in mind by those carrying out the subsequent structural design work.

5.2. Recommendations for further research.

(1) In the southern group of sites there were conclusive grounds for eliminating all of the winnowed data except those from the Glendale site (F088). Since the extremes of the distribution of k-values depend quite critically upon the winnowing, it is of some importance to resolve the cause of the anomalously high amplitudes recorded at 1 and 2 Hz at Glendale. Furthermore, if the anomaly has a geophysical cause, that in itself should make an interesting study. Vibration tests of both the Municipal Services Building itself, and the adjacent Public Services Building should resolve whether or not the structural response of either building was responsible for the anomaly.

(2) Similar remarks apply to the high k-values from the Wheeler Ridge site (E071) at 16 Hz, and from the Fairmont Reservoir (O207) at 0.4, 1 and 4 Hz.

(3) The spotty distribution of recordings shown in Figure 2.4 indicates the non-uniform distribution of strong-motion accelerographs in the Los Angeles region. A better distribution of instruments would not only record more earthquakes, but also would enable the rupture process to be studied in more detail. The successful application of earthquake engineering depends upon both the estimation of design earthquakes, and the subsequent structural analysis. The behavior of buildings during earthquakes is now relatively well understood. However, it should be clear from this study that the same cannot be said of the seismological phenomena contributing to earthquake ground motion. It therefore seems reasonable, that some portion of the funds now being spent in placing instruments on the upper floors of tall buildings would be better spent in improving the distribution of ground level or free-field instruments. Similarly, there seems little point in placing an instrument on the crest of a dam when there is no instrument at the base or in the nearby free field to record the dam excitation.

Specifically, a more even distribution of accelerographs, particularly those with radio time-signal capability, should enable better investigations to be made of:

(a) The rupture mechanism, in particular the study of fine details of the dislocation time-function,

(b) details of rupture propagation, in particular, the velocity and coherence of propagation, and how this acts to modify the classical radiation pattern, $\Re_{\theta\varphi}$, at frequencies of engineering interest (i.e. say 0.05 to 20 Hz).

(4) A closer examination of the San Fernando strong-motion data could be made for details of the radiation pattern, to study both its frequency and directional dependence.

(5) Consideration should be given to model studies. While these may not give quantitative information, they should lead to a better qualitative understanding of the rupture process, and point to improved ways of using existing and future seismological data.

(6) The marked drop-off in A(f) values at frequencies above 8 Hz may contain useful information about details of the San Fernando source, and may be worthy of consideration by theoretical seismologists.

(7) Further checks of simple source model against existing and future strong-motion records should be made if it is to be used with confidence in design earthquake prediction.

APPENDIX 1: SMOOTHING BANDWIDTH

In smoothing Fourier amplitude spectra to bring out general trends, a balance should be struck between the reduction of the apparently random fluctuations of individual spectrum ordinates about the smoother, underlying base function, and the introduction of bias errors into the base function itself. This point is illustrated in Figure A1. 1, in which the underlying base function has been sketched by hand. It can be seen that smoothing by averaging over a bandwidth B_e centered about the frequency f_1 results in a bias error b_e, in the smoothed estimate of the base function at f_1. In general, bias errors will be introduced by smoothing whenever the base function has a non-zero second derivative.

To determine the minimum amount of smoothing required to reduce the random fluctuations in the spectra without introducing large biases, the following simple experiment was performed. Twelve spectra were selected at random from the set of 15-second accelerogram spectra, and they were smoothed over $N = 2M+1$ spectral points at each of the discrete sampling frequencies used in the study: 0.4, 1, 2, 4, 8, and 16 Hz. The resulting averaged amplitude ordinates $\langle X \rangle$, were plotted against N, for N in the range of 1 to 49. Three typical plots are shown in Figure A1. 2. It can be seen that for small N the random fluctuations in the spectra cause large changes in $\langle X \rangle$ with N. But by about N = 11, $\langle X \rangle$ has settled down, and little appears to be gained by further smoothing. Similar behavior was also observed in the other 9 spectra tested; in all cases N = 9 or 11

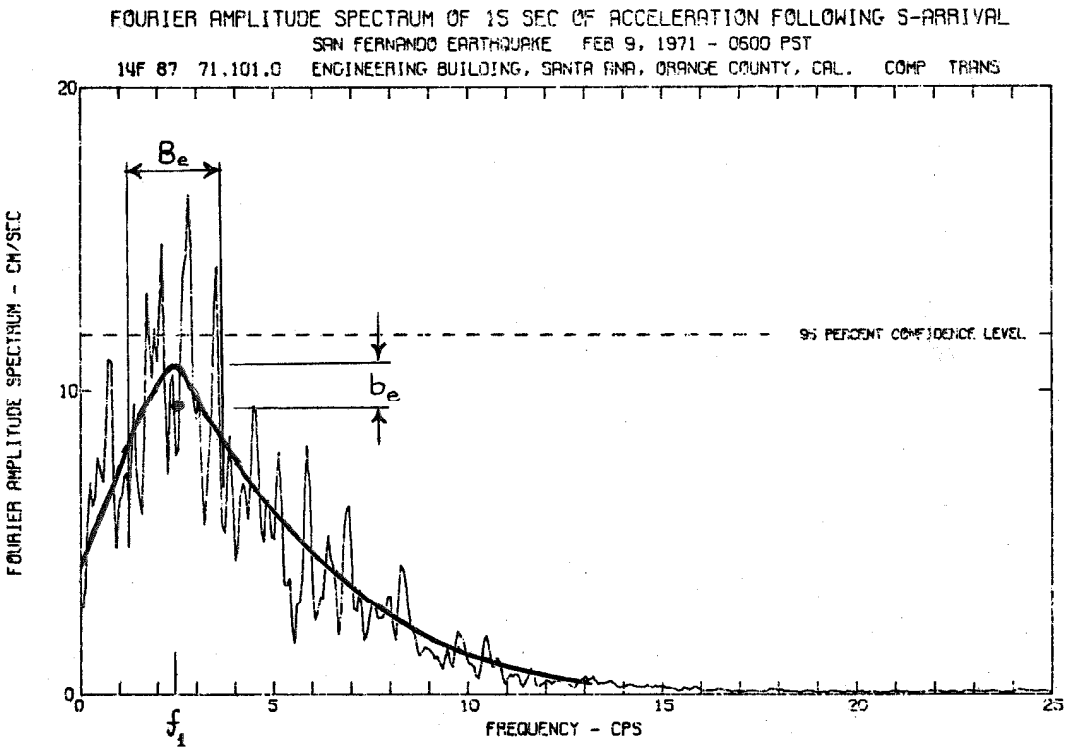

Figure A1.1. Illustration of bias error, b_e, introduced to the smoothed spectrum ordinate at f_1 by smoothing over bandwidth, B_e.

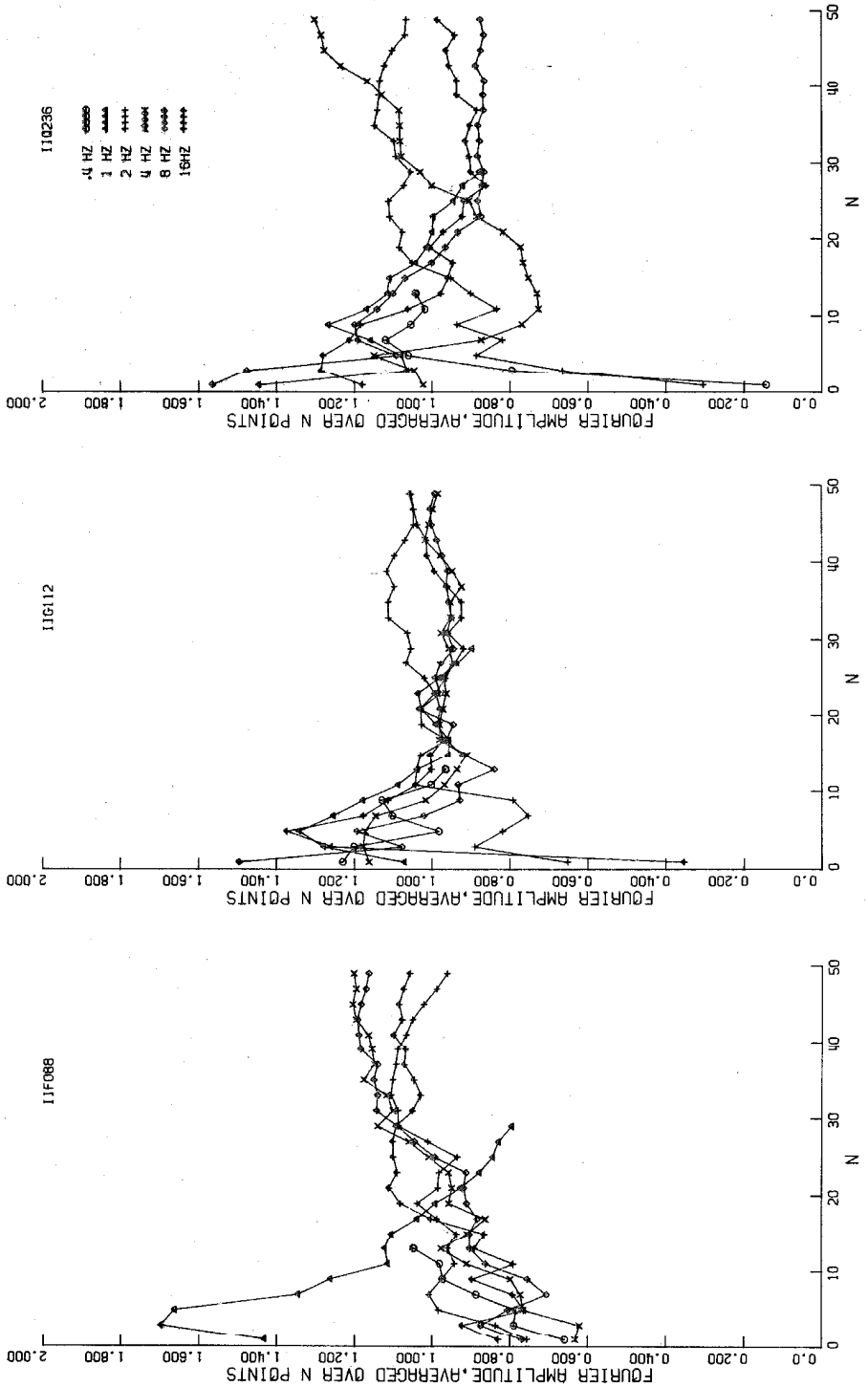

Figure A1.2. Normalized, smoothed Fourier amplitude, smoothed by averaging over N amplitude points.

appeared optimum, and N = 11 (M = 5) was chosen for smoothing the 15-second spectra.

A similar experiment was made with the full-length Volume IV spectra, and N = 21 (M = 10) appeared optimum, and was used throughout for smoothing the Volume IV data.

APPENDIX 2: LISTINGS OF FOURIER AMPLITUDES

The various sets of Fourier amplitude data used in this investigation are listed below. Details of their computation and smoothing are given in sections 2.2 and 2.3 of Chapter 2. Section 2.3 refers to Appendix 1.

SAN FERNANDO EARTHQUAKE
130 < PHI < 200 DEGREES
15 SECOND SAMPLE
142 COMPONENTS

RECORD	R (KM)	FOURIER AMPLITUDE OF ACCELERATION (CM/SEC) (0.4 HZ)	(1 HZ)	(2 HZ)	(4 HZ)	(8 HZ)	(16 HZ)
C041 R	16	92.700	134.000	66.200	134.000	69.700	15.500
C041 T	16	114.000	265.000	236.000	129.000	58.200	16.800
C046 R	26	70.900	79.900	81.200	37.600	11.000*	1.120*
C048 T	26	55.100	77.400	69.000	35.300	8.880*	1.190*
C051 R	45	21.700	26.900	39.600	20.000	10.600	1.810
C051 T	45	27.300	45.300	24.700	14.600	10.300	1.360
C054 R	44	25.200	33.300	43.200	19.100	7.400	0.985
C054 T	44	31.500	43.800	28.300	26.500	7.520	0.761
D057 R	39	27.400	33.800	36.600	27.700	10.700	0.595
D057 T	39	40.800	55.100	27.400	30.800	8.680	0.715
D058 R	39	26.400	35.900	33.900	44.400	27.300	2.150
D058 T	39	43.300	56.900	36.300	40.300	27.700	1.390
D059 R	42	30.600	33.000	26.100	17.400	21.900	3.766
D059 T	42	18.200	18.700	15.900	17.300	15.200	0.559
D062 R	45	26.700	29.200	28.200	26.000	7.790	1.210
D062 T	45	29.500	58.700	40.400	36.000	14.800	1.180
D065 R	42	27.300	37.100	43.500	16.900	5.850	0.406
D065 T	42	43.400	36.000	28.900	23.100	10.900	0.782
D068 R	37	16.000	17.500	30.100	19.900	5.750	1.010
D068 T	37	27.300	31.300	19.700	11.000	9.070	0.844
E072 R	42	24.800	36.500	35.000	11.400	8.300	1.500
E072 T	42	40.000	31.700	23.300	16.300	5.560	1.680
E075 R	42	36.800	49.100	44.300	22.800	8.350	1.050
E075 T	42	33.000	43.700	27.100	27.300	10.400	0.654
E078 R	45	27.000	28.400	26.200	15.600	16.800	1.080
E078 T	45	28.000	45.700	22.600	13.500	12.500	0.976
E083 R	42	30.400	45.600	52.200	30.600	17.100	1.610
E083 T	42	30.100	46.000	27.200	21.000	21.000	1.170
F086 R	51	24.400	22.900	23.800	19.300	5.530	0.590
F086 T	51	29.900	40.800	27.500	20.600	5.450	0.632
F087 R	89	3.650	5.220	11.200	4.240	3.030	0.189*
F087 T	89	6.150	7.660	11.100	7.290	2.580	0.153*
F088 R	37	36.600	115.000*	66.600*	24.800	9.470	0.949
F088 T	37	30.700	65.700*	87.500*	24.500	17.200	1.080
F089 R	46	26.900	35.500	31.900	18.700	8.380	2.480
F089 T	46	33.600	49.900	30.800	19.700	9.940	1.010
F092 R	45	20.700	22.900	13.600	12.900	4.140	1.400
F092 T	45	22.800	32.400	17.300	16.900	4.570	1.340
F095 R	40	29.500	32.100	35.100	15.800	10.800	0.873
F095 T	40	26.300	40.400	16.000	14.800	4.800	0.887
F098 R	45	24.300	26.600	34.100	22.600	14.300	1.320
F098 T	45	36.900	47.600	43.700	18.200	13.400	3.400
F105 R	41	11.300	12.300	13.400	23.300	4.800	0.777
F105 T	41	14.400	16.600	16.600	13.300	7.830	0.598
G106 R	38	8.360	10.000	21.600	41.900	7.250	1.590
G106 T	38	12.300	24.500	22.200	48.700	9.120	1.500
G107 R	42	16.100	34.600	32.300	16.700	6.640	0.961
G107 T	42	16.800	35.300	26.200	16.900	9.940	1.520
G108 R	42	22.600	43.200	30.700	26.600	5.480	0.761
G108 T	42	22.800	46.900	37.000	45.700	6.780	1.100
G110 R	34	10.500	24.400	19.200	39.500	8.160	3.200
G110 T	34	17.900	30.900	20.400	36.000	8.120	3.620
G112 R	45	24.400	27.100	32.300	9.420	10.300	1.270
G112 T	45	30.700	40.600	22.900	10.500	7.540	1.860
H115 R	32	55.300	39.100	41.900	63.200	17.300	2.800
H115 T	32	30.200	19.800	40.300	31.600	10.500	0.830
H118 R	52	14.200	14.900	14.400	6.950	2.670	0.463
H118 T	52	13.100	15.400	14.000	10.400	2.320	0.263
H121 R	45	19.900	25.700	31.400	14.400	8.350	1.750
H121 T	45	28.500	56.100	28.900	22.900	16.200	2.110

* DATA POINT NOT USED

TABLE A2.1. M5H15 Fourier amplitudes of acceleration, southern group.

RECORD	R (KM)	FOURIER AMPLITUDE OF ACCELERATION (CM/SEC) (0.4 HZ)	(1 HZ)	(2 HZ)	(4 HZ)	(8 HZ)	(16 HZ)
H124 R	77	6.090	7.020	8.560	9.440	2.790	0.191*
H124 T	77	5.750	7.970	14.000	11.100	2.730	0.177*
I128 R	39	23.400	22.500	24.100	9.490	5.810	0.672
I128 T	39	21.600	25.900	14.700	11.400	6.110	0.395
I131 R	40	24.100	21.800	28.600	24.700	15.100	0.843
I131 T	40	20.100	24.800	27.500	48.900	17.300	1.120
I134 R	41	22.200	21.100	23.000	12.800	6.400	1.140
I134 T	41	21.600	17.200	34.100	18.800	6.570	0.832
I137 R	32	63.600	72.600	34.800	27.700	16.500	3.190
I137 T	32	21.400	30.900	34.800	19.500	14.900	2.360
J145 R	28	69.800	70.300	35.800	25.200	9.010*	0.857*
J145 T	28	44.700	50.500	43.600	30.500	12.700*	0.877*
J148 R	42	33.600	47.500	36.800	24.200	18.400	1.150
J148 T	42	30.800	32.800	29.100	33.900	12.600	2.290
L166 R	33	19.900	29.400	23.900	20.900	10.800	1.270
L166 T	33	18.900	30.500	34.000	49.500	8.800	1.710
L171 R	140	3.310*	6.080*	4.170*	2.080*	0.845*	0.089*
L171 T	140	2.640*	5.310*	4.460*	2.460*	1.320*	0.101*
M176 R	45	41.400	49.100	24.500	10.000	13.800	1.230
M176 T	45	39.100	36.900	22.200	9.740	8.100	0.729
M180 R	85	4.200	7.270	11.500	7.500	1.690	0.192*
M180 T	85	6.510	7.610	7.870	6.700	1.880	0.174*
N185 R	77	3.870	6.750	11.900	21.300*	11.100*	0.581*
N185 T	77	4.300	5.710	16.300	28.600*	7.080*	0.729*
N186 R	56	15.300	15.000	13.700	26.700*	9.450*	0.851*
N186 T	56	15.600	16.400	22.700	17.200*	15.800*	0.746*
N188 R	41	25.800	22.400	18.800	32.700	11.100	1.580
N188 T	41	20.200	17.300	21.800	19.600	10.000	0.886
N191 R	69	3.570	9.090	9.970	7.900	1.740	0.184*
N191 T	69	5.510	11.000	7.860	7.480	2.320	0.103*
N192 R	43	31.800	43.100	14.600	9.750	12.200	2.140
N192 T	43	32.400	41.000	26.500	15.800	15.500	1.500
N196 R	77	12.400	14.000	16.100	7.940	2.480	0.244*
N196 T	77	9.130	18.500	18.300	12.100	2.240	0.227*
N195 R	123	5.590*	13.500*	11.400*	6.450*	3.960*	0.185*
N195 T	123	5.200*	14.900*	17.600*	7.970*	4.350*	0.211*
O198 R	36	21.800	42.900	65.700	34.400	7.850	3.250
O198 T	36	19.400	52.500	45.800	39.900	9.560	3.710
O199 R	44	30.900	43.000	33.300	30.700	15.700	1.730
O199 T	44	31.500	55.500	48.100	30.700	23.400	0.699
O204 R	75	8.410	6.260	8.440	7.160	1.540	0.167*
O204 T	75	6.000	10.300	10.800	5.780	1.510	0.108*
O205 R	75	8.580	8.720	10.500	6.160	2.490	0.146*
O205 T	75	5.460	8.320	13.500	7.400	1.500	0.124*
P214 R	39	23.800	33.900	46.700	42.200	6.890	1.330
P214 T	39	30.900	58.800	32.500	32.800	13.400	1.540
P217 R	42	29.200	42.100	39.200	16.600	8.410	0.615
P217 T	42	31.400	41.100	16.100	13.000	7.880	0.631
P220 R	97	5.450	8.680	10.300	8.420	2.090	0.188*
P220 T	97	6.720	11.300	13.300	6.390	2.430	0.154*
P231 R	53	17.300	17.000	13.700	6.160	2.380	0.469
P231 T	53	12.600	17.000	16.900	6.140	3.070	0.431
Q233 R	32	45.700	39.400	60.600	67.300	18.200	3.910
Q233 T	32	38.200	28.600	48.600	48.800	17.200	6.250
Q236 R	37	15.400	15.200	11.700	28.800	11.700	1.950
Q236 T	37	24.600	35.500	27.800	19.600	21.600	1.900
Q239 R	41	31.800	21.600	39.700	24.400	19.400	2.230
Q239 T	41	31.300	30.500	38.000	29.700	14.200	1.140
Q241 R	44	29.400	34.300	38.300	16.500	10.700	0.923
Q241 T	44	38.400	56.500	17.500	16.600	12.500	1.390

* DATA POINT NOT USED

TABLE A2.1 Continued

RECORD	R (KM)	FOURIER AMPLITUDE OF ACCELERATION (CM/SEC) (0.4 HZ)	(1 HZ)	(2 HZ)	(4 HZ)	(8 HZ)	(16 HZ)
R244 R	44	24.200	29.900	39.300	17.100	6.810	0.845
R244 T	44	27.400	44.800	28.800	22.300	5.790	0.877
R246 R	38	22.400	38.600	28.300	18.000	8.410	0.957
R246 T	38	35.000	37.400	24.000	22.800	9.420	1.320
R249 R	41	29.300	29.500	22.200	16.500	8.710	1.510
R249 T	41	19.700	18.100	15.100	7.770	12.200	1.340
R251 R	44	25.100	34.400	56.200	23.500	4.520	0.980
R251 T	44	31.600	56.700	32.400	27.400	9.600	1.190
R253 R	44	27.500	44.500	49.000	37.500	16.800	1.830
R253 T	44	35.800	45.300	38.100	42.800	14.000	1.920
S255 R	41	31.500	27.600	25.300	25.000	13.400	0.796
S255 T	41	37.600	33.000	40.000	25.600	12.000	0.825
S258 R	47	30.600	33.900	25.900	9.910	3.370	0.928
S258 T	47	24.800	36.200	14.700	12.800	4.060	0.912
S261 R	42	26.500	27.000	24.500	16.000	11.500	1.370
S261 T	42	24.700	26.600	23.100	17.000	9.060	1.820
S265 R	42	29.700	42.000	24.700	21.400	13.400	1.330
S265 T	42	32.400	34.800	16.600	24.000	20.800	1.830
S266 R	42	33.600	49.500	38.000	21.100	11.900	2.390
S266 T	42	33.900	43.200	35.100	31.000	9.410	1.690
S267 R	54	17.000	19.900	17.300	11.200	5.400	0.800
S267 T	54	15.100	20.000	14.000	10.400	8.480	0.738

* DATA POINT NOT USED

TABLE A2.1 Continued

SAN FERNANDO EARTHQUAKE
310 < PHI < 360 DEGREES
15 SECOND SAMPLE
16 COMPONENTS

RECORD	R (KM)	FOURIER AMPLITUDE OF ACCELERATION (CM/SEC) (0.4 HZ)	(1 HZ)	(2 HZ)	(4 HZ)	(8 HZ)	(16 HZ)
E071 R	87	3.210	4.180	2.880	3.240	2.630	0.789
E071 T	87	2.940	4.520	4.220	4.300	2.450	0.396
F102 R	70	1.340	1.250	1.700	5.530	2.680	0.232
F102 T	70	1.750	2.000	2.830	3.210	2.240	0.219
F104 R	54	10.200	15.600	11.200	21.200	4.290	0.424
F104 T	54	12.500	14.300	16.100	10.800	3.920	0.529
J141 R	32	13.200*	60.300*	34.700*	16.200	4.510	0.428
J141 T	32	14.200*	39.900*	33.700*	17.700	8.860	0.605
J142 R	30	10.100	20.100	29.500	22.400	32.300	5.140
J142 T	30	3.660	8.590	9.500	6.910	17.600	2.570
J143 R	30	9.410	10.600	10.900	11.100	9.350	2.910
J143 T	30	4.080	9.750	11.300	14.200	9.140	5.880
J144 R	27	12.400	20.700	19.500	57.300	16.100	4.320
J144 T	27	5.750	23.200	19.200	81.400	16.100	4.480
M179 R	72	1.880	1.340	2.790	2.810	4.310*	1.050*
M179 T	72	1.810	1.610	4.510	3.040	5.520*	0.792*
0207 R	35	7.960*	18.700*	11.500	33.100*	5.600	1.140
0207 T	35	3.610*	7.380*	7.690	10.800*	5.910	0.753

* DATA POINT NOT USED

TABLE A2.2. M5H15 Fourier amplitudes of acceleration, northern group.

SAN FERNANDO EARTHQUAKE
90 < PHI < 150 DEGREES
15 SECOND SAMPLE
34 COMPONENTS

RECORD	R (KM)	FOURIER AMPLITUDE OF ACCELERATION (CM/SEC) (0.4 HZ)	(1 HZ)	(2 HZ)	(4 HZ)	(8 HZ)	(16 HZ)
F087 R	89	3.650	5.220	11.200	4.240	3.030	0.189*
F087 T	89	6.150	7.660	11.100	7.290	2.580	0.153*
F101 R	108	2.970	3.920	6.620	10.600	3.920	0.221
F101 T	108	2.140	4.100	8.730	5.820	2.520	0.185
G106 R	38	8.360	10.000	21.600	41.900	7.250	1.590
G106 T	38	12.300	24.500	22.200	48.700	9.120	1.500
G107 R	42	16.100	34.600	32.300	16.700	6.640	0.961
G107 T	42	16.800	35.300	26.200	16.900	9.940	1.520
G108 R	42	22.600	43.200	30.700	26.600	5.480	0.761
G108 T	42	22.800	46.900	37.000	45.700	6.780	1.100
G110 R	34	10.500	24.400	19.200	39.500	8.160	1.200
G110 T	34	17.900	30.900	20.400	36.000	8.120	1.620
H121 T	45	28.500*	56.100*	28.900	22.900	16.200	2.110
H121 R	45	19.900*	25.700*	31.400	14.400	8.350	1.750
H124 R	77	6.090	7.020	8.560	9.440	2.790	0.191*
H124 T	77	5.730	7.970	14.000	11.100	2.730	0.177*
M180 R	85	4.200	7.270	11.500	7.500	1.690	0.192*
M180 T	85	6.510	7.610	7.870	6.700	1.880	0.174*
M183 R	72	3.520	8.640	13.300	7.170	4.170	0.684
M183 T	72	2.340	4.460	11.000	12.600	3.420	0.793
M184 R	72	3.790	8.960	12.800	8.090	3.860	0.521
M184 T	72	2.350	4.410	10.700	16.200	3.790	0.612
N185 T	77	4.300	5.710	16.300	28.800*	7.080*	0.729*
N185 R	77	3.870	6.750	11.900	21.300*	11.100*	0.581*
N186 R	56	15.300	15.000	13.700	26.700*	9.450*	0.851*
N186 T	56	15.600	16.400	22.700	17.200*	15.800*	0.746*
N187 R	73	3.030	5.870	11.800	19.800*	9.790*	0.553*
N187 T	73	2.840	5.430	11.700	12.800*	9.640*	0.606*
0206 R	109	4.440	8.970	11.700	10.600	2.910	0.196
0206 T	109	4.640	8.210	14.400	9.400	2.260	0.135
P221 R	45	6.640	6.250	9.050	13.900	17.300	3.110
P221 T	45	7.680	6.800	7.250	33.400	37.500	2.260
P223 R	66	5.760	12.300	14.200	4.470	8.540	0.245
P223 T	66	5.170	9.680	14.100	7.360	5.070	0.246

* DATA POINT NOT USED

TABLE A2.3. M5H15 Fourier amplitudes of acceleration, south-eastern group.

SAN FERNANDO EARTHQUAKE
130 < PHI < 200 DEGREES
UNSMOOTHED,.15 SECOND SAMPLE
142 COMPONENTS

RECORD	R (KM)	FOURIER AMPLITUDE OF ACCELERATION (CM/SEC) (0.4 HZ)	(1 HZ)	(2 HZ)	(4 HZ)	(8 HZ)	(16 HZ)
C041 R	16	79.500	193.000	61.800	154.000	123.000	10.500
C041 T	16	86.700	334.000	375.000	64.100	15.400	13.300
C048 R	26	3.530	54.100	19.000	9.100	6.210*	0.629*
C048 T	26	6.870	61.800	61.000	42.400	10.000*	2.080*
C051 R	45	64.900	7.830	15.800	16.800	17.100	1.230
C051 T	45	28.100	27.200	22.000	11.900	19.100	1.610
C054 R	44	69.000	67.400	59.900	13.700	5.730	0.581
C054 T	44	39.500	41.100	8.730	3.230	4.800	0.512
D057 R	39	47.400	36.900	24.300	67.200	2.620	0.341
D057 T	39	28.200	46.400	5.340	9.940	1.730	1.190
D058 R	39	43.800	38.000	10.600	30.000	39.400	1.930
D058 T	39	25.100	42.000	14.500	46.200	22.600	2.820
D059 R	42	39.300	45.900	3.630	31.000	29.700	0.053
D059 T	42	15.400	24.200	9.450	23.000	18.200	1.030
D062 R	45	57.500	29.700	25.900	14.700	5.870	0.595
D062 T	45	6.730	71.300	42.000	19.900	12.200	0.908
D065 R	42	55.100	37.400	30.800	36.400	10.300	0.794
D065 T	42	34.800	61.000	16.700	2.400	12.900	0.899
D068 R	37	17.100	15.500	15.300	8.940	5.850	1.360
D068 T	37	26.400	33.400	13.700	0.394	8.160	1.210
E072 R	42	17.400	21.600	51.900	10.900	10.200	1.390
E072 T	42	21.000	36.600	4.280	29.300	3.480	1.770
E075 R	42	45.000	81.100	24.000	23.100	0.763	1.200
E075 T	42	18.900	44.400	32.400	26.000	8.420	0.763
E078 R	45	77.200	12.700	24.700	18.200	20.400	1.110
E078 T	45	34.300	32.700	8.520	31.100	9.060	0.930
E083 R	42	45.100	25.900	90.600	38.300	18.300	1.720
E083 T	42	32.800	78.500	4.930	64.700	13.100	1.560
F086 R	51	43.400	32.900	13.500	12.000	6.260	1.050
F086 T	51	18.400	63.300	24.200	12.600	5.400	0.569
F087 R	89	3.610	3.730	19.100	9.740	2.640	0.122*
F087 T	89	6.230	4.560	8.270	11.600	3.120	0.071*
F088 R	37	24.500	146.000*	53.400*	17.400	8.500	0.977
F088 T	37	17.300	58.600*	16.900*	45.900	17.700	1.180
F089 R	46	86.800	65.500	73.100	21.200	5.220	1.600
F089 T	46	29.900	90.900	58.800	13.000	11.400	2.230
F092 R	45	56.800	12.300	6.640	13.000	8.810	3.310
F092 T	45	13.800	55.200	13.200	12.800	6.790	1.360
F095 R	40	59.400	17.400	26.400	30.400	1.940	1.340
F095 T	40	27.800	51.900	9.200	7.310	10.200	0.778
F098 R	45	70.400	49.000	27.400	18.600	2.660	0.706
F098 T	45	35.800	75.100	53.400	12.100	7.430	2.710
F105 R	41	18.200	13.400	6.830	26.400	4.610	0.570
F105 T	41	10.800	16.500	7.560	9.790	2.890	0.837
G106 R	38	5.450	6.700	10.200	30.500	10.200	0.407
G106 T	38	16.600	48.200	9.580	26.200	4.480	1.110
G107 R	42	25.100	69.000	39.700	11.000	11.700	0.810
G107 T	42	7.780	72.600	48.000	6.610	2.830	0.806
G108 R	42	32.400	60.000	32.100	24.700	2.800	1.340
G108 T	42	32.600	61.000	29.300	10.700	4.530	2.140
G110 R	34	8.540	11.700	12.300	31.400	8.250	1.990
G110 T	34	27.500	37.200	42.200	32.200	4.390	4.730
G112 R	45	71.900	34.100	56.500	8.490	10.400	0.884
G112 T	45	37.300	39.800	14.600	12.700	12.200	0.631
H115 R	32	49.500	66.800	55.900	19.100	20.400	0.161
H115 T	32	24.400	18.300	25.700	38.800	8.010	0.666
H118 R	52	3.450	8.770	25.600	9.550	2.200	0.264
H118 T	52	1.040	6.340	13.800	8.490	2.110	0.547
H121 R	45	50.100	33.100	22.100	7.740	8.070	2.680
H121 T	45	9.280	46.400	8.510	52.400	14.900	2.300

* DATA POINT NOT USED

TABLE A2.4. M0H15 (Unsmoothed) Fourier amplitudes of acceleration, southern group.

RECORD	R (KM)	FOURIER AMPLITUDE OF ACCELERATION (CM/SEC) (0.4 HZ)	(1 HZ)	(2 HZ)	(4 HZ)	(8 HZ)	(16 HZ)
H124 R	77	7.160	6.790	2.460	7.080	4.930	0.364*
H124 T	77	3.230	3.280	14.000	15.700	1.040	0.279*
I128 R	39	28.600	31.200	22.700	6.740	4.720	0.617
I128 T	39	48.200	27.000	9.170	10.500	8.490	0.307
I131 R	40	55.500	2.310	80.600	29.800	13.100	1.090
I131 T	40	21.500	41.300	23.700	30.100	8.230	1.530
I134 R	41	46.300	6.540	22.300	19.700	7.300	1.540
I134 T	41	18.600	11.400	20.300	13.800	3.850	0.759
I137 R	32	41.900	97.400	46.900	11.600	17.300	2.600
I137 T	32	16.900	25.400	49.600	25.700	19.700	0.758
J145 R	28	97.700	27.900	64.500	56.200	8.560*	0.679*
J145 T	28	24.600	63.300	11.800	39.000	2.560*	2.010*
J148 R	42	41.300	26.100	77.800	10.800	11.900	0.247
J148 T	42	16.500	27.600	77.800	54.500	4.190	2.010
L166 R	33	11.500	16.600	22.400	13.900	8.940	0.955
L166 T	33	20.500	6.840	14.900	54.300	5.450	1.980
L171 R	140	0.953*	6.170*	7.880*	2.260*	0.885*	0.031*
L171 T	140	2.490*	9.540*	5.950*	0.737*	1.130*	0.111*
M176 R	45	68.400	76.900	17.500	1.890	16.400	1.010
M176 T	45	21.800	6.000	17.100	7.060	13.700	0.356
M180 R	85	3.510	4.830	13.500	6.920	1.560	0.284*
M180 T	85	8.490	3.280	6.660	14.400	2.860	0.184*
N185 R	77	2.310	5.500	11.000	14.300*	13.500*	1.040*
N185 T	77	2.830	1.760	15.300	23.900*	6.960*	1.510*
N186 R	56	15.400	18.300	9.750	31.700*	13.600*	0.800*
N186 T	56	19.300	20.300	13.800	27.500*	17.900*	0.901*
N188 R	41	43.600	13.600	16.800	30.300	2.450	0.638
N188 T	41	14.600	16.100	20.400	9.410	8.520	0.742
N191 R	69	2.110	5.000	19.300	1.180	1.930	0.080*
N191 T	69	4.100	25.600	12.300	6.630	1.110	0.198*
N192 R	43	59.700	60.100	22.600	8.430	16.100	0.699
N192 T	43	46.900	66.200	46.500	29.500	28.000	0.745
N195 R	123	9.150*	12.900*	26.300*	7.160*	5.740*	0.173*
N195 T	123	3.480*	9.700*	37.500*	5.090*	4.620*	0.289*
N196 R	77	2.640	19.300	20.700	8.110	2.670	0.191*
N196 T	77	13.800	19.300	24.900	4.720	1.110	0.251*
O198 R	36	12.600	50.200	70.100	14.100	9.230	6.210
O198 T	36	17.800	79.600	65.400	31.700	26.500	4.950
O199 R	44	51.600	39.600	58.900	62.200	29.000	2.130
O199 T	44	24.000	81.100	47.600	14.300	21.300	1.110
O204 R	75	4.220	3.380	5.330	4.740	1.560	0.173*
O204 T	75	6.680	8.920	15.000	2.170	1.640	0.085*
O205 R	75	5.290	11.500	5.420	6.270	2.260	0.094*
O205 T	75	4.640	5.650	22.100	15.300	2.110	0.129*
P214 R	39	31.000	14.900	40.600	40.100	6.940	2.900
P214 T	39	22.700	95.900	51.500	22.900	9.420	1.050
P217 R	42	41.600	25.900	33.100	6.600	8.970	1.430
P217 T	42	14.000	15.500	16.600	10.100	11.300	1.630
P220 R	97	3.160	6.750	8.200	15.200	0.428	0.051*
P220 T	97	5.510	11.800	6.560	4.670	2.590	0.120*
P231 R	53	11.800	5.540	9.350	8.500	0.499	0.121
P231 T	53	13.200	13.100	15.600	3.500	0.551	0.373
Q233 R	32	17.000	74.300	59.200	34.800	8.000	3.360
Q233 T	32	85.200	18.500	116.000	13.000	9.740	0.482
Q236 R	37	7.920	33.900	21.100	16.700	20.200	4.110
Q236 T	37	3.490	43.400	10.000	27.600	29.500	2.090
Q239 R	41	25.800	6.270	7.700	30.100	13.900	2.120
Q239 T	41	37.100	27.600	31.400	26.500	12.200	0.685
Q241 R	44	34.700	31.600	26.700	16.700	13.500	0.698
Q241 T	44	21.000	47.800	4.500	9.320	12.500	1.310

* DATA POINT NOT USED

TABLE A2.4 Continued

RECORD	R (KM)	FOURIER AMPLITUDE OF ACCELERATION (CM/SEC) (0.4 HZ)	(1 HZ)	(2 HZ)	(4 HZ)	(8 HZ)	(16 HZ)
R244 R	44	80.700	11.900	41.600	28.700	5.000	0.796
R244 T	44	40.200	59.100	8.040	36.300	8.590	0.470
R246 R	38	44.800	23.800	15.900	18.000	7.690	0.372
R246 T	38	19.700	44.000	12.800	32.700	9.200	1.990
R249 R	41	40.400	37.900	18.400	14.300	20.300	1.240
R249 T	41	12.800	23.200	5.540	10.000	9.770	0.385
R251 R	44	73.800	50.600	49.000	36.000	4.060	0.775
R251 T	44	41.200	77.500	27.100	8.330	4.920	0.334
R253 R	44	14.700	55.000	10.300	28.000	18.300	2.780
R253 T	44	16.200	65.700	63.200	26.200	19.300	2.150
S255 R	41	16.300	21.300	12.200	39.600	16.800	0.699
S255 T	41	68.400	17.600	39.900	62.500	13.800	0.516
S258 R	47	42.800	24.600	34.500	18.900	1.590	0.485
S258 T	47	15.300	63.400	12.200	23.700	5.040	0.353
S261 R	42	43.400	22.500	2.510	7.810	15.000	1.520
S261 T	42	15.600	7.200	39.000	28.100	7.750	1.870
S265 R	42	50.500	43.500	27.000	5.580	14.500	2.290
S265 T	42	38.100	78.100	7.850	19.300	21.400	2.220
S266 R	42	54.700	47.800	57.800	27.500	7.250	4.100
S266 T	42	8.070	46.300	19.700	25.000	17.500	2.090
S267 R	54	12.700	10.900	4.520	9.020	3.270	0.646
S267 T	54	8.860	9.860	10.200	6.770	6.460	0.607

* DATA POINT NOT USED

TABLE A2.4 Continued

SAN FERNANDO EARTHQUAKE
130 < PHI < 200 DEGREES
FULL RECORDS - SMOOTHED
142 COMPONENTS

RECORD	COMPONENT BEARING	R (KM)	FOURIER AMPLITUDE OF ACCELERATION (CM/SEC) (0.4 HZ)	(1 HZ)	(2 HZ)	(4 HZ)	(8 HZ)	(16 HZ)
C041	164	16	173.000	248.000	165.000	138.000	83.400	18.700
C041	254	16	77.800	171.000	203.000	105.000	67.300	14.100
C048	0	26	104.000	66.300	66.500	37.400	12.600*	1.310*
C048	270	26	111.000	57.100	32.400	30.200	8.170*	1.170*
C051	36	45	29.200	39.500	25.300	15.200	15.000	1.650
C051	306	45	22.000	42.300	29.300	19.300	9.650	1.510
C054	308	44	26.400	58.800	40.500	17.000	8.140	0.934
C054	218	44	32.500	36.800	27.500	40.200	8.550	0.734
D057	180	39	42.100	39.800	39.300	35.300	18.100	0.371
D057	90	39	32.000	49.600	27.200	28.400	11.400	0.781
D058	180	39	37.300	38.500	40.200	46.700	44.600	1.560
D058	90	39	32.700	46.100	38.200	44.100	25.200	1.290
D059	314	42	32.700	30.400	19.100	18.100	11.700	0.631
D059	224	42	37.700	24.000	15.400	16.300	21.300	0.864
D062	322	45	23.900	38.200	21.400	21.400	4.910	1.390
D062	232	45	27.700	51.800	34.500	34.300	11.600	1.210
D065	180	42	36.600	39.700	39.200	22.700	7.140	0.470
D065	270	42	42.300	46.900	36.400	22.500	9.250	0.465
D068	0	37	18.800	18.000	31.700	17.200	6.480	0.860
D068	90	37	36.200	34.700	21.100	11.900	8.850	0.802
E072	285	42	37.800	31.900	23.500	18.600	9.980	1.240
E072	15	42	31.100	54.800	29.500	17.800	11.600	0.550
E075	0	42	53.400	50.300	47.400	21.300	8.260	0.650
E075	270	42	31.800	52.200	39.300	29.800	11.400	0.648
E078	310	45	29.500	43.000	26.200	8.110	12.100	0.607
E078	220	45	36.600	28.400	12.100	19.400	18.600	1.730
E083	180	42	34.200	53.000	54.100	30.700	18.100	1.470
E083	90	42	24.800	49.900	27.200	28.100	13.600	1.310
F086	277	51	24.900	52.000	26.400	22.400	5.610	0.878
F086	187	51	16.500	23.200	19.900	19.300	3.690	0.446
F087	176	89	10.900	15.000	13.200	7.720	3.300	0.182*
F087	266	89	16.400	13.900	13.300	3.530	1.990	0.179*
F088	110	37	43.700	132.000*	105.000*	20.500	17.100	0.880
F088	200	37	37.500	93.800*	58.100*	29.400	13.500	0.844
F089	127	46	31.600	63.300	38.900	29.200	8.420	2.130
F089	217	46	37.800	35.300	17.300	12.500	8.770	1.130
F092	118	45	28.100	34.500	13.900	12.300	4.780	1.180
F092	208	45	26.700	22.400	15.900	17.900	4.170	1.510
F095	92	40	29.900	55.200	19.300	14.600	4.850	1.190
F095	182	40	36.600	44.600	44.400	16.200	9.500	0.938
F098	127	45	23.500	48.700	36.500	23.200	13.000	2.100
F098	217	45	39.200	30.600	37.400	31.500	8.330	2.180
F105	180	41	17.800	12.900	11.100	26.900	3.560	0.712
F105	90	41	17.200	19.700	10.300	19.600	6.730	0.550
G106	180	38	10.600	16.200	10.700	26.200	5.260	1.110
G106	270	38	17.900	33.100	28.100	54.900	7.290	1.360
G107	0	42	16.800	30.500	23.300	16.900	9.030	1.780
G107	90	42	25.300	41.900	39.800	14.700	7.890	0.893
G108	0	42	28.600	28.900	37.400	28.400	6.660	1.100
G108	90	42	35.600	65.100	67.900	17.800	7.020	0.640
G110	98	34	15.900	26.300	11.900	59.500	11.800	3.090
G110	188	34	23.900	33.600	15.200	34.900	6.160	4.840
G112	38	45	26.100	44.300	24.200	9.770	12.000	1.600
G112	308	45	34.400	35.500	23.400	12.000	9.900	1.950
H115	11	32	102.000	39.100	45.000	59.200	16.600	3.140
H115	281	32	72.900	41.500	40.700	27.800	8.810	0.839
H118	135	52	20.300	19.800	18.600	12.300	2.440	0.444
H118	225	52	21.100	15.000	13.900	6.160	3.380	0.389
H121	270	45	42.000	52.400	23.400	20.400	13.200	1.920
H121	180	45	26.300	32.700	30.500	27.200	9.500	1.690

* DATA POINT NOT USED

TABLE A2.5. M10HIV Fourier amplitudes of acceleration, southern group.

RECORD	COMPONENT BEARING	R (KM)	FOURIER AMPLITUDE OF ACCELERATION (CM/SEC) (0.4 HZ)	(1 HZ)	(2 HZ)	(4 HZ)	(8 HZ)	(16 HZ)
H124	270	77	9.780	9.950	9.940	9.020	3.070	0.194*
H124	180	77	11.600	9.920	15.100	8.430	2.600	0.245*
I128	0	39	24.900	22.400	24.000	12.300	5.810	0.865
I128	270	39	27.000	24.600	19.200	13.000	6.530	0.661
I131	50	40	30.500	26.800	31.700	41.300	16.900	1.570
I131	320	40	28.400	29.000	38.700	27.300	10.300	0.657
I134	54	41	33.400	20.100	35.000	13.100	5.320	1.400
I134	144	41	32.200	22.800	25.800	13.900	10.200	1.020
I137	99	32	83.500	46.000	34.400	24.500	10.500	1.510
I137	189	32	105.000	62.400	37.500	38.400	16.900	3.570
J145	180	28	109.000	46.800	44.200	30.000	12.700*	0.776*
J145	270	28	129.000	43.300	22.800	41.700	10.000*	1.020*
J148	0	42	29.900	37.300	28.400	23.700	17.000	1.410
J148	270	42	28.900	34.800	30.300	35.300	13.700	1.810
L166	0	33	16.800	23.700	28.000	16.000	9.260	1.200
L166	270	33	18.400	29.200	42.300	52.300	7.780	2.000
L171	33	140	6.790*	7.560*	4.150*	2.000*	1.290*	0.118*
L171	303	140	6.470*	8.820*	6.250*	2.720*	1.160*	0.079*
M176	37	45	38.600	30.000	14.900	9.040	10.200	0.952
M176	127	45	29.100	68.100	24.600	14.600	4.440	0.872
M180	180	85	11.800	10.600	15.500	11.400	1.440	0.285*
M180	270	85	16.900	13.700	10.700	5.410	1.210	0.152*
N185	130	77	6.970	8.080	12.700	18.900*	15.100*	0.588*
N185	220	77	7.140	8.320	15.300	35.000*	6.440*	0.794*
N186	143	56	21.000	15.100	18.700	27.900*	12.400*	0.754*
N186	233	56	24.900	17.700	22.500	21.900*	17.800*	0.490*
N188	54	41	31.300	20.000	16.900	15.400	12.300	1.490
N188	324	41	30.500	24.200	19.500	31.700	7.230	0.936
N191	65	69	14.900	17.600	5.950	6.330	1.800	0.134*
N191	155	69	12.100	20.500	13.800	4.270	1.660	0.103*
N192	29	43	38.600	30.800	18.300	14.200	12.200	1.690
N192	299	43	35.600	48.000	21.200	10.300	14.200	1.940
N195	33	123	10.900*	23.800*	15.200*	6.580*	4.270*	0.237*
N195	303	123	11.600*	23.900*	17.400*	5.810*	4.090*	0.321*
N196	284	77	23.300	26.500	14.800	13.900	1.980	0.241*
N196	194	77	17.900	24.300	22.400	9.440	2.620	0.191*
O198	180	36	29.400	54.100	64.500	32.400	8.360	3.940
O196	270	36	17.900	64.000	51.500	43.400	13.700	4.740
O199	28	44	39.400	29.800	33.800	24.000	13.700	1.620
O199	298	44	32.100	75.500	48.400	45.900	17.900	1.090
O204	0	75	20.900	12.600	10.400	9.340	1.880	0.164*
O204	90	75	20.500	16.400	12.000	6.170	1.530	0.098*
O205	339	75	18.600	11.200	9.850	3.480	1.820	0.088*
O205	249	75	15.500	13.100	18.000	7.650	1.430	0.157*
P214	269	39	34.400	75.400	37.200	32.100	15.000	1.280
P214	179	39	35.700	43.300	43.100	51.800	5.570	1.430
P217	180	42	40.800	44.200	41.100	17.100	9.140	0.776
P217	90	42	28.200	47.200	19.000	14.400	7.950	0.656
P220	180	97	12.500	15.900	6.860	9.820	1.470	0.144*
P220	90	97	15.300	17.200	13.900	5.290	2.930	0.164*
P231	0	53	29.600	17.400	13.300	6.130	2.460	0.280
P231	270	53	27.900	20.900	18.400	6.840	2.080	0.380
Q233	192	32	79.100	44.100	56.300	64.500	14.200	3.250
Q233	282	32	65.100	33.800	53.400	46.800	13.200	6.260
Q236	180	37	28.900	35.700	29.900	26.100	23.700	1.940
Q236	90	37	16.800	21.800	13.700	27.400	13.800	1.900
Q239	180	41	38.500	23.700	39.900	20.600	17.400	2.290
Q239	90	41	30.000	35.300	36.300	29.500	16.400	1.250
Q241	37	44	40.700	34.000	18.200	18.200	15.000	1.890
Q241	307	44	30.400	49.100	30.200	15.200	7.020	1.350

* DATA POINT NOT USED

TABLE A2.5 Continued

RECORD	COMPONENT BEARING	R (KM)	FOURIER AMPLITUDE OF ACCELERATION (CM/SEC) (0.4 HZ)	(1 HZ)	(2 HZ)	(4 HZ)	(8 HZ)	(16 HZ)
R244	307	44	28.400	50.300	37.400	11.800	6.460	0.952
R244	217	44	42.000	36.400	22.200	30.400	6.190	0.772
R246	180	38	27.100	43.000	28.800	19.200	10.500	1.060
R246	90	38	41.000	48.000	23.600	21.400	7.730	1.260
R249	44	41	35.400	21.800	18.500	13.400	11.100	1.440
R249	134	41	30.900	27.600	20.400	11.000	9.030	1.450
R251	37	44	37.800	34.900	48.800	27.000	7.010	1.470
R251	127	44	28.000	59.400	48.200	22.000	7.150	0.795
R253	330	44	31.400	52.400	46.500	44.500	14.200	2.000
R253	240	44	43.500	39.900	34.200	34.600	14.500	2.400
S255	8	41	40.500	36.000	25.700	24.100	14.800	0.772
S255	278	41	45.400	32.200	42.600	26.200	9.080	0.914
S258	29	47	29.600	30.500	23.600	10.300	3.360	0.698
S258	119	47	34.900	43.600	21.400	12.000	3.540	1.090
S261	59	42	42.300	33.400	19.600	18.300	10.000	1.600
S261	329	42	26.700	22.600	26.800	12.300	12.200	1.480
S265	180	42	29.200	34.800	21.400	20.200	15.000	1.210
S265	270	42	31.500	31.200	19.400	22.800	19.300	1.700
S266	0	42	47.800	43.600	37.600	25.900	10.900	2.720
S266	270	42	34.900	56.100	40.000	51.700	9.270	1.750
S267	0	54	24.000	23.300	16.300	9.240	4.470	0.591
S267	90	54	31.400	25.500	18.000	8.320	6.340	0.893

* DATA POINT NOT USED

TABLE A2.5 Continued

APPENDIX 3: LISTINGS OF UNCERTAINTY FACTORS, K.

The uncertainty factors, k, introduced in Chapter 2 and computed from equation (2.13) provide a quantitative measure of how each site behaved relative to its group as a whole during the San Fernando earthquake. This information may be of use in future investigations of either individual sites or classes of sites.

A complete listing of the k-values used in this study is given below. The amplitude decay parameters from which the k-values were computed are given in the table caption. For convenience of presentation, the A_i values are given in vector notation thus:

$$\underset{\sim}{A} = (A_1,\ A_2,\ A_3,\ A_4,\ A_5,\ A_6)$$

SAN FERNANDO EARTHQUAKE
130 < PHI < 200 DEGREES
15 SECOND SAMPLE

RECORD	R (KM)	UNCERTAINTY FACTOR, K (0.4 HZ)	(1 HZ)	(2 HZ)	(4 HZ)	(8 HZ)	(16 HZ)
C041 T	16	1.78	3.07	2.87	1.72	1.24	1.56
C041 R	16	1.45	1.55	0.80	1.79	1.49	1.44
C046 T	26	1.42	1.50	1.45	0.86	0.39*	0.29*
C046 R	26	1.83	1.55	1.70	0.92	0.48*	0.27*
J145 T	28	1.24	1.06	1.00	0.82	0.63*	0.25*
J145 R	28	1.94	1.48	0.82	0.68	0.45*	0.25*
H115 T	32	0.97	0.48	1.08	1.02	0.66	0.33
H115 R	32	1.77	0.95	1.12	2.05	1.11	1.12
I137 T	32	0.68	0.75	0.93	0.63	0.93	0.94
Q233 T	32	1.22	0.69	1.30	1.58	1.08	2.50
Q233 R	32	1.46	0.96	1.62	2.18	1.14	1.56
I137 R	32	2.03	1.76	0.93	0.90	1.03	1.28
L166 R	33	0.66	0.74	0.66	0.71	0.71	0.55
L166 T	33	0.62	0.77	0.94	1.67	0.58	0.74
G110 T	34	0.61	0.80	0.59	1.27	0.57	1.69
G110 R	34	0.36	0.63	0.55	1.39	0.57	1.50
D198 T	36	0.70	1.45	1.41	1.52	0.74	2.02
D198 R	36	0.79	1.19	2.02	1.31	0.61	1.77
F088 T	37	1.14	1.87*	2.79*	0.97	1.40	0.63
Q236 R	37	0.57	0.43	0.37	1.14	0.95	1.15
D068 T	37	1.02	0.89	0.63	0.44	0.74	0.50
D068 R	37	0.60	0.50	0.96	0.79	0.47	0.59
Q236 T	37	0.92	1.01	0.89	0.78	1.76	1.12
F088 R	37	1.36	3.28*	2.12*	0.99	0.77	0.56
G106 T	38	0.47	0.72	0.73	2.01	0.78	0.95
R246 R	38	0.80	1.13	0.93	0.74	0.72	0.61
R246 T	38	1.34	1.10	0.79	0.94	0.81	0.84
G106 R	38	0.32	0.29	0.71	1.73	0.62	1.01
D058 T	39	1.70	1.72	1.23	1.73	2.50	0.95
P214 R	39	0.94	1.02	1.59	1.61	0.62	0.91
D057 T	39	1.61	1.67	0.93	1.32	0.78	0.49
D058 R	39	1.04	1.09	1.15	1.90	2.46	1.47
D057 R	39	1.08	1.02	1.24	1.19	0.96	0.41
I128 R	39	0.92	0.68	0.82	0.41	0.52	0.46
P214 T	39	1.22	1.78	1.10	1.41	1.21	1.05
I128 T	39	0.85	0.78	0.50	0.49	0.55	0.27
I131 T	40	0.81	0.77	0.96	2.18	1.64	0.82
I131 R	40	0.97	0.68	1.00	1.10	1.43	0.62
F095 T	40	1.06	1.26	0.56	0.66	0.45	0.65
F095 R	40	1.19	1.00	1.23	0.70	1.02	0.64
R249 R	41	1.22	0.94	0.80	0.76	0.87	1.19
Q239 R	41	1.32	0.69	1.43	1.13	1.93	1.76
N188 R	41	1.07	0.72	0.68	1.51	1.10	1.25
S255 R	41	1.31	0.88	0.91	1.15	1.33	0.63
N188 T	41	0.84	0.55	0.79	0.91	0.99	0.70
F105 R	41	0.47	0.39	0.48	1.08	0.48	0.61
I134 R	41	0.92	0.67	0.83	0.59	0.64	0.90
R249 T	41	0.82	0.58	0.55	0.36	1.21	1.06
F105 T	41	0.60	0.53	0.60	0.61	0.78	0.47
Q239 T	41	1.30	0.97	1.37	1.37	1.41	0.90
I134 T	41	0.90	0.55	1.23	0.87	0.65	0.66
S255 T	41	1.56	1.05	1.45	1.18	1.19	0.65
G107 R	42	0.69	1.14	1.20	0.80	0.69	0.81
D059 T	42	0.78	0.61	0.59	0.83	1.59	0.47
E083 T	42	1.28	1.51	1.01	1.01	2.19	0.99
D059 R	42	1.30	1.08	0.97	0.83	2.29	0.65
P217 T	42	1.34	1.35	0.60	0.62	0.82	0.53
P217 R	42	1.24	1.38	1.46	0.79	0.88	0.52
S266 R	42	1.43	1.63	1.42	1.01	1.24	2.03
G108 T	42	0.97	1.54	1.38	2.19	0.71	0.93

* DATA POINT NOT USED

TABLE A3.1. k-values for M5H15 data, southern group. $Q = 330$, $\underset{\sim}{A} = (1050, 1450, 1450, 1450, 1100, 370)$

RECORD	R (KM)	UNCERTAINTY FACTOR, K (0.4 HZ)	(1 HZ)	(2 HZ)	(4 HZ)	(8 HZ)	(16 HZ)
G108 R	42	0.96	1.42	1.14	1.27	0.57	0.65
G107 T	42	0.72	1.16	0.98	0.81	1.04	1.29
E075 T	42	1.41	1.44	1.01	1.31	1.09	0.55
E075 R	42	1.57	1.61	1.65	1.09	0.87	0.89
E072 T	42	1.70	1.04	0.87	0.78	0.58	1.42
E072 R	42	1.06	1.20	1.30	0.55	0.87	1.27
S261 R	42	1.13	0.89	0.91	0.79	1.20	1.16
J148 T	42	1.31	1.08	1.08	1.62	1.31	1.94
J148 R	42	1.43	1.56	1.37	1.16	1.92	0.97
D065 T	42	1.85	1.18	1.08	1.11	1.14	0.66
D065 R	42	1.16	1.22	1.62	0.61	0.61	0.34
S266 T	42	1.44	1.42	1.31	1.48	0.98	1.43
S265 T	42	1.38	1.14	0.62	1.15	2.17	1.55
S265 R	42	1.27	1.38	0.92	1.02	1.40	1.13
S261 T	42	1.05	0.87	0.86	0.81	0.95	1.54
E083 R	42	1.29	1.50	1.94	1.47	1.78	1.36
N192 T	43	1.42	1.38	1.02	0.78	1.70	1.37
N192 R	43	1.39	1.45	0.56	0.48	1.33	1.95
R251 R	44	1.12	1.19	2.22	1.21	0.52	0.96
C054 R	44	1.13	1.15	1.71	0.98	0.85	0.96
Q241 T	44	1.72	1.96	0.69	0.85	1.43	1.36
R253 R	44	1.23	1.54	1.93	1.93	1.93	1.79
0199 T	44	1.41	1.92	1.90	1.58	2.68	0.68
0199 R	44	1.38	1.49	1.31	1.58	1.80	1.69
R244 T	44	1.23	1.55	1.14	1.13	0.66	0.86
R244 R	44	1.08	1.03	1.55	0.88	0.78	0.83
C054 T	44	1.41	1.52	1.12	1.36	0.86	0.74
R253 T	44	1.60	1.57	1.50	2.20	1.61	1.88
R251 T	44	1.41	1.96	1.28	1.41	1.10	1.16
Q241 R	44	1.32	1.19	1.51	0.85	1.23	0.90
J062 R	45	1.22	1.04	1.15	1.38	0.94	1.27
H121 T	45	1.31	1.99	1.17	1.22	1.95	2.21
H121 R	45	0.91	0.91	1.28	0.77	1.00	1.83
G112 T	45	1.41	1.44	0.93	0.56	0.91	1.95
G112 R	45	1.12	0.96	1.31	0.50	1.24	1.33
E078 T	45	1.28	1.62	0.92	0.72	1.50	1.02
C051 T	45	1.25	1.61	1.00	0.78	1.24	1.43
E078 R	45	1.24	1.01	1.06	0.83	2.02	1.13
C051 R	45	0.99	0.96	1.61	1.06	1.27	1.90
F098 T	45	1.69	1.69	1.76	0.97	1.61	3.57
F098 R	45	1.11	0.94	1.39	1.20	1.72	1.38
M176 T	45	1.79	1.31	0.90	0.52	0.97	0.76
M176 R	45	1.90	1.74	1.00	0.53	1.66	1.29
F092 T	45	1.05	1.15	0.70	0.90	0.55	1.41
F092 R	45	0.95	0.81	0.55	0.69	0.50	1.47
D062 T	45	1.35	2.08	1.64	1.91	1.78	1.24
F089 T	46	1.58	1.82	1.29	1.08	1.25	1.14
F089 R	46	1.26	1.29	1.33	1.03	1.05	2.79
S258 T	47	1.19	1.35	0.63	0.73	0.53	1.10
S258 R	47	1.47	1.26	1.11	0.56	0.44	1.12
F086 T	51	1.57	1.67	1.31	1.33	0.86	1.00
F086 R	51	1.28	0.94	1.14	1.25	0.87	0.93
H118 T	52	0.70	0.65	0.69	0.69	0.38	0.48
H118 R	52	0.76	0.62	0.70	0.46	0.44	0.78
P231 T	53	0.69	0.73	0.85	0.42	0.53	0.78
P231 R	53	0.95	0.73	0.69	0.42	0.41	0.85
S267 T	54	0.84	0.88	0.72	0.74	1.52	1.43
S267 R	54	0.95	0.87	0.89	0.80	0.97	1.55
N186 T	56	0.90	0.75	1.23	1.30*	3.07*	1.65*
N186 R	56	0.89	0.68	0.74	2.02*	1.84*	1.88*

* DATA POINT NOT USED

TABLE A3.1 Continued

RECORD	R (KM)	UNCERTAINTY FACTOR,K (0.4 HZ)	(1 HZ)	(2 HZ)	(4 HZ)	(8 HZ)	(16 HZ)
N191 T	69	0.40	0.64	0.57	0.81	0.76	0.52*
N191 R	69	0.26	0.53	0.72	0.86	0.57	0.93*
Q205 T	75	0.44	0.54	1.09	0.94	0.62	0.91*
Q205 R	75	0.69	0.56	0.85	0.78	1.02	1.07*
Q204 T	75	0.48	0.67	0.88	0.73	0.62	0.79*
Q204 R	75	0.67	0.41	0.68	0.91	0.63	1.23*
H124 T	77	0.47	0.53	1.18	1.48	1.21	1.47*
H124 R	77	0.50	0.47	0.72	1.26	1.23	1.59*
N196 T	77	0.75	1.24	1.54	1.61	0.99	1.88*
N196 R	77	1.02	0.94	1.36	1.06	1.10	2.03*
N185 T	77	0.36	0.38	1.37	3.84*	3.13*	6.05*
N185 R	77	0.32	0.45	1.00	2.84*	4.91*	4.82*
M180 T	85	0.60	0.58	0.77	1.09	1.11	2.34*
M180 R	85	0.39	0.55	1.12	1.22	1.00	2.58*
F087 R	89	0.36	0.42	1.17	0.76	2.06	3.22*
F087 T	89	0.60	0.61	1.16	1.30	1.76	2.61*
P220 T	97	0.72	1.01	1.59	1.36	2.18	4.20*
P220 R	97	0.58	0.78	1.23	1.80	1.88	5.12*
N195 T	123	0.73*	1.83*	3.12*	2.95*	9.24*	25.31*
N195 R	123	0.79*	1.65*	2.02*	2.38*	8.41*	22.19*
L171 T	140	0.47*	0.78*	1.00*	1.27*	4.79*	31.11*
L171 R	140	0.54*	0.89*	0.93*	1.07*	3.07*	27.41*

* DATA POINT NOT USED

TABLE A3.1 Continued

SAN FERNANDO EARTHQUAKE
130 < PHI < 200 DEGREES
UNSMOOTHED,15 SECOND SAMPLE

RECORD	R (KM)	UNCERTAINTY FACTOR,K (0.4 HZ)	(1 HZ)	(2 HZ)	(4 HZ)	(8 HZ)	(16 HZ)
C041 R	16	1.24	2.23	0.75	2.06	2.62	0.98
C041 T	16	1.35	3.87	4.55	0.86	0.33	1.24
C048 R	26	0.09	1.05	0.40	0.22	0.27*	0.15*
C048 T	26	0.18	1.20	1.28	1.04	0.44*	0.51*
J145 R	28	2.72	0.59	1.47	1.52	0.43*	0.20*
J145 T	28	0.68	1.33	0.27	1.05	0.13*	0.58*
I137 T	32	0.54	0.62	1.33	0.83	1.23	0.30
H115 T	32	0.78	0.44	0.69	1.19	0.50	0.27
H115 R	32	1.58	1.67	1.49	0.62	1.28	0.06
Q233 T	32	2.72	0.45	3.10	0.42	0.61	0.19
I137 R	32	1.34	2.37	1.25	0.38	1.08	1.04
Q233 R	32	0.54	1.80	1.58	1.13	0.50	1.34
L166 T	33	0.68	0.17	0.41	1.83	0.36	0.86
L166 R	33	0.38	0.42	0.62	0.47	0.59	0.41
G110 R	34	0.29	0.30	0.35	1.11	0.58	0.93
G110 T	34	0.94	0.97	1.21	1.13	0.31	2.21
D198 R	36	0.46	1.39	2.16	0.54	0.72	3.39
D198 T	36	0.64	2.20	2.01	1.21	2.05	2.70
Q236 T	37	0.13	1.24	0.32	1.10	2.41	1.23
Q236 R	37	0.29	0.97	0.67	0.66	1.65	2.42
F088 T	37	0.64	1.67*	0.54*	1.82	1.44	0.69
D068 T	37	0.98	0.95	0.44	0.82	0.67	0.71
F088 R	37	0.91	4.16*	1.70*	0.69	0.69	0.57
D068 R	37	0.64	0.44	0.49	0.36	0.48	0.80
G106 T	38	0.64	1.42	0.32	1.08	0.38	0.70
R246 R	38	1.72	0.70	0.52	0.74	0.66	0.24
R246 T	38	0.75	1.29	0.47	1.35	0.79	1.26
G106 R	38	0.21	0.20	0.34	1.26	0.88	0.26
D057 T	39	1.11	1.46	0.18	0.43	0.16	0.81
D058 T	39	0.99	1.27	0.49	1.98	2.04	1.92
P214 T	39	0.89	2.90	1.75	0.98	0.85	0.72
P214 R	39	1.22	0.45	1.38	1.72	0.63	1.98
D057 R	39	1.87	1.12	0.83	2.88	0.24	0.23
I128 R	39	1.13	0.94	0.77	0.29	0.43	0.42
D058 R	39	1.72	1.15	0.36	1.29	3.55	1.32
I128 T	39	1.90	0.82	0.31	0.45	0.77	0.21
I131 T	40	0.87	1.28	0.83	1.34	0.78	1.12
F095 T	40	1.12	1.61	0.32	0.33	0.97	0.57
F095 R	40	2.40	0.54	0.93	1.35	0.18	0.98
I131 R	40	2.24	0.07	2.82	1.33	1.24	0.80
R249 R	41	1.68	1.21	0.66	0.66	2.02	0.98
Q239 R	41	1.07	0.20	0.28	1.39	1.38	1.67
S255 R	41	0.68	0.68	0.44	1.83	1.67	0.55
N188 R	41	1.81	0.43	0.61	1.40	0.24	0.50
N188 T	41	0.61	0.51	0.74	0.43	0.85	0.59
F105 R	41	0.76	0.43	0.25	1.22	0.46	0.45
I134 R	41	1.92	0.21	0.81	0.91	0.73	1.21
I134 T	41	0.77	0.36	0.73	0.64	0.38	0.60
R249 T	41	0.53	0.74	0.20	0.46	0.97	0.30
Q239 T	41	1.54	0.88	1.13	1.22	1.21	0.54
S255 T	41	2.84	0.56	1.44	2.89	1.37	0.41
F105 T	41	0.45	0.53	0.27	0.45	0.29	0.66
D059 T	42	0.66	0.79	0.35	1.10	1.90	0.87
E083 T	42	1.40	2.58	0.18	3.10	1.37	1.32
P217 T	42	0.60	0.51	0.62	0.48	1.18	1.38
P217 R	42	1.77	0.78	1.23	0.32	0.94	1.21
S266 R	42	2.33	1.57	2.15	1.32	0.76	3.48
G108 T	42	1.39	2.00	1.09	0.51	0.47	1.81
G108 R	42	1.36	1.97	1.20	1.16	0.29	1.14
G107 T	42	0.33	2.38	1.79	0.32	0.30	0.68

* DATA POINT NOT USED

TABLE A3.2. k-values M0H15 data, southern group. $Q = 330$, $\underset{\sim}{A} = (1050, 1450, 1450, 1450, 1100, 370)$

RECORD	R (KM)	UNCERTAINTY FACTOR, K (0.4 HZ)	(1 HZ)	(2 HZ)	(4 HZ)	(8 HZ)	(16 HZ)
E075 T	42	0.81	1.46	1.21	1.24	0.88	0.65
G107 R	42	1.07	2.27	1.48	0.53	1.22	0.69
E075 R	42	1.92	2.66	0.89	1.11	0.08	1.02
E072 T	42	0.89	1.20	0.16	1.40	0.36	1.50
E072 R	42	0.74	0.71	1.93	0.52	1.06	1.18
S261 R	42	1.85	0.74	0.09	0.37	1.57	1.29
J148 T	42	0.70	0.91	2.90	3.09	0.44	1.70
J148 R	42	1.76	0.86	2.90	0.52	1.24	0.21
D065 T	42	1.44	2.00	0.62	0.11	1.35	0.76
D065 R	42	2.35	1.23	1.15	1.74	1.07	0.67
S266 T	42	0.34	1.52	0.73	1.20	1.83	1.77
S265 T	42	1.62	2.57	0.29	0.92	2.23	1.88
S265 R	42	2.15	1.43	1.01	0.27	1.51	1.94
S261 T	42	0.66	0.24	1.45	1.35	0.81	1.59
E083 R	42	1.92	0.85	3.37	1.83	1.91	1.46
D059 R	42	1.67	1.51	0.14	1.46	3.10	0.05
N192 T	43	2.05	2.23	1.78	1.46	3.06	0.68
N192 R	43	2.61	2.03	0.87	0.42	1.76	0.82
R251 R	44	3.30	1.75	1.93	1.85	0.47	0.76
C054 R	44	3.09	2.53	2.37	0.70	0.66	0.57
Q241 T	44	0.94	1.65	0.18	0.48	1.43	1.28
R253 R	44	0.65	1.90	0.41	1.44	2.10	2.72
D199 T	44	1.07	2.81	1.88	0.73	2.44	1.08
D199 R	44	2.31	1.37	2.33	3.20	3.33	2.08
R244 T	44	1.80	2.05	0.32	1.87	0.99	0.46
R244 R	44	3.61	0.41	1.64	1.47	0.57	0.78
C054 T	44	1.77	1.42	0.34	0.17	0.55	0.50
R253 T	44	0.73	2.27	2.50	1.35	2.21	2.10
R251 T	44	1.84	2.68	1.07	0.43	0.56	0.33
Q241 R	44	1.55	1.09	1.05	0.86	1.55	0.68
D062 R	45	2.64	1.05	1.05	0.78	0.71	0.62
H121 T	45	0.43	1.65	0.35	2.79	1.79	2.41
H121 R	45	2.30	1.18	0.90	0.41	0.97	2.81
C051 T	45	1.29	0.97	0.89	0.63	2.29	1.69
G112 T	45	1.71	1.41	0.59	0.68	1.47	0.66
G112 R	45	3.30	1.21	2.30	0.45	1.25	0.93
E078 T	45	1.57	1.16	0.35	1.65	1.09	0.98
E076 R	45	3.54	0.45	1.00	0.97	2.45	1.16
C051 R	45	2.98	0.28	0.64	0.89	2.05	1.29
F098 T	45	1.64	2.67	2.17	0.64	0.89	2.84
F098 R	45	3.23	1.74	1.11	0.99	0.32	0.74
M176 T	45	1.00	0.21	0.69	0.38	1.65	0.37
M176 R	45	3.14	2.73	0.71	0.10	1.97	1.06
F092 T	45	0.63	1.96	0.54	0.68	0.82	1.43
F092 R	45	2.60	0.44	0.27	0.69	1.06	3.47
D062 T	45	0.31	2.53	1.71	1.06	1.47	0.95
F089 T	46	1.40	3.31	2.46	0.72	1.43	2.51
F089 R	46	4.07	2.38	3.05	1.17	0.66	1.80
S258 T	47	0.73	2.37	0.52	1.35	0.66	0.43
S258 R	47	2.06	0.92	1.48	1.08	0.21	0.58
F086 T	51	0.96	2.68	1.15	0.82	0.85	0.90
F086 R	51	2.28	1.35	0.64	0.78	0.98	1.66
H118 T	52	0.06	0.27	0.68	0.57	0.35	0.93
H118 R	52	0.18	0.37	1.25	0.64	0.36	0.45
P231 T	53	0.72	0.56	0.78	0.24	0.09	0.68
P231 R	53	0.64	0.24	0.47	0.59	0.09	0.22
S267 T	54	0.49	0.43	0.52	0.48	1.16	1.18
S267 R	54	0.71	0.48	0.23	0.64	0.58	1.25
N186 T	56	1.12	0.93	0.75	2.08*	3.48*	1.99*
N186 R	56	0.89	0.84	0.53	2.39*	2.65*	1.77*

* DATA POINT NOT USED

TABLE A3.2 Continued

RECORD	R (KM)	UNCERTAINTY FACTOR, K (0.4 HZ)	(1 HZ)	(2 HZ)	(4 HZ)	(8 HZ)	(16 HZ)
N191 T	69	0.30	1.50	0.88	0.72	0.36	1.00*
N191 R	69	0.15	0.29	1.39	0.13	0.63	0.41*
U205 T	75	0.37	0.37	1.79	1.94	0.87	0.95*
U205 R	75	0.42	0.74	0.44	0.80	0.93	0.69*
U204 T	75	0.53	0.58	1.22	0.28	0.67	0.62*
U204 R	75	0.34	0.22	0.43	0.60	0.64	1.27*
H124 T	77	0.27	0.22	1.18	2.10	0.46	2.32*
H124 R	77	0.59	0.45	0.21	0.94	2.18	3.02*
N196 T	77	1.14	1.29	2.10	0.63	0.49	2.08*
N196 R	77	0.22	1.29	1.74	1.08	1.18	1.59*
N185 T	77	0.23	0.12	1.29	3.19*	3.08*	12.54*
N185 R	77	0.19	0.37	0.93	1.91*	5.97*	8.63*
M180 T	85	0.78	0.25	0.65	2.33	1.69	2.47*
M180 R	85	0.30	0.37	1.32	1.45	0.92	3.82*
F087 R	89	0.35	0.30	2.00	1.73	1.80	2.08*
F087 T	89	0.60	0.37	0.86	2.07	2.12	1.21*
P220 T	97	0.59	1.06	0.78	1.00	2.33	3.27*
P220 R	97	0.34	0.60	0.98	3.25	0.38	1.39*
N195 T	123	0.49*	1.19*	6.64*	1.88*	9.81*	34.66*
N195 R	123	1.29*	1.58*	4.66*	2.65*	12.19*	20.75*
L171 T	140	0.41*	1.40*	1.33*	0.38*	4.10*	34.19*
L171 R	140	0.16*	0.91*	1.76*	1.17*	3.21*	9.67*

* DATA POINT NOT USED

TABLE A3.2 Continued

SAN FERNANDO EARTHQUAKE
130 < PHI < 200 DEGREES
FULL RECORDS - SMOOTHED

RECORD	COMPONENT BEARING	R (KM)	UNCERTAINTY FACTOR,K (0.4 HZ)	(1 HZ)	(2 HZ)	(4 HZ)	(8 HZ)	(16 HZ)
C041	164	16	1.94	2.54	1.95	1.83	1.83	1.74
C041	254	16	0.87	1.75	2.40	1.39	1.47	1.31
C048	0	26	1.93	1.14	1.36	0.91	0.57*	0.32*
C048	270	26	2.05	0.98	0.66	0.73	0.37*	0.28*
J145	180	28	2.18	0.87	0.98	0.80	0.65*	0.22*
J145	270	28	2.58	0.80	0.51	1.12	0.51*	0.29*
I137	189	32	2.41	1.34	0.97	1.23	1.09	1.42
H115	281	32	1.68	0.89	1.06	0.89	0.57	0.36
H115	11	32	2.34	0.84	1.17	1.90	1.07	1.25
Q233	282	32	1.50	0.73	1.39	1.50	0.85	2.50
I137	99	32	1.92	0.99	0.89	0.79	0.67	0.60
Q233	192	32	1.82	0.95	1.46	2.07	0.91	1.30
L166	270	33	0.44	0.65	1.14	1.75	0.53	0.86
L166	0	33	0.40	0.53	0.76	0.54	0.63	0.52
G110	98	34	0.39	0.60	0.33	2.08	0.84	1.44
G110	188	34	0.59	0.77	0.42	1.22	0.44	2.26
D198	180	36	0.76	1.32	1.93	1.23	0.66	2.14
D198	270	36	0.47	1.56	1.54	1.64	1.09	2.57
Q236	90	37	0.45	0.55	0.42	1.08	1.15	1.11
Q236	180	37	0.77	0.90	0.93	1.03	1.98	1.14
F088	200	37	1.00	2.36*	1.80*	1.16	1.13	0.49
D068	90	37	0.97	0.87	0.65	0.47	0.74	0.47
F088	110	37	1.17	3.33*	3.25*	0.81	1.43	0.52
D068	0	37	0.50	0.45	0.98	0.68	0.54	0.50
G106	270	38	0.49	0.86	0.90	2.25	0.64	0.86
R246	180	38	0.75	1.12	0.92	0.79	0.92	0.67
R246	90	38	1.13	1.25	0.76	0.88	0.68	0.79
G106	180	38	0.29	0.42	0.34	1.07	0.46	0.70
D057	90	39	0.91	1.33	0.90	1.21	1.05	0.53
D058	90	39	0.93	1.23	1.26	1.88	2.33	0.88
P214	179	39	1.01	1.16	1.42	2.20	0.52	0.97
P214	269	39	0.97	2.01	1.23	1.37	1.39	0.87
D057	180	39	1.19	1.06	1.30	1.49	1.67	0.25
I128	0	39	0.71	0.60	0.79	0.52	0.54	0.59
D058	180	39	1.06	1.03	1.33	1.99	4.13	1.07
I128	270	39	0.76	0.66	0.63	0.55	0.60	0.45
I131	320	40	0.83	0.80	1.32	1.21	1.00	0.48
F095	182	40	1.05	1.23	1.51	0.72	0.92	0.69
F095	92	40	0.87	1.52	0.66	0.64	0.47	0.87
I131	50	40	0.89	0.74	1.08	1.82	1.64	1.15
R249	44	41	1.06	0.62	0.65	0.61	1.13	1.13
Q239	180	41	1.15	0.67	1.40	0.94	1.77	1.80
S255	8	41	1.21	1.02	0.90	1.10	1.51	0.61
N188	54	41	0.93	0.57	0.59	0.71	1.25	1.17
N188	324	41	0.91	0.68	0.69	1.45	0.74	0.73
F105	180	41	0.53	0.36	0.39	1.23	0.36	0.56
I134	54	41	1.00	0.57	1.23	0.60	0.54	1.10
I134	144	41	0.96	0.64	0.91	0.64	1.04	0.80
R249	134	41	0.92	0.78	0.72	0.50	0.92	1.14
Q239	90	41	0.90	1.00	1.28	1.35	1.67	0.98
S255	278	41	1.36	0.91	1.50	1.20	0.93	0.72
F105	90	41	0.51	0.56	0.36	0.90	0.69	0.43
D059	224	42	1.15	0.70	0.56	0.77	2.28	0.73
E083	90	42	0.76	1.45	0.99	1.33	1.48	1.11
P217	90	42	0.86	1.37	0.69	0.68	0.85	0.55
P217	180	42	1.25	1.28	1.49	0.81	0.98	0.65
S266	0	42	1.46	1.27	1.36	1.23	1.17	2.29
G108	90	42	1.10	1.89	2.46	0.85	0.75	0.54
G108	0	42	0.88	0.84	1.35	1.35	0.71	0.93
G107	90	42	0.77	1.22	1.44	0.70	0.84	0.75

* DATA POINT NOT USED

TABLE A3.3. k-values, M10HIV data, southern group. $Q = 330$, $\underline{A} = (1460, 1640, 1490, 1460, 1070, 370)$.

RECORD	COMPONENT BEARING	R (KM)	UNCERTAINTY FACTOR,K (0.4 HZ)	(1 HZ)	(2 HZ)	(4 HZ)	(8 HZ)	(16 HZ)
E075	270	42	0.97	1.52	1.42	1.42	1.22	0.55
G107	0	42	0.51	0.89	0.84	0.80	0.97	1.50
E075	0	42	1.64	1.46	1.72	1.01	0.88	0.55
E072	15	42	0.95	1.59	1.07	0.85	1.26	0.80
E072	285	42	1.16	0.93	0.85	0.88	1.07	1.05
S261	59	42	1.30	0.97	0.71	0.87	1.07	1.35
J148	270	42	0.89	1.01	1.10	1.68	1.47	1.53
J148	0	42	0.92	1.08	1.03	1.13	1.82	1.19
D065	270	42	1.30	1.36	1.32	1.07	0.99	0.39
D065	180	42	1.12	1.15	1.42	1.08	0.76	0.40
S266	270	42	1.07	1.63	1.45	1.51	0.99	1.48
S265	270	42	0.96	0.91	0.70	1.08	2.07	1.43
S265	180	42	0.89	1.01	0.78	0.96	1.61	1.02
S261	329	42	0.82	0.66	0.97	0.58	1.31	1.25
E083	180	42	1.05	1.54	1.96	1.46	1.94	1.24
D059	314	42	1.00	0.88	0.69	0.86	1.25	0.53
N192	299	43	1.12	1.43	0.79	0.51	1.59	1.76
N192	29	43	1.22	0.92	0.68	0.70	1.37	1.53
R251	37	44	1.22	1.07	1.87	1.38	0.82	1.43
C054	308	44	0.85	1.80	1.56	0.87	0.72	0.93
Q241	307	44	0.98	1.50	1.16	0.77	0.83	1.31
R253	330	44	1.01	1.60	1.79	2.27	1.67	1.94
D199	298	44	1.03	2.31	1.86	2.34	2.10	1.06
D199	28	44	1.27	0.91	1.30	1.22	1.61	1.58
R244	217	44	1.35	1.11	0.85	1.55	0.73	0.75
R244	307	44	0.91	1.54	1.44	0.60	0.76	0.93
C054	218	44	1.05	1.13	1.06	2.05	1.01	0.71
R253	240	44	1.40	1.22	1.31	1.76	1.71	2.33
R251	127	44	0.90	1.82	1.85	1.12	0.84	0.77
Q241	37	44	1.31	1.04	0.70	0.93	1.76	1.84
D062	322	45	0.79	1.20	0.85	1.13	0.60	1.45
H121	180	45	0.87	1.03	1.21	1.43	1.17	1.76
H121	270	45	1.38	1.64	0.92	1.08	1.63	2.00
C051	306	45	0.73	1.33	1.16	1.02	1.19	1.58
G112	308	45	1.13	1.11	0.92	0.63	1.22	2.03
G112	38	45	0.86	1.39	0.96	0.52	1.48	1.67
E078	220	45	1.21	0.89	0.48	1.02	2.29	1.80
E078	310	45	0.97	1.35	1.04	0.43	1.49	0.84
C051	36	45	0.96	1.24	1.00	0.80	1.85	1.72
F098	217	45	1.29	0.96	1.48	1.66	1.03	2.27
F098	127	45	0.77	1.53	1.44	1.22	1.60	2.19
M176	127	45	0.96	2.14	0.97	0.77	0.55	0.91
M176	37	45	1.27	0.94	0.59	0.48	1.26	0.99
F092	208	45	0.88	0.70	0.63	0.94	0.51	1.58
F092	118	45	0.93	1.08	0.55	0.65	0.59	1.23
D062	232	45	0.91	1.63	1.36	1.81	1.43	1.26
F089	217	46	1.28	1.14	0.70	0.68	1.13	1.26
F089	127	46	1.07	2.04	1.58	1.59	1.09	2.38
S258	119	47	1.21	1.44	0.89	0.68	0.48	1.31
S258	29	47	1.02	1.01	0.99	0.58	0.45	0.84
F086	187	51	0.62	0.84	0.92	1.24	0.59	0.70
F086	277	51	0.94	1.88	1.23	1.44	0.90	1.38
H118	225	52	0.81	0.56	0.66	0.41	0.57	0.66
H118	135	52	0.78	0.73	0.89	0.82	0.41	0.75
P231	270	53	1.10	0.79	0.90	0.47	0.37	0.68
P231	0	53	1.16	0.66	0.65	0.42	0.43	0.50
S267	90	54	1.26	0.99	0.90	0.59	1.16	1.72
S267	0	54	0.96	0.90	0.82	0.65	0.82	1.14
N186	233	56	1.04	0.71	1.18	1.64*	3.55*	1.06*
N186	143	56	0.88	0.61	0.98	2.09*	2.47*	1.66*

* DATA POINT NOT USED

TABLE A3.3 Continued

RECORD	COMPONENT BEARING	R (KM)	UNCERTAINTY FACTOR,K (0.4 HZ)	(1 HZ)	(2 HZ)	(4 HZ)	(8 HZ)	(16 HZ)
N191	155	69	0.63	1.06	0.96	0.46	0.56	0.52*
N191	65	69	0.78	0.91	0.42	0.68	0.60	0.67*
0205	249	75	0.89	0.75	1.42	0.96	0.60	1.14*
0205	339	75	1.07	0.64	0.78	0.44	0.76	0.64*
0204	90	75	1.18	0.94	0.95	0.78	0.64	0.71*
0204	0	75	1.20	0.72	0.82	1.17	0.79	1.19*
H124	180	77	0.69	0.59	1.24	1.11	1.27	2.02*
H124	270	77	0.58	0.59	0.81	1.19	1.39	1.60*
N196	194	77	1.06	1.44	1.83	1.25	1.19	1.57*
N196	284	77	1.38	1.57	1.21	1.84	0.90	1.98*
N185	220	77	0.42	0.49	1.25	4.03*	2.91*	6.55*
N185	130	77	0.41	0.48	1.04	2.50*	6.83*	4.84*
M180	270	85	1.12	0.92	1.01	0.87	0.73	2.02*
M180	180	85	0.78	0.71	1.47	1.83	0.87	3.79*
F087	176	89	0.76	1.06	1.34	1.36	2.30	3.07*
F087	266	89	1.14	0.98	1.35	0.62	1.39	3.02*
P220	90	97	1.17	1.36	1.61	1.12	2.69	4.42*
P220	180	97	0.96	1.26	0.80	2.08	1.35	3.88*
N195	303	123	1.17*	2.59*	2.99*	2.13*	8.87*	37.96*
N195	33	123	1.10*	2.58*	2.61*	2.41*	9.26*	28.03*
L171	303	140	0.76*	1.14*	1.35*	1.39*	4.30*	24.07*
L171	33	140	0.80*	0.98*	0.90*	1.02*	4.78*	35.77*

* DATA POINT NOT USED

TABLE A3. 3 Continued

SAN FERNANDO EARTHQUAKE
310 < PHI < 360 DEGREES
15 SECOND SAMPLE

RECORD	R (KM)	UNCERTAINTY FACTOR,K (0.4 HZ)	(1 HZ)	(2 HZ)	(4 HZ)	(8 HZ)	(16 HZ)
J144 R	27	1.62	1.81	1.38	2.96	1.32	1.73
J144 T	27	0.75	2.03	1.36	4.23	1.32	1.80
J143 T	30	0.59	0.95	0.90	0.83	0.86	2.79
J142 R	30	1.47	1.96	2.34	1.31	3.04	2.44
J143 R	30	1.37	1.03	0.86	0.65	0.88	1.38
J142 T	30	0.53	0.84	0.75	0.41	1.65	1.22
J141 R	32	2.05*	0.29*	2.95*	1.05	0.46	0.23
J141 T	32	2.21*	4.16*	2.87*	1.12	0.91	0.32
0207 T	35	0.62*	0.85*	0.72	0.76*	0.68	0.46
0207 R	35	1.36*	2.14*	1.08	2.33*	0.65	0.70
F104 T	54	3.33	2.59	2.45	1.30	0.86	0.76
F104 R	54	2.72	2.83	1.70	2.55	0.94	0.61
F102 R	70	0.47	0.30	0.35	0.94	0.90	0.60
F102 T	70	0.61	0.48	0.58	0.54	0.75	0.57
M179 R	72	0.68	0.33	0.59	0.50	1.52*	2.94*
M179 T	72	0.65	0.40	0.96	0.54	1.95*	2.22*
E071 T	87	1.29	1.38	1.13	0.99	1.23	1.85
E071 R	87	1.41	1.28	0.77	0.75	1.32	3.68

* DATA POINT NOT USED

TABLE A3.4. k-values, M5H15 data, complete northern group. $Q = 700$, $\underset{\sim}{A} = (210, 320, 410, 600, 440, 120)$

SAN FERNANDO EARTHQUAKE
310 < PHI < 360 DEGREES
15 SECOND SAMPLE

RECORD	R (KM)	UNCERTAINTY FACTOR,K (0.4 HZ)	(1 HZ)	(2 HZ)	(4 HZ)	(8 HZ)	(16 HZ)
J142 R	30	1.98	2.43	2.76	1.66	2.60	1.79
J143 T	30	0.80	1.18	1.06	1.05	0.74	2.04
J142 T	30	0.72	1.04	0.89	0.51	1.42	0.89
J143 R	30	1.84	1.28	1.02	0.82	0.75	1.01
0207 R	35	1.83*	2.68*	1.29	3.03*	0.59	0.58
0207 T	35	0.83*	1.06*	0.87	0.99*	0.62	0.38
F102 T	70	0.85	0.63	0.78	0.88	1.05	1.10
F102 R	70	0.65	0.40	0.47	1.51	1.25	1.17

* DATA POINT NOT USED

TABLE A3.5. k-values, M5H15 data, basement rock sites in northern group. $Q = 350$, $\underset{\sim}{A} = (160, 270, 380, 570, 740, 340)$

SAN FERNANDO EARTHQUAKE
310 < PHI < 360 DEGREES
15 SECOND SAMPLE

RECORD	R (KM)	UNCERTAINTY FACTOR,K (0.4 HZ)	(1 HZ)	(2 HZ)	(4 HZ)	(8 HZ)	(16 HZ)
J144 R	27	2.17	2.24	1.62	3.69	1.09	1.18
J144 T	27	1.01	2.51	1.59	5.25	1.09	1.22
F104 T	54	4.56	3.34	3.11	1.90	0.98	0.99
F104 R	54	3.72	3.64	2.17	3.72	1.08	0.79
M179 R	72	0.94	0.44	0.80	0.81	2.17*	5.97*
M179 T	72	0.90	0.53	1.29	0.87	2.78*	4.50*
E071 T	87	1.81	1.87	1.59	1.77	2.10	5.40
E071 R	87	1.98	1.73	1.08	1.34	2.26	10.76

* DATA POINT NOT USED

TABLE A3.6. k-values for sedimentary sites in northern group, computed with respect to basement rock curves, M5H15 data. $Q = 400$, $\underset{\sim}{A} = (160, 270, 380, 570, 740, 340)$

SAN FERNANDO EARTHQUAKE
310 < PHI < 360 DEGREES
15 SECOND SAMPLE

RECORD	R (KM)	UNCERTAINTY FACTOR,K (0.4 HZ)	(1 HZ)	(2 HZ)	(4 HZ)	(8 HZ)	(16 HZ)
J144 R	27	2.16	2.21	1.58	3.51	0.98	0.96
J144 T	27	1.00	2.47	1.55	4.99	0.98	1.00
J143 T	30	0.79	1.16	1.03	1.00	0.66	1.63
J142 R	30	1.96	2.40	2.69	1.57	2.32	1.43
J143 R	30	1.83	1.27	0.99	0.76	0.67	0.81
J142 T	30	0.71	1.03	0.87	0.48	1.27	0.71
J141 R	32	2.74*	7.71*	3.40*	1.23	0.36	0.14
J141 T	32	2.95*	5.10*	3.31*	1.35	0.71	0.19
U207 T	35	0.82*	1.04*	0.84	0.93*	0.55	0.30
U207 R	35	1.82*	2.64*	1.25	2.84*	0.52	0.45
F104 T	54	4.50	3.25	2.96	1.71	0.80	0.66
F104 R	54	3.67	3.55	2.06	3.36	0.88	0.53
F102 R	70	0.64	0.38	0.44	1.33	0.97	0.69
F102 T	70	0.83	0.61	0.73	0.77	0.81	0.65
M179 R	72	0.92	0.42	0.75	0.71	1.66*	3.49*
M179 T	72	0.89	0.51	1.21	0.76	2.13*	2.63*
E071 T	87	1.77	1.79	1.46	1.51	1.52	2.82
E071 R	87	1.94	1.66	1.00	1.14	1.63	5.62

* DATA POINT NOT USED

TABLE A3.7. k-values, M5H15 data, northern group. $Q = 400$, $\underset{\sim}{A} = (160, 270, 380, 570, 740, 340)$. This is the "best fit" Q with $\underset{\sim}{A}$ set to basement values.

SAN FERNANDO EARTHQUAKE
90 < PHI < 150 DEGREES
15 SECOND SAMPLE

RECORD	R (KM)	UNCERTAINTY FACTOR, K (0.4 HZ)	(1 HZ)	(2 HZ)	(4 HZ)	(8 HZ)	(16 HZ)
G110 T	34	1.51	1.68	0.70	1.27	0.65	1.64
G110 R	34	0.89	1.33	0.66	1.39	0.65	1.45
G106 R	38	0.79	0.61	0.84	1.68	0.67	0.86
G106 T	38	1.17	1.50	0.86	1.95	0.85	0.82
G107 R	42	1.69	2.35	1.40	0.75	0.71	0.62
G107 T	42	1.76	2.39	1.13	0.76	1.06	0.98
G108 T	42	2.39	3.18	1.60	2.06	0.72	0.71
G108 R	42	2.37	2.93	1.33	1.20	0.58	0.49
P221 T	45	0.86	0.50	0.34	1.63	4.39	1.65
H121 T	45	3.21*	4.09*	1.35	1.12	1.90	1.54
P221 R	45	0.75	0.46	0.42	0.68	2.03	2.28
H121 R	45	2.24*	1.87*	1.46	0.70	0.98	1.28
N186 T	56	2.20	1.51	1.35	1.10*	2.54*	0.83*
N186 R	56	2.16	1.38	0.81	1.71*	1.52*	0.95*
P223 T	66	0.86	1.06	1.01	0.58	1.05	0.39
P223 R	66	0.96	1.35	1.02	0.35	1.78	0.39
M184 T	72	0.45	0.55	0.85	1.43	0.91	1.17
M184 R	72	0.69	1.08	1.02	0.72	0.93	1.00
M183 T	72	0.43	0.54	0.87	1.12	0.82	1.52
M183 R	72	0.64	1.04	1.05	0.63	1.00	1.31
N187 T	73	0.53	0.66	0.94	1.15*	2.36*	1.20*
N187 R	73	0.56	0.72	0.95	1.79*	2.40*	1.09*
H124 R	77	1.20	0.91	0.73	0.91	0.75	0.43*
N185 R	77	0.76	0.87	1.02	2.06*	2.98*	1.31*
N185 T	77	0.84	0.74	1.40	2.79*	1.90*	1.64*
H124 T	77	1.12	1.03	1.20	1.08	0.73	0.40*
M180 T	85	1.42	1.10	0.76	0.74	0.60	0.50*
M180 R	85	0.91	1.05	1.11	0.83	0.54	0.55*
F087 R	89	0.83	0.79	1.14	0.50	1.05	0.61*
F087 T	89	1.40	1.16	1.13	0.86	0.89	0.49*
F101 R	108	0.83	0.74	0.86	1.66	1.96	1.23
F101 T	108	0.60	0.77	1.13	0.91	1.26	1.03
0206 T	109	1.31	1.56	1.88	1.49	1.15	0.77
0206 R	109	1.26	1.70	1.53	1.68	1.48	1.12

* DATA POINT NOT USED

TABLE A3.8. k-values, M5H15 data, complete south-eastern group. $Q = 860$, $\underset{\sim}{A} = (410, 650, 1070, 1130, 580, 140)$

SAN FERNANDO EARTHQUAKE
90 < PHI < 150 DEGREES
15 SECOND SAMPLE

RECORD	R (KM)	UNCERTAINTY FACTOR,K (0.4 HZ)	(1 HZ)	(2 HZ)	(4 HZ)	(8 HZ)	(16 HZ)
G106 R	38	1.13	0.78	1.01	1.69	0.51	0.71
G106 T	38	1.07	1.91	1.04	1.97	0.64	0.67
P221 R	45	1.07	0.59	0.51	0.70	1.58	1.99
P221 T	45	1.24	0.64	0.41	1.68	3.45	1.45
P223 T	66	1.25	1.38	1.26	0.63	0.91	0.42
P223 R	66	1.39	1.75	1.27	0.38	1.54	0.42
M183 R	72	0.93	1.36	1.33	0.70	0.89	1.50
M184 T	72	0.62	0.69	1.07	1.56	0.81	1.35
M184 R	72	1.00	1.41	1.28	0.79	0.83	1.15
M183 T	72	0.62	0.70	1.10	1.23	0.73	1.74
N187 R	73	0.81	0.94	1.20	1.97*	2.15*	1.27*
N187 T	73	0.76	0.87	1.19	1.27*	2.12*	1.39*

* DATA POINT NOT USED

TABLE A3.9. k-values, M5H15 data, basement rock sites of south-eastern group. $Q = 550$, $\underset{\sim}{A} = (290, 520, 930, 1230, 930, 250)$

SAN FERNANDO EARTHQUAKE
90 < PHI < 150 DEGREES
15 SECOND SAMPLE

RECORD	R (KM)	UNCERTAINTY FACTOR,K (0.4 HZ)	(1 HZ)	(2 HZ)	(4 HZ)	(8 HZ)	(16 HZ)
G110 T	34	2.16	2.15	0.84	1.27	0.48	1.29
G110 R	34	1.27	1.69	0.79	1.39	0.48	1.14
G108 T	42	3.43	4.08	1.94	2.10	0.55	0.61
G107 R	42	2.42	3.01	1.69	0.77	0.54	0.53
G108 R	42	3.40	3.76	1.61	1.22	0.45	0.42
G107 T	42	2.52	3.07	1.37	0.78	0.81	0.84
H121 R	45	3.21*	2.41*	1.78	0.72	0.76	1.12
H121 T	45	4.60*	5.26*	1.64	1.15	1.48	1.35
N186 T	56	3.17	1.95	1.67	1.16*	2.10*	0.81*
N186 R	56	3.10	1.78	1.01	1.81*	1.25*	0.93*
H124 R	77	1.73	1.19	0.93	1.02	0.69	0.52*
H124 T	77	1.63	1.35	1.52	1.20	0.67	0.48*
N185 R	77	1.10	1.15	1.29	2.30*	2.73*	1.57*
N185 T	77	1.22	0.97	1.77	3.10*	1.74*	1.98*
M180 R	85	1.33	1.38	1.42	0.94	0.51	0.72*
M180 T	85	2.06	1.45	0.97	0.84	0.57	0.65*
F087 T	89	2.04	1.53	1.45	0.99	0.87	0.67*
F087 R	89	1.21	1.05	1.47	0.58	1.02	0.83*
F101 R	108	1.22	0.99	1.13	2.00	2.09	2.02
F101 T	108	0.88	1.03	1.48	1.10	1.54	1.69
0206 T	109	1.92	2.09	2.48	1.80	1.23	1.28
0206 R	109	1.84	2.28	2.01	2.03	1.59	1.86

* DATA POINT NOT USED

TABLE A3.10. k-values, M5H15 data, sedimentary site in south-eastern group, computed with respect to basement rock decay curves. $Q = 550$, $\underset{\sim}{A} = (290, 520, 930, 1230, 930, 250)$

APPENDIX 4: K-VALUE DISTRIBUTIONS FOR ENGINEERING APPLICATION

The effect of smoothing bandwidth B_e on scatter in the amplitude data has been discussed in Chapter 2. In order that the statistics of scatter observed in the San Fernando data may be more easily applied to engineering design problems, the distribution of k-values for the southern group of Volume IV Fourier amplitudes of acceleration has been recomputed for a variety of frequencies and values of γ, where γ is defined as

$$\gamma = \frac{B_e}{f} \qquad \text{(A4. 1)}$$

As before, f is frequency in Hz.

If the assumption is made, as discussed in Section 2. 7. 3, that B_e corresponds to the half-power bandwidth, Δf, of a resonance peak at frequency f, then γ may be related to the fraction of critical equivalent viscous damping ζ, through equation (2. 16). That is

$$\zeta = \tfrac{1}{2}\gamma \qquad \text{(A4. 2)}$$

Figures A4. 1 show the accumulated relative frequency distributions F(k) of k at the six sampling frequencies and for the values of $\gamma = 0.04$, 0. 1 and 0. 2. Only one plot is shown for f = 8 and 16 Hz since their distributions coincide.

It is seen from the figures that:

(a) the amount of scatter decreases with increasing structural damping, represented by γ, and

(b) the scatter decreases with increasing frequency when constant

B_e/f smoothing is employed.

Since $\zeta = 0.02$ is a fairly common value of damping in real structures, the large uncertainties shown by the $\gamma = 0.04$ ($\zeta = 0.02$) curves, particularly at low frequencies, is noteworthy.

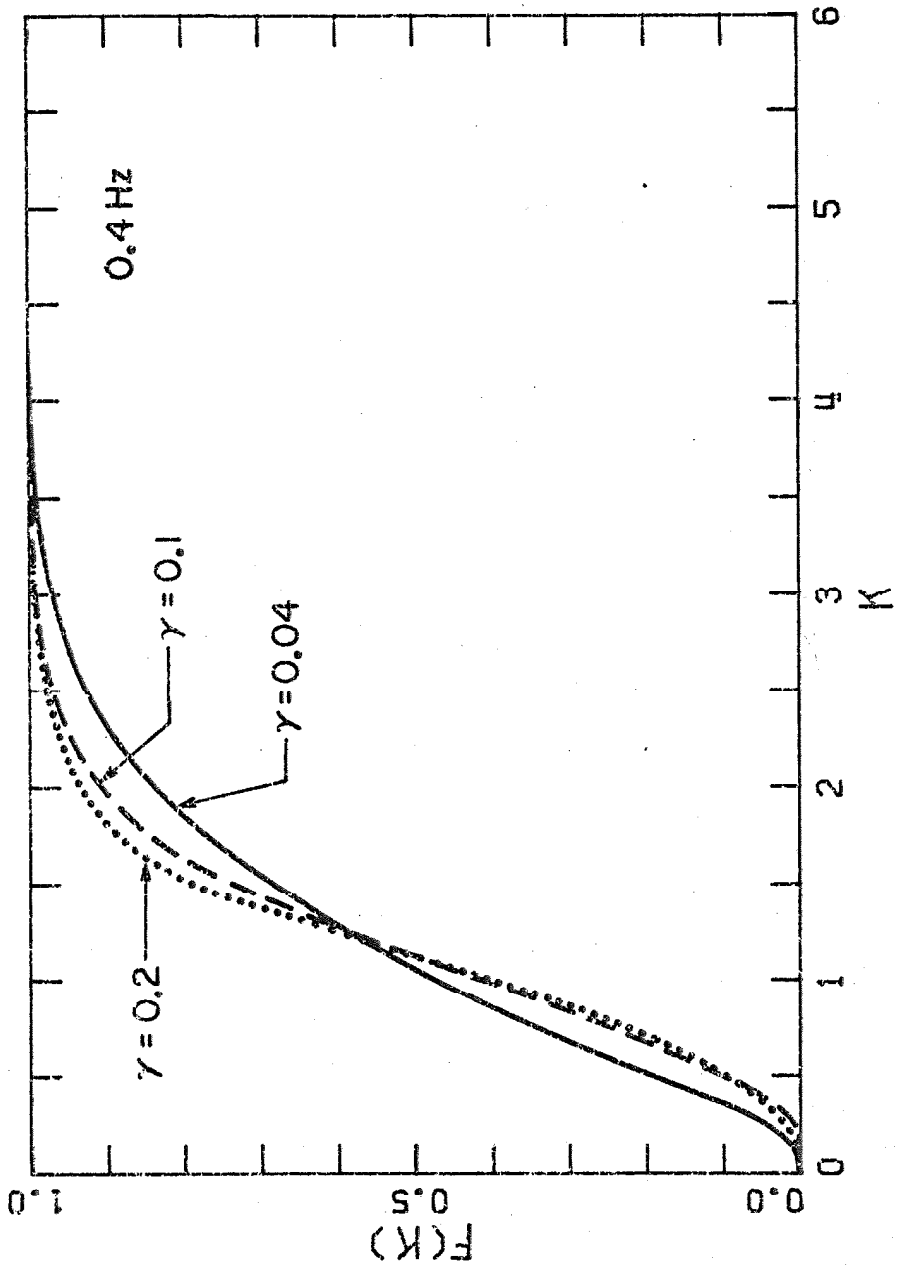

Figure A4.1. Accumulated relative frequency distribution of k for various values of γ and at sampling frequency f, shown in upper right-hand corner of plot. Note that $\gamma \approx 2\zeta$, where ζ is fraction of critical, equivalent viscous damping.

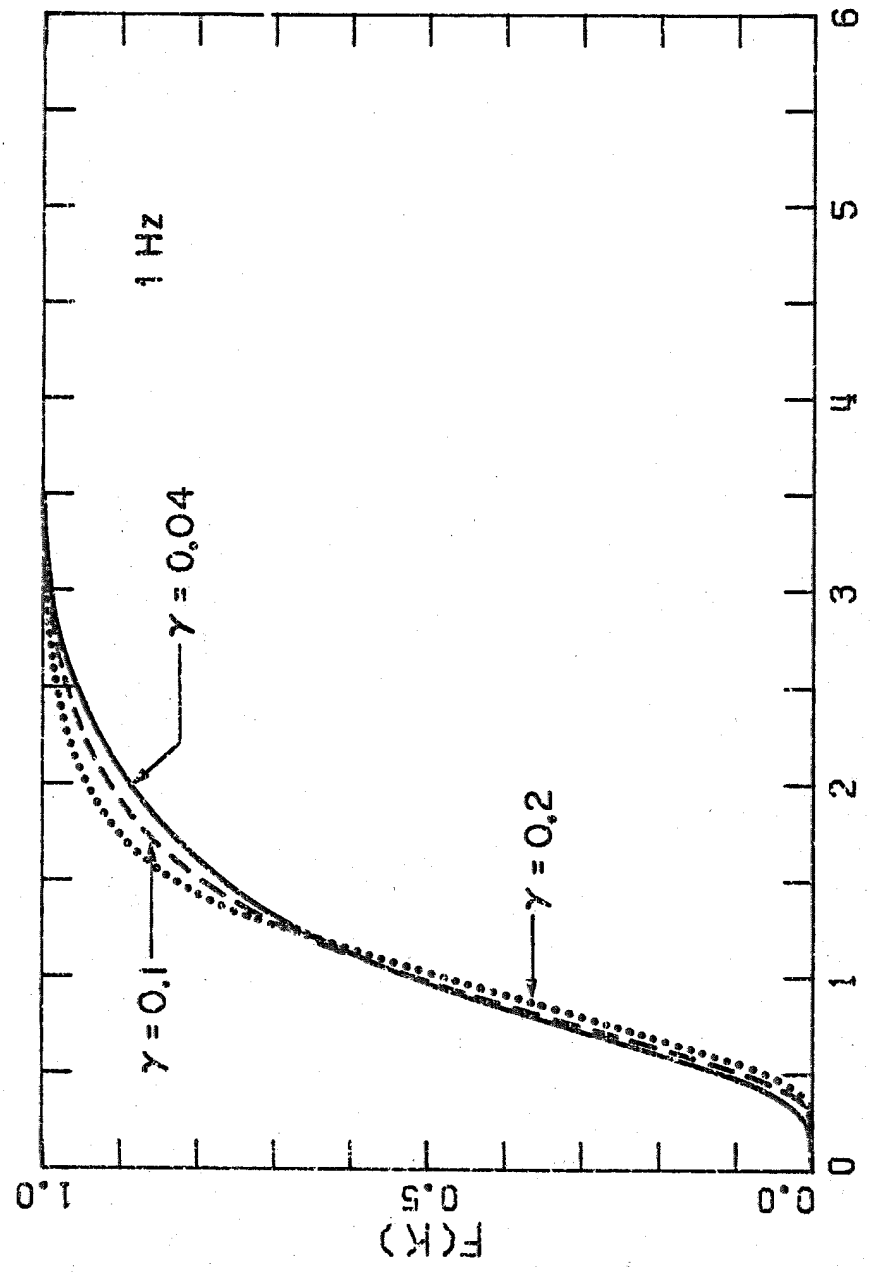

Figure A4.1. Continued.

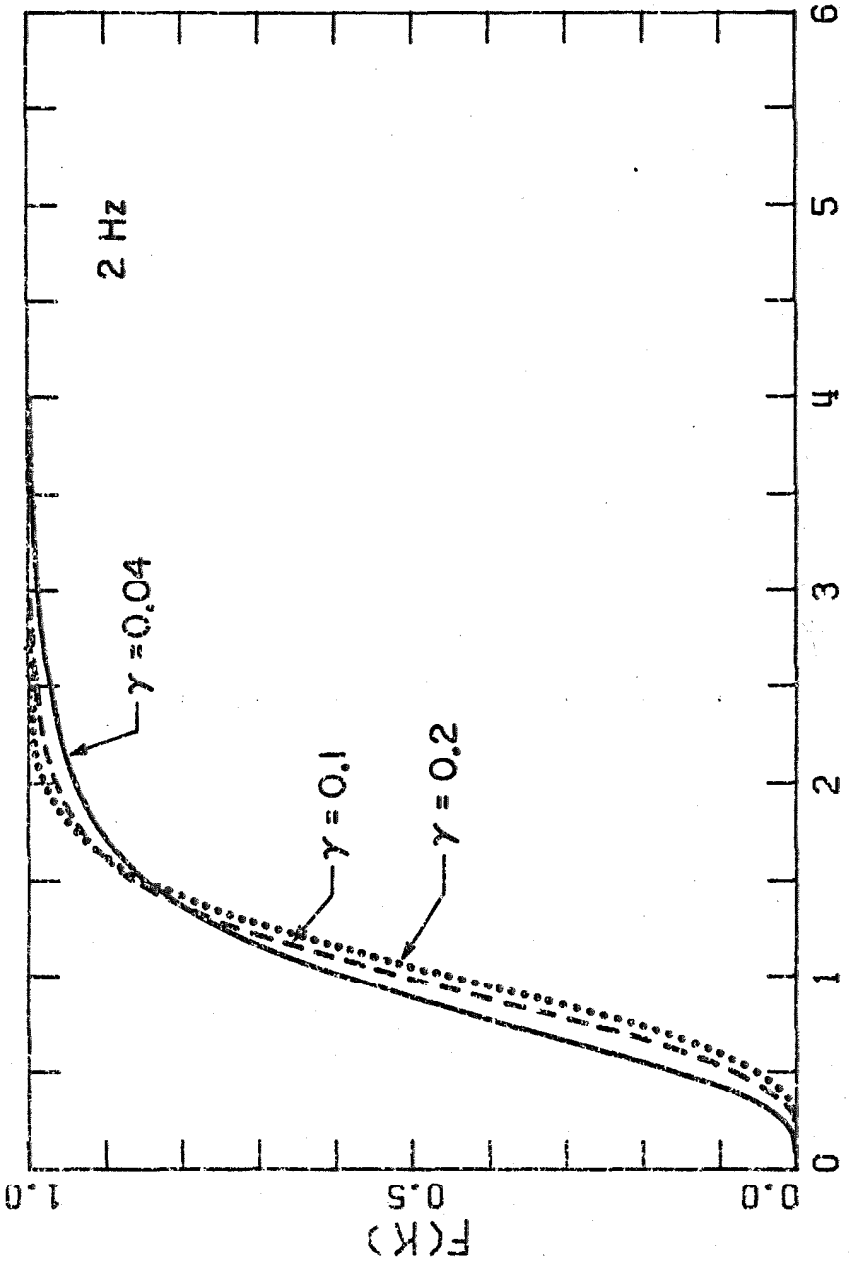

Figure A4.1. Continued.

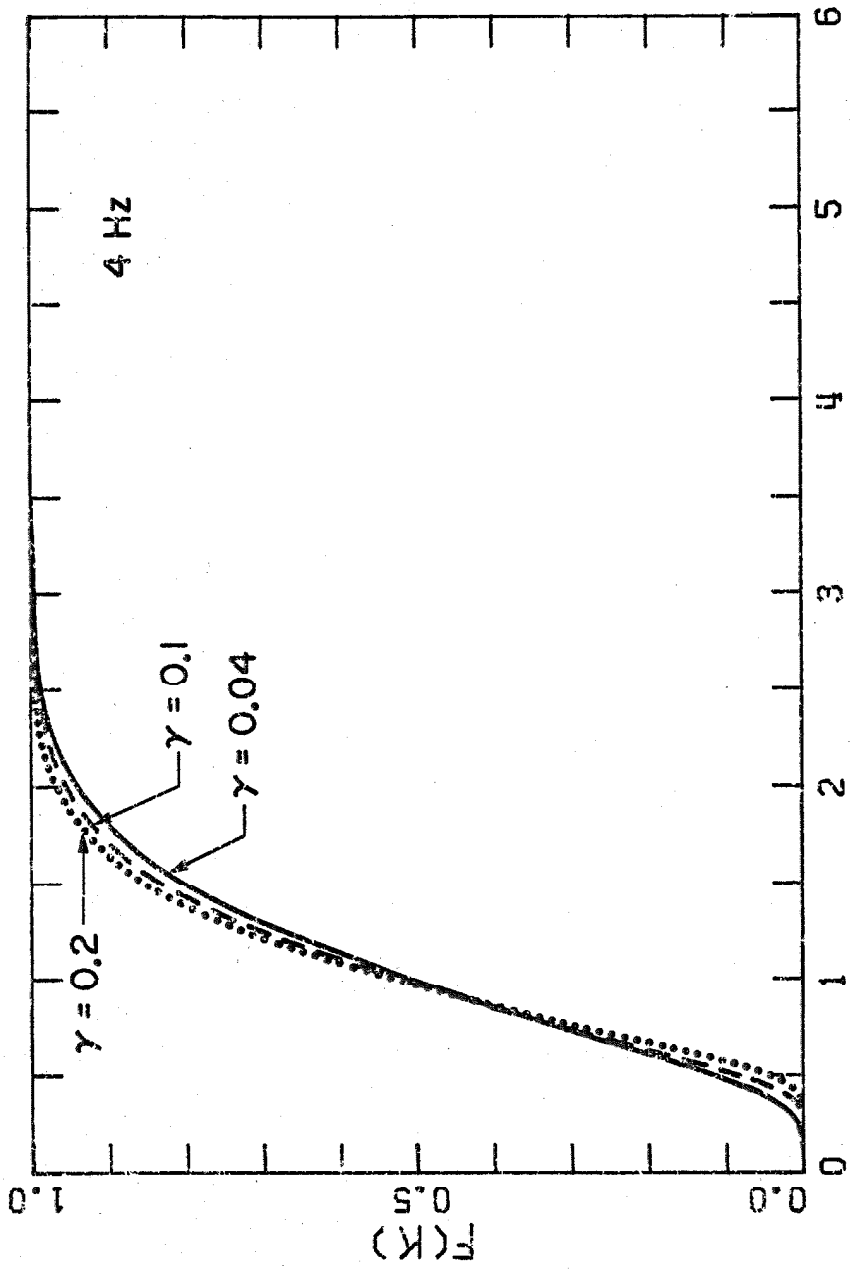

Figure A4.1. Continued.

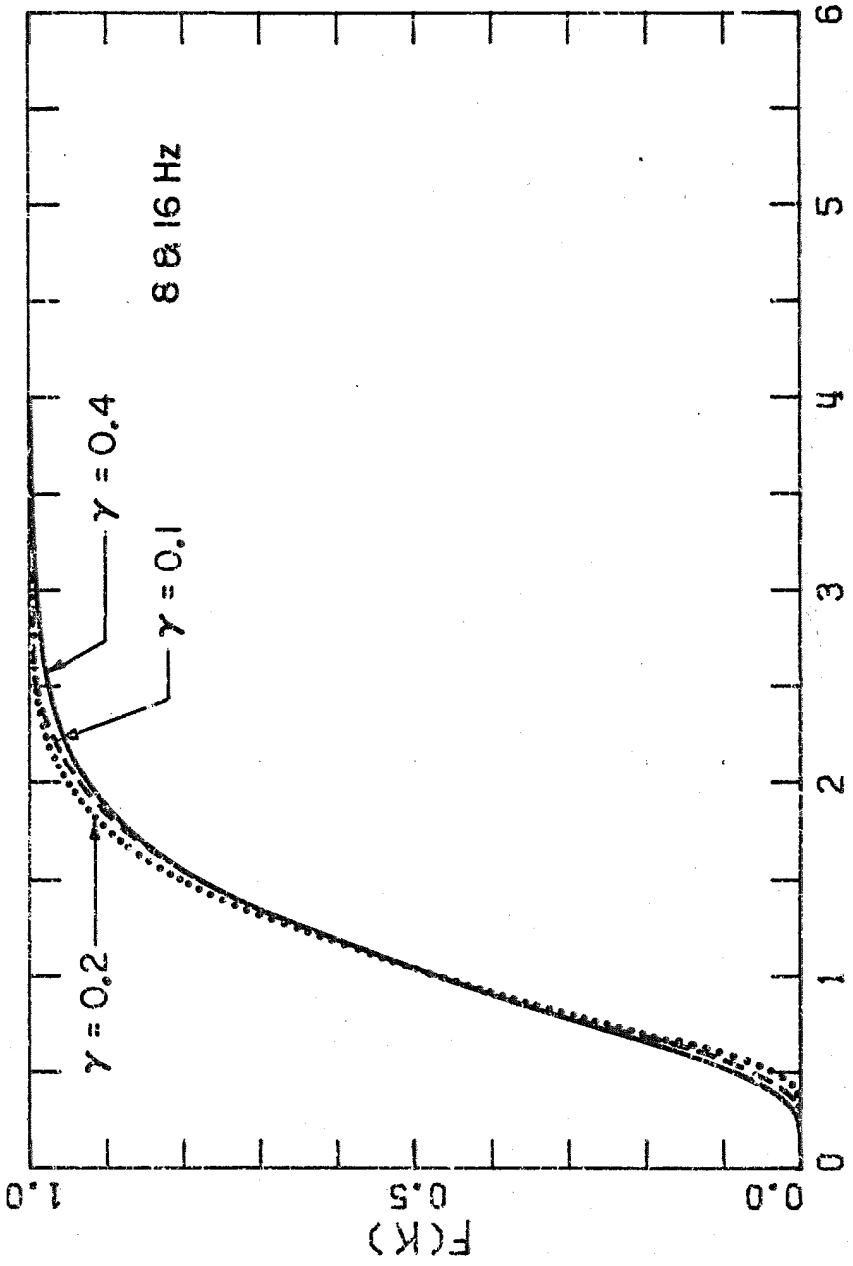

Figure A4.1. Continued.

APPENDIX 5: GLOSSARY AND LIST OF SYMBOLS

Coherence: Used loosely, coherence implies regulatory or consistency. More precisely, two functions are said to be coherent if their frequency contents are similar.

Engineering or Strong-Motion Seismology: That part of seismology dealing with the study of earthquakes sufficiently close to the fault rupture that ground motion is strong enough to pose a threat to engineering structures.

Epicentral, Focal and Hypocentral Distances: The point on a fault at which rupture initiates is known as the focus or hypocenter. The point on the ground surface directly above the focus is known as the epicenter. Distances referred to these points are known as focal, hypocentral and epicentral distances respectively.

Far Field: A point at distance r is said to be in the far field with respect to a fault rupture if $Kr \gg 1$, where K is the wave number, and if $r/R \gg 1$, where R is the source dimension. Conversely, a point is said to be in the near field if either $Kr \ll 1$ or $r/R \ll 1$.

Magnitude: In this study magnitude, M, refers specifically to local magnitude (Richter, 1958) unless otherwise stated.

Near Field: See far field.

Strong (Ground) Motion: Strong ground motion is a general term referring to ground motions strong enough to pose a threat to engineering structures. In effect, this implies peak accelerations of a few percent of gravity, or more.

Source Parameters: A set of several parameters which measure the average properties of the fault rupture mechanism. The rupture mechanism, in general, is referred to as the earthquake source.

List of Symbols

$A(f)$	Source excitation in equation (2.6)
A_i	$A(f)$ evaluated at sampling frequency f_i
$\overline{A}(f)$	$A(f)$ predicted by the two-parameter source model
A_o	The high frequency limit of $\overline{A}(f)$
a	Peak ground acceleration
$a(s)$	Wave amplitude (used in this sense in equation (2.11))
$\langle a \rangle$	Root mean square acceleration
B_e	Resolution bandwidth
C	A parameter in equation (1.6)
c	Wave velocity
c_1, c_2	Constants in equation (2.2)
D	Fault offset
d_{max}	Peak ground displacement
E	Peak stored energy
F	Accumulated relative frequency (frequency here is used in the statistical sense)
f	Frequency (in Hertz)
f_o	Corner frequency
$f_{m,n}$	Natural frequency of m, nth mode of vibration
$G(f)$	Power spectral density
$g(t)$	An arbitrary time function
$\hat{g}(f)$	Fourier transform of $g(t)$
h	Fault depth
k	Uncertainty factor
k_a	Uncertainty factor for predicted accelerations

k_v	Uncertainty factor for predicted velocities
$\bar{k}$	Arithmetic mean of k
k_G	Geometric mean of k
L	Fault length
M	Local magnitude
M	A measure of Fourier amplitude smoothing (see N, below) (used in Section 2. 3 and Appendix 1)
M_o	Seismic moment
m	Exponent of s in equation (1. 6)
m_k	Third moment
N	The number of raw spectral ordinates averaged to obtain a smoothed Fourier amplitude value; N = 2M+1
1/Q	Specific attenuation
$\Re_{\theta\varphi}$	Radiation pattern
r	Focal distance or, equivalently, hypocentral distance
S	Fault area
S_v	Pseudo-velocity response
s	Epicentral distance
t	Time
T	Time length of accelerogram
T_e	Length of strong-motion part of accelerogram
$\bar{u}$	Average dislocation
u_{max}	Maximum dislocation
v	Peak ground velocity
X(f, r)	Fourier amplitude of acceleration
$\bar{X}$(f, r)	Fourier amplitude of acceleration predicted by equation (2. 6)

$\overline{X}_{90}$	$\overline{X}$ at 90 percent confidence level
x(t)	Ground acceleration
$\hat{x}(f)$	Fourier transform of x(t)
$\langle x \rangle$	Root mean square acceleration
y	Relative displacement of a single-degree-of-freedom oscillator
y_{max}	Maximum relative displacement
α	P-wave velocity
α	A parameter in equation (1.6)
β	Shear-wave velocity
γ	Exponent of f (in Chapter 3)
γ	Ratio of resolution bandwidth to frequency (in Appendix 4)
ΔB	Frequency increment
$\Delta\sigma$	Static stress drop
ϵ_{max}	Peak strain
ζ	Fraction of critical viscous damping
κ	Wave number
μ	Shear modulus
$\sum$	Summation
σ_e	Effective stress
σ_k	Standard deviation of k
$\sigma_{\log_e k}$	Standard deviation of $\log_e k$
Φ	The function minimized in the least-squares parameter estimation
ϕ	Phase angle

φ	Source-station azimuth
$\Omega(f)$	Fourier amplitude of displacement
Ω_o	Low frequency limit of $\Omega(f)$

REFERENCES

Adu, R. A. (1971). "Response and failure of structures under stationary random excitation", Ph. D. Thesis, Calif. Inst. of Tech., Pasadena.

Aki, K. (1966). "Generation and propagation of G waves from the Niigata earthquake of June 16, 1964", Bull. Earthquake Research Inst. 44, 73-88.

Aki, K. (1972a). "Earthquake mechanism", Tectonophysics, 13, 423-446.

Aki, K. (1972b). "Scaling law of earthquake source time-function", Geophys. J. R. astr. Soc. 31, 3-25.

Ambaseys, N. N. (1960). "On the shear response of a two-dimensional truncated wedge subjected to an arbitrary disturbance", Bull. Seism. Soc. Am. 50, 45-56.

Ambraseys, N. N. (1961). "On the seismicity of South-west Asia (I) Data from a XV-century arabic manuscript", Report for Union Internationale de Secours, Geneva.

Archambeau, C. B. (1968). "General theory of elastodynamic source fields", Rev. Geophys. 6, 241-288.

Ben-Menahem, A. (1961). "Radiation of seismic surface waves from finite moving sources", Bull. Seism. Soc. Am. 51, 401-435.

Bendat, J. S. and A. G. Piersol (1971). Random Data: Analysis and Measurement Procedures, Wiley-Interscience, New York.

Berrill, J. B. and T. C. Hanks (1974). "High frequency amplitude errors in digitized strong motion accelerograms", in Vol. IV, Part Q, Analysis of Strong Motion Accelerograms, Earthquake Eng. Research Lab., Calif. Inst. of Tech., Pasadena.

Bolt, B. A. (1970a). "Elastic waves in the vicinity of the earthquake source", in Earthquake Engineering, ed. R. L. Wiegel, Prentice-Hall, Englewood Cliffs, N. J., pp. 1-20.

Bolt, B. A. (1970b). "Causes of earthquakes", in Earthquake Engineering, ed. R. L. Wiegel, Prentice-Hall, Englewood Cliffs, N. J., pp. 21-45.

Borcherdt, R. D. (1970). "Effects of local geology on ground motion near San Francisco Bay", Bull. Seism. Soc. Am. 60, 29-61.

Bradley, J. J. and A. N. Fort (1966). "Internal friction in rocks", Handbook of Physical Constants, Geological Soc. of America Memoir 97, 175-193.

Brady, A. G. and M. D. Trifunac (1975). "Experimental relationships between response spectra and peak ground motions", (to be published).

Brune, J. N. (1970). "Tectonic stress and the spectra of seismic shear waves", J. Geophys. Res. 75, 4997-5009.

Brune, J. N. (1971a). Correction, J. Geophys. Res. 76, 5002.

Brune, J. N. (1971b). "Seismic sources, fault plane studies and tectonics", Trans. Am. Geophys. Union 52 (5), 178-187.

Bullen, K. E. (1963). An Introduction to the Theory of Seismology, 3rd ed. Cambridge.

Caughey, T. K. and H. J. Stumpf (1961). "Transient response of a dynamic system under random excitation", J. Applied Mech. 87, 563-566.

Crandall, S. H. and W. D. Mark (1963). Random Vibrations in Mechanical Systems, Academic Press, New York and London.

Crouse, C. B. (1973). "Engineering studies of the San Fernando earthquake", Ph. D. Thesis, Calif. Inst. of Tech., Pasadena.

Davenport, A. G. (1972). "A statistical relationship between shock amplitude and epicentral distance and its application to seismic zoning", Report BLWT-4-72, University of Western Ontario, London, Ontario.

Donovan, N. C. (1972). "Earthquake hazards for buildings", Report No. EE72-4, Dames and Moore, San Francisco.

Donovan, N. C. (1973). "A statistical evaluation of strong motion data including the February 9, 1971, San Fernando earthquake", Proc. 5th World Conf. on Earthquake Eng., Rome, 1252-1261.

Drake, L. A. and A. K. Mal (1972). "Love and Rayleigh waves in the San Fernando Valley", Bull. Seism. Soc. Am. 62, 1673-1690.

Duke, C. M., J. A. Johnson, Y. Kharraz, K. W. Campbell and N. A. Malpiede (1971). "Subsurface site conditions and geology in the San Fernando earthquake area", Report No. UCLA-ENG-7206, University of California, Los Angeles.

Esteva, L. and E. Rosenblueth (1963). "Espectros de Temblores a Distancios Moderadas y Grandes", Proc. Chilean Conference on Seismology and Earthquake Engineering, Vol. 1, Univ. of Chile.

Hall, W.J., N.M. Newmark and B. Mobray (1973). "Comments on earthquake transmission from basement rock to surface", Proc. 5th World Conf. on Earthquake Eng., Rome, 737-740.

Hanks, T.C. (1973). "Current assessment of long period errors", in Vol. II, Part G, Strong Motion Earthquake Accelerograms, ed. Trifunac, M.D. et al., Earthquake Eng. Research Lab., Calif. Inst. of Tech., Pasadena, pp. 6-38.

Hanks, T.C. (1974a). "The faulting mechanism of the San Fernando earthquake", J. Geophys. Res., 79, 1215-1229.

Hanks, T.C. (1974b). "Strong ground motion following the San Fernando, California, earthquake: ground displacements", to appear in Bull. Seism. Soc. Am.

Hanks, T.C. (1975). "Observation and estimation of long-period strong ground motion in the Los Angeles Basin", (in manuscript).

Hanks, T.C., J.A. Hileman, and W. Thatcher (1975). "Seismic moments of the larger earthquakes of the Southern California region", (in manuscript).

Hanks, T.C. and W. Thatcher (1972). "A graphical representation of seismic source parameters," J. Geophys. Res., 77, 4393-4405.

Hanks, T.C. and M. Wyss (1972). "The use of body-wave spectra in the determination of seismic-source parameters", Bull. Seism. Soc. Am. 62, 561-589.

Haskell, N.A. (1964). "Total energy and energy spectral density of elastic wave radiation from propagating faults", Bull. Seism. Soc. Am. 54, 1811-1841.

Housner, G.W. (1955). "Properties of strong-motion earthquakes", Bull. Seism. Soc. Am. 45, 197-218.

Housner, G.W. (1965). "Intensity of ground shaking near the causative fault", Proc. 3rd World Conf. on Earthquake Eng., Vol. 1, New Zealand.

Housner, G.W. (1973a). "The role of earthquake ground motions in earthquake engineering", Proc. 5th World Conf. on Earthquake Engineering, Rome.

Housner, G.W. (1973b). "Earthquake resistant design of high-rise buildings", Earthquake Eng. Research Lab., Calif. Inst. of Tech., Pasadena.

Hudson, D. E. (1956). "Response spectrum techniques in engineering seismology", Proc. 1st World Conf. on Earthquake Eng., Berkeley, California.

Hudson, D. E. (1972a). "Strong motion seismology", Proc. Int'l. Conf. on Microzonation, Seattle, pp. 29-60.

Hudson, D. E. (1972b). "Local distribution of strong earthquake ground motions", Bull. Seism. Soc. Am. 62, 1765, 1786.

Hudson, D. E. (1974). "Destructive earthquake ground motions", in Applied Mechanics in Earthquake Engineering, ed. W. D. Iwan, AMD-Vol. 8, ASME, New York, New York.

Hudson, D. E. (ed.) (1971). Strong Motion Instrumental Data on the San Fernando Earthquake of February 9, 1971. Earthquake Eng. Research Lab., Calif. Inst. of Tech., Pasadena, and Seismological Field Survey.

Hudson, D. E. (ed.) (1972). Analyses of Strong Motion Earthquake Accelerograms, Vol. IV, Earthquake Eng. Research Lab., Calif. Inst. of Tech., Pasadena.

Hudson, D. E., A. G. Brady, M. D. Trifunac and A. Vijayaraghavan (1971). Strong Motion Earthquake Accelerograms – Vol. II. Corrected Accelerograms and Integrated Ground Velocity on Displacement Curves. Earthquake Eng. Research Lab., Calif. Inst. of Tech., Pasadena.

Idriss, I. M. and H. B. Seed (1968). "Seismic response of horizontal soil layers", J. Soil Mech. Found. Div., ASCE 94, 1003-1031.

Jacobs, J. A., R. D. Russell and J. Tuzo Wilson (1974). Physics and Geology, 2nd ed. McGraw-Hill, New York, New York.

Jennings, P. C., G. W. Housner and N. C. Tsai (1968). "Simulated earthquake motions", Earthquake Eng. Research Lab., Calif. Inst. of Tech., Pasadena.

Johnson, R. A. (1973). "An earthquake spectrum prediction technique", Bull. Seism. Soc. Am. 63, 1255-1274.

Kanamori, H. (1972). "Determination of effective tectonic stress associated with earthquake faulting. The Tottori earthquake of 1943", Phys. Earth. and Planet. Interiors 5, 426-434.

Keilis-Borok, V. I. (1959). "On the estimation of the displacement in an earthquake source and of source dimensions", Ann. Geofis. 12, 205-214.

Keilis-Borok, V. I. (1960). "Investigation of the mechanism of earthquakes", Soc. Res. Geophys. 4, Am. Geophys. Union, Consultants Bureau, New York, 201 pp.

Knopoff, L. (1958). "Energy release in earthquakes", Geophys. J. R. astr. Soc. 1, 44-52.

Knopoff, L. (1964). "Q", Rev. Geophys. 2, 625-660.

Lin, Y. K. (1967). Probabilistic Theory of Structural Dynamics, McGraw-Hill, New York, New York.

Lord, J. (1974). Personal communication.

Lynch, R. D. (1969). "Response spectra for Pahute Mesa nuclear events", Bull. Seism. Soc. Am. 59, 2295-2309.

Mal, A. K. (1974). "Applications of continuum mechanics", in Applied Mechanics in Earthquake Engineering, ed. Iwan, W. D., ASME, New York, 205-224.

Marquandt, D. W. (1963). "An algorithm for least-squares estimation of nonlinear parameters", J. Soc. Indust. Appl. Math. 11, 431-441.

Marquandt, D. W. (1964). "Least squares estimation of nonlinear parameters", Documentation for IBM Share Library program No. 3094.

Maruyama, T. (1963). "On the force equivalents of dynamical elastic dislocations with reference to the earthquake mechanism", Bull. Earthquake Research Inst., 41, 467-486.

Mason, W. P. (1958). Physical Acoustics and Properties of Solids, Van Nostrand, Princeton, N. J.

Mei, Shi-Yun (1960). "The seismic activity of China", (in Russian) Izvestia Geophysics Series, 381-395.

Merchant, H. C. and D. E. Hudson (1962). "Mode superposition in multi-degree-of-freedom structures using earthquake response spectrum data", Bull. Seism. Soc. Am. 52, 405-416.

Newmark, N. M. and E. Rosenblueth (1971). Fundamentals of Earthquake Engineering, Prentice-Hall, Englewood Cliffs, N. J.

Randall, M. J. (1966). "Seismic radiation from a sudden phase transition", J. Geophys. Res. 71, 5297-5302.

Randall, M. J. (1973a). "The spectral theory of seismic sources", Bull. Seism. Soc. Am. 63, 1133-1144.

Randall, M. J. (1973b). "Spectral peaks and earthquake source dimension", J. Geophys. Res. 78, 2609-2611.

Reid, H. F. (1911). "The elastic-rebound theory of earthquakes", Calif. Univ. Publ. in the Geological Sciences Bull. 6, 413-443.

Richter, C. F. (1958). Elementary Seismology, Freeman, San Francisco.

Salt, P. E. (1974). "Seismic site response", Bull. of N. Z. Nat. Soc. for Earthquake Eng., 7, 62-77.

Savage, J. C. (1972). "Relation of corner frequency to fault dimensions", J. Geophys. Res. 77, 3788-3795.

Schnabel, D. and H. B. Seed (1973). "Accelerations in rock for earthquakes in the Western United States", Bull. Scism. Soc. Am. 62, 501-576.

Scott, R. F. (1972). "A comparative study of strong ground motions", Proc. 4th European Conf. on Earthquake. Eng., London.

Seed, H. B., I. M. Idriss and F. W. Kiefer (1969). "Characteristics of rock motions during earthquakes", J. Soil Mech. Found Div., ASCE, 95, 1199-1218.

Seed, H. B. and I. M. Idriss (1970). "Soil moduli and damping factors for dynamic response analysis", Report No. EERC 70-10, Univ. of California, Berkeley.

Starr, A. T. (1928). "Slip in a crystal and rupture in a solid due to shear", Proc. Camb. Phil. Soc. 24, 489-500.

Steketee, J. A. (1958). "Some geophysical applications of the elasticity theory of dislocations", Can. J. of Phys. 36, 1168-1198.

Thatcher, W. (1972). "Regional variations of seismic source parameters in Northern Baja California area", J. Geophys. Res. 77, 1549-1565.

Thatcher, W. and T. C. Hanks (1973). "Source parameters of Southern California earthquakes", J. Geophys. Res. 78, 8547-8576.

Thomson, W. T. (1965). Vibration Theory and Applications, Prentice-Hall, Englewood Cliffs, N. J.

Tolstoy, I. (1973). Wave Propagation, McGraw-Hill, New York, N. Y.

Trifunac, M. D. (1971). "Surface motion of a semi-cylindrical alluvial valley for indecent plane SH waves", Bull. Seism. Soc. Am. 61, 1739-1753.

Trifunac, M. D. (1972). "Stress estimates for the San Fernando, California earthquake of February 9, 1971: Main event and thirteen aftershocks", Bull. Seism. Soc. Am. 62, 721-750.

Trifunac, M. D. (1973). "Analysis of strong earthquake ground motion for prediction of response spectra", J. Earthquake Eng. and Struct. Dyn. 2, 59-69.

Trifunac, M. D. (1974). "A three-dimensional dislocation model for the San Fernando, California, earthquake of February 9, 1971", Bull. Seism. Soc. Am. 64, 149-172.

Trifunac, M. D. and A. G. Brady (1975). "On the correlation of seismic intensity scales with the peaks of recorded strong ground motion", (to be published in Bull. Seism. Soc. Am.).

Trifunac, M. D. and V. Lee (1973). "Routine Computer Processing of Strong-Motion Accelerograms", Earthquake Eng. Res. Lab., Calif. Inst. of Tech., Pasadena.

Trifunac, M. D. and F. E. Udwadia (1972). "Fourier spectra", in Analyses of Strong Motion Earthquake Accelerograms, Vol. IV, Earthquake Eng. Res. Lab., Calif. Inst. of Tech., Pasadena.

Trifunac, M. D. and F. E. Udwadia (1974). "Variations of strong earthquake ground motion in the Los Angeles area", Bull. Seism. Soc. Am. 64, 1429-1454.

Trifunac, M. D., F. E. Udwadia and A. G. Brady (1973). "Analysis of errors in digitized strong-motion accelerograms", Bull. Seism. Soc. Am. 63, 157-187.

Tsai, N.-C. (1969). "Influence of local geology on earthquake ground motion", Ph. D. Thesis, Calif. Inst. of Tech., Pasadena.

Tucker, B. E. and J. N. Brune (1973). "Seismograms, S-wave spectra, and source parameters for aftershocks of the San Fernando earthquake of February 9, 1971", in Geological and Geophysical Studies, Vol. 3, San Fernando Earthquake of February 9, 1971, NOAA, Washington, D. C.

Tukey, J. W. (1965). "Data analysis and the frontiers of geophysics", Science 148, 1283-1289.

Udwadia, F. E. (1972). "Investigation of earthquake and microtremor ground motions", Ph. D. Thesis, Calif. Inst. of Tech., Pasadena.

Wong, H. L. and P. C. Jennings (1975). "Effects of canyon topography on strong ground motion", (in manuscript).

Wong, H. L. and M. D. Trifunac (1974). "Surface motion of a semi-elliptical alluvial valley for incident plane SH-waves", Bull. Seism. Soc. Am. 64, 1389-1408.

Wood, J. H. (1973). "Earthquake-induced soil pressures on structures", Ph. D. Thesis, Calif. Inst. of Tech., Pasadena.

Woodward-Lundgren and Associates (1973). Geotechnical Data Compilation for Selected Strong Motion Seismograph Sites in California, Report to the U. S. National Oceanic and Atmospheric Administration, Washington, D. C.

Wyss, M. and T. C. Hanks (1972). "The source parameters of the San Fernando Earthquake inferred from teleseismic body waves", Bull. Seism. Soc. Am. 62, 591-602.

Yerkes, R. F., T. H. McCulloh, J. E. Schoellhamer, and J. G. Vedder (1965). "Geology of the Los Angeles Basin – an introduction", U. S. Geol. Survey, Professional Paper 420-A, 57 pp.

Zeevaert, L. (1964). "Strong ground motions recorded during earthquakes of May the 11th and 19th, 1962, in Mexico City", Bull. Seism. Soc. Am. 54, 209-231.